

**More Medicines for Tuberculosis:
Fuelling Drug Discovery against
*Mycobacterium tuberculosis***

THÈSE N° 8906 (2018)

PRÉSENTÉE LE 5 OCTOBRE 2018

À LA FACULTÉ DES SCIENCES DE LA VIE

UNITÉ DU PROF. COLE

PROGRAMME DOCTORAL EN BIOTECHNOLOGIE ET GÉNIE BIOLOGIQUE

ÉCOLE POLYTECHNIQUE FÉDÉRALE DE LAUSANNE

POUR L'OBTENTION DU GRADE DE DOCTEUR ÈS SCIENCES

PAR

Shi-Yan Caroline FOO

acceptée sur proposition du jury:

Prof. M. Blokesch, présidente du jury

Prof. S. Cole, directeur de thèse

Prof. P. Sander, rapporteur

Prof. M. Jackson, rapporteuse

Prof. K.-H. Altmann, rapporteur



ÉCOLE POLYTECHNIQUE
FÉDÉRALE DE LAUSANNE

Suisse
2018

Summary

Tuberculosis (TB), whose etiological agent is *Mycobacterium tuberculosis* (*M. tuberculosis*), has plagued humanity since antiquity. Even with chemotherapy available today, TB is the leading cause of death due to an infectious disease. Modern day factors, such as the HIV epidemic and the emergence of drug-resistant TB strains, have redefined the complexities and challenges of tackling the TB pandemic. Current treatments for TB are lengthy, and poor adherence to such prolonged treatment further exacerbates the issue of drug resistance. Moreover, therapies for drug-resistant TB have low cure rates. There is therefore a pressing need for improved therapies that are short and efficacious against all TB strains, which can be achieved through new antimicrobials that are more potent and have novel mechanisms of action, in addition to being affordable, orally bioavailable, and without drug-drug interactions.

Such new anti-TB drugs need to be discovered and developed through a long, risky, and costly process, in which attrition rates are high. While there are promising compounds currently being developed, including the benzothiazinones (BTZs), it is necessary to further populate and enhance the Global TB drug pipeline to ensure the availability of new drugs. This thesis aims to address this need through the discovery work of two new, highly promising families, the AX and PB compounds, and of BTZs.

The piperazine-based AX analogs are easily synthesised and demonstrate potent activity against *M. tuberculosis* *in vitro* and *in vivo*. Their target, identified in this work, is the QcrB subunit of the cytochrome *bc₁-aa₃* complex, a terminal oxidase of the mycobacterial respiratory chain. Notably, AX compounds are bactericidal in the absence of the alternate terminal oxidase, cytochrome *bd*. As this family interacts differently in the same binding site of QcrB as Q203, a drug candidate in clinical trials, AX compounds could potentially serve as a backup series for QcrB inhibitors.

The PB family, derived from the natural product lapachol, is also easily synthesised and shows substantially improved activity against *M. tuberculosis* *in vitro* compared to the parent compound. PB analogs also demonstrated activity against the non-replicating bacillus and in infected macrophages. The mechanism of action of PB compounds relies on the F420 cofactor, although not on the F420-dependent nitroreductase Ddn, therefore this family has a novel mechanism of action which is highly specific to *M. tuberculosis*.

To support the clinical development of PBTZ169, the mechanism of resistance to BTZs was further elucidated in this thesis. Five mutations at cysteine 387 of the target enzyme, DprE1, were identified as mediating resistance to BTZs, which would serve as resistance markers for clinical screening. The impact of these mutations on *M. tuberculosis* and on DprE1 was further characterised, revealing a fitness cost imposed on the bacillus intracellularly and reduced catalytic efficiency of the enzyme. This thesis additionally contributed to the characterisation of a PBTZ169 backup series and the design of an optimal regimen with other TB drugs.

The compounds presented herein merit further optimisation so their full antibiotic potential may be realised for TB, and possibly for other mycobacterial diseases as well. Altogether, this thesis has contributed to the fuelling of drug discovery against *M. tuberculosis*, and a step towards more medicines for TB.

Keywords: tuberculosis, anti-TB drugs, drug discovery and development, drug resistance, QcrB inhibitors, natural product lapachol, F420 cofactor, benzothiazinone, PBTZ169

Résumé

La tuberculose (TB), dont l'agent étiologique est *Mycobacterium tuberculosis* (*M. tb*), affecte l'humanité depuis l'antiquité. Malgré la disponibilité d'une antibiothérapie, elle est la principale cause de décès dû à une maladie infectieuse. Les facteurs modernes, tels que l'épidémie du VIH et l'apparition de souches multi-résistantes, ont redéfini les défis de la lutte contre la pandémie causée par le bacille de Koch. Les traitements actuels sont longs, et le manque d'observance entraîne la résistance aux antibiotiques. De plus, les traitements contre la TB résistante ont de faibles taux de guérison. Il y a donc un besoin urgent d'améliorer les médicaments offerts afin de diminuer le temps de traitement et d'augmenter l'efficacité de ceux-ci contre l'ensemble des souches de *M. tb*. Par conséquent, la découverte de nouveaux antimycobactériens abordables, ne présentant aucune interaction médicamenteuse, ayant de nouveaux mode d'actions et biodisponibles par voie orale est l'un des nerfs de la guerre afin de contrer la TB dans le monde.

Ces nouveaux médicaments sont mis au point dans le cadre d'un processus long et coûteux dans lequel les taux d'attrition sont élevés. Bien que des composés prometteurs soient en cours de développement, dont les benzothiazinones (BTZ), il est nécessaire d'alimenter le pipeline de nouveaux médicaments contre la TB. Cette thèse répond à cette problématique par la découverte de deux nouvelles familles très prometteuses, les composés AX et PB, ainsi que les BTZ. Les analogues AX sont faciles à synthétiser et démontrent une bonne activité contre *M. tb in vitro* et *in vivo*. La cible, identifiée dans ce travail, est la sous-unité QcrB du complexe cytochrome bc1-aa3, une oxydase terminale de la chaîne respiratoire mycobactérienne. Les composés AX sont bactéricides en l'absence de l'oxydase terminale alternative, le cytochrome bd. Puisque cette famille interagit différemment au même site de liaison que le Q203, les composés AX pourraient servir de série alternative pour les inhibiteurs de QcrB.

La famille PB est dérivée du lapachol, un produit naturel. Les composés sont facilement synthétisables et présentent une amélioration substantielle de l'activité contre *M. tb* par rapport au lapachol. Les analogues PB ont démontré une activité contre le bacille non-réplicatif ainsi que dans les macrophages infectés. Le mécanisme d'action repose sur le cofacteur F420, mais est indépendant de la nitroréductase Ddn, ce qui suggère que cette famille possède un nouveau mécanisme d'action très spécifique à *M. tb*. Pour soutenir le développement clinique du PBTZ169, le mécanisme de résistance aux BTZ a été caractérisé. Cinq mutations de la cystéine 387 de l'enzyme cible, DprE1, ont été identifiées et impliquées dans cette résistance. La présence de ces mutations diminue la virulence *ex vivo*, ainsi qu'elle altère l'efficacité catalytique de l'enzyme DprE1. Ces mutations pourraient servir de marqueurs de résistance pour le dépistage clinique. Cette thèse a également contribué à la caractérisation d'une série alternative du PBTZ169 et à la conception d'une combinaison optimale avec d'autres antituberculeux.

Les composés présentés ici méritent d'être améliorés afin que leur activité soit optimale contre *M. tb* et possiblement contre d'autres mycobactéries. Dans l'ensemble, cette thèse a contribué à la découverte de nouveaux antituberculeux afin d'élargir le spectre des outils permettant de lutter contre la TB.

Mots-clés : tuberculose, médicaments antituberculeux, découverte et développement d'antibiotiques, pharmacorésistance, inhibiteur de QcrB, produit naturel lapachol, cofacteur F420, benzothiazinone, PBTZ169

Table of Contents

Abbreviations	3
Chapter 1: Tuberculosis – past and present.....	5
Chapter 2: Arylvinylpiperazine amides, a new class of potent inhibitors targeting QcrB of <i>Mycobacterium tuberculosis</i>	63
Chapter 3: Discovery of new plant-derived inhibitors with potent F420-dependent activity against <i>Mycobacterium tuberculosis</i>	129
Chapter 4: Characterization of DprE1-mediated Benzothiazinone Resistance in <i>Mycobacterium tuberculosis</i>	159
Chapter 5: Conclusions and Perspectives.....	177
Appendix Chapter A1: Structural studies of <i>Mycobacterium tuberculosis</i> DprE1 interacting with its inhibitors.....	189
Appendix Chapter A2: Structure-based drug design and characterization of sulfonyl- piperazine benzothiazinone inhibitors of DprE1 from <i>Mycobacterium tuberculosis</i>	199
Appendix Chapter A3: An optimized background regimen for treatment of active tuberculosis with the next-generation benzothiazinone Macozinone (PBTZ169)	237
Acknowledgements	271
Curriculum Vitae.....	273

Abbreviations

TB	tuberculosis
ABC transporters	ATP-binding cassette transporters
ADME	adsorption, distribution, metabolism, and excretion
BCG vaccine	Bacilli Calmette-Guérin vaccine
BDQ	bedaquiline, Sirturo
BTZs	benzothiazinones
CFM / CLO	clofazimine
Ddn	deazaflavin-dependent nitroreductase
DOT	directly-observed therapy
DprE1	decaprenylphosphoryl-beta-D-ribose 2' epimerase
DR-TB	drug-resistant TB
ESX-1	6-kDa early secreted antigen or ESAT-6 secretion system 1
ETC	electron transport chain
FDA	U.S. Food and Drug Administration
Fgd1	F420-dependent glucose-6-phosphate dehydrogenase
GLP	good laboratory practice
GMP	good manufacturing practices
GSK	GlaxoSmithKline
IFN- γ	interferon- γ
IGRAs	IFN- γ release assays
INH	isoniazid
LAM	lipoarabinomannan
LM	lipomannan
LPZ(S)	lansoprazole (sulphide)
LTBI	latent TB infection
<i>M. bovis</i>	<i>Mycobacterium bovis</i>
<i>M. tuberculosis</i>	<i>Mycobacterium tuberculosis</i>
MABSC	<i>Mycobacterium abscessus</i> complex
MBC	minimal bactericidal concentration
MCZ	Macozinone, PBTZ169
MDR-TB	multi-drug resistant TB
MIC	minimal inhibitory concentration
MM4TB	More Medicine for Tuberculosis consortium
MTBC	<i>M. tuberculosis</i> complex
NCEs	new chemical entities
NDH-2	type 2 NADH-quinone oxidoreductase
NO	nitric oxide
NTM	non-tuberculous mycobacteria
PA-824	Pretomanid
PAS	<i>para</i> -aminosalicylic acid
PBTZ	piperazine-based BTZ
PDIM	phthiocerol dimycocerosate
PK	pharmacokinetics
PMF	proton motive force
PPD	purified protein derivative
PZA	pyrazinamide
RD-1	region of difference 1

RIF	rifampicin
RND	resistance, nodulation and division
RNS	reactive nitrogen species
ROS	reactive oxygen species
RR-TB	rifampicin-resistant TB
SAR	structure-activity relationship
SS18b	streptomycin-starved 18b strain
TMM or TDM	trehalose monomycolate or trehalose dimycolate
TST	tuberculin skin test
WGS	whole-genome sequencing
WHO	World Health Organisation
XDR-TB	extensively drug-resistant TB

Chapter 1: Tuberculosis – past and present

Chapter 1 - Table of Contents

1.1 A Brief History of Tuberculosis.....	10
1.1.1 TB – an ancient disease.....	10
1.1.2 Treatment of TB in the pre-antibiotic era.....	10
1.1.3 New approaches to TB management.....	11
1.2 Epidemiology	15
1.3 <i>M. tuberculosis</i> , the bug behind the disease.....	16
1.3.1 Mycobacteria classification.....	16
1.3.2 Pathogenesis.....	17
1.3.3 Characteristics of <i>M. tuberculosis</i>	19
1.4 Current approaches to tackling TB.....	21
1.4.1 Vaccination.....	21
1.4.2 Diagnosis of TB infection and disease.....	22
1.4.3 Treatment of TB	24
1.5 The search for new TB drugs	25
1.5.1 The need for new drugs and regimens	25
1.5.2 Strategies for improved TB therapy through new anti-TB drugs.....	28
1.5.3 TB drug discovery and development	29
1.5.4 Global TB drug pipeline.....	34
1.6 Thesis rationale and outline.....	41
References	43

Tuberculosis (TB) is one of the deadliest diseases from antiquity. It is one of the top ten causes of death worldwide today, and remains the leading cause of death due to an infectious disease (1). In 2016 alone, TB claimed 1.7 million lives, contributing to three percent of deaths globally (2). On a broader time scale, the death toll due to TB over the past two centuries is estimated at one billion (3), hence its moniker ‘Captain of all these Men of Death’ (4).

TB, as we know it today, is a contemporary term for the disease. Historically, it has been referred to as consumption, the White Plague, or phthisis by Hippocrates. Although a disease which primarily affects the lungs, TB also manifests itself in other organs such as the spine (Pott’s disease), the lymph nodes (scrofula), and the skin (lupus vulgaris).

For all its different labels and forms, the disease caused by *Mycobacterium tuberculosis* (*M. tuberculosis*) that has afflicted mankind since thousands of years is the one and the same which persists as a global health problem today. The juxtaposition of an age-old disease against a modern backdrop highlights similarities and contrasts between past and present contexts. While overcrowding and impoverished living conditions (which still unfortunately exist in many areas of the world today) continue to contribute to the spread and mortality of TB, new factors, including the HIV epidemic and drug resistance, add modern complexities to an old problem.

Up until now, the history of TB and humankind has been very much intertwined and will remain so in the foreseeable future. As we continue to seek to tackle TB globally, building upon the work of a great many before us, it is with the aspirations of closing this chapter of history definitively and to put to rest the ‘Captain of all these Men of Death’.

1.1 A Brief History of Tuberculosis

1.1.1 TB – an ancient disease

Historical evidence for the existence of TB in humans has been derived from prehistoric art, archaeological artefacts, and literary writings (5). The detection of *M. tuberculosis*-specific DNA and lipids in mummy specimens, including those from ancient Egypt (dated 600 BC) (6) and pre-Columbian Peru (dated 1000 AC) (7) provide concrete proof for TB affecting humans in the past. Thus far, the evidence gathered traces TB in humans to more than 8000 years ago with specimens from Atlit Yam in east Mediterranean (5, 8), and paints a picture of a disease with a wide geographical reach with TB epidemics having occurred in ancient Egypt, Greece, the Americas, and Europe (9).

1.1.2 Treatment of TB in the pre-antibiotic era

Treatments for the disease varied greatly throughout different periods of history (9). Ancient Greek physicians prescribed milk, mild exercise, and warm climates for consumption, while it was believed that the touch of royalty would cure scrofula in Europe during the middle ages. Common practices during the TB epidemic in Europe in the 17th and 19th centuries included body-cleansing techniques such as sweating, bleeding, and vomiting. Horseback riding and sea voyages were also commonly prescribed to TB patients. These remedies would remain largely ineffective as the White Plague ravaged on.

Sanatoria were associated with TB treatment in the late 19th and early 20th century. Generally considered as the first sanatorium dedicated to TB treatment, Heilanstalt was established in 1859 in the German Silesian Mountains by a German physician, Herman Brehmer (10). Many other TB sanatoria followed suit, including those of Davos (Switzerland) and Seranac Lake (North America), with Dr. Brehmer's regimen of bed rest, mountainous outdoor air, exercise

and a good diet often being implemented. For the TB patients, there was some success of sanatorium treatment, although its efficacy largely depended on the extent of the disease at the point of hospitalisation (9).

Another procedure performed that was not uncommon during this period was the surgical induction of lung collapse in patients with unilateral TB, on the presumption that limiting lung motions and promoting healing of scarred lung tissue could cure the patient (11). This involved either the injection of air into the pleural cavity (pneumothorax) or removing a portion of the ribs (thoracoplasty). Although this procedure was reported to benefit numerous TB patients, undesirable consequences included embolism, bleeding, and permanent deformity.

While these treatments may have alleviated and treated TB in many cases, and while TB sanatoria contributed to containing the spread of TB from a public health viewpoint, all these practices have since been relegated to history as scientific advancements in the TB field ushered in the antibiotic era.

1.1.3 New approaches to TB management

The defining moment in our understanding of TB arrived with the discovery of its etiological agent, presented by the German scientist Robert Koch in 1882 (12). Previously thought to be hereditary, TB was proven based on Koch's postulates to be in fact an infectious disease caused by the tubercle bacillus, *M. tuberculosis*. The immense impact of Koch's work on TB would later earn him the Nobel Prize in Medicine in 1905.

Koch also created the first diagnostic tool for TB in 1890. Tuberculin, a liquid comprising sterilised, filtered *M. tuberculosis* culture, was initially aimed at treating TB (13). Although it would prove ineffective for its original purposes, it was further developed into a skin test by an

Austrian physician, Clemens Freiherr Baron von Pirquet, to detect prior and ongoing TB infection regardless of disease manifestation (14). The administration of the skin test was further modified by Charles Mantoux such that tuberculin was injected into the skin. The principle active component of Koch's tuberculin termed as purified protein derivative (PPD) was identified and led to the increased purity and reliability of tuberculin skin tests (15). The batch of PPD produced by Florence Seibert in 1940 still remains as the international reference for the manufacturing of PPD (16).

Eighteen years after Koch's presentation of his discovery of *M. tuberculosis*, Albert Calmette and Camille Guérin began work on developing a TB vaccine. After passaging a culture of bovine tubercle bacilli *Mycobacterium bovis* (*M. bovis*) 269 times, they obtained a live, attenuated vaccine strain found to be safe in non-human primates (9, 17). The vaccine was named *Bacilli Calmette-Guérin* (BCG) and was first administered in 1921 in a newborn at high risk of death due to TB, successfully protecting the infant from the disease. Apart from being implicated in a catastrophe in 1930 in Lübeck, Germany, in which a mix-up of strains resulted in children being mistakenly vaccinated with live virulent strains and dying from TB, BCG has demonstrated from widespread vaccination programs to be a safe vaccine, with more than 3 billion doses having been administered worldwide to date (18).

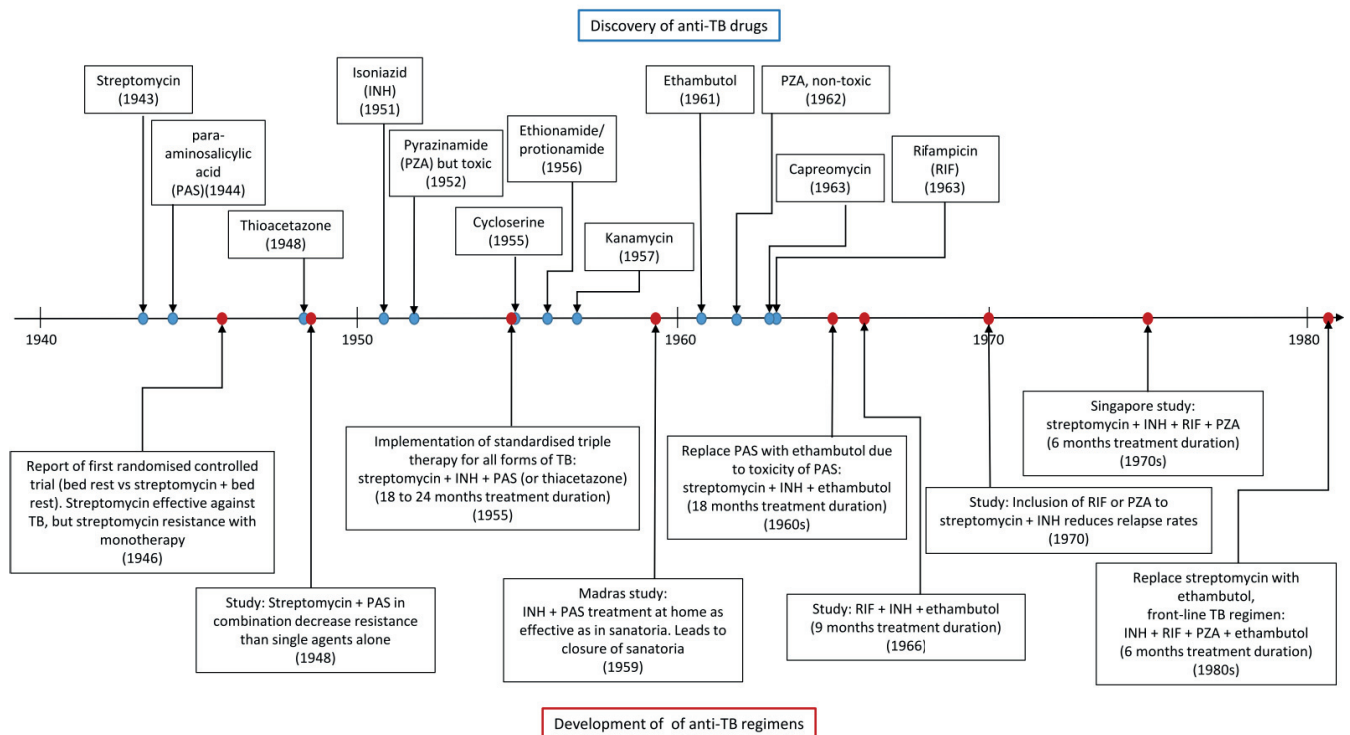


Figure 1: A timeline of TB drug discovery and regimen development. Adapted from (19).

The emergence of the TB drug discovery field (Fig. 1) originated on the basis of ‘magic bullets’ designed to specifically target microorganisms without harming the human host. This idea of molecules with selective activity was conceptualised by Paul Ehrlich, and successfully demonstrated when his arsenic-derived drug Salvarsan was used to treat syphilis by targeting *Treponema pallidum* in 1910 (20). A breakthrough in anti-TB chemotherapy occurred about 30 years later with the discovery of streptomycin, an antibiotic isolated from a soil actinomycete *Streptomyces griseus* (21). Its potent activity was first demonstrated in a guinea pig model of TB (22), and further validated in the first ever randomised controlled trial conducted in medical history, in which streptomycin was clearly more efficacious than bed rest (23). Resistance to streptomycin emerged within a year of its use (24), which led to the introduction of combination therapy for TB. The first combination of streptomycin and *para*-aminosalicylic acid (PAS),

another TB drug discovered around the same time as streptomycin, demonstrated that resistance emerged less frequently when both agents were used (25, 26).

More anti-TB drugs were discovered in the 1950s and 1960s. A significant point was the simultaneous discovery of isoniazid (INH) by three pharmaceutical companies, Hoffman-La Roche, Squibb and Bayer with potent anti-TB activity *in vivo* (27). This led to the first TB regimen implemented in 1955 consisting of a triple therapy of streptomycin, PAS and INH for 18 to 24 months (28, 29), which would remain as the standard treatment for all forms of TB for the next 15 years (30).

With the discovery of new anti-TB drugs, treatment toxicity was reduced and treatment duration was shortened (Fig. 1). While INH remained the cornerstone for building regimens, major advancements included the replacement of PAS with ethambutol, which reduced toxicity and shortened treatment duration to 18 months, as well as the inclusion of rifampicin (RIF) and pyrazinamide (PZA) which further decreased therapy length to 6 months with reduced relapse rates (31). This 6-month regimen of INH, RIF, PZA, and ethambutol has remained as the front-line TB treatment until today, 38 years after its implementation in the 1980s.

The period between the 1940s and 1960s was a productive era for TB drug discovery, with many significant contributions made by pharmaceutical companies and academics. As TB incidences declined, the disease became less prominent and efforts in TB drug discovery came to a halt. Unfortunately, the late 1980s and early 1990s saw a resurgence in TB cases worldwide driven by the onset of the HIV epidemic and the emergence and transmission of drug-resistant TB strains (32–34), threatening the efficacy of the front-line regimen. This led to the declaration of TB as a global public health emergency by the World Health Organisation (WHO) in 1993.

1.2 Epidemiology (2)

A quarter of the world population has latent TB, defined as an infection with *M. tuberculosis* without existing clinical disease manifestation. 5 to 15% are predicted to develop active TB within their lifetime, with certain populations at higher risk such as HIV, diabetic, and other immunosuppressed patients. This presents a large potential reservoir of at least 285 million new TB cases.

In 2016, 10.4 million people fell ill with active TB. 18% of these cases were attributed to undernourishment, 10% to HIV-TB co-infection and about 8% to diabetes. Seven countries accounted for 64% of TB incidence, namely India with the largest incidence, followed by Indonesia, China, Philippines, Pakistan, Nigeria, and South Africa.

Even with the availability of chemotherapy, TB continues to claim many lives globally. An estimated 1.7 million people died from TB in 2016, of which about 22% were attributed to HIV-associated TB. The HIV-TB co-infection burden is evident: TB is the biggest killer of HIV patients, with 40% of them dying of TB. Since TB remains largely a poverty-related disease, 85% of TB deaths are located in the WHO African and South East Asia Regions, areas of lower socioeconomic status.

Another cause for alarm is the emergence and transmission of drug-resistant TB (DR-TB). Rifampicin-resistant TB (RR-TB) is TB resistant to RIF, while multi-drug resistant TB (MDR-TB) is defined as resistance to both RIF and INH, cornerstones of the front-line regimen. Both these cases require second-line treatment regimens comprising fluoroquinolones and injectable agents such as amikacin, capreomycin or kanamycin. Extensively drug-resistant TB (XDR-TB) is defined as MDR-TB with additional resistance to any fluoroquinolone and at least one of the

above mentioned injectable agents. In 2016, 600 000 new cases of DR-TB were reported amounting to about 6% of total TB incidence. Of these DR-TB cases, 20% were RR-TB, 80% were MDR-TB cases and 6% of MDR-TB cases were classified as XDR-TB. DR-TB has been reported in 123 countries, with India, China and the Russian Federation alone accounting for half of the cases. Treatment success rates for RR-/MDR-TB and XDR-TB were low, with estimates at 54% and 30%, respectively.

Globally, although there is a decreasing trend in TB mortality rates and incidence rates of 3% and 2% per year, these rates need to be significantly improved in order to meet the milestones of the WHO End TB Strategy as part of the Sustainable Development Goals to end the TB epidemic by 2030.

1.3 *M. tuberculosis*, the bug behind the disease

1.3.1 Mycobacteria classification

The genus mycobacteria belongs to the actinobacteria family and consists of more than 170 species, including a majority of environmental organisms and several important human pathogens (35). Mycobacteria can be classified as slow- and fast-growers, as defined by colony formation within seven days (36, 37). Most mycobacteria causing diseases in humans are slow-growers, including pathogens within the *M. tuberculosis* complex (MTBC), *M. ulcerans*, and *M. leprae*, which are the causative agents of TB, Buruli ulcer and leprosy, respectively. The MTBC comprises human-adapted strains (*M. tuberculosis*, *M. africanum*) and animal-adapted strains (e.g. *M. bovis* which infects cattle, *M. microti*, the vole bacillus, *M. caprae* infecting goats, and *M. pinipedi* that causes TB in seals). Non-tuberculous mycobacteria (NTM), another group of mycobacteria which do not cause TB nor leprosy, are opportunistic environmental

pathogens and include slow-growers *M. avium* and fast-growers of the *M. abscessus* complex (MABSC).

1.3.2 Pathogenesis

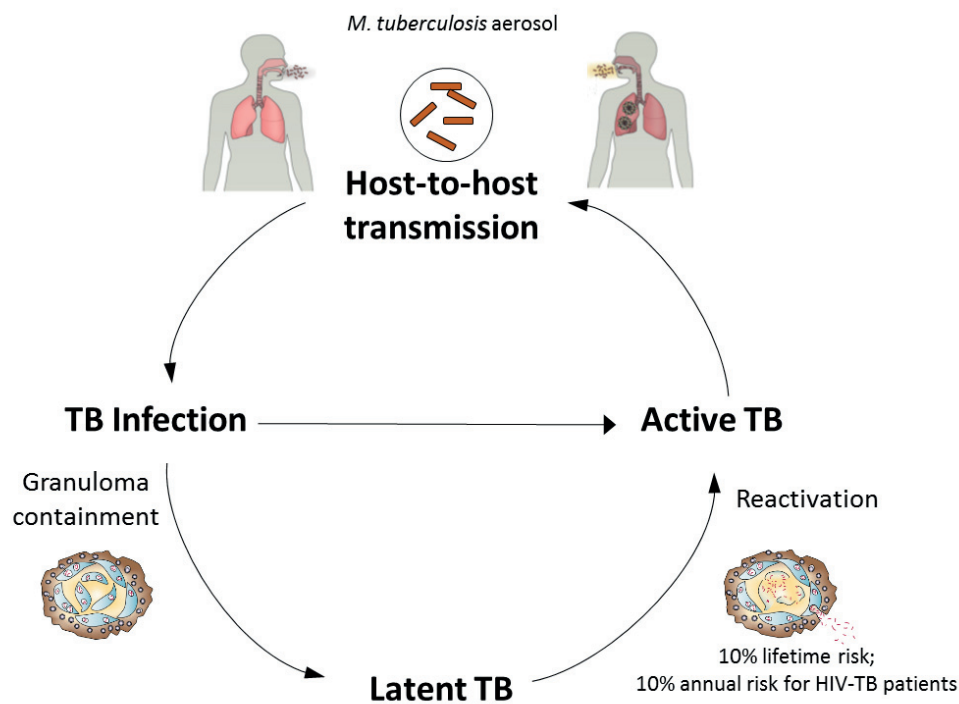


Figure 2: The cycle of *M. tuberculosis* infection. The transmission of *M. tuberculosis* occurs through the inhalation of the mycobacteria in aerosols, whereby an infection is established primarily in the lungs. In most cases, *M. tuberculosis* is contained by the host immune system in granulomas, resulting in asymptomatic, non-transmissible latent TB. However, there is a risk of the bacillus escaping the granuloma and reactivating, which increases drastically in immunocompromised individuals, such as HIV-TB patients. This results in active TB, in which *M. tuberculosis* spreads within the host and is transmitted between individuals to establish infections in new hosts. Adapted from (38, 39).

M. tuberculosis is transmitted between individuals in aerosols which are formed when coughing or sneezing, with a single bacterium estimated to be sufficient for establishing an infection (40). When inhaled, *M. tuberculosis* cells reach the lung alveoli and are phagocytosed primarily by

alveolar macrophages, which are at the front-line of the innate immune response. Intracellularly, pathogens are typically compartmentalised in the phagosome, which undergoes maturation by fusion with a lysosome to form the phagolysosome. Pathogens face a myriad of host defence mechanisms within the phagolysosome, including an acidic environment, reactive oxygen and nitrogen species (ROS and RNS), lysosomal enzymes, and antimicrobial peptides (41, 42). However, *M. tuberculosis* has evolved tactics through a variety of virulence factors to overcome these host defences. It is capable of inhibiting phagolysosome formation and acidification, escaping into the cytosol by lysing the phagosomal membrane, and overcoming xenophagy in the cytosol by preventing the formation of autophagosomes and autolysosomes (43, 44). In addition, it can induce necrosis instead of apoptosis of the infected macrophage such that upon macrophage death, the bacilli can enter the extracellular space and infect other cells (45).

Infected macrophages produce inflammatory cytokines, triggering the host innate immune response. Neutrophils, monocytes, and lymphocytes recruited to the infection site phagocytose more bacteria and amplify the immune signal through the secretion of even more cytokines (46). As dendritic cells phagocytose the bacilli, they mature and migrate to regional draining lymph nodes to present mycobacterial antigens, which then trigger the adaptive immune response (47). Antigen-specific T-cells are primed and differentiate to effector T-cells, which then migrate back to the infection site (39). CD4⁺ T-cells have a key role in protective immunity against *M. tuberculosis* by secreting predominantly interferon- γ (IFN- γ), which activates macrophages to kill intracellular *M. tuberculosis* by further stimulating antimicrobial processes such as the generation of more RNS (48–50).

The entire immune response to the infection results in granuloma formation, with a caseous centre containing lipids and cellular debris of necrotic macrophages surrounded by cellular zones of macrophages, fibroblasts and lymphocytes (51). The granuloma structure is a histopathological hallmark of TB, and this aggregation of immune cells is meant to contain bacilli which cannot be eradicated. Within the granuloma core, *M. tuberculosis* encounter a variety of microenvironments including low oxygen availability, nutrient deprivation and acidic pH (42, 52). These conditions drive the bacilli into a metabolically-altered dormant state (52), which can last for years.

In most TB-infected individuals, this stalemate between host immune system and pathogen is maintained and enables the containment of bacilli without the manifestation of clinical symptoms. This condition is termed as latent TB infection (LTBI) in which *M. tuberculosis* is non-transmissible. Immunosuppression, particularly as a result of HIV co-infection, greatly increases the risk of reactivation of the bacilli, leading to their replication and escape from the confinement of the granuloma. They spread in the lung tissue (pulmonary TB), and can also spread through the lymphatic system and blood to other organs (extra-pulmonary or disseminated TB). In this state of active TB, the bacilli can be further transmitted to other hosts, completing the infection cycle of *M. tuberculosis* (Fig. 2).

1.3.3 Characteristics of *M. tuberculosis*

M. tuberculosis is a rod-shaped, weakly Gram-staining and acid-fast bacterium with a slow growth rate of 24 h *in vitro* and *in vivo*, a highly unusual cell wall, and natural resistance to many antibiotics. The complete sequence of the reference strain *M. tuberculosis* H37Rv revealed a 4.4 Mbp circular chromosome rich in G + C bases (65%) (53). Its genome indicates a self-sufficient and versatile microorganism as enzymes necessary for the biosynthesis of all

essential amino acids, vitamins and enzyme co-factors and for glycolysis, the pentose phosphate pathway, tricarboxylic and glyoxylate metabolic pathways are present, with an unusually large repertoire of enzymes involved in lipid metabolism (53). Furthermore, the genome revealed antibiotic resistance entities such as β -lactamase, aminoglycoside acetyl transferases and drug-efflux systems such as the ATP-binding cassette (ABC) transporters (53).

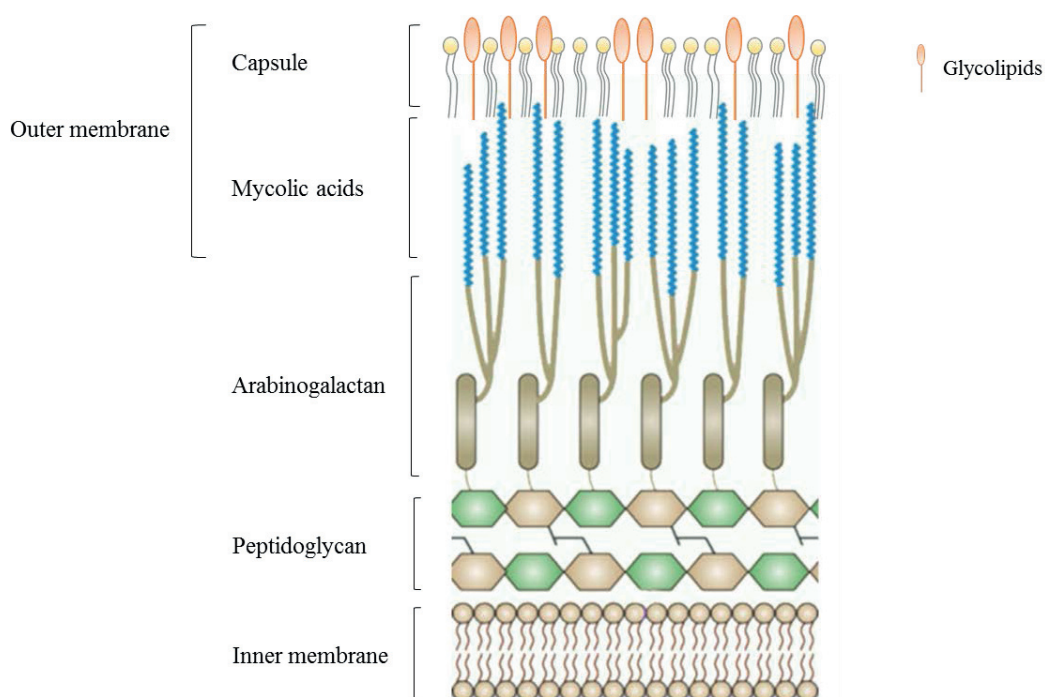


Figure 3: Schematic representing a simplified view of the mycobacterial cell envelope. Adapted from (54).

The cell wall of mycobacteria differs from those of Gram-positive and Gram-negative bacteria in that apart from the inner cell membrane and core peptidoglycan structure, there are additional arabinogalactan and mycolic acid components (55) (Fig. 3). The arabinogalactan layer is covalently attached to the peptidoglycan layer, and is composed of highly-branched arabinose sugars attached to linear chains of galactose sugars, both in the furanose form (56). Long-chain alpha-alkyl-beta-hydroxy C₇₀-C₉₀ fatty acids form the mycolic acid layer, and these molecules

can either be covalently bound to arabinogalactan or esterified to sugars, in particular trehalose (57). These esters of trehalose, trehalose monomycolate or trehalose dimycolate (TMM or TDM), are located in the outer membrane segment, which intercalates with mycolic acids (58). The outer membrane segment also contains non-covalently linked glycolipids including lipomannan (LM) and lipoarabinomannan (LAM). Many outer membrane lipids such as TDM, LAM and phthiocerol dimycocerosate (PDIM) have important roles in mediating host interactions and pathogenesis (59–61). Altogether, these layers of polysaccharides, lipids and glycolipids create a highly hydrophobic barrier between the external environment and the bacillus, largely contributing to the natural resistance of *M. tuberculosis* to many antibiotics.

1.4 Current approaches to tackling TB

1.4.1 Vaccination

One important approach to TB eradication is the vaccination of the population against the pathogen. The only licensed vaccine against TB currently available is BCG, an attenuated form of *M. bovis*. Its loss of virulence is attributed to the deletion of genomic locus region of difference 1 (RD-1), which encodes components of the ESX-1 (6-kDa early secreted antigen or ESAT-6 secretion system 1) secretion system, including immunodominant T-cell antigens EsxA (or ESAT-6) and EsxB (or CFP-10 for 10-kDa cultured filtered protein) (62). Although BCG highly protects infants and children against disseminated TB, its efficacy against pulmonary TB in the adult population varies widely for reasons which remain unclear (63). This limited efficacy of BCG thus necessitates the development of new, improved vaccines that protect both children and adults against pulmonary TB.

Current vaccine candidates aim at being administered either upon pre-exposure to *M. tuberculosis* to protect against active TB, or post-exposure for individuals with LTBI to prevent

re-activation (64). Three main strategies are undertaken, mainly the development of live mycobacterial vaccines whereby BCG is improved with the addition of appropriate genes or with the removal of virulence genes from *M. tuberculosis*, subunit and live vector-based vaccines as boosters after priming by BCG, or killed whole bacterial vaccines (65). Much of the focus of these candidates has been to develop a strong cellular-mediated T-helper 1 cell and IFN-gamma immune response. However, the lack of correlation between such a response and efficacy as demonstrated by a highly promising vaccine candidate MVA85A failing in Phase IIb clinical trials underscores the potential need for a more comprehensive set of protective immune markers (66).

1.4.2 Diagnosis of TB infection and disease

Clinical symptoms of pulmonary TB disease include persistent coughing, weight loss, night sweats and fever (67). These symptoms are not specific to TB however, and as individuals with LTBI are asymptomatic, the diagnosis of TB infection and disease requires a complete medical evaluation. This involves obtaining a medical history of the individual, a physical examination, detection of *M. tuberculosis* infection, performing a chest radiography, and bacteriological examination of clinical specimens (67).

The detection of *M. tuberculosis* infection is determined by the Mantoux tuberculin skin test (TST) and IFN- γ release assays (IGRAs) (68). In the case of TST, PPD is injected under the skin and the diameter of an indurated area is measured 48 to 72 hours later. TST is well-established and extensively used, however several instances can affect its accuracy, including NTM infections or a previous vaccination with BCG (69). IGRAs such as QuantiFERON-TB Gold and T-SPOT.TB measure the production of IFN-gamma in the blood induced by TB-specific antigens EsxA and EsxB and are highly specific for *M. tuberculosis* (68, 69). With the

validation of a TB infection, further tests are required to distinguish between LTBI and active TB.

One test performed is with chest radiographs to detect pulmonary TB, which appears as lung abnormalities such as lesions. Another is the bacteriological examination of clinical specimens, which plays an important role in the diagnosis of TB disease. Sputum smear microscopy involves the staining of acid-fast bacilli from the sputum and detection by microscopy. It is a rapid detection method, although its sensitivity is poor, at around 50%, as more than 10^4 bacilli per ml of sputum is required for reliable detection (67). Acid-fast organisms other than *M. tuberculosis* can also generate false-positives (69). A more accurate method of detecting *M. tuberculosis* is nucleic acid amplification (NAA), which amplifies *M. tuberculosis*-specific DNA and RNA segments from clinical specimens. An example is the Xpert MTB/RIF assay (Cepheid, USA), which is recommended by WHO as a rapid molecular test (2). The reference standard for the confirmation of TB disease is the culturing of specimens for the bacillus (2), which can be performed either on solid growth media or in broth culture systems such as BACTEC or MGIT (69). This method is highly sensitive, however the long doubling time of *M. tuberculosis* leads to a slow diagnosis.

With the diagnosis of TB, drug-susceptibility testing should be conducted. Molecular tests for DR-TB such as Xpert MTB/RIF assay, HAIN GenoType MTBDRplus and HAIN GenoType MTBDRsl are useful in providing rapid information for guiding decisions in treatment regimens and resistance surveillance. However, culture-based methods remain the reference standard for the testing of resistance to anti-TB drugs (67).

1.4.3 Treatment of TB

The front-line regimen which emerged in the 1980s from drug discovery efforts and clinical trials still remains as the current treatment for drug-susceptible TB (DS-TB). It consists of a six-month, directly-observed therapy (DOT) in which INH, RIF, PZA and ethambutol for the initial two months followed by INH and RIF for the next four months are administered under supervision (2). With complete adherence to the treatment, success rates are at least 85%, and costs US\$40 per individual (2).

DR-TB treatment regimens are more complex. Forming a core regimen for MDR-TB treatment involves at least five drugs, including PZA, a fluoroquinolone (levofloxacin, moxifloxacin or gatifloxacin), a second-line injectable (amikacin, kanamycin or capreomycin) and two other core second-line agents such as ethionamide/prothionamide and cycloserine (70, 71). Standard MDR-TB therapy lasts for 20 months with DOT, including an initial phase of 8 months with the injectable (70). Since 2016, a shorter MDR-TB regimen lasting 9 to 11 months has been recommended by WHO in certain cases. This regimen consists of add-on agents PZA, ethambutol, and high-dose INH in addition to moxifloxacin, kanamycin, prothionamide and clofazimine (70). There is currently no standardised regimen for XDR-TB, and like MDR-TB, regimens are built depending on strain susceptibility and patient tolerability. Altogether, the treatment for DR-TB is costly, more than a hundred times that of DS-TB (2), and long treatment durations are often accompanied by severe side effects.

1.5 The search for new TB drugs

1.5.1 The need for new drugs and regimens

There is a pressing need for new TB drugs and regimens, mainly due to two phenomena: (i) resistance towards current antibiotics and (ii) a persistent state of tubercle bacilli which contributes to long treatment durations.

(i) Resistance

Drug-resistant TB either originates from a wild-type strain acquiring resistance within the host (secondary resistance) or a resistant strain being transmitted between hosts (primary resistance) (72). Acquired resistance in *M. tuberculosis* is derived through spontaneous mutations in the chromosome rather than through horizontal gene transfer of mobile elements carrying resistance genes as in other bacteria (73). Such spontaneous mutations occur at a rate estimated at 10^{-6} to 10^{-8} replications in *M. tuberculosis*, and those that impart a survival advantage would be selected for in the presence of a single antibiotic, leading to the multiplication of the resistant strain (74). The probability of such an event occurring theoretically is greatly decreased, to less than 10^{-24} , by combination therapy with four effective TB drugs, that is, effectively negligible (74). However, sub-optimal combination therapy, in cases for instance of inappropriate prescription, poor compliance, and compartmentalisation of bacilli, increases the likelihood of the selection of spontaneous mutations for resistance towards an antibiotic. In this manner, step-wise acquisition of mutations leads to the emergence of MDR- and XDR-TB strains (75).

Although resistant strains with accumulation of mutations in essential genes should have incurred a certain fitness cost (76), several appear to have retained their virulence and transmissibility with low- or no-cost mutations (77–79), as evident from cases of primary resistance in which individuals having never undergone TB treatment are infected with a

resistant strain. Compensatory mutations can also contribute towards lessening the fitness cost of the initial mutation, particularly for initial costly mutations (77), as exemplified by the overexpression of alkyl hydroperoxidase AhpC in INH-resistant strains to compensate for the loss of function of catalase-peroxidase KatG (80).

Table 1 summarises the main genes mediating resistance to front-line and second-line anti-TB agents, as well as their corresponding roles in the mechanism of drug action and cellular processes in which they are involved.

Table 1: Genes involved in resistance to conventional front-line and second-line anti-TB agents.
Adapted from (75).

Drug	Genes involved in resistance	Gene function	Role in mechanism of drug action	Cellular process inhibited
Isoniazid	<i>katG</i>	Catalase-peroxidase	Activator	Resistance to oxidative stress
	<i>inhA</i>	Enoyl acyl carrier protein (ACP) reductase	Target	Cell wall synthesis (mycolic acid)
Rifampicin	<i>rpoB</i>	RNA polymerase beta-subunit	Target	RNA synthesis
Pyrazinamide	<i>pncA</i>	Nicotinamidase/pyrazinamidase	Activator	Membrane energetics
	<i>rpsA</i>	Ribosomal protein S1	Likely Target	Trans-translation
	<i>panD</i>	Aspartate decarboxylase	Likely Target	Pantothenate and co-enzyme A synthesis
Ethambutol	<i>embB</i>	Arabinosyl transferase	Target	Cell wall synthesis (arabinogalactan)
Fluoroquinolones	<i>gyrA</i>	DNA gyrase subunit A	Target	DNA synthesis
	<i>gyrB</i>	DNA gyrase subunit B	Target	
Amikacin	<i>rrs</i>	16S rRNA of 30S ribosomal subunit	Target	Protein synthesis
Kanamycin	<i>rrs</i>	16S rRNA of 30S ribosomal subunit	Target	Protein synthesis
Capreomycin	<i>rrs</i>	16S rRNA of 30S ribosomal subunit	Target	Protein synthesis
	<i>thyA</i>	2'-O-methyltransferase	Target	
Streptomycin	<i>rpsL</i>	S12 ribosomal protein	Target	Protein synthesis
	<i>rrs</i>	16S rRNA	Target	
Ethionamide	<i>ethA</i>	Flavin monooxygenase	Activator	Cell wall synthesis (mycolic acid)
	<i>inhA</i>	Enoyl acyl carrier protein (ACP) reductase	Target	
Cycloserine	<i>alr</i>	Alanine racemase	Target	Cell wall synthesis (peptidoglycan)
	<i>ddl</i>	D-alanine:D-alanine ligase	Target	
PAS	<i>thyA</i>	Thymidylate synthase	Activator?	Folate metabolism

(ii) Persistence

The idea that distinct sub-populations of tubercle bacilli, existing in different metabolic states during TB infection in the host, was put forward by Mitchison (81). The heterogeneous nature of these populations may be a stochastic process, or can arise as a response to drugs, the immune response and/or hostile local microenvironments of low oxygen, nutrient deprivation and acidity (82). Bacilli which are either rapidly multiplying, sporadically multiplying, or are in acidic phagolysosomal compartments are killed by conventional anti-TB drugs (83), which inhibit cellular processes involved during active replication (Table 1).

A sub-population, however, displays drug tolerance and are termed as persisters for their phenotypic resistance to chemotherapy without signs of inheritable genetic mutations (84). Persistence stems from an altered metabolic state in which bacilli are non-replicating or dormant, and as such these bacilli are difficult to eradicate completely as many targets of conventional anti-TB agents are rendered irrelevant in their case (85). As a result, TB therapy requires a longer continuation phase in addition to an initial intensive phase. Persisters therefore contribute to lengthy treatment durations and increasing the probability of resistance.

In summary, there remains much room for improving current TB treatments. Apart from drug-resistance and long treatment durations, drug-drug interactions of RIF with components of HIV therapy pose problems in HIV-TB cases (86). Moreover, DR-TB regimens are extremely costly and highly toxic with limited efficacy, and the use of injectables is cumbersome for drug administration. Therefore, new regimens comprising new drugs should seek to address these issues.

1.5.2 Strategies for improved TB therapy through new anti-TB drugs

Treatment durations can be shortened by using combinations of more potent and sterilising drugs against drug-susceptible and drug-resistant TB strains, which are effective against bacilli in different metabolic and replicating states. This requires drugs with new mechanisms of action. For regimens which are well-tolerated and simple to administer, new drugs need to have good safety profiles with reduced toxicities, as well as high oral bioavailability with preferably not more than once a day dosing. Drugs which are easy to synthesise and have few or no drug-drug interactions would result in more affordable and compatible treatments, such as with anti-retroviral therapy for HIV for instance.

Table 2: Goals for new TB regimens and corresponding characteristics of new anti-TB drugs

Desirable attributes of new TB regimens	Characteristics of new anti-TB drugs
Shorter treatment duration	More potent and sterilising drugs, New mechanisms of action
Well-tolerated	Good safety profile, reduced toxicity
Simple administration	High oral bioavailability, once a day dosing
Affordable	Easy synthesis
Compatible within and without	Few or no drug-drug interactions

In particular, new anti-TB drugs can seek to target either *M. tuberculosis* as (i) antimicrobials, or (ii) be directed at the host as immunotherapy.

(i) Antimicrobials

For new antimicrobials effective against *M. tuberculosis*, existing drugs for TB can be further optimised, existing antimicrobials can repurposed for TB, or new chemical entities (NCEs) can be explored for their activity against the pathogen and safety in humans through drug discovery and development (87). This will be discussed in further detail in the next sections.

(ii) Host-directed therapy

In the case of host-directed therapy, repurposed drugs and NCEs are assessed for their abilities to modulate host immune responses to eradicate *M. tuberculosis* more rapidly and/or to prevent lung tissue damage as a consequence of inflammatory processes induced by the immune system reacting to the pathogen (88). Although an important point of consideration in the development of such inhibitors is the potential toxicity due to off-target effects (89), host-directed therapy offers an avenue as adjunct therapy for TB, and in particular for DR-TB.

1.5.3 TB drug discovery and development

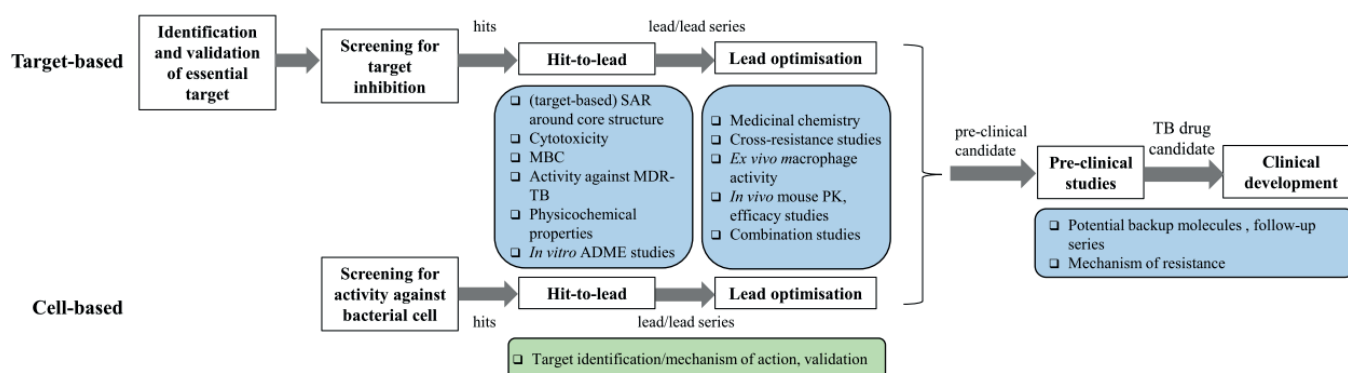


Figure 4: Flow of TB drug discovery and development. Some key activities performed at each stage are listed in coloured boxes, with blue being common to both target-based and cell-based approaches and green for the cell-based approach. Adapted from (90).

(i) TB drug discovery: hit-identification, hit-to-lead generation, lead optimisation

Two main strategies can be undertaken for TB drug discovery, namely target-based or phenotypic, whole-cell based approaches (Fig. 4). For both these approaches, the main stages involve hit identification, hit-to-lead generation, and lead optimisation.

Hit identification

Identification and validation of the target is the first step towards hit identification in the target-based approach. The complete sequencing of *M. tuberculosis* has enabled the identification of essential genes for infection *in vivo* (91, 92). Further validation studies on the essentiality of these genes *in vivo* and databases such as TuberQ can aid in deciding on a relevant, vulnerable, and druggable target for the drug discovery program (93). Subsequently, screening of compounds is conducted against the target to identify hits. Compounds screened include synthetic, small, drug-like molecules and semi-synthetic, larger molecules derived from natural scaffolds (94). The screening phase can be performed in a high-throughput manner based on compound libraries, either biochemically against the purified enzyme or *in silico* using its 3D structure (95, 96). Molecules which have a validated activity against the target below a threshold are advanced as hits to the next phase.

For the cell-based approach, hit identification begins with the screening of compounds against the whole bacterial cell and assessing activity of the molecules through growth inhibition or killing of the bacteria (97). Screening conditions, such as growth medium composition (98), models of bacilli mimicking various metabolic states, such as non-replicating *M. tuberculosis* as induced by microaerophilic and anaerobic conditions in the Wayne model (99), or by withdrawal of streptomycin in the streptomycin-starved 18b strain (SS18b) (100, 101), and intracellular screens (102), are important determinants influencing the susceptibility of *M. tuberculosis* towards the compounds screened.

A third approach of identifying hits involves target-based, whole-cell screens which combines both of the strategies mentioned above (103). The basis of these screens is the increased

susceptibility of a bacterial strain under-expressing the target to the target-specific inhibitor. Such screens are meant to overcome difficulties often encountered in the subsequent phases of drug discovery such as translation of *in vitro* activity of hits into whole-cell activity for the target-based approach, and target identification for the cell-based approach (94).

Hit-to-lead generation

Identified hits are advanced to the next stage of hit-to-lead generation. At this stage, hits with promising drug-like features are narrowed down and are refined by medicinal chemistry to improve their potency and selectivity to generate a lead or lead series (104), whereby a lead can be defined as ‘a chemical structure or a series of structures which demonstrate activity and selectivity in a pharmacological or biochemically relevant screen’ (105). Notably, hits identified from target-based screens need to demonstrate activity against whole bacterial cells.

Activities at this stage include more intensive structure-activity-relationship (SAR) studies around the core hit structure which can be rationally guided by the 3D structure of the target and inhibitor-target complex if available, assessing cytotoxicity, determining the minimal bactericidal concentration (MBC) and activity against MDR-TB strains, and profiling of physicochemical and *in vitro* adsorption, distribution, metabolism, and excretion (ADME) properties (Fig. 4) (90, 104). This information guides generating a lead that has an acceptable, balanced trade-off between potency, selectivity, and physicochemical and ADME properties which have the potential for improvement in the next stage.

In parallel to these activities, studies to identify the target and/or the mechanism of action are undertaken for hits identified through whole-cell screens. With its increasing accessibility and decreasing costs, genomics is a commonly-used technique nowadays, with whole genome

sequencing (WGS) of spontaneous resistant mutants to identify targets and/or transcriptomics to aid in deciphering the mechanism of action (106). Validation of the target encompasses confirming the essentiality of the target *in vivo*, and also genetic and biochemical verification of the specific interaction of the inhibitor with the target. Although the inability to identify the target or the mechanism of action may not necessarily hinder the progress of a compound through the discovery pipeline, it is nevertheless an important step towards understanding its efficacy and safety, both critical parameters for drug development afterwards.

Lead optimisation

The aim of this stage is of lead refinement, in that favourable properties of the lead are maintained while deficiencies of the lead structure are improved upon (104). Lead analogues, which are generated guided by medicinal chemistry, are subjected to further evaluation such as cross-resistance studies with other drugs or leads to verify the target and *ex vivo* activity in *M. tuberculosis*-infected macrophages (if this was not determined in the initial screen). *In vivo* pharmacokinetics (PK) and efficacy studies in mouse TB models give preliminary insight into the metabolism and oral bioavailability of the compound *in vivo*. At this stage, combination studies may be performed to evaluate potential drug interactions of the lead with other TB drugs or candidates.

A decision is made on the lead analogue to be advanced based on the extensive profiling and evaluation studies performed. During the pre-clinical and clinical development stages of the candidate compound where the risk of failure remains high, drug discovery work continues to generate potential backup molecules and follow-up series (104). Further characterisation studies of the candidate compound such as potential mechanisms of resistance provide more comprehensive insight for its clinical use.

(ii) TB drug development: pre-clinical and clinical trials

Pre-clinical studies are designed to assess the efficacy and safety of the pre-clinical candidate using animal models. As they provide a convenient, robust and reproducible model of TB, mice are most commonly used, although studies are also conducted in rats, guinea pigs, rabbits and non-human primates (107). Efficacy is determined alone and in combination with other drugs for assessing potential drug interactions within a regimen (107). To determine a safe window of dosage for human clinical trials, toxicology studies are performed in compliance with good laboratory practice (GLP) (107). In addition, standardising compound formulation and production under good manufacturing practices (GMP) is also required for further clinical development (107).

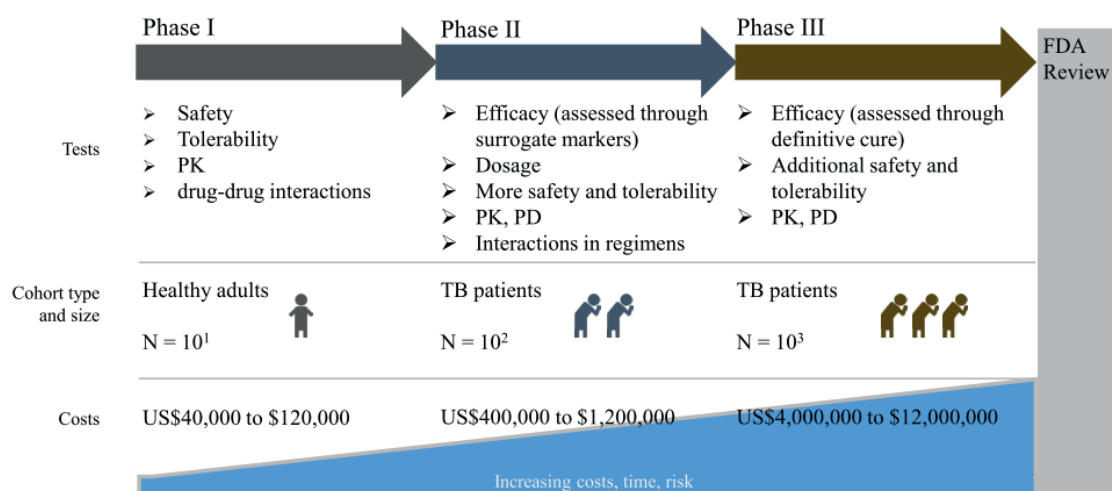


Figure 5: Stages of clinical trials. The tests conducted, cohort type and size, and costs are indicated for Phase I, II, and III of clinical trials for TB. Costs vary depending on several factors, including the study site, and are estimated based on numbers from (108). Adapted from (109).

Clinical trials are designed to assess the efficacy and safety of the drug candidate in humans. Phase I trials are conducted in a small number of healthy adults to identify a safe dose range

and additional pharmacokinetic data can be obtained from participants (107, 110) (Fig. 5). Phase II trials are conducted on a larger group of about 100 to 200 TB patients and are meant to determine the efficacy of the compound alone and then in combination with other approved TB drugs, to establish an optimal dosage, and to gather more pharmacokinetics and safety data (107, 110) (Fig. 5). An early bactericidal activity (EBA) study is carried out at the beginning of the trial whereby participants are treated with the candidate drug alone over 2 to 14 days to obtain preliminary efficacy results, after which the candidate drug is administered as part of a regimen (111, 112). The current gold-standard for the end-point of the Phase II trials is sputum culture conversion after 2 months (110). Phase III trials are much larger, recruiting in the range of 1000 TB patients (107) (Fig. 5). The aim is to assess the efficacy of the new regimen with the candidate drug and its sterilising ability. As such, patients are followed up for TB relapse for up to 2 years, which is the endpoint for Phase III trials (107).

The entire process from discovering to developing a TB drug is lengthy, costly, complex, and highly risky, calling for much collaborative effort and the involvement of pharmaceutical companies, academic institutions, governmental and non-governmental organisation. The creation of large consortia such as the TB Drug Accelerator (113), the Lilly TB Drug Discovery (114), and the previously EU-funded More Medicines for Tuberculosis (MM4TB) consortia (115) dedicated to developing new TB drugs has led to more candidates present in the Global TB drug pipeline.

1.5.4 Global TB drug pipeline

The current global TB drug and regimen pipeline consists of candidates which are existing TB drugs undergoing optimisation, repurposed drugs or NCEs (Fig. 6).

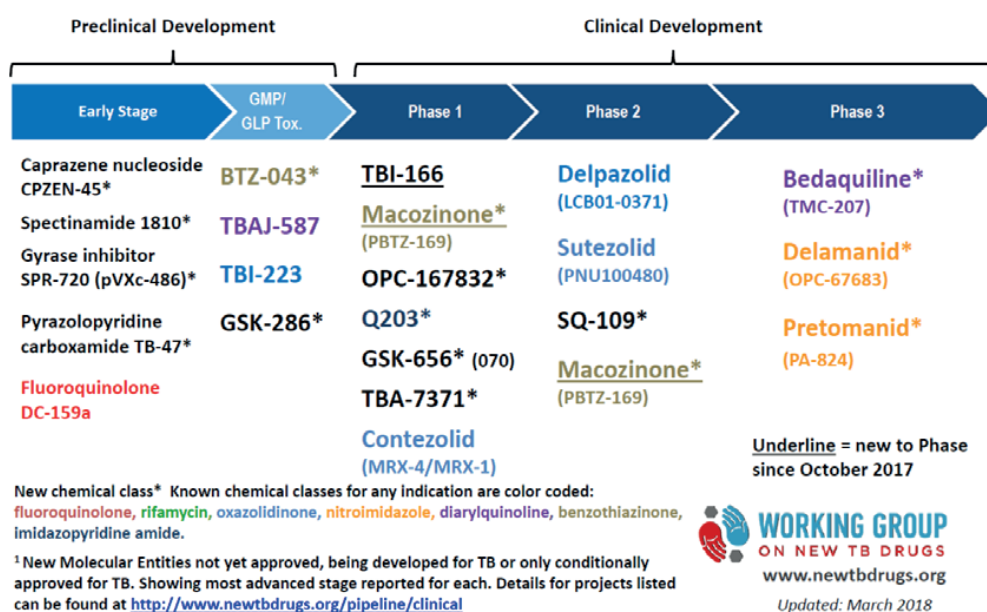


Figure 6: The Global TB Drug Development Pipeline (2018). Repurposed compounds or NCEs currently undergoing pre-clinical and development for TB, as published by the Working Group on New TB drugs in March 2018 (87).

(i) Optimising existing TB drugs/Repurposed drugs

Optimising existing TB drugs and repurposing drugs used in other therapeutic areas are strategies to hasten the availability of new TB drugs. Since these drugs have already been approved by the U.S. Food and Drug Administration, they have validated safety profiles and resources can be diverted to evaluating efficacy against TB. They are also starting scaffolds for improving anti-mycobacterial potency and liabilities of the parent drug.

RIF belongs to the rifamycin class of natural products and is a main sterilising component of front-line TB treatment by binding to bacterial RNA polymerase and inhibiting RNA synthesis (116). Current clinical trials aim to determine if DS-TB treatment durations can be shortened with higher doses of RIF and with substitution of RIF by rifapentine, a derivative with a longer half-life (117, 118).

Fluoroquinolones are broad-spectrum antibiotics repurposed as anti-TB drugs, whereby they inhibit bacterial DNA gyrase, preventing DNA synthesis. Since the 1980s when ciprofloxacin was demonstrated to be useful against DR-TB (119), fluoroquinolones have formed a key component of DR-TB treatment. Today, newer generations of fluoroquinolones such as moxifloxacin, levofloxacin, and gatifloxacin with improved activity against TB are preferred over older generations for MDR-TB treatment (70). Ongoing clinical trials involve assessing moxifloxacin as part of new regimens for DS- and DR-TB treatment (117).

Clofazimine, a member of the riminophenazines, is an anti-leprosy drug being repurposed for treating TB. While its exact mechanism of action is not fully understood, it is considered a prodrug which first requires reduction by type 2 NADH-quinone oxidoreductase (NDH-2) of the mycobacterial electron transport chain (ETC) before releasing ROS upon spontaneous re-oxidation by oxygen (120). Clofazimine is recommended by the WHO as a second-line agent for MDR-TB (70). New riminophenazines, such as TBI-166, are intended to overcome issues of compound solubility and skin discoloration caused by clofazimine (121).

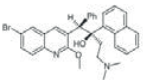
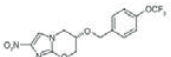
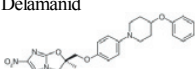
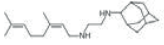
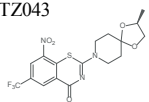
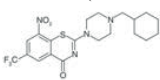
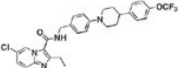
Linezolid is an oxazolidinone used in the treatment of Gram-positive infections (122) which has been repurposed for TB. It is active against *M. tuberculosis* by targeting the 23S RNA of the 50S ribosomal subunit, inhibiting protein synthesis (123). Linezolid is a recommended second-line agent for MDR-TB treatment, and is evaluated as part of new regimens for DS- and DR-TB although it has been reported to induce significant toxicities (87, 124). Newer oxazolidinones with improved safety profiles such as sutezolid are being currently developed (87).

Carbapenems belong to the beta-lactam class of broad-spectrum antibiotics inhibiting cell wall peptidoglycan synthesis. Due to beta-lactamase BlaC in *M. tuberculosis* limiting the efficacy of beta-lactams (125), meropenem and faropenem are being assessed in combination with clavulanate, a beta-lactamase inhibitor, as potential treatment options in clinical trials (126, 87).

(ii) New chemical entities (NCEs)

NCEs contain active moieties which have not been previously approved by the FDA, and thus have the potential to kill *M. tuberculosis* through new mechanisms of action. All the NCEs currently undergoing development in the Global TB drug pipeline have been identified through cell-based approaches in the discovery stage (Table 3).

Table 3: NCEs in the Global TB drug pipeline. Adapted from (106, 87).

New Chemical Entities (NCEs)						
Class	Compound	Hit identification approach	Target	Mechanism of Action	Clinical Development	Comments
Diarylquinolones	Bedaquiline 	Whole-cell screen of quinolone derivatives	ATP synthase	Inhibition of energy production	Phase 3	MDR-TB FDA approval, add-on agent for MDR-TB
Nitroimidazoles	Pretomanid 	Whole-cell screen of metronidazole derivatives	Unknown	Inhibition of cell wall synthesis (mycolic acid), respiratory poisoning	Phase 3	
	Delamanid 	Whole-cell screen of inhibitors of mycolic acid synthesis	Unknown	Inhibition of cell wall synthesis (mycolic acid), likely respiratory poisoning	Phase 3	add-on agent for MDR-TB
Diethylamines	SQ109 	Whole-cell screen of ethambutol derivatives	MmpL3	Inhibition of cell wall synthesis (mycolic acid)	Phase 2	
Benzothiazinones	BTZ043 	Whole-cell screen	DprE1	Inhibition of cell wall synthesis (arabinogalactan)	Pre-clinical	
	Macozinone (PBTZ169) 	Piperazine-derivative of BTZ	DprE1	Inhibition of cell wall synthesis (arabinogalactan)	Phase 1, 2	
Imidazopyridines	Q203 	Whole-cell screen in <i>M. tuberculosis</i> -infected macrophages	QcrB	Perturbation of respiration	Phase 1	

Bedaquiline (BDQ, Sirturo) belongs to a new chemical class of the diarylquinolones (Table 3). It is considered a milestone in the context of contemporary TB drug development as it gained FDA approval in 2012 and became the first new anti-TB drug to be approved in more than 40 years (127). The target of BDQ was identified by WGS of spontaneous resistant mutants isolated in *M. tuberculosis*, which revealed missense mutations in *atpE* encoding for the *c* subunit of ATP synthase (128, 129). BDQ acts by inhibiting ATP synthesis, an essential process for both replicating and non-replicating states of *M. tuberculosis* (130), and thus is bactericidal against these populations albeit with a delayed onset of killing (131). Not all clinical isolates resistant to BDQ have mutations in *atpE*, implying that there is another target or that there are other mechanisms of resistance (132). This has been demonstrated as upregulation of MmpL5, a multi-substrate efflux pump of the MmpL proteins, causes resistance to both BDQ and clofazimine (133, 134). Recommended as an add-on agent for MDR-TB treatment, BDQ has a long oral bioavailability, however it has been associated with the potential induction of arrhythmia and an increased risk of death (127).

Delamanid and PA-824 (also known as Pretomanid) (Table 3) are two new nitroimidazoles identified independently in whole-cell screens (135, 136). Both compounds are active against MDR-TB and against replicating and non-replicating *M. tuberculosis*. They have similar mechanisms of action, in that their aerobic activity is attributed to the inhibition of mycolic acid synthesis (135, 137). The anaerobic activity of PA-824 relies on its nitro-reduction by F420-deazaflavin-dependent nitroreductase (Ddn) of *M. tuberculosis* (138), which results in the release of nitric oxide (NO) causing subsequent respiratory poisoning of the pathogen (139). Mutations in enzymes of the F420 cofactor biosynthesis pathway, or in F420-dependent glucose-6-phosphate dehydrogenase (Fgd1) which generates reduced F420 required for Ddn

activity, or in Ddn itself are associated with resistance to these compounds (140, 141). Both are in advanced clinical trials, with Delamanid having been approved for MDR-TB treatment by the European Commission (142).

SQ109 is an ethylenediamine-based analogue (Table 3) originating from a whole-cell screen which aimed at generating more potent diamines than ethambutol (143). A target of SQ109 was identified as MmpL3 (144), an essential protein belonging to the resistance, nodulation and division (RND) family which transports trehalose monomycolate to the cell envelope for mycolic acid synthesis (145). Apart from inhibiting cell wall synthesis, it has been demonstrated that SQ109 also interferes with menaquinone synthesis and dissipates the proton motive force (PMF) across the mycobacterial membrane, resulting in perturbation of respiration (146). This multi-modal mechanism of action would imply lower resistance frequencies to SQ109, which is currently being developed in Phase II clinical trials (87).

Benzothiazinones (BTZs) (Table 3) are a new class of extremely potent inhibitors against *M. tuberculosis*, with the original lead BTZ043 identified in a whole-cell screen (147), and improved upon with a more potent, safer piperazine-containing benzothiazinone PBTZ169 (148). These BTZs have low nanomolar activity against mycobacteria *in vitro* and *ex vivo* and are active against DS- and DR-TB clinical isolates (147–149). Through genetic, biochemical, transcriptomic and proteomic analyses, the target was identified and validated as decaprenylphosphoryl-beta-D-ribose 2' epimerase (DprE1) (147). DprE1 is an essential flavoenzyme of *M. tuberculosis*, and acts in concert with DprE2 to convert decaprenylphosphoryl-D-ribose to decaprenyl-phosphoryl-D-arabinose, the sole precursor for the biosynthesis of the arabinogalactan and lipoarabinomannan components of the mycobacterial cell wall (150). BTZs are prodrugs requiring activation by reduced FAD of DprE1 (151). The

nitro group undergoes nitroreduction to form a nitroso species, which covalently binds to cysteine 387 in the active site of DprE1 (152–154). This irreversible interaction results in the inhibition of cell wall arabinan synthesis, causing lysis of the mycobacterial cell (147). Synergy has been demonstrated for PBTZ169 with BDQ, which is promising for a novel TB regimen (148, 155). PBTZ169 is undergoing Phase I and II clinical trials, while BTZ043 is in pre-clinical trials as a backup compound (87).

Q203, the most advanced candidate of the imidazopyridine amides class (Table 3), was identified in a whole-cell screen in *M. tuberculosis*-infected macrophages (156). It has an MIC in the nanomolar range, and is active against MDR-TB clinical isolates (156). Resistance to Q203 is mediated by mutations in QcrB (156), the *b* subunit of cytochrome *bc_L* complex, one of two terminal oxidases in mycobacteria (157). Inhibition of QcrB by Q203 results in rapid depletion of intracellular ATP levels (156) and enhanced killing of *M. tuberculosis* in mice with the genetic deletion of the alternate terminal oxidase cytochrome *bd* (158). This emphasises the extreme vulnerability of the bacillus when both terminal respiratory oxidases are simultaneously targeted. With its good oral bioavailability in mice and long half-life, Q203 is undergoing Phase I clinical trials (87).

Although promising compounds with new mechanisms of action are currently present in the Global TB drug pipeline, there remains nevertheless a need to enhance the pipeline due to the high attrition rates in pre-clinical development and clinical trials that is the very nature of drug discovery and development.

1.6 Thesis rationale and outline

The broader aim of this thesis is to address the ongoing global health issue by contributing to the search for new, efficacious, and safe TB antimicrobials. In particular, the scope of this thesis is to enhance the Global TB drug pipeline through the discovery work on several new compounds, including BTZs.

Chapter 2 focuses on hit/lead optimisation activities of new piperazine-based AX compounds, of which the lead molecule, AX-35, was previously identified in a large phenotypic screening campaign conducted by GlaxoSmithKline (GSK) in 2013. Due to its micromolar potency against *M. tuberculosis* and structural simplicity, AX-35 was deemed as an attractive starting point for lead analogue generation. In this chapter, the characterisation of AX-35 and its four most potent analogues are described, as well as target identification and validation studies undertaken to elucidate their mechanism of action.

The ongoing discovery work of new derivatives of lapachol, the PB compounds, is detailed in Chapter 3. Lapachol is a natural product originating from trees of the Bignoniaceae family, and its availability and simple structure provides an attractive starting scaffold for analogue generation. PB compounds demonstrate potent activity against *M. tuberculosis in vitro* in the micromolar range, thus forming the basis of further characterisation work of these series, including some insight into their mechanism of action.

Continued discovery work on the BTZs, BTZ043 and PBTZ169 (Macozinone, MCZ), is intended to support their development as they undergo pre-clinical and phase I/II clinical trials respectively. One aspect is in the understanding of the mechanism of resistance, which can enable the identification of a diagnostic marker for drug-susceptibility and can be screened for

over the course of clinical trials to monitor acquired resistance. Through a comprehensive biological and biochemical characterisation of BTZ-resistant mutants, Chapter 4 sheds more light on the underlying mechanisms of BTZ resistance and the impact of these mutations at cysteine 387 of DprE1 on *M. tuberculosis* fitness, DprE1 enzymatic activity, and the binding of covalent and non-covalent DprE1 inhibitors.

To address potential resistance issues with MCZ and as part of the MCZ back-up program, sulfone-containing derivatives were envisioned by structure-based drug design then generated, with the aim of increasing compound activity against wild-type and BTZ-resistant *M. tuberculosis* and improving physicochemical properties of MCZ. Chapters A1 and A2 of the annex describes the rationale of generating the sulfone-containing MCZ series and the comprehensive characterisation of these derivatives.

Since TB treatment requires combination therapy and as new TB regimens are needed to improve upon existing ones, Chapter A3 of the annex seeks to explore the potential of MCZ as a part of novel TB regimens by a thorough evaluation of its interactions with other conventional and new TB drugs through *in vitro* and *in vivo* combination studies.

Lastly, Chapter 5 concludes the thesis with a summary of the main contributions, as well as some perspectives on the future directions of the work presented here.

References

1. 2017. The top 10 causes of death. WHO.
2. World Health Organization. 2017. Global Tuberculosis Report 2017. S.l.
3. Koehler CSW. 2002. Consumption, the great killer. *Mod Drug Discov* 5.
4. Bunyan J. 1680. The Life And Death Of Mr Badman (The Twin Book To The Pilgrim's Progress).
5. Donoghue HD. 2016. Paleomicrobiology of Human Tuberculosis, p. 113–130. *In* Drancourt, M, Raoult, D (eds.), *Paleomicrobiology of Humans*. American Society of Microbiology.
6. Donoghue HD, Lee OY-C, Minnikin DE, Besra GS, Taylor JH, Spigelman M. 2010. Tuberculosis in Dr Granville's mummy: a molecular re-examination of the earliest known Egyptian mummy to be scientifically examined and given a medical diagnosis. *Proc R Soc B Biol Sci* 277:51–56.
7. Salo WL, Aufderheide AC, Buikstra J, Holcomb TA. 1994. Identification of *Mycobacterium tuberculosis* DNA in a pre-Columbian Peruvian mummy. *Proc Natl Acad Sci* 91:2091–2094.
8. HersHKovitz I, Donoghue HD, Minnikin DE, May H, Lee OY-C, Feldman M, Galili E, Spigelman M, Rothschild BM, Bar-Gal GK. 2015. Tuberculosis origin: The Neolithic scenario. *Tuberculosis* 95:S122–S126.
9. Daniel TM. 1999. *Captain of Death: The Story of Tuberculosis*.

10. Daniel TM. 2011. Hermann Brehmer and the origins of tuberculosis sanatoria [Founders of our knowledge]. *Int J Tuberc Lung Dis* 15:161–162.
11. The Surgery for Pulmonary Tuberculosis | American Review of Respiratory Disease.
12. Koch R. 2010. Die aetiologie der tuberkulose.
13. Koch R. 1890. A Further Communication on a Remedy for Tuberculosis. *Br Med J* 2:1193–1199.
14. Pirquet CV. 1909. Frequency of Tuberculosis in Childhood. *J Am Med Assoc* LII:675–678.
15. Long ER, Seibert FB, Aronson JD. 1934. A standardised tuberculin (purified protein derivative) for uniformity in diagnosis and epidemiology. *Tubercle* 16:304–322.
16. Seibert FB, Glenn JT. 1941. Tuberculin Purified Protein Derivative. Preparation and Analyses of a Large Quantity for Standard. *Am Rev Tuberc Pulm Dis* 44:9–25.
17. Bloom BR, Fine PEM. 1994. The BCG Experience: Implications for Future Vaccines against Tuberculosis. *Tuberculosis: Pathogenesis, Protection, and Control*. American Society of Microbiology, Washington, DC 200005.
18. SAGE Working Group on BCG Vaccines, WHO. 2017. Report on BCG vaccine use for protection against mycobacterial infections including tuberculosis, leprosy, and other nontuberculous mycobacteria (NTM) infections.
19. Ma Z, Lienhardt C, McIlleron H, Nunn AJ, Wang X. 2010. Global tuberculosis drug development pipeline: the need and the reality. *The Lancet* 375:2100–2109.
20. Thorburn AL. 1983. Paul Ehrlich: pioneer of chemotherapy and cure by arsenic (1854–1915). *Sex Transm Infect* 59:404–405.

21. Schatz A, Bugle E, Waksman SA. 1944. Streptomycin, a Substance Exhibiting Antibiotic Activity Against Gram-Positive and Gram-Negative Bacteria.*†. *Proc Soc Exp Biol Med* 55:66–69.
22. Feldman WH, Karlson AG, Hinshaw HC. 1947. Streptomycin in Experimental Tuberculosis. The Effects in Guinea Pigs following Infection by Intravenous Inoculation. *Am Rev Tuberc Pulm Dis* 56:346–59.
23. 1948. Streptomycin Treatment of Pulmonary Tuberculosis. *Br Med J* 2:769–782.
24. Hinshaw C, Feldman WH, Pfuetze KH. 1946. Treatment of Tuberculosis with Streptomycin: A Summary of Observations on One Hundred Cases. *J Am Med Assoc* 132:778–782.
25. Lehmann J. 1946. Para-aminosalicylic acid in the treatment of tuberculosis. *The Lancet* 247:15–16.
26. 1950. Treatment of Pulmonary Tuberculosis with Streptomycin and Para-Amino-Salicylic Acid. *Br Med J* 2:1073–1085.
27. Bernstein J, Lott WA, Steinberg BA, Yale HL. 1952. Chemotherapy of Experimental Tuberculosis. V. Isonicotinic Acid Hydrazide (Nydrazid) and Related Compounds. *Am Rev Tuberc Pulm Dis* 65:357–64.
28. Group BMJP. 1955. Various Combinations of Isoniazid with Streptomycin or with P.A.S. in the Treatment of Pulmonary Tuberculosis: Seventh Report to the Medical Research Council. *Br Med J* 1:435–445.
29. Iseman MD. 2002. Tuberculosis therapy: past, present and future. *Eur Respir J* 20:87S–94s.

30. Murray JF, Schraufnagel DE, Hopewell PC. 2015. Treatment of Tuberculosis. A Historical Perspective. *Ann Am Thorac Soc* 12:1749–1759.
31. Fox W, Ellard GA, Mitchison DA. 1999. Studies on the treatment of tuberculosis undertaken by the British Medical Research Council Tuberculosis Units, 1946 to 1986, with relevant subsequent publications. Text.
32. Giovanni D, Danzi MC, Checchi GD, Pizzighella S, Solbiati M, Cruciani M, Luzzati R, Malena M, Mazzi R, Concia E, Bassetti D. 1989. Nosocomial Epidemic of Active Tuberculosis Among HIV-infected Patients. *The Lancet* 334:1502–1504.
33. Daley CL, Small PM, Schechter GF, Schoolnik GK, McAdam RA, Jacobs WRJ, Hopewell PC. 2010. An Outbreak of Tuberculosis with Accelerated Progression among Persons Infected with the Human Immunodeficiency Virus. <http://dx.doi.org/10.1056/NEJM199201233260404>. research-article.
34. Frieden TR, Sterling T, Pablos-Mendez A, Kilburn JO, Cauthen GM, Dooley SW. 2010. The Emergence of Drug-Resistant Tuberculosis in New York City. <http://dx.doi.org/10.1056/NEJM199302253280801>. research-article.
35. Gagneux S. 2018. Ecology and evolution of *Mycobacterium tuberculosis*. *Nat Rev Microbiol* 16:202–213.
36. Springer B, Stockman L, Teschner K, Roberts GD, Böttger EC. 1996. Two-laboratory collaborative study on identification of mycobacteria: molecular versus phenotypic methods. *J Clin Microbiol* 34:296–303.
37. Rastogi N, Legrand E, Sola C. 2001. The mycobacteria: an introduction to nomenclature and pathogenesis. *Rev Sci Tech-Off Int Epizoot* 20:21–54.

38. Kaufmann SHE. 2001. How can immunology contribute to the control of tuberculosis? *Nat Rev Immunol* 1:20–30.
39. Nunes-Alves C, Booty MG, Carpenter SM, Jayaraman P, Rothchild AC, Behar SM. 2014. In search of a new paradigm for protective immunity to TB. *Nat Rev Microbiol* 12:289–299.
40. Russell DG, Barry CE, Flynn JL. 2010. Tuberculosis: What We Don't Know Can, and Does, Hurt Us. *Science* 328:852–856.
41. Nathan CF, Hibbs Jr JB. 1991. Role of nitric oxide synthesis in macrophage antimicrobial activity. *Curr Opin Immunol* 3:65–70.
42. Smith I. 2003. *Mycobacterium tuberculosis* Pathogenesis and Molecular Determinants of Virulence. *Clin Microbiol Rev* 16:463–496.
43. Frehel C, Chastellier C de, Lang T, Rastogi N. 1986. Evidence for inhibition of fusion of lysosomal and prelysosomal compartments with phagosomes in macrophages infected with pathogenic *Mycobacterium avium*. *Infect Immun* 52:252–262.
44. Crowle AJ, Dahl R, Ross E, May MH. 1991. Evidence that vesicles containing living, virulent *Mycobacterium tuberculosis* or *Mycobacterium avium* in cultured human macrophages are not acidic. *Infect Immun* 59:1823–1831.
45. Philips JA, Ernst JD. 2012. Tuberculosis Pathogenesis and Immunity. *Annu Rev Pathol Mech Dis* 7:353–384.
46. Crevel R van, Ottenhoff THM, Meer JWM van der. 2002. Innate Immunity to *Mycobacterium tuberculosis*. *Clin Microbiol Rev* 15:294–309.

47. Wolf AJ, Desvignes L, Linas B, Banaiee N, Tamura T, Takatsu K, Ernst JD. 2008. Initiation of the adaptive immune response to *Mycobacterium tuberculosis* depends on antigen production in the local lymph node, not the lungs. *J Exp Med* 205:105–115.
48. Orme IM, Roberts AD, Griffin JP, Abrams JS. 1993. Cytokine secretion by CD4 T lymphocytes acquired in response to *Mycobacterium tuberculosis* infection. *J Immunol* 151:518–525.
49. Flynn JL, Chan J, Triebold KJ, Dalton DK, Stewart TA, Bloom BR. 1993. An essential role for interferon gamma in resistance to *Mycobacterium tuberculosis* infection. *J Exp Med* 178:2249–2254.
50. Chan J, Xing Y, Magliozzo RS, Bloom BR. 1992. Killing of virulent *Mycobacterium tuberculosis* by reactive nitrogen intermediates produced by activated murine macrophages. *J Exp Med* 175:1111–1122.
51. Russell DG. 2007. Who puts the tubercle in tuberculosis? *Nat Rev Microbiol* 5:39–47.
52. Timm J, Post FA, Bekker L-G, Walther GB, Wainwright HC, Manganelli R, Chan W-T, Tsenova L, Gold B, Smith I, Kaplan G, McKinney JD. 2003. Differential expression of iron-, carbon-, and oxygen-responsive mycobacterial genes in the lungs of chronically infected mice and tuberculosis patients. *Proc Natl Acad Sci* 100:14321–14326.
53. Cole ST, Brosch R, Parkhill J, Garnier T, Churcher C, Harris D, Gordon SV, Eiglmeier K, Gas S, Iii CEB, Tekaia F, Badcock K, Basham D, Brown D, Chillingworth T, Connor R, Davies R, Devlin K, Feltwell T, Gentles S, Hamlin N, Holroyd S, Hornsby T, Jagels K, Krogh A, McLean J, Moule S, Murphy L, Oliver K, Osborne J, Quail MA, Rajandream M-A, Rogers J, Rutter S, Seeger K, Skelton J, Squares R, Squares S, Sulston JE, Taylor K,

- Whitehead S, Barrell BG. 1998. Deciphering the biology of *Mycobacterium tuberculosis* from the complete genome sequence. *Nature* 393:537–544.
54. Brown L, Wolf JM, Prados-Rosales R, Casadevall A. 2015. Through the wall: extracellular vesicles in Gram-positive bacteria, mycobacteria and fungi. *Nat Rev Microbiol* 13:620–630.
55. Brennan PJ, Nikaido H. 1995. The Envelope of Mycobacteria. *Annu Rev Biochem* 64:29–63.
56. McNeil M, Wallner SJ, Hunter SW, Brennan PJ. 1987. Demonstration that the galactosyl and arabinosyl residues in the cell-wall arabinogalactan of *Mycobacterium leprae* and *Mycobacterium tuberculosis* are furanoid. *Carbohydr Res* 166:299–308.
57. Cole ST. 2012. Infectious diseases: Transporter targeted in tuberculosis. *Nat Chem Biol* 8:326–327.
58. Jankute M, Cox JAG, Harrison J, Besra GS. 2015. Assembly of the Mycobacterial Cell Wall. *Annu Rev Microbiol* 69:405–423.
59. Briken V, Porcelli SA, Besra GS, Kremer L. 2004. Mycobacterial lipoarabinomannan and related lipoglycans: from biogenesis to modulation of the immune response. *Mol Microbiol* 53:391–403.
60. Camacho LR, Ensergueix D, Perez E, Gicquel B, Guilhot C. Identification of a virulence gene cluster of *Mycobacterium tuberculosis* by signature-tagged transposon mutagenesis. *Mol Microbiol* 34:257–267.
61. Cox JS, Chen B, McNeil M, Jr WRJ. 1999. Complex lipid determines tissue-specific replication of *Mycobacterium tuberculosis* in mice. *Nature* 402:79–83.

62. Pym AS, Brodin P, Brosch R, Huerre M, Cole ST. 2002. Loss of RD1 contributed to the attenuation of the live tuberculosis vaccines *Mycobacterium bovis* BCG and *Mycobacterium microti*. *Mol Microbiol* 46:709–717.
63. Colditz GA, Brewer TF, Berkey CS, Wilson ME, Burdick E, Fineberg HV, Mosteller F. 1994. Efficacy of BCG Vaccine in the Prevention of Tuberculosis: Meta-analysis of the Published Literature. *JAMA* 271:698–702.
64. Andersen P, Woodworth JS. 2014. Tuberculosis vaccines – rethinking the current paradigm. *Trends Immunol* 35:387–395.
65. Kaufmann SH, Hussey G, Lambert P-H. 2010. New vaccines for tuberculosis. *The Lancet* 375:2110–2119.
66. Tameris MD, Hatherill M, Landry BS, Scriba TJ, Snowden MA, Lockhart S, Shea JE, McClain JB, Hussey GD, Hanekom WA, Mahomed H, McShane H. 2013. Safety and efficacy of MVA85A, a new tuberculosis vaccine, in infants previously vaccinated with BCG: a randomised, placebo-controlled phase 2b trial. *The Lancet* 381:1021–1028.
67. Centers for Disease Control and Prevention. Diagnosis of Tuberculosis Disease. *Diagnosis of Tuberculosis Disease*.
68. Centers for Disease Control and Prevention. Testing for Tuberculosis Infection and Disease. *Testing for Tuberculosis Infection and Disease*.
69. Dorman SE. 2010. New Diagnostic Tests for Tuberculosis: Bench, Bedside, and Beyond. *Clin Infect Dis* 50:S173–S177.
70. World Health Organization, Global Tuberculosis Programme. 2016. WHO treatment guidelines for drug-resistant tuberculosis: 2016 update.

71. 2015. Companion Handbook to the 2011 Who Guidelines for the Programmatic Management of Multidrug-resistant Tuberculosis. World Health Organization.
72. Kochi A, Vareldzis B, Styblo K. 1993. Multidrug-resistant tuberculosis and its control. *Res Microbiol* 144:104–110.
73. McGrath M, Pittius G van, C N, Helden V, D P, Warren RM, Warner DF. 2014. Mutation rate and the emergence of drug resistance in *Mycobacterium tuberculosis*. *J Antimicrob Chemother* 69:292–302.
74. Gillespie SH. 2002. Evolution of Drug Resistance in *Mycobacterium tuberculosis*: Clinical and Molecular Perspective. *Antimicrob Agents Chemother* 46:267–274.
75. Zhang Y, Yew WW. 2009. Mechanisms of drug resistance in *Mycobacterium tuberculosis* [State of the art series. Drug-resistant tuberculosis. Edited by CY. Chiang. Number 1 in the series]. *Int J Tuberc Lung Dis* 13:1320–1330.
76. Spratt BG. 1996. Antibiotic resistance: Counting the cost. *Curr Biol* 6:1219–1221.
77. Sander P, Springer B, Prammananan T, Sturmfels A, Kappler M, Pletschette M, Böttger EC. 2002. Fitness Cost of Chromosomal Drug Resistance-Confering Mutations. *Antimicrob Agents Chemother* 46:1204–1211.
78. Davies A., Billington O., Bannister B., Weir WR., McHugh T., Gillespie S. 2000. Comparison of Fitness of Two Isolates of *Mycobacterium tuberculosis*, one of Which had Developed Multi-drug Resistance During the Course of Treatment. *J Infect* 41:184–187.
79. Gagneux S, Long CD, Small PM, Van T, Schoolnik GK, Bohannon BJM. 2006. The Competitive Cost of Antibiotic Resistance in *Mycobacterium tuberculosis*. *Science* 312:1944–1946.

80. Sherman DR, Mdluli K, Hickey MJ, Arain TM, Morris SL, Barry CE, Stover CK. 1996. Compensatory *ahpC* Gene Expression in Isoniazid-Resistant *Mycobacterium tuberculosis*. *Science* 272:1641–1643.
81. Mitchison DA. 1979. Basic Mechanisms of Chemotherapy. *Chest* 76:771–780.
82. Sacchettini JC, Rubin EJ, Freundlich JS. 2008. Drugs versus bugs: in pursuit of the persistent predator *Mycobacterium tuberculosis*. *Nat Rev Microbiol* 6:41–52.
83. McKinney JD. 2000. *In vivo veritas*: The search for TB drug targets goes live. *Nat Med* 6:1330–1333.
84. Dhar N, McKinney JD. 2007. Microbial phenotypic heterogeneity and antibiotic tolerance. *Curr Opin Microbiol* 10:30–38.
85. Gomez JE, McKinney JD. 2004. *M. tuberculosis* persistence, latency, and drug tolerance. *Tuberculosis* 84:29–44.
86. McIlleron H, Meintjes G, Burman WJ, Maartens G. 2007. Complications of Antiretroviral Therapy in Patients with Tuberculosis: Drug Interactions, Toxicity, and Immune Reconstitution Inflammatory Syndrome. *J Infect Dis* 196:S63–S75.
87. Working Group for New TB Drugs |.
88. Wallis RS, Maeurer M, Mwaba P, Chakaya J, Rustonjee R, Migliori GB, Marais B, Schito M, Churchyard G, Swaminathan S, Hoelscher M, Zumla A. 2016. Tuberculosis—advances in development of new drugs, treatment regimens, host-directed therapies, and biomarkers. *Lancet Infect Dis* 16:e34–e46.

89. Lechartier B, Rybniker J, Zumla A, Cole ST. 2014. Tuberculosis drug discovery in the post-post-genomic era. *EMBO Mol Med* 6:158–168.
90. Manjunatha UH, Smith PW. 2015. Perspective: Challenges and opportunities in TB drug discovery from phenotypic screening. *Bioorg Med Chem* 23:5087–5097.
91. McKinney JD, Bentrup KH zu, Muñoz-Elías EJ, Miczak A, Chen B, Chan W-T, Swenson D, Sacchettini JC, Jr WRJ, Russell DG. 2000. Persistence of *Mycobacterium tuberculosis* in macrophages and mice requires the glyoxylate shunt enzyme isocitrate lyase. *Nature* 406:735–738.
92. Sasseti CM, Rubin EJ. 2003. Genetic requirements for mycobacterial survival during infection. *Proc Natl Acad Sci U S A* 100:12989–12994.
93. Radusky L, Defelipe LA, Lanzarotti E, Luque J, Barril X, Marti MA, Turjanski AG. 2014. TuberQ: a *Mycobacterium tuberculosis* protein druggability database. Database 2014.
94. Zuniga ES, Early J, Parish T. 2015. The future for early-stage tuberculosis drug discovery. *Future Microbiol* 10:217–229.
95. Wilsey C, Gurka J, Toth D, Franco J. 2013. A large scale virtual screen of DprE1. *Comput Biol Chem* 47:121–125.
96. Pauli I, dos Santos RN, Rostirolla DC, Martinelli LK, Ducati RG, Timmers LFSM, Basso LA, Santos DS, Guido RVC, Andricopulo AD, Norberto de Souza O. 2013. Discovery of New Inhibitors of *Mycobacterium tuberculosis* InhA Enzyme Using Virtual Screening and a 3D-Pharmacophore-Based Approach. *J Chem Inf Model* 53:2390–2401.
97. Sala C, Hartkoorn RC. 2011. Tuberculosis drugs: new candidates and how to find more. *Future Microbiol* 6:617–633.

98. Franzblau SG, DeGroot MA, Cho SH, Andries K, Nuermberger E, Orme IM, Mdluli K, Angulo-Barturen I, Dick T, Dartois V, Lenaerts AJ. 2012. Comprehensive analysis of methods used for the evaluation of compounds against *Mycobacterium tuberculosis*. *Tuberculosis* 92:453–488.
99. Wayne LG, Hayes LG. 1996. An in vitro model for sequential study of shutdown of *Mycobacterium tuberculosis* through two stages of nonreplicating persistence. *Infect Immun* 64:2062–2069.
100. Deb C, Lee C-M, Dubey VS, Daniel J, Abomoelak B, Sirakova TD, Pawar S, Rogers L, Kolattukudy PE. 2009. A Novel In Vitro Multiple-Stress Dormancy Model for *Mycobacterium tuberculosis* Generates a Lipid-Loaded, Drug-Tolerant, Dormant Pathogen. *PLOS ONE* 4:e6077.
101. Sala C, Dhar N, Hartkoorn RC, Zhang M, Ha YH, Schneider P, Cole ST. 2010. Simple Model for Testing Drugs against Nonreplicating *Mycobacterium tuberculosis*. *Antimicrob Agents Chemother* 54:4150–4158.
102. Christophe T, Jackson M, Jeon HK, Fenistein D, Contreras-Dominguez M, Kim J, Genovesio A, Carralet J-P, Ewann F, Kim EH, Lee SY, Kang S, Seo MJ, Park EJ, Škovierová H, Pham H, Riccardi G, Nam JY, Marsollier L, Kempf M, Joly-Guillou M-L, Oh T, Shin WK, No Z, Nehrbass U, Brosch R, Cole ST, Brodin P. 2009. High Content Screening Identifies Decaprenyl-Phosphoribose 2' Epimerase as a Target for Intracellular Antimycobacterial Inhibitors. *PLOS Pathog* 5:e1000645.
103. Abrahams GL, Kumar A, Savvi S, Hung AW, Wen S, Abell C, Barry CE, Sherman DR, Boshoff HIM, Mizrahi V. 2012. Pathway-Selective Sensitization of *Mycobacterium tuberculosis* for Target-Based Whole-Cell Screening. *Chem Biol* 19:844–854.

104. Hughes JP, Rees S, Kalindjian SB, Philpott KL. 2011. Principles of early drug discovery. *Br J Pharmacol* 162:1239–1249.
105. Bleicher KH, Böhm H-J, Müller K, Alanine AI. 2003. A guide to drug discovery: Hit and lead generation: beyond high-throughput screening. *Nat Rev Drug Discov* 2:369–378.
106. Lechartier B, Rybniker J, Zumla A, Cole ST. 2014. Tuberculosis drug discovery in the post-post-genomic era. *EMBO Mol Med* n/a-n/a.
107. Global Alliance for TB Drug Development. 2001. Tuberculosis. Scientific blueprint for tuberculosis drug development. *Tuberc Edinb Scotl* 81 Suppl 1:1–52.
108. Schluger N, Karunakara U, Lienhardt C, Nyirenda T, Chaisson R. 2007. Building Clinical Trials Capacity for Tuberculosis Drugs in High-Burden Countries. *PLOS Med* 4:e302.
109. Dorman S. New Drugs, New Regimens, Clinical Trials.
110. Bark CM, Furin JJ, Johnson JL. 2012. Approaches to clinical trials of new anti-TB drugs. *Clin Investig* 2:359–370.
111. Jindani A, Aber VR, Edwards EA, Mitchison DA. 1980. The Early Bactericidal Activity of Drugs in Patients with Pulmonary Tuberculosis. *Am Rev Respir Dis* 121:939–949.
112. Donald PR, Diacon AH. 2008. The early bactericidal activity of anti-tuberculosis drugs: a literature review. *Tuberculosis* 88:S75–S83.
113. Berthel S. Tuberculosis Drug Accelerator.
114. Dang A. Lilly TB Drug Discovery Initiative. IDRI.
115. More Medicines For Tuberculosis (MM4TB). <http://mm4tb.org/>.

116. Wehrli W, Staehelin M. 1971. Actions of the rifamycins. *Bacteriol Rev* 35:290–309.
117. Tiberi S, Plessis N du, Walzl G, Vjecha MJ, Rao M, Ntouni F, Mfinanga S, Kapata N, Mwaba P, McHugh TD, Ippolito G, Migliori GB, Maeurer MJ, Zumla A. 2018. Tuberculosis: progress and advances in development of new drugs, treatment regimens, and host-directed therapies. *Lancet Infect Dis* 0.
118. Munsiff SS, Kambili C, Ahuja SD. 2006. Rifapentine for the Treatment of Pulmonary Tuberculosis. *Clin Infect Dis* 43:1468–1475.
119. Gay JD, DeYoung DR, Roberts GD. 1984. In vitro activities of norfloxacin and ciprofloxacin against *Mycobacterium tuberculosis*, *M. avium* complex, *M. chelonae*, *M. fortuitum*, and *M. kansasii*. *Antimicrob Agents Chemother* 26:94–96.
120. Yano T, Kassovska-Bratinova S, Teh JS, Winkler J, Sullivan K, Isaacs A, Schechter NM, Rubin H. 2011. Reduction of Clofazimine by *Mycobacterial* Type 2 NADH:Quinone Oxidoreductase. *J Biol Chem* 286:10276–10287.
121. Zhang D, Lu Y, Liu K, Liu B, Wang J, Zhang G, Zhang H, Liu Y, Wang B, Zheng M, Fu L, Hou Y, Gong N, Lv Y, Li C, Cooper CB, Upton AM, Yin D, Ma Z, Huang H. 2012. Identification of less lipophilic riminophenazine derivatives for the treatment of drug-resistant tuberculosis. *J Med Chem* 55:8409–8417.
122. Ford CW, Hamel JC, Wilson DM, Moerman JK, Stapert D, Yancey RJ, Hutchinson DK, Barbachyn MR, Brickner SJ. 1996. In vivo activities of U-100592 and U-100766, novel oxazolidinone antimicrobial agents, against experimental bacterial infections. *Antimicrob Agents Chemother* 40:1508–1513.

123. Livermore DM. 2003. Linezolid in vitro : mechanism and antibacterial spectrum. *J Antimicrob Chemother* 51:ii9-ii16.
124. Lippe B von der, Sandven P, Brubakk O. 2006. Efficacy and safety of linezolid in multidrug resistant tuberculosis (MDR-TB)—a report of ten cases. *J Infect* 52:92–96.
125. Flores AR, Parsons LM, Pavelka. 2005. Genetic analysis of the β -lactamases of *Mycobacterium tuberculosis* and *Mycobacterium smegmatis* and susceptibility to β -lactam antibiotics. *Microbiology* 151:521–532.
126. Hugonnet J-E, Blanchard JS. 2007. Irreversible Inhibition of the *Mycobacterium tuberculosis* β -lactamase by Clavulanate. *Biochemistry (Mosc)* 46:11998–12004.
127. Sirturo (bedaquiline) product insert. Silver Spring, MD: Food and Drug Administration.
128. Andries K, Verhasselt P, Guillemont J, Göhlmann HWH, Neefs J-M, Winkler H, Gestel JV, Timmerman P, Zhu M, Lee E, Williams P, Chaffoy D de, Huitric E, Hoffner S, Cambau E, Truffot-Pernot C, Lounis N, Jarlier V. 2005. A Diarylquinoline Drug Active on the ATP Synthase of *Mycobacterium tuberculosis*. *Science* 307:223–227.
129. Koul A, Dendouga N, Vergauwen K, Molenberghs B, Vranckx L, Willebrords R, Ristic Z, Lill H, Dorange I, Guillemont J, Bald D, Andries K. 2007. Diarylquinolines target subunit c of mycobacterial ATP synthase. *Nat Chem Biol* 3:323.
130. Rao SPS, Alonso S, Rand L, Dick T, Pethe K. 2008. The protonmotive force is required for maintaining ATP homeostasis and viability of hypoxic, nonreplicating *Mycobacterium tuberculosis*. *Proc Natl Acad Sci* 105:11945–11950.

131. Koul A, Vranckx L, Dhar N, Göhlmann HWH, Özdemir E, Neefs J-M, Schulz M, Lu P, Mørtz E, McKinney JD, Andries K, Bald D. 2014. Delayed bactericidal response of *Mycobacterium tuberculosis* to bedaquiline involves remodelling of bacterial metabolism. *Nat Commun* 5.
132. Huitric E, Verhasselt P, Koul A, Andries K, Hoffner S, Andersson DI. 2010. Rates and Mechanisms of Resistance Development in *Mycobacterium tuberculosis* to a Novel Diarylquinoline ATP Synthase Inhibitor. *Antimicrob Agents Chemother* 54:1022–1028.
133. Hartkoorn RC, Uplekar S, Cole ST. 2014. Cross-Resistance between Clofazimine and Bedaquiline through Upregulation of MmpL5 in *Mycobacterium tuberculosis*. *Antimicrob Agents Chemother* 58:2979–2981.
134. Andries K, Villellas C, Coeck N, Thys K, Gevers T, Vranckx L, Lounis N, Jong BC de, Koul A. 2014. Acquired Resistance of *Mycobacterium tuberculosis* to Bedaquiline. *PLOS ONE* 9:e102135.
135. Matsumoto M, Hashizume H, Tomishige T, Kawasaki M, Tsubouchi H, Sasaki H, Shimokawa Y, Komatsu M. 2006. OPC-67683, a Nitro-Dihydro-Imidazooxazole Derivative with Promising Action against Tuberculosis In Vitro and In Mice. *PLOS Med* 3:e466.
136. Stover CK, Warrener P, VanDevanter DR, Sherman DR, Arain TM, Langhorne MH, Anderson SW, Towell JA, Yuan Y, McMurray DN, Kreiswirth BN, Barry CE, Baker WR. 2000. A small-molecule nitroimidazopyran drug candidate for the treatment of tuberculosis. *Nature* 405:962–966.
137. Manjunatha U, Boshoff HI, Barry CE. 2009. The mechanism of action of PA-824. *Commun Integr Biol* 2:215–218.

138. Manjunatha UH, Boshoff H, Dowd CS, Zhang L, Albert TJ, Norton JE, Daniels L, Dick T, Pang SS, Barry CE. 2006. Identification of a nitroimidazo-oxazine-specific protein involved in PA-824 resistance in *Mycobacterium tuberculosis*. *Proc Natl Acad Sci U S A* 103:431–436.
139. Singh R, Manjunatha U, Boshoff HIM, Ha YH, Niyomrattanakit P, Ledwidge R, Dowd CS, Lee IY, Kim P, Zhang L, Kang S, Keller TH, Jiricek J, Barry CE. 2008. PA-824 Kills Nonreplicating *Mycobacterium tuberculosis* by Intracellular NO Release. *Science* 322:1392–1395.
140. Haver HL, Chua A, Ghode P, Lakshminarayana SB, Singhal A, Mathema B, Wintjens R, Bifani P. 2015. Mutations in Genes for the F420 Biosynthetic Pathway and a Nitroreductase Enzyme Are the Primary Resistance Determinants in Spontaneous In Vitro-Selected PA-824-Resistant Mutants of *Mycobacterium tuberculosis*. *Antimicrob Agents Chemother* 59:5316–5323.
141. Fujiwara M, Kawasaki M, Hariguchi N, Liu Y, Matsumoto M. 2018. Mechanisms of resistance to delamanid, a drug for *Mycobacterium tuberculosis*. *Tuberculosis* 108:186–194.
142. 2014. Otsuka Wins European Marketing Authorization for Deltyba™ (delamanid).
143. Protopopova M, Hanrahan C, Nikonenko B, Samala R, Chen P, Gearhart J, Einck L, Nacy CA. 2005. Identification of a new antitubercular drug candidate, SQ109, from a combinatorial library of 1,2-ethylenediamines. *J Antimicrob Chemother* 56:968–974.
144. Tahlan K, Wilson R, Kastrinsky DB, Arora K, Nair V, Fischer E, Barnes SW, Walker JR, Alland D, Barry CE, Boshoff HI. 2012. SQ109 Targets MmpL3, a Membrane

Transporter of Trehalose Monomycolate Involved in Mycolic Acid Donation to the Cell Wall Core of *Mycobacterium tuberculosis*. *Antimicrob Agents Chemother* 56:1797–1809.

145. Grzegorzewicz AE, Pham H, Gundi VAKB, Scherman MS, North EJ, Hess T, Jones V, Gruppo V, Born SEM, Korduláková J, Chavadi SS, Morisseau C, Lenaerts AJ, Lee RE, McNeil MR, Jackson M. 2012. Inhibition of mycolic acid transport across the *Mycobacterium tuberculosis* plasma membrane. *Nat Chem Biol* 8:334–341.
146. Li K, Schurig-Briccio LA, Feng X, Upadhyay A, Pujari V, Lechartier B, Fontes FL, Yang H, Rao G, Zhu W, Gulati A, No JH, Cintra G, Bogue S, Liu Y-L, Molohon K, Orlean P, Mitchell DA, Freitas-Junior L, Ren F, Sun H, Jiang T, Li Y, Guo R-T, Cole ST, Gennis RB, Crick DC, Oldfield E. 2014. Multitarget Drug Discovery for Tuberculosis and Other Infectious Diseases. *J Med Chem* 57:3126–3139.
147. Makarov V, Manina G, Mikusova K, Mollmann U, Ryabova O, Saint-Joanis B, Dhar N, Pasca MR, Buroni S, Lucarelli AP, Milano A, De Rossi E, Belanova M, Bobovska A, Dianiskova P, Kordulakova J, Sala C, Fullam E, Schneider P, McKinney JD, Brodin P, Christophe T, Waddell S, Butcher P, Albrethsen J, Rosenkrands I, Brosch R, Nandi V, Bharath S, Gaonkar S, Shandil RK, Balasubramanian V, Balganesch T, Tyagi S, Grosset J, Riccardi G, Cole ST. 2009. Benzothiazinones Kill *Mycobacterium tuberculosis* by Blocking Arabinan Synthesis. *Science* 324:801–804.
148. Makarov V, Lechartier B, Zhang M, Neres J, van der Sar AM, Raadsen SA, Hartkoorn RC, Ryabova OB, Vocat A, Decosterd LA, Widmer N, Buclin T, Bitter W, Andries K, Pojer F, Dyson PJ, Cole ST. 2014. Towards a new combination therapy for tuberculosis with next generation benzothiazinones. *EMBO Mol Med* 6:372–383.

149. Pasca MR, Degiacomi G, Ribeiro AL d. JL, Zara F, De Mori P, Heym B, Mirrione M, Brerra R, Pagani L, Pucillo L, Troupioti P, Makarov V, Cole ST, Riccardi G. 2010. Clinical Isolates of *Mycobacterium tuberculosis* in Four European Hospitals Are Uniformly Susceptible to Benzothiazinones. *Antimicrob Agents Chemother* 54:1616–1618.
150. Mikusova K, Huang H, Yagi T, Holsters M, Vereecke D, D’Haeze W, Scherman MS, Brennan PJ, McNeil MR, Crick DC. 2005. Decaprenylphosphoryl Arabinofuranose, the Donor of the D-Arabinofuranosyl Residues of Mycobacterial Arabinan, Is Formed via a Two-Step Epimerization of Decaprenylphosphoryl Ribose. *J Bacteriol* 187:8020–8025.
151. Trefzer C, Rengifo-Gonzalez M, Hinner MJ, Schneider P, Makarov V, Cole ST, Johnsson K. 2010. Benzothiazinones: Prodrugs That Covalently Modify the Decaprenylphosphoryl- β -D-ribose 2’-epimerase DprE1 of *Mycobacterium tuberculosis*. *J Am Chem Soc* 132:13663–13665.
152. Trefzer C, Škovierová H, Buroni S, Bobovská A, Nenci S, Molteni E, Pojer F, Pasca MR, Makarov V, Cole ST, Riccardi G, Mikušová K, Johnsson K. 2012. Benzothiazinones Are Suicide Inhibitors of Mycobacterial Decaprenylphosphoryl- β - d-ribofuranose 2’-Oxidase DprE1. *J Am Chem Soc* 134:912–915.
153. Neres J, Pojer F, Molteni E, Chiarelli LR, Dhar N, Boy-Rottger S, Buroni S, Fullam E, Degiacomi G, Lucarelli AP, Read RJ, Zanoni G, Edmondson DE, De Rossi E, Pasca MR, McKinney JD, Dyson PJ, Riccardi G, Mattevi A, Cole ST, Binda C. 2012. Structural Basis for Benzothiazinone-Mediated Killing of *Mycobacterium tuberculosis*. *Sci Transl Med* 4:150ra121-150ra121.

154. Batt SM, Jabeen T, Bhowruth V, Quill L, Lund PA, Eggeling L, Alderwick LJ, Futterer K, Besra GS. 2012. Structural basis of inhibition of *Mycobacterium tuberculosis* DprE1 by benzothiazinone inhibitors. *Proc Natl Acad Sci* 109:11354–11359.
155. Lechartier B, Hartkoorn RC, Cole ST. 2012. In Vitro Combination Studies of Benzothiazinone Lead Compound BTZ043 against *Mycobacterium tuberculosis*. *Antimicrob Agents Chemother* 56:5790–5793.
156. Pethe K, Bifani P, Jang J, Kang S, Park S, Ahn S, Jiricek J, Jung J, Jeon HK, Cechetto J, Christophe T, Lee H, Kempf M, Jackson M, Lenaerts AJ, Pham H, Jones V, Seo MJ, Kim YM, Seo M, Seo JJ, Park D, Ko Y, Choi I, Kim R, Kim SY, Lim S, Yim S-A, Nam J, Kang H, Kwon H, Oh C-T, Cho Y, Jang Y, Kim J, Chua A, Tan BH, Nanjundappa MB, Rao SPS, Barnes WS, Wintjens R, Walker JR, Alonso S, Lee S, Kim J, Oh S, Oh T, Nehrbass U, Han S-J, No Z, Lee J, Brodin P, Cho S-N, Nam K, Kim J. 2013. Discovery of Q203, a potent clinical candidate for the treatment of tuberculosis. *Nat Med* 19:1157–1160.
157. Cook GM, Hards K, Vilchèze C, Hartman T, Berney M. 2014. Energetics of Respiration and Oxidative Phosphorylation in *Mycobacteria*. *Microbiol Spectr* 2.
158. Kalia NP, Hasenoehrl EJ, Rahman NBA, Koh VH, Ang MLT, Sajorda DR, Hards K, Grüber G, Alonso S, Cook GM, Berney M, Pethe K. 2017. Exploiting the synthetic lethality between terminal respiratory oxidases to kill *Mycobacterium tuberculosis* and clear host infection. *Proc Natl Acad Sci* 201706139.

Chapter 2: Arylvinylpiperazine amides, a new class of potent inhibitors targeting QcrB of *Mycobacterium tuberculosis*

Caroline S. Foo^{1§}, Andréanne Lupien^{1§}, Maryline Kienle², Anthony Vocat¹, Andrej Benjak¹, Raphael Sommer¹, Dirk A. Lamprecht^{3#}, Adrie JC Steyn^{3,4}, Kevin Pethe⁵, Jérémie Piton¹, Karl-Heinz Altmann², Stewart T. Cole^{1#}

¹Global Health Institute, École Polytechnique Fédérale de Lausanne, Switzerland

²Institute of Pharmaceutical Sciences, Department of Chemistry and Applied Biosciences, ETH Zürich, Switzerland

³Africa Health Research Institute, South Africa

⁴Department of Microbiology, University of Alabama at Birmingham, Birmingham, AL, United States

⁵ Lee Kong Chian School of Medicine and School of Biological Sciences, Nanyang Technological University, Singapore

[§]These authors contributed equally to the design and execution of experiments

[#] current affiliations: D.A.L. - Janssen Pharmaceutica, Turnhoutweg 30, 2340, Beerse, Belgium; S.T.C. – Institut Pasteur, Paris, France

Manuscript accepted, mBio, August 2018

Contributions: design and execution of experiments, data analysis, manuscript preparation

ABSTRACT

New drugs are needed to control the current tuberculosis (TB) pandemic caused by infection with *Mycobacterium tuberculosis*. We report here on our work with **AX-35**, an arylvinylpiperazine amide and four related analogs, which are potent anti-tubercular agents *in vitro*. All five compounds showed good activity against *M. tuberculosis* *in vitro* and in infected THP-1 macrophages, while displaying only mild cytotoxicity. Isolation and characterization of *M. tuberculosis* resistant mutants to the arylvinylpiperazine amide derivative AX-35 revealed mutations in the *qcrB* gene encoding a subunit of cytochrome *bc₁* oxidase, one of two terminal oxidases of the electron transport chain. Cross-resistance studies, allelic exchange, transcriptomic analyses and bioenergetics flux assays provided conclusive evidence that the cytochrome *bc₁-aa₃* is the target of **AX-35**, although the compound appears to interact differently with the quinol binding pocket compared to previous QcrB inhibitors. The transcriptomic and bioenergetic profiles of *M. tuberculosis* treated with **AX-35** were similar to those generated by other cytochrome *bc₁* oxidase inhibitors, including the compensatory role of the alternate terminal oxidase cytochrome *bd* in respiratory adaptation. In the absence of cytochrome *bd* oxidase, **AX-35** was bactericidal against *M. tuberculosis*. Finally, **AX-35** and its analogs were active in an acute mouse model of TB infection, with two analogs displaying improved activity over the parent compound. Our findings will guide future lead optimization to produce a drug candidate for the treatment of TB and other mycobacterial diseases, including Buruli ulcer and leprosy. (235 words)

IMPORTANCE

New drugs against *Mycobacterium tuberculosis* are urgently needed to deal with the current global TB pandemic. We report here on the discovery of a series of arylvinylpiperazine amides (**AX-35 – AX-39**), which represent a promising new family of compounds with potent *in vitro* and *in vivo* activity against *M. tuberculosis*. AX compounds target the QcrB subunit of the cytochrome *bc₁* terminal oxidase with a different mode of interaction compared to known QcrB inhibitors. This study provides the first multi-faceted validation of QcrB inhibition by recombineering-mediated allelic exchange, gene expression profiling and bioenergetic flux studies. It also provides further evidence for the compensatory role of cytochrome *bd* oxidase upon QcrB inhibition. In the absence of cytochrome *bd* oxidase, AX compounds are bactericidal, an encouraging property for future antimycobacterial drug development.

KEYWORDS tuberculosis, QcrB inhibitor, cytochrome *bc₁* oxidase, cytochrome *bd* oxidase, mycobacterial respiration, mycobacterial diseases

INTRODUCTION

Mycobacterium tuberculosis, the causative agent of tuberculosis (TB), is at the origin of a severe global health problem. TB is the leading cause of death due to an infectious agent, with an estimated death toll of 1.6 million in 2016 (1). Drug-susceptible TB is typically treated over the course of six months with a combination of the first-line drugs isoniazid, rifampicin, pyrazinamide and ethambutol; however, this regimen has been rendered ineffective nowadays in many cases, due to the emergence of drug-resistant TB (1). Treatment of multi-drug resistant TB (MDR-TB), whose defining characteristics are resistance to both rifampicin and isoniazid, requires a regimen of second-line drugs including a fluoroquinolone and injectable agents, but treatment success rates are lower than 50% (1–3). In addition to resistance to rifampicin and isoniazid, extensively-drug resistant TB (XDR-TB) strains are resistant to at least one of the fluoroquinolones and an injectable. XDR-TB cure rates are low at 30% (1). Long treatment duration, toxicity issues, drug resistance and the expense of the second-line regimens are important factors driving the search for new anti-TB drugs with novel mechanisms of action.

To generate new anti-TB candidates, drug screening efforts have employed phenotypic or whole-cell screening approaches recently, whereby compound libraries of new chemical entities are screened against *M. tuberculosis* for inhibition of bacterial growth in various settings which, ideally, should recapitulate pathophysiological conditions (4–6). Attempts are subsequently made to identify and validate the target(s) of hits to enable and facilitate further compound optimization. The diarylquinoline bedaquiline (BDQ), which targets the subunit *c* of mycobacterial ATP synthase (7, 8), emerged from such a compound-to-target approach and has been hailed as a milestone for TB drug discovery and, with its approval in 2012, became the first anti-TB drug to be approved in more than 40 years. The imidazopyrimidine amide Q203 and lansoprazole sulfide (LPZS) both target the QcrB subunit of cytochrome *bc₁* oxidase and were identified from intracellular screens with *M. tuberculosis*-infected macrophages and fibroblasts, respectively (9, 10). The approval of BDQ for the treatment of

MDR-TB, inclusion of BDQ as a component of the highly promising NIX-TB combination trial for XDR-TB treatment (11), and the fact that Q203 is currently in Phase I clinical development (2, 12), altogether validate mycobacterial respiration as a new, relevant and attractive target for an obligate aerobic pathogen.

In 2013, GlaxoSmithKline published the results of a large phenotypic screening campaign against *Mycobacterium bovis* BCG and *M. tuberculosis*, which yielded a total of 177 low-molecular weight hits (13). One of these compounds was **GW861072X** (referred to here as **AX-35**) (Fig. 1), which exhibited potent activity against both *M. bovis* BCG and *M. tuberculosis* H37Rv (MIC of 0.3 μ M against both species).

Due to its structural simplicity, we considered **AX-35** as an attractive starting point for lead optimization and prepared a series of analogs for structure-activity-relationship (SAR) studies, the full details of which will be published in a forthcoming report. In this paper, we describe the characterization of **AX-35** and four of the most potent analogs that have emerged from our SAR work (**AX-36** – **AX-39**) and are active against *M. tuberculosis* replicating *in vitro* and in infected macrophages. Subsequent work validated the target of these compounds as QcrB, the *b* subunit of the cytochrome *bc₁* oxidase, based on the isolation of resistant mutants, cross-resistance studies, RNA-seq and bioenergetics flux assays. Finally, further characterization of three AX compounds in an acute mouse model of TB demonstrated *in vivo* efficacy against *M. tuberculosis*.

RESULTS

Initial characterization of AX-35 and its analogs. The synthesis of **AX-35** – **AX-39** is described in the supporting information (for structures see Table 1). Analog **AX-36** served to assess the importance of the position of the sulfur atom in the thiophene ring for antimycobacterial activity, while thiazole derivatives **AX-37** and **AX-39** were designed to probe the effect of enhanced compound polarity. In addition, replacement of the thiophene ring by a thiazole moiety could mitigate the toxicity

risk often associated with thiophene derivatives. For the same reason, the thiophene moiety in **AX-35** was also replaced by a phenyl ring, as an established bioisostere (**AX-38**). As shown in the data in Table 1, **AX-35** is the most active compound within this series, with an MIC of 0.05 µg/ml against *M. tuberculosis* H37Rv; **AX-36**, **AX-37**, **AX-38**, and **AX-39** have somewhat higher MIC values ranging from 0.1 to 0.3 µg/ml (Table 1). The activity of AX compounds is selective for pathogenic mycobacteria in the panel of bacterial strains and fungi tested (Table 2). Members of the *M. tuberculosis* complex were especially susceptible, notably *Mycobacterium canettii*, followed by *Mycobacterium ulcerans*. Most of the microorganisms tested were resistant to both **AX-35** and **AX-36**. Mild to no cytotoxicity was observed in human HepG2 cells, resulting in selectivity indices (HepG2 TD₅₀/MIC) above 250 for all compounds, with **AX-35** being the most selective (Table 1). The IC₅₀ values for *M. tuberculosis* H37Rv-infected THP-1 macrophages ranged from 0.1 to 1.8 µg/ml (Table 1), reflecting the potent *ex vivo* activity of these molecules. The metabolic stability of the compounds in mouse and human liver microsomes was moderate to low (Table S1).

Evidence of AX compounds targeting QcrB of *M. tuberculosis*. Initial attempts to raise spontaneous resistant mutants in *M. tuberculosis* H37Rv to **AX-35** and **AX-36** on solid 7H10 medium failed, even at exposures of up to 100x MIC. An alternative method of continual passaging of H37Rv in complete 7H9 liquid medium containing **AX-35** or **AX-36** at concentrations above the MIC, beginning at 2x MIC and increasing to 100x MIC over five passages, proved to be more successful. Increasing MICs reflected the gradual selection of a resistant sub-population in the culture on constant exposure to the compounds, especially after the fourth and fifth passages. Single clones isolated on 7H10 plates at passage five were subsequently tested for resistance to **AX-35** or **AX-36** by MIC determinations using the resazurin microtiter assay plate (REMA) method (Fig. 2a).

To identify mutations associated with resistance to **AX-35** or **AX-36**, whole-genome sequencing (WGS) analysis was performed on six clones with a 50-fold increase in MIC compared to the parental strain H37Rv (Fig. 2a). Three missense mutations in *qcrB* were revealed, leading to non-synonymous

substitutions in QcrB, the *b* subunit of cytochrome *bc₁* oxidase. S182P and M342V mutations were associated with **AX-35** resistance and M342I with **AX-36** resistance. The specific contribution of these substitutions to **AX-35** and **AX-36** resistance was confirmed by the generation of the same missense mutations in chromosomal *qcrB* of wild-type H37Rv by recombineering and MIC determination (Fig. S1).

Since mutations in *qcrB* have also been identified in mutants of *M. tuberculosis* H37Rv resistant to Q203 and LPZS, two compounds known to target QcrB, cross-resistance studies were performed to investigate if **AX-35** and **AX-36** behaved in a similar manner. Q203- and LPZS-resistant strains, harbouring single-nucleotide polymorphisms leading to T313A and L176P in QcrB, respectively, are cross-resistant to **AX-35** and **AX-36** (Fig. 2b). These results indicate that the binding mode of the AX compound with QcrB shares some similarities with Q203 and LPZS. However, not all **AX**-resistant mutants were fully resistant to Q203 and LPZS (Fig. 2b), thus suggesting a distinct mode of binding for these QcrB inhibitors. On inspection of a model of *M. tuberculosis* QcrB, residues S182, M342, T313 and L176 were found to cluster around the quinol oxidation site of the enzyme (Fig. 2c), implying that **AX-35** and **AX-36** bind to QcrB at this pocket, similar to Q203 and LPZS.

As QcrB is one of the respiratory subunits of the cytochrome *bc₁* oxidase, a consequence of its inhibition is depletion of ATP levels in the bacterium (9, 10). The intracellular ATP level was measured in wild-type H37Rv after 24 h exposure to **AX-35** or **AX-36** and found to be ~90% lower than for the untreated control, similar to the effect of treatment with the ATP-synthase inhibitor BDQ or with Q203 under the same conditions (Fig. 2d), thus indicating that AX compounds do indeed affect ATP levels. ATP was also depleted in BDQ- or Q203-exposed AX-resistant mutants, with ATP levels similar to that in BDQ- or Q203-exposed wild-type *M. tuberculosis*. However, ATP levels were essentially unaffected in the AX-resistant strains in the presence of **AX-35** or **AX-36** (Fig. 2d). This demonstrates that the mutations in QcrB associated with AX-resistance do not greatly impact the activity of BDQ nor Q203, indicating that AX compounds do not have off-target effects on the ATP synthase and that

they interact in a different manner with QcrB compared to Q203. Taken together these findings indicate that QcrB is the direct target of the AX compounds.

Transcriptional response of *M. tuberculosis* to AX-35 treatment. To gain insight into the initial adaptive response of *M. tuberculosis* to **AX-35** treatment, the transcriptomes of wild-type H37Rv exposed to **AX-35** at 10x and 30x MIC for a duration of 4h were examined. Of 81 genes significantly down-regulated (fold-change (FC) ≤ -2 , Benjamini and Hochberg's adjusted p-value (p_{adj}) ≤ 0.05), *leuC* and *leuD* (involved in leucine biosynthesis) were the most extensively down-regulated (Fig. 3a, b). Thirteen genes were significantly up-regulated (FC ≥ 2 , $p_{adj} \leq 0.05$) in the presence of **AX-35**, seven of which were involved in intermediary metabolism and respiration (Fig. 3a, b). The most highly up-regulated gene was *lipU*, a gene implicated in lipid hydrolysis. Notably, two main operons in the *M. tuberculosis* transcriptome were up-regulated, namely the *cyd* and *mymA* operons. The *cyd* operon consists of *cydA*, *cydB* and *cydD* (*cydA* and *cydB* were close to the cutoff with FC 1.97 and 1.99 respectively), with *cydA* and *cydB* coding for subunits I and II, respectively, of the cytochrome *bd* oxidase, while *cydDC* encodes an ABC transporter involved in cytochrome *bd* assembly. The *mymA* operon from Rv3083 to Rv3089 (14) includes *tgs4* and *rv3088* encoding triacylglycerol synthases (15) *lipR*, *rv3085* and *rv3086* encoding short-chain dehydrogenases, and an acyl-CoA synthase gene, *fadD13*.

To validate the RNA-seq data, qRT-PCR was performed targeting *lipU*, *cydB*, and *tgs4* in both wild-type H37Rv and its AX-resistant mutants after exposure to **AX-35** at 30x MIC (Fig. 3c). The up-regulation of all three genes in wild-type H37Rv upon **AX-35** treatment detected by qRT-PCR is consistent with the RNA-seq data, with *lipU* having the highest relative expression of around 6-fold compared to the control, i.e. H37Rv treated with DMSO alone. No significant differences in the expression levels of these three genes were measured for the AX-resistant mutant when treated with DMSO or with **AX-35**, therefore establishing that their up-regulation and, by extension, the de-

regulation of genes observed by RNA-seq, is indeed a consequence of **AX-35** treatment in *M. tuberculosis*.

Respiratory response of *M. tuberculosis* to AX-35 treatment. Bioenergetic flux studies were carried out to assess the respiratory response of *M. tuberculosis* to **AX-35**, with Q203 used as a control. Oxygen consumption rate (OCR) was first measured in *M. tuberculosis* H37Rv in the presence of glucose to determine the basal OCR and the subsequent addition of **AX-35** or Q203 resulted in an increase in OCR (Fig. 4a, b). Lastly, the protonophore carbonyl cyanide *m*-chlorophenyl hydrazine (CCCP) was added, depolarising the bacterial membrane and enabling the measurement of the maximum respiration capability of the bacteria.

The increase in OCR upon the addition of **AX-35** or Q203 can be attributed to cytochrome *bd* oxidase, since this increase was no longer observed in the presence of either compound in the $\Delta cydAB$ strain (Fig. 4a, b). This switch in *M. tuberculosis* respiration to the *bd* oxidase has previously been validated as a respiratory signature of cytochrome *bc₁* oxidase inhibitors such as Q203 (16), and our results indicate a similar bioenergetic profile of **AX-35** to that of Q203.

Interestingly, a difference can be observed in the bioenergetic profiles, on exposure of the cytochrome *bd* oxidase KO strain harbouring a QcrB A317V mutation to these two QcrB inhibitors. Addition of **AX-35** decreases the OCR of this strain, generating a profile similar to that of H37Rv $\Delta cydAB$ (Fig. 4a), implying that respiration is via the *bd* oxidase branch and that QcrB remains fully inhibited despite the A317V mutation. The basal OCR remains unaffected by the addition of Q203, however (Fig. 4b), which would suggest a partial inhibition of QcrB and thus inability of the drug to fully inhibit QcrB due to the mutation. This therefore reveals additional differences in the binding modes of **AX-35** and Q203 to QcrB.

Taken together, these results demonstrate the capability of respiratory adaptation of *M. tuberculosis* via the *bd* oxidase upon treatment with **AX-35**, generating a respiratory signature similar to that of

another established QcrB inhibitor, Q203, albeit highlighting different modes of interaction of the two compounds within the binding pocket.

Cidality, drug interactions, and *in vivo* efficacy of AX compounds. QcrB inhibitors described to date are bacteriostatic due to the compensatory role of the cytochrome *bd* oxidase. To determine the mode of action of AX compounds against *M. tuberculosis*, minimum bactericidal concentrations (MBC) were determined in *M. tuberculosis* H37Rv, H37RvΔ*cydAB*, and complemented H37RvΔ*cydAB*::*cydAB* strains (Fig. S2). In H37Rv, **AX-35** is bacteriostatic with an MBC up to a concentration 32-fold higher than the MIC. Conversely, **AX-35** was bactericidal against the H37RvΔ*cydAB* strain at a concentration 4-fold in excess of its MIC. Cidality of **AX-35** can be specifically attributed to the lack of the cytochrome *bd* oxidase, as evident from the survival of the bacteria in the complemented strain treated with **AX-35**.

Since synergistic interactions have been previously reported between the cell wall inhibitor PBTZ169 and BDQ (17), as well as between compounds targeting the mycobacterial respiratory chain (16, 18), checkerboard assays for two-drug combinations were performed to determine the nature of interactions between **AX-35** with PBTZ169, BDQ, or clofazimine (CFZ) in *M. tuberculosis* H37Rv. The ΣFIC indices obtained for all three combinations range from 0.8 to 1.6 for concentrations of **AX-35** less than or equal to 0.5-fold MIC (Table S2), indicating non-antagonistic, additive interactions.

The activity of AX compounds *in vivo* was determined in mouse models of chronic and acute TB. None of the AX compounds reduced the bacterial burden in mice at the dose of 100 mg/kg in the chronic model (Fig. S3). In the acute model, however, **AX-35** at an oral dose of 200 mg/kg, **AX-37** and **AX-39** at 100 mg/kg significantly reduced the bacterial load in mouse lungs by 0.4 log₁₀, 0.6 log₁₀ and 0.9log₁₀, respectively, compared to the TPGS vehicle control (Fig. 5).

DISCUSSION

The compounds investigated in this study are chemically distinct and different from the diverse QcrB inhibitors described in recent years (9, 19–25). Of the three mutations in QcrB identified here in spontaneous mutants resistant to **AX-35** and **AX-36**, namely S182P, M342V, and M342I, the first two have been previously reported (20). Cross-resistance studies and bioenergetic flux assays highlight influential residues for the interaction of **AX-35** and **AX-36** with QcrB, which occurs in the same binding site as Q203 and LPZS. In particular, mutations S182P, M342V/I, T313A, L176P, impair the interaction of **AX-35** and **AX-36** with QcrB, resulting in resistance of *M. tuberculosis* to the compounds. The substitution A317V, however, does not interfere with this interaction. This highlights the different modes of interaction of **AX-35** and **AX-36** with QcrB compared with Q203 or LPZS, and this information will be useful for further optimization of the compounds through structure-based drug design.

In addition to cross-resistance studies, transcriptomic and bioenergetic flux studies provided further evidence of QcrB as the primary target of **AX-35/36**. Treatment of *M. tuberculosis* with **AX-35** results in the up-regulation of the *cydABD* operon, but not the *dosR* regulon, which is consistent with the transcriptomic signature of respiratory inhibitors specifically inhibiting the cytochrome *bc₁-aa₃* terminal oxidase (26). In line with this, exposure of *M. tuberculosis* to **AX-35** results in an increase in OCR due to activity of the cytochrome *bd* oxidase, generating a bioenergetic profile similar to that of the respiratory signature of cytochrome *bc₁* oxidase inhibitors such as Q203 (16).

Cytochrome *bd* oxidase is non-proton translocating and thus the less bioenergetically efficient of the two terminal oxidases of *M. tuberculosis* (27). It has been demonstrated that the *bd* oxidase is up-regulated under conditions where the function of the cytochrome *bc₁-aa₃* is compromised (20, 28–30). In addition, inhibitors of respiration such as BDQ and QcrB inhibitors have markedly improved activity upon deletion or inhibition of *bd* oxidase (20, 31–33). The pronounced compensatory role of this alternate oxidase in the respiratory adaptation of *M. tuberculosis* for its survival is also apparent

in our study, where the absence of *bd* oxidase is associated with AX-mediated bactericidal activity. Targeting both terminal oxidases simultaneously may therefore be a novel and effective strategy against *M. tuberculosis*. Although the increase in respiration, up-regulation of cytochrome *bd* oxidase, and enhanced killing of $\Delta cydAB$ mutants upon inhibition of ATP synthase by BDQ in *M. smegmatis* (38) have been attributed to the ionophoric/off-target effect of BDQ (39), it is unlikely that AX compounds behave in a similar manner as uncouplers, based on the bioenergetic flux data.

It is also of note that AX treatment of *M. tuberculosis* results in the up-regulation of *tgs* genes (*tgs4* and *rv3087*) and lipases (*lipU* and *lipR*). *tgs* genes are involved in the biosynthesis of triacylglycerol (TAG), the predominant energy source for *M. tuberculosis* in host macrophages (15, 34), while *lip* genes encode lipolytic enzymes thought to be involved in the utilization of host TAG (35). Such up-regulation of *tgs* and *lip* genes has been observed in various models of host stress (36, 37), and similarly AX-induced stress re-models central carbon metabolism in *M. tuberculosis* toward lipid metabolism.

The compounds investigated here show promising properties as anti-TB agents. **AX-35** to **AX-39** demonstrated potent activity against *M. tuberculosis in vitro* and in macrophages, while having mild to no cytotoxicity. When tested in an acute mouse model of TB, **AX-35**, **AX-37** and **AX-39** were capable of reducing the bacterial burden in the lungs of mice. This *in vivo* activity can likely be improved further by addressing metabolic stability issues, such as those observed in mouse microsomes, although the compounds appear to be more stable in human microsomes.

The fact that activity of the AX compounds was only observed in the acute rather than the chronic mouse model of TB could be attributed to the difference in expression levels of the terminal oxidases found between these two stages of *M. tuberculosis* lung infection (29). The cytochrome *bc₁-aa₃* oxidase is more highly expressed than the *bd* oxidase during the exponential phase of growth of *M. tuberculosis* in mice, whereas it is down-regulated as a response to host immunity and remains down-regulated as the bacteria enter a non-replicating state in the chronic phase (29). Thus, targeting QcrB

during the exponential phase of *M. tuberculosis* growth would have a bigger impact on bacterial viability despite any compensatory response by *bd* oxidase. Another potential application of the AX-inhibitors could be in the treatment of the human diseases Buruli ulcer and leprosy as their causative agents, *M. ulcerans* and *M. leprae*, respectively, lack the cytochrome *bd* oxidase.

In conclusion, our SAR data prove that structural changes to **AX-35 (GW861072X)** can lead to improved *in vivo* activity against *M. tuberculosis* and that the arylvinylpiperazine amide series target the QcrB subunit of the cytochrome *bc₁-aa₃* oxidase. As part of the mycobacterial respiratory chain, QcrB is an attractive target for combination therapy. Furthermore, the biochemical information obtained from this study could guide future lead optimization work to enhance potency and stability of the compounds.

MATERIALS AND METHODS

Drugs used in this study. Q203 was synthesized as described before (9, 40), LPZS was purchased from Santa Cruz biotechnology, Toronto Research Chemicals Inc., BDQ was a gift from Janssen Pharmaceutica NV, PBTZ169 (Macozinone) was provided by Innovative Medicines for Tuberculosis, while CFZ, INH and RIF were from Sigma Aldrich.

Culture conditions of *M. tuberculosis* strains, other bacteria and eukaryotic cell lines.

Mycobacterial strains were grown at 37°C in Middlebrook 7H9 broth (Difco) supplemented with 0.2% glycerol, 0.05% Tween-80 and 10% albumin dextrose catalase (ADC) (7H9 complete) or on 7H10 agar plates supplemented with 0.5% glycerol and 10% oleic ADC. *Bacillus subtilis*, *Candida albicans*, *Corynebacterium diphtheriae*, *Corynebacterium glutamicum*, *Escherichia coli*, *Micrococcus luteus*, *Pseudomonas putida*, *Salmonella typhimurium*, and *Staphylococcus aureus* were grown in LB broth. *Enterococcus faecalis*, *Listeria monocytogenes*, and *Pseudomonas aeruginosa* were grown in brain heart infusion (BHI) broth. HepG2 cells were grown in DMEM (Gibco) media supplemented with 10% fetal bovine serum at 37°C with 5% CO₂. THP-1 macrophages were grown in RPMI medium supplemented with 10% fetal bovine serum and 1 mM sodium pyruvate at 37°C with 5% CO₂.

Determination of MICs. MICs were determined using the resazurin reduction microplate assay (REMA) as previously described (41). Strains were grown to log-phase (OD₆₀₀ 0.4 to 0.8) and diluted to an OD₆₀₀ of 0.0001. Two-fold serial dilutions of each test compound were prepared in 96-well plates containing 100 µl of bacteria per well (3 x 10³ cells per well). Plates were incubated either at 30°C or 37°C as required with appropriate incubation times (e.g. for *M. tuberculosis* at 37°C, 6 days). 10 µl of resazurin (0.0025% w/v) was added to each well, after which the fluorescence intensity of the resorufin metabolite (excitation/emission: 560/590 nm) was read using an Infinite F200 Tecan plate reader. MIC values representing 90% growth inhibition were determined by a non-linear fitting of the data to the Gompertz equation using GraphPad Prism.

Cytotoxicity for HepG2 cells. Human HepG2 cells (4,000 cells/well) were incubated for 3 days with two-fold serially diluted compounds at 37°C, under an atmosphere of 5% CO₂. Cell viability was determined by the addition of resazurin (0.0025% w/v) for 4 h at 37°C and the fluorescence intensity measured as in REMA.

Assessment of drug activity in THP-1 macrophages. THP-1 human monocytic cells (10⁵/well) were seeded in 96-well plates and incubated with 100 nM phorbol-12-myristate-13-acetate (PMA) overnight to stimulate macrophage differentiation. Differentiated macrophages were infected with *M. tuberculosis* H37Rv grown to log phase (OD₆₀₀ 0.4 to 0.8) at MOI 5. Extracellular bacteria were removed after 3-4 h incubation at 37°C with 5% CO₂ by removing the RPMI medium and washing with PBS. Compounds to be tested were prepared in separate 96-well plates by two-fold serial dilutions in a final volume of 100 µl RPMI which was then transferred to the plates of infected THP-1 macrophages. Plates were sealed and incubated for 48 h at 37°C with 5% CO₂. 10 µl of PrestoBlue® (ThermoFischer Scientific) was added and plates were incubated for up to 1 h at 37°C with 5% CO₂ before the fluorescence intensity (excitation/emission: 560/590 nm) was measured using Infinite F200 Tecan plate reader. Dose-response curves were plotted and IC₅₀ values obtained using a non-linear regression fit equation (log[inhibitor] vs response, variable slope) in GraphPad Prism.

Microsomal stability studies. Metabolic stability of the compounds was measured based on intrinsic clearance (Cl_{int}) in mouse and human liver microsomes as previously described (42). Final compound concentration in the mixture of microsomes and NADPH-regeneration system was 2 µg/ml, and a mixture without NADPH-regeneration was also prepared for each compound as a control of the stability of the compound with time. Carbamazepine and nifedipine at 2 µg/ml were used as low and high intrinsic clearance controls, respectively.

Mouse studies. To assess compound activity in an acute mouse model of TB, female BALB/c mice from Charles River Laboratories (7-8 weeks old, 20g, 5 mice per group) were aerosol-infected

with *M. tuberculosis* H37Rv at a low dose and treated by oral gavage the following day with either vehicle controls (TPGS 20% or TPGS 20% containing 1% DMSO) or test compounds once daily for 10 days. AX compounds were prepared in TPGS 20%, Q203 in TPGS 20% containing 1% DMSO (as described in (32) and INH in ddH₂O. Compounds were ground with a pestle and mortar followed by sonication at room temperature for 30 min. Compound solutions were stored at 4°C and prepared freshly after 5 days. The day after the final treatment, mice were sacrificed and serial dilutions of lung homogenates were plated on 7H10 agar containing 10 µg/ml cyclohexamide and 50 µg/ml ampicillin. Experiments were approved by the Swiss Cantonal Veterinary Authority (authorization number 3082).

Isolation and characterization of AX-resistant mutants. AX-resistant mutants of *M. tuberculosis* H37Rv were isolated from 7H9 cultures over 5 passages with increasing concentrations of **AX-35** or **AX-36** starting from 2x, 5x, 10x MIC to a final concentration of 50x and 100x MIC. Single colonies were obtained from three independent cultures by streaking on 7H10 agar plates and resistance to AX was measured by REMA. Genomic DNA extraction was performed using the QiaAMP UCP Pathogen Minikit (Qiagen) as per the manufacturer's instructions. Whole genome sequencing was performed using Illumina technology with sequencing libraries prepared using the KAPA HyperPrep kit (Roche) and sequenced on an Illumina HiSeq 2500 instrument. All raw reads were adapter- and quality-trimmed with Trimmomatic v0.33 (43) and mapped onto the *M. tuberculosis* H37Rv reference genome (RefSeq NC_000962.3) using Bowtie2 v2.2.5 (44). The bamleftalign program from the FreeBayes package v0.9.20-18 (45) was used to left-align indels. Reads with mapping quality below 8 and duplicate reads were omitted.

Variant analysis. Variant calling was done using VarScan v2.3.9 (46) using the following cut-offs: minimum overall coverage of ten non-duplicated reads, minimum of five non-duplicated reads supporting the SNP, base quality score >15, and a SNP frequency above 30%. The rather low thresholds, especially the SNP frequency, were deliberately chosen to avoid missing potential variants

in alignment-difficult regions, or in case of mixed population. All putative variants unique to the mutant strains were manually checked by inspecting the alignments.

Recombineering for target confirmation. Insertion of mutations associated with AX resistance in chromosomal *qcrB* of *M. tuberculosis* was done based on a recombineering method (47). Desired mutations were centered in lagging strand oligos of 70 nucleotides. *M. tuberculosis* H37Rv containing plasmid pJV53 was grown to OD₆₀₀ of 0.8 in 7H9 liquid media containing 25 µg/ml kanamycin and exposed to 0.2% acetamide for 24 h and 0.2 M glycine for 16 h. Competent cells were prepared and co-transformed with 100 ng of lagging oligo and 50 ng of pYub412 carrying a hygromycin selection marker. After a rescue of 3 days at 37°C, cells were plated on 7H10 plates containing hygromycin at 50 µg/ml and transformants were evaluated for resistance to AX by REMA. Desired mutations associated with AX resistance were subsequently confirmed by Sanger sequencing across *qcrB* and the absence of other mutations was confirmed by whole-genome sequencing.

Modelling of *M. tuberculosis* QcrB. The QcrB protein of *M. tuberculosis* was modelled using the homology modelling web server (SWISS) (48) and the chain A of the crystal structure of the mutant *Rhodobacter sphaeroides* cytochrome *bc₁* oxidase (PDB code: 2QJK). Illustrations were made using Pymol software (49).

Quantification of intracellular ATP. Log-phase cultures of wild-type H37Rv or AX-resistant mutants (about 10⁶ CFU/ml) were exposed to test compounds at 2.5x MIC for 24 h in a final volume of 100 µl and incubated with BacTiter Glo Reagent (Promega) (v/v 4:1) for 5 min in the dark. Luminescence was measured on a TECAN Infinite M200 in relative light units (RLU) with an integration time of 1s.

Total RNA extraction and RNA-seq. Wild-type and AX-resistant H37Rv cultures were grown to mid-log phase and exposed to DMSO (vehicle control) or compounds for 4 h at 37°C. Cells were harvested by centrifugation and pellets were stored with 1 ml of TRIzol reagent (Thermo Fisher

Scientific) at -80°C until further processed. Cells were lysed by bead-beating and total RNA was extracted by phenol-chloroform with DNase treatment (RQ1 RNase-free DNase, Promega). Library preparation was done using the Ribo-zero rRNA removal kit (Illumina) for Gram-positive bacteria to deplete rRNA from total RNA. Two biological replicates for each strain were prepared for RNA-seq. Reads were adapter- and quality-trimmed with Trimmomatic v0.33 (43) and mapped onto the *M. tuberculosis* H37Rv reference genome (RefSeq NC_000962.3) using Bowtie2 v2.2.5 (44). Counting reads over features was done with featureCounts from the Subread package v1.4.6 (50). DESeq2 (51) as used to infer differentially expressed genes.

Quantitative PCR. cDNA was prepared from total RNA using SuperScript III First-strand Synthesis kit (Invitrogen) and analysed by qPCR for targeted gene expression in duplicates using Power SYBR Green PR Master Mix (Applied Biosystems) on a QuantStudio 5 Real-Time PCR system (Thermo Fisher Scientific). *sigA* was used as a house-keeping gene for normalization and the $\Delta\Delta C_t$ method was used for quantification.

Extracellular Flux Analysis. All strains of *M. tuberculosis* used were cultured in Middlebrook 7H9 media (Difco) supplemented with 10% OADC (Difco) and 0.01% Tyloxapol (Sigma) at 37°C, to an OD₆₀₀ ~ 0.6 – 0.8. *M. tuberculosis* H37Rv was obtained from BEI Resources (NR-123), *M. tuberculosis* H37Rv $\Delta cydAB$ (52) and *M. tuberculosis* H37Rv $\Delta cydKO$ A317V (20) were gifts from Dr. Digby Warner and Dr. Helena Boshoff, respectively. *M. tuberculosis* oxygen consumption rate (OCR) was measured using the Seahorse XF96 Analyzer (Agilent) as previously described (16). In short, *M. tuberculosis* bacilli were adhered to the bottom of a XF96 cell culture microplate (Agilent) at a density of 2×10^6 bacilli/well using Cell-Tak™ cell adhesive (Corning). Extra cellular flux analysis was carried out in unbuffered 7H9 media, at pH 7.35, containing 0.2% glucose. Basal OCR was measured for ~19 min before the automatic addition, through the drug ports of the XF96 sensory cartridge (Agilent), of either Q203 (final concentration of 0.3 μ M, 100x the MIC₅₀) or AX-35 (final concentration of 14 μ M, 100x the MIC₅₀) to the three different *M. tuberculosis* strains. Q203 was a

gift from Dr. Helena Boshoff. The deviations from basal respiration, caused by compound addition, were measured for ~35 min before the addition of the uncoupler CCCP (final concentration of 2 μ M, Sigma) to induce maximal OCR, after which OCR was measured for a final ~19 min. The points of compound addition are indicated by vertical dotted lines. OCR data points are representative of the average OCR after 3 minutes of continuous measurement, the error calculated automatically by the Seahorse Wave Desktop 2.3.0 software (Agilent) from the OCR measurements from at least four replicate wells. OCR plots are representative of two independent experiments performed and data representation was done using GraphPad Prism 7.02.

Data Availability. Sequence data were deposited at the NCBI Sequence Read Archive under the accession number **SRP142469** (<https://www.ncbi.nlm.nih.gov/sra/SRP142469>). RNA-seq data were deposited at the NCBI Gene Expression Omnibus under the accession number **GSE113683** (<https://www.ncbi.nlm.nih.gov/geo/query/acc.cgi?acc=GSE113683>).

ACKNOWLEDGEMENTS

We would like to thank Dr. Digby Warner and Dr. Helena Boshoff for providing *M. tuberculosis* H37Rv $\Delta cydAB$ and *M. tuberculosis* H37Rv $\Delta cydKO$ A317V strains used in the bioenergetics flux assays. We also greatly appreciate the technical help and expertise of Dr. Claudia Sala and Dr. Charlotte Avanzi in RNA-seq and insightful discussions, and library preparation, respectively. The research was also co-funded by the South African Medical Research Council to AJCS. The research leading to these results received funding from the European Community's Seventh Framework Programme (MM4TB, Grant 260872).

REFERENCES

1. World Health Organization. 2017. Global Tuberculosis Report 2017. S.l.
2. World Health Organization, Global Tuberculosis Programme. 2016. WHO treatment guidelines for drug-resistant tuberculosis: 2016 update.
3. Caminero JA, Sotgiu G, Zumla A, Migliori GB. 2010. Best drug treatment for multidrug-resistant and extensively drug-resistant tuberculosis. *Lancet Infect Dis* 10:621–629.
4. Lechartier B, Rybniker J, Zumla A, Cole ST. 2014. Tuberculosis drug discovery in the post-post-genomic era. *EMBO Mol Med* 6:158–168.
5. Manjunatha UH, Smith PW. 2015. Perspective: Challenges and opportunities in TB drug discovery from phenotypic screening. *Bioorg Med Chem* 23:5087–5097.
6. Mdluli K, Kaneko T, Upton A. 2014. Tuberculosis drug discovery and emerging targets. *Ann N Y Acad Sci* 1323:56–75.
7. Andries K, Verhasselt P, Guillemont J, Göhlmann HWH, Neefs J-M, Winkler H, Gestel JV, Timmerman P, Zhu M, Lee E, Williams P, Chaffoy D de, Huitric E, Hoffner S, Cambau E, Truffot-Pernot C, Lounis N, Jarlier V. 2005. A Diarylquinoline Drug Active on the ATP Synthase of *Mycobacterium tuberculosis*. *Science* 307:223–227.
8. Koul A, Dendouga N, Vergauwen K, Molenberghs B, Vranckx L, Willebrords R, Ristic Z, Lill H, Dorange I, Guillemont J, Bald D, Andries K. 2007. Diarylquinolines target subunit c of mycobacterial ATP synthase. *Nat Chem Biol* 3:323.
9. Pethe K, Bifani P, Jang J, Kang S, Park S, Ahn S, Jiricek J, Jung J, Jeon HK, Cechetto J, Christophe T, Lee H, Kempf M, Jackson M, Lenaerts AJ, Pham H, Jones V, Seo MJ, Kim YM, Seo M, Seo JJ, Park D, Ko Y, Choi I, Kim R, Kim SY, Lim S, Yim S-A, Nam J, Kang H, Kwon

- H, Oh C-T, Cho Y, Jang Y, Kim J, Chua A, Tan BH, Nanjundappa MB, Rao SPS, Barnes WS, Wintjens R, Walker JR, Alonso S, Lee S, Kim J, Oh S, Oh T, Nehrbass U, Han S-J, No Z, Lee J, Brodin P, Cho S-N, Nam K, Kim J. 2013. Discovery of Q203, a potent clinical candidate for the treatment of tuberculosis. *Nat Med* 19:1157.
10. Rybníček J, Vocat A, Sala C, Busso P, Pojer F, Benjak A, Cole ST. 2015. Lansoprazole is an antituberculous prodrug targeting cytochrome *bc₁*. *Nat Commun* 6:7659.
 11. THE NIX-TB TRIAL OF PRETOMANID, BEDAQUILINE AND LINEZOLID TO TREAT XDR-TB | CROI Conference.
 12. Working Group for New TB Drugs. Pipeline | Working Group for New TB Drugs.
 13. Ballell L, Bates RH, Young RJ, Alvarez-Gomez D, Alvarez-Ruiz E, Barroso V, Blanco D, Crespo B, Escribano J, González R, Lozano S, Huss S, Santos-Villarejo A, Martín-Plaza JJ, Mendoza A, Rebollo-Lopez MJ, Remuiñán-Blanco M, Lavandera JL, Pérez-Herran E, Gamo-Benito FJ, García-Bustos JF, Barros D, Castro JP, Cammack N. 2013. Fueling Open-Source Drug Discovery: 177 Small-Molecule Leads against Tuberculosis. *Chemmedchem* 8:313–321.
 14. Singh A, Jain S, Gupta S, Das T, Tyagi AK. 2003. *mymA* operon of *Mycobacterium tuberculosis*: its regulation and importance in the cell envelope. *FEMS Microbiol Lett* 227:53–63.
 15. Daniel J, Deb C, Dubey VS, Sirakova TD, Abomoelak B, Morbidoni HR, Kolattukudy PE. 2004. Induction of a Novel Class of Diacylglycerol Acyltransferases and Triacylglycerol Accumulation in *Mycobacterium tuberculosis* as It Goes into a Dormancy-Like State in Culture. *J Bacteriol* 186:5017–5030.

16. Lamprecht DA, Finin PM, Rahman MA, Cumming BM, Russell SL, Jonnala SR, Adamson JH, Steyn AJC. 2016. Turning the respiratory flexibility of *Mycobacterium tuberculosis* against itself. *Nat Commun* 7:12393.
17. Lechartier B, Hartkoorn RC, Cole ST. 2012. In Vitro Combination Studies of Benzothiazinone Lead Compound BTZ043 against *Mycobacterium tuberculosis*. *Antimicrob Agents Chemother* 56:5790–5793.
18. Berube BJ, Parish T. 2018. Combinations of Respiratory Chain Inhibitors Have Enhanced Bactericidal Activity against *Mycobacterium tuberculosis*. *Antimicrob Agents Chemother* 62:e01677-17.
19. Abrahams KA, Cox JAG, Spivey VL, Loman NJ, Pallen MJ, Constantinidou C, Fernández R, Alemparte C, Remuiñán MJ, Barros D, Ballell L, Besra GS. 2012. Identification of Novel Imidazo[1,2-a]pyridine Inhibitors Targeting *M. tuberculosis* QcrB. *PLoS ONE* 7.
20. Arora K, Ochoa-Montaña B, Tsang PS, Blundell TL, Dawes SS, Mizrahi V, Bayliss T, Mackenzie CJ, Cleghorn LAT, Ray PC, Wyatt PG, Uh E, Lee J, Barry CE, Boshoff HI. 2014. Respiratory Flexibility in Response to Inhibition of Cytochrome c Oxidase in *Mycobacterium tuberculosis*. *Antimicrob Agents Chemother* 58:6962–6965.
21. Chandrasekera NS, Berube BJ, Shetye G, Chettiar S, O'Malley T, Manning A, Flint L, Awasthi D, Ioerger TR, Sacchettini J, Masquelin T, Hipskind PA, Odingo J, Parish T. 2017. Improved Phenoxyalkylbenzimidazoles with Activity against *Mycobacterium tuberculosis* Appear to Target QcrB. *ACS Infect Dis* 3:898–916.
22. Moraski GC, Seeger N, Miller PA, Oliver AG, Boshoff HI, Cho S, Mulugeta S, Anderson JR, Franzblau SG, Miller MJ. 2016. Arrival of Imidazo[2,1-b]thiazole-5-carboxamides: Potent Anti-tuberculosis Agents That Target QcrB. *ACS Infect Dis* 2:393–398.

23. Phummarin N, Boshoff HI, Tsang PS, Dalton J, Wiles S, Barry 3rd CE, Copp BR. 2016. SAR and identification of 2-(quinolin-4-yloxy)acetamides as *Mycobacterium tuberculosis* cytochrome bc 1 inhibitors. *Medchemcomm* 7:2122–2127.
24. Subtil FT, Villela AD, Abbadi BL, Rodrigues-Junior VS, Bizarro CV, Timmers LFSM, de Souza ON, Pissinate K, Machado P, López-Gavín A, Tudó G, González-Martín J, Basso LA, Santos DS. 2017. Activity of 2-(quinolin-4-yloxy)acetamides in *mycobacterium tuberculosis* clinical isolates and identification of their molecular target by whole genome sequencing. *Int J Antimicrob Agents*.
25. van der Westhuyzen R, Winks S, Wilson CR, Boyle GA, Gessner RK, Soares de Melo C, Taylor D, de Kock C, Njoroge M, Brunschwig C, Lawrence N, Rao SPS, Sirgel F, van Helden P, Seldon R, Moosa A, Warner DF, Arista L, Manjunatha UH, Smith PW, Street LJ, Chibale K. 2015. Pyrrolo[3,4-c]pyridine-1,3(2H)-diones: A Novel Antimycobacterial Class Targeting Mycobacterial Respiration. *J Med Chem* 58:9371–9381.
26. Boshoff HIM, Myers TG, Copp BR, McNeil MR, Wilson MA, Barry CE. 2004. The Transcriptional Responses of *Mycobacterium tuberculosis* to Inhibitors of Metabolism NOVEL INSIGHTS INTO DRUG MECHANISMS OF ACTION. *J Biol Chem* 279:40174–40184.
27. Puustinen A, Finel M, Haltia T, Gennis RB, Wikström M. 1991. Properties of the two terminal oxidases of *Escherichia coli*. *Biochemistry (Mosc)* 30:3936–3942.
28. Matsoso LG, Kana BD, Crellin PK, Lea-Smith DJ, Pelosi A, Powell D, Dawes SS, Rubin H, Coppel RL, Mizrahi V. 2005. Function of the Cytochrome bc1-aa3 Branch of the Respiratory Network in *Mycobacteria* and Network Adaptation Occurring in Response to Its Disruption. *J Bacteriol* 187:6300–6308.

29. Shi L, Sohaskey CD, Kana BD, Dawes S, North RJ, Mizrahi V, Gennaro ML. 2005. Changes in energy metabolism of *Mycobacterium tuberculosis* in mouse lung and under in vitro conditions affecting aerobic respiration. *Proc Natl Acad Sci* 102:15629–15634.
30. Small JL, Park SW, Kana BD, Ioerger TR, Sacchettini JC, Ehrt S. 2013. Perturbation of Cytochrome c Maturation Reveals Adaptability of the Respiratory Chain in *Mycobacterium tuberculosis*. *mBio* 4:e00475-13.
31. Berney M, Hartman TE, Jacobs WR. 2014. A *Mycobacterium tuberculosis* Cytochrome bd Oxidase Mutant Is Hypersensitive to Bedaquiline. *mBio* 5.
32. Kalia NP, Hasenoehrl EJ, Rahman NBA, Koh VH, Ang MLT, Sajorda DR, Hards K, Grüber G, Alonso S, Cook GM, Berney M, Pethe K. 2017. Exploiting the synthetic lethality between terminal respiratory oxidases to kill *Mycobacterium tuberculosis* and clear host infection. *Proc Natl Acad Sci* 114:7426–7431.
33. Lu P, Asseri AH, Kremer M, Maaskant J, Ummels R, Lill H, Bald D. 2018. The anti-mycobacterial activity of the cytochrome bcc inhibitor Q203 can be enhanced by small-molecule inhibition of cytochrome bd. *Sci Rep* 8:2625.
34. Segal W, Bloch H. 1956. Biochemical Differentiation of *Mycobacterium Tuberculosis* Grown in Vivo and in Vitro. *J Bacteriol* 72:132–141.
35. Daniel J, Maamar H, Deb C, Sirakova TD, Kolattukudy PE. 2011. *Mycobacterium tuberculosis* Uses Host Triacylglycerol to Accumulate Lipid Droplets and Acquires a Dormancy-Like Phenotype in Lipid-Loaded Macrophages. *PLOS Pathog* 7:e1002093.

36. Fisher MA, Plikaytis BB, Shinnick TM. 2002. Microarray Analysis of the Mycobacterium tuberculosis Transcriptional Response to the Acidic Conditions Found in Phagosomes. *J Bacteriol* 184:4025–4032.
37. Betts JC, Lukey PT, Robb LC, McAdam RA, Duncan K. 2002. Evaluation of a nutrient starvation model of Mycobacterium tuberculosis persistence by gene and protein expression profiling. *Mol Microbiol* 43:717–731.
38. Hards K, Robson JR, Berney M, Shaw L, Bald D, Koul A, Andries K, Cook GM. 2015. Bactericidal mode of action of bedaquiline. *J Antimicrob Chemother* 70:2028–2037.
39. Hards K, McMillan DGG, Schurig-Briccio LA, Gennis RB, Lill H, Bald D, Cook GM. 2018. Ionophoric effects of the antitubercular drug bedaquiline. *Proc Natl Acad Sci* 115:7326–7331.
40. Kang S, Kim RY, Seo MJ, Lee S, Kim YM, Seo M, Seo JJ, Ko Y, Choi I, Jang J, Nam J, Park S, Kang H, Kim HJ, Kim J, Ahn S, Pethe K, Nam K, No Z, Kim J. 2014. Lead Optimization of a Novel Series of Imidazo[1,2-a]pyridine Amides Leading to a Clinical Candidate (Q203) as a Multi- and Extensively-Drug-Resistant Anti-tuberculosis Agent. *J Med Chem* 57:5293–5305.
41. Palomino J-C, Martin A, Camacho M, Guerra H, Swings J, Portaels F. 2002. Resazurin Microtiter Assay Plate: Simple and Inexpensive Method for Detection of Drug Resistance in Mycobacterium tuberculosis. *Antimicrob Agents Chemother* 46:2720–2722.
42. Makarov V, Neres J, Hartkoorn RC, Ryabova OB, Kazakova E, Šarkan M, Huszár S, Piton J, Kolly GS, Vocat A, Conroy TM, Mikušová K, Cole ST. 2015. The 8-Pyrrole-Benzothiazinones Are Noncovalent Inhibitors of DprE1 from Mycobacterium tuberculosis. *Antimicrob Agents Chemother* 59:4446–4452.

43. Bolger AM, Lohse M, Usadel B. 2014. Trimmomatic: a flexible trimmer for Illumina sequence data. *Bioinformatics* 30:2114–2120.
44. Langmead B, Salzberg SL. 2012. Fast gapped-read alignment with Bowtie 2. *Nat Methods* 9:357–359.
45. Garrison E, Marth G. 2012. Haplotype-based variant detection from short-read sequencing. *ArXiv12073907 Q-Bio*.
46. Koboldt DC, Zhang Q, Larson DE, Shen D, McLellan MD, Lin L, Miller CA, Mardis ER, Ding L, Wilson RK. 2012. VarScan 2: Somatic mutation and copy number alteration discovery in cancer by exome sequencing. *Genome Res* 22:568–576.
47. van Kessel JC, Marinelli LJ, Hatfull GF. 2008. Recombineering mycobacteria and their phages. *Nat Rev Microbiol* 6:851–857.
48. Biasini M, Bienert S, Waterhouse A, Arnold K, Studer G, Schmidt T, Kiefer F, Cassarino TG, Bertoni M, Bordoli L, Schwede T. 2014. SWISS-MODEL: modelling protein tertiary and quaternary structure using evolutionary information. *Nucleic Acids Res* 42:W252–W258.
49. Schrödinger LLC. 2015. The PyMOL molecular graphics systems, version 1.8.
50. Liao Y, Smyth GK, Shi W. 2014. featureCounts: an efficient general purpose program for assigning sequence reads to genomic features. *Bioinformatics* 30:923–930.
51. Love MI, Huber W, Anders S. 2014. Moderated estimation of fold change and dispersion for RNA-seq data with DESeq2. *Genome Biol* 15:550.
52. Moosa A, Lamprecht DA, Arora K, Barry CE, Boshoff HIM, Ioerger TR, Steyn AJC, Mizrahi V, Warner DF. 2017. Susceptibility of *Mycobacterium tuberculosis* Cytochrome bd Oxidase

Mutants to Compounds Targeting the Terminal Respiratory Oxidase, Cytochrome c.

Antimicrob Agents Chemother 61:e01338-17.

TABLES AND FIGURES

Table 1 Characterization of AX series: activity against *M. tuberculosis* H37Rv, cytotoxicity and selective index

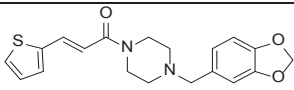
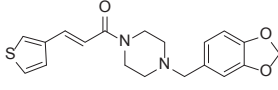
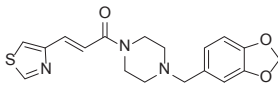
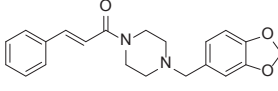
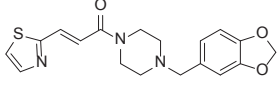
Compound ID	Structure	Anti-mycobacterial activity against <i>M. tuberculosis</i> H37Rv		Cytotoxicity in HepG2 cells TD ₅₀ (µg/ml)	Selective Index (TD ₅₀ /MIC)
		<i>in vitro</i> MIC (µg/ml)	<i>ex vivo</i> in THP-1 macrophages IC ₅₀ (µg/ml)		
AX-35		0.05	0.1	50	1000
AX-36		0.1	0.3	37.5	375
AX-37		0.1	0.2	25	250
AX-38		0.2	0.3	37.5	188
AX-39		0.3	1.8	75	250
Rifampicin		0.0008	0.1	75	93750

Table 2 Activity of **AX-35** and **AX-36** against selected microorganisms

<i>Microorganisms</i>	MIC (µg/ml)		
	AX-35	AX-36	RIF
<i>Bacillus subtilis</i>	>100	>100	0.3
<i>Candida albicans</i>	>100	>100	1.5
<i>Corynebacterium diphtheriae</i>	>100	>100	0.0004
<i>Corynebacterium glutamicum</i>	>100	>100	0.004
<i>Enterococcus faecalis</i>	>100	>100	0.6
<i>Escherichia coli</i>	74	100	6.7
<i>Listeria monocytogenes</i>	>100	>100	0.8
<i>Micrococcus luteus</i>	>100	>100	0.7
<i>Mycobacterium avium</i>	8.2	12.8	25
<i>Mycobacterium bovis BCG</i>	0.8	0.8	0.0008
<i>Mycobacterium canettii STB-L</i>	0.003	0.01	0.002
<i>Mycobacterium marinum</i>	11.5	19.6	0.5
<i>Mycobacterium massiliense</i>	7.7	10.4	26.9
<i>Mycobacterium smegmatis</i>	100	63	1.7
<i>Mycobacterium tuberculosis</i>	0.05	0.1	0.001
<i>Mycobacterium ulcerans</i>	1.6	1.6	0.01
<i>Mycobacterium vaccae</i>	12.1	26.9	2.5
<i>Pseudomonas aeruginosa</i>	>100	>100	1
<i>Pseudomonas putida</i>	>100	>100	0.2
<i>Salmonella typhimurium</i>	>100	>100	0.7
<i>Staphylococcus aureus</i>	>100	>100	3.8

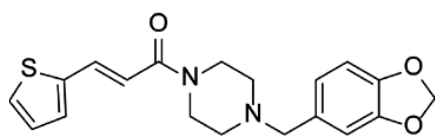


FIG 1 Molecular structure of **AX-35** (**GW861072X**)

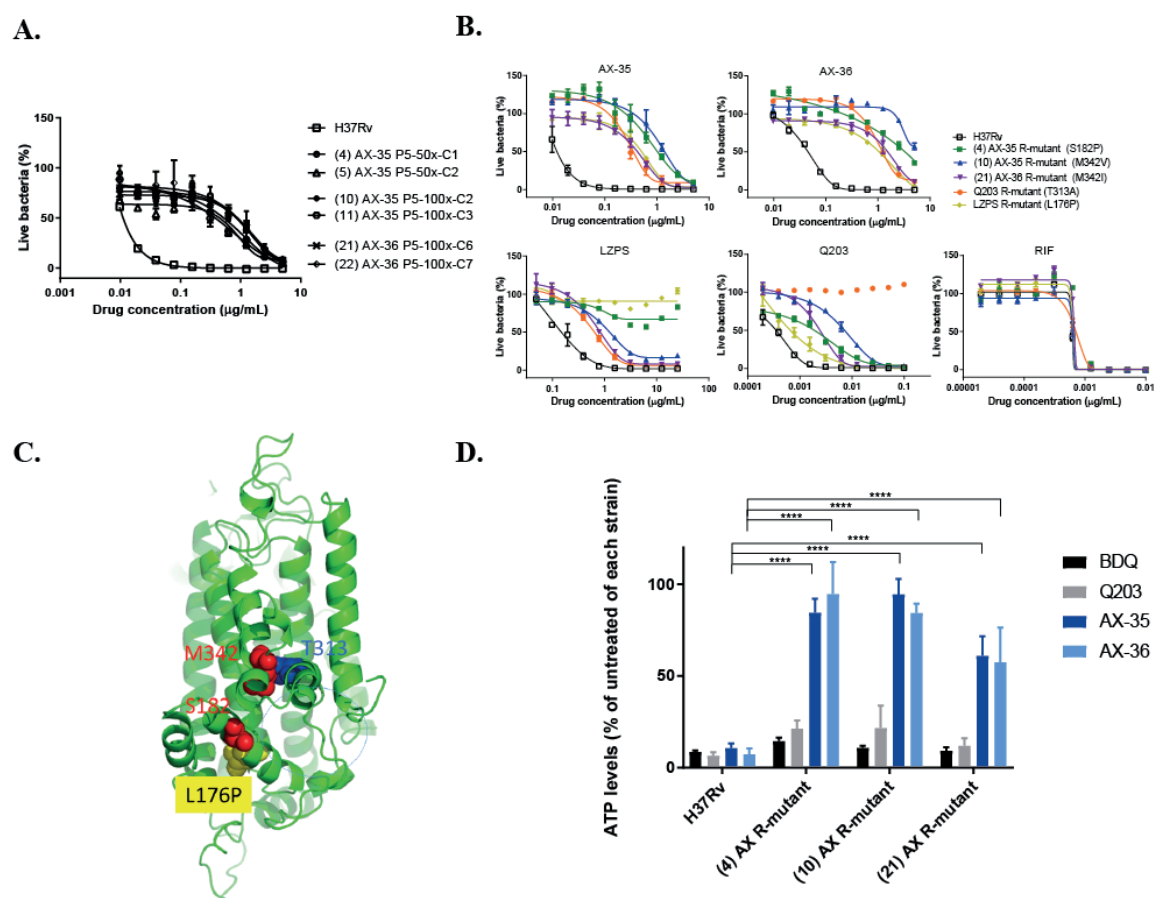


FIG 2 Evidence of AX compounds targeting QcrB of *M. tuberculosis*. (A) Dose-response curves of isolated mutants resistant to either **AX-35** or **AX-36** compared to wild-type H37Rv. Three independent 7H9 liquid cultures of *M. tuberculosis* containing 50x or 100x MIC of **AX-35** or **AX-36** at passage 5 were plated on 7H10 medium to obtain single colonies. WGS results of AX-resistant mutants reveal mutations in QcrB. (B) Dose-response curves of AX-resistant, Q203-resistant, LPZS-resistant mutants to **AX-35**, **AX-36**, LPZS, Q203, and RIF for cross-resistance studies. Data plotted are presented as mean \pm SD, curves are representative of at least two independent experiments. (C) The QcrB protein of *M. tuberculosis* was modelled on chain A of the crystal structure of the mutant *Rhodobacter sphaeroides* cytochrome *bc₁* oxidase (PDB code: 2QJK). Clustering of mutations associated with resistance to AX, Q203 and LPZS around the quinol oxidation site of QcrB, indicated by dotted blue line. (D) Intracellular ATP levels in H37Rv and AX-resistant strains were measured in the absence and presence of BDQ, Q203, **AX-35** and **AX-36** at 2.5x MIC after 24 h using BacTiter-Glo™ (Promega). Data from two independent experiments are presented as mean \pm SD. Statistical analysis was performed using two-way ANOVA, Tukey's multiple comparison test (**** p <0.0001).

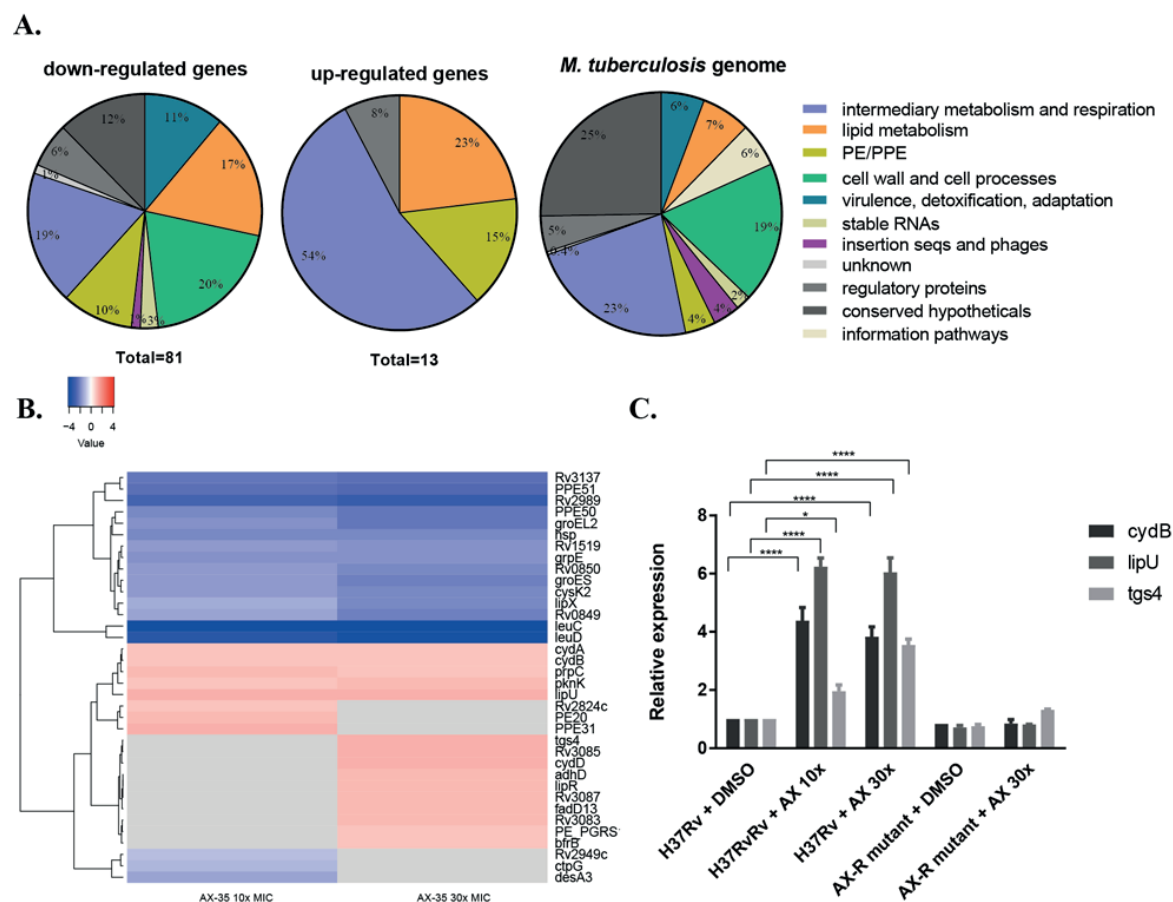


FIG 3 Transcriptional response of *M. tuberculosis* to **AX-35** treatment by RNA-seq. (A) Global transcriptomic response and involvement of different metabolic responses, based on TubercuList classification (<https://mycobrowser.epfl.ch/>), after exposure of two independent cultures of *M. tuberculosis* H37Rv to **AX-35** at 10x and 30x MIC for 4 h. (B) Heat map representing top significantly differentially regulated *M. tuberculosis* genes ($p_{adj} \leq 0.05$). Colour scale indicates differential regulation as \log_2 fold-change of H37Rv with **AX-35** treatment relative to H37Rv with vehicle control, DMSO. Up-regulation is indicated in red, down-regulation in blue and insignificant \log_2 fold-change values for the condition are in grey. Data are from two independent experiments. (C) qPCR validation of genes, *cydB*, *lipU*, and *tgs4* in H37Rv and AX-resistant mutant strains treated with vehicle (DMSO) or **AX-35**. Data are presented as mean \pm SD of two independent cultures. Statistical analysis was performed using two-way ANOVA with Tukey's multiple comparison test ($*p < 0.05$, $****p < 0.0001$).

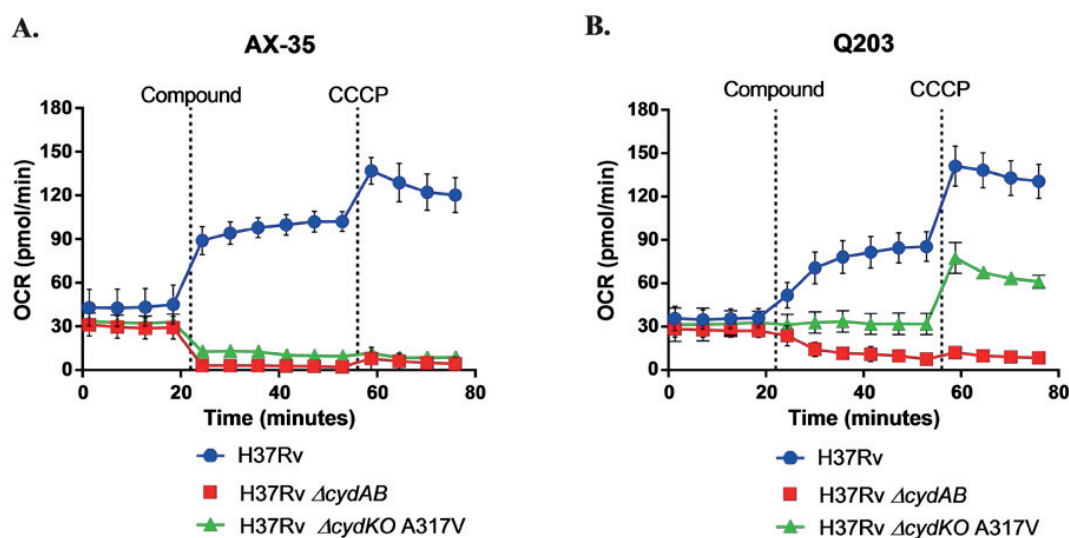


FIG 4 Bioenergetic flux profiles of *M. tuberculosis* with **AX-35** or **Q203** treatment. Oxygen consumption rate of wild-type H37Rv, H37Rv $\Delta cydAB$ and H37Rv $\Delta cydKO$ with a QcrB A317V mutation (Q203-resistance SNP) measured at basal levels, then in the presence of (A) **AX-35** (final concentration of 14 μ M, 100x MIC₅₀) or (B) **Q203** (final concentration of 0.3 μ M, 100x MIC₅₀), and then at maximum capability with the depolarization of the bacterial membrane by the protonophore carbonyl cyanide *m*-chlorophenyl hydrazine (CCCP).

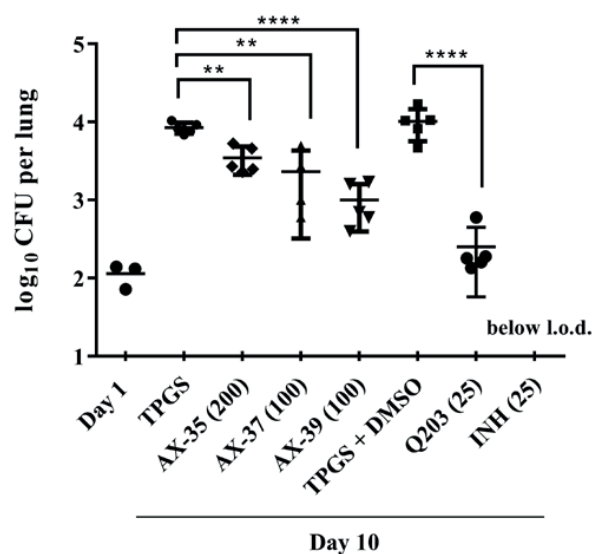
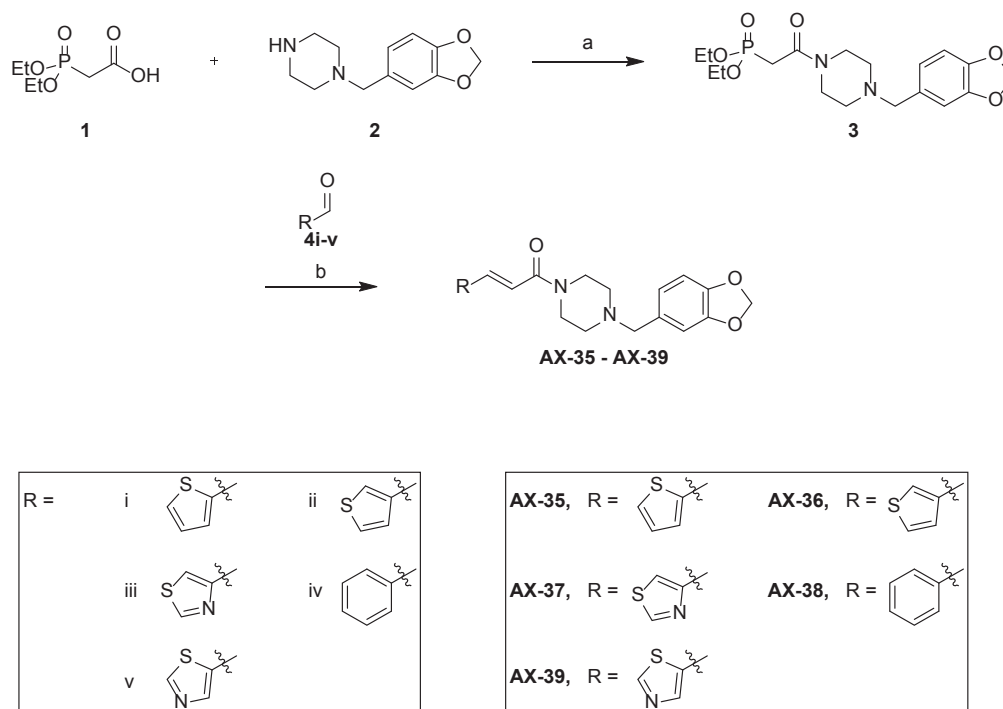


FIG 5 Activity of AX compounds assessed in a mouse model of acute TB. One day after low-dose aerosol M. tuberculosis infection, groups of five mice were treated with vehicle controls (TPGS 20% or TPGS 20% with 1% DMSO) or with compounds administered by oral gavage for ten days daily at the doses indicated (mg/kg). AX compounds were prepared in TPGS 20%, Q203 in TPGS 20% with 1% DMSO and INH in ddH₂O. Bacterial burden (CFU) was determined from lung homogenates. Data from one experiment is presented as mean \pm SD. Statistical analysis was performed using one-way ANOVA, Tukey's multiple comparison test (** $p < 0.01$, **** $p < 0.0001$). L.o.d. indicates limit of detection.

SUPPLEMENTAL MATERIAL - SYNTHESIS AND CHARACTERIZATION DATA OF AX-35 AND ANALOGS

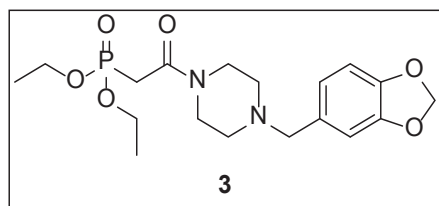
General information. All reactions were performed under an argon atmosphere using flame-dried glassware and standard syringe/septa techniques. CH₂Cl₂ and THF used for reactions were distilled under argon prior to use (CH₂Cl₂ from CaH₂ and THF from Na/benzophenone). All other absolute solvents were purchased as anhydrous grade from Acros (puriss.; dried over molecular sieves; H₂O <0.005 %) and used without further purification. Solvents for extractions, flash column chromatography and thin layer chromatography (TLC) were either purchased as commercial grade and distilled prior to use or purchased as HPLC grade. All other commercially available reagents were used without further purification. Reactions were magnetically stirred and monitored by TLC performed on Merck TLC aluminum sheets (silica gel 60 F254). Spots were visualized with UV light ($\lambda = 254$ nm) or through staining with Ce₂(SO₄)₃/phosphomolybdic acid/H₂SO₄ (CPS), or KMnO₄/K₂CO₃. NaHCO₃ and brine (NaCl) refer to aqueous saturated solutions. Chromatographic purification of products was performed using either Sigma-Aldrich or SiliCycle silica gel 60 for preparative column chromatography (particle size 40-63 μ m). ¹H-, ¹³C- and ³¹P-NMR spectra were recorded on a Bruker AV-400 400 MHz. Chemical shifts (δ) are reported in ppm and are referenced to chloroform (δ 7.26 ppm for ¹H, δ 77.16 ppm for ¹³C). All ¹³C-NMR spectra were measured with complete proton decoupling. Data for NMR spectra are reported as follows: s = singlet, d = doublet, t = triplet, q = quartet, quint = quintet, sept = septet, m = multiplet, br = broad signal, app. = apparent. Infrared spectra (IR) were recorded on a Jasco FT/IR-6200 instrument. Resonance frequencies are given as wavenumbers in cm⁻¹. High resolution mass spectra (HRMS) were recorded on a Bruker maXis (ESI) by the ETH Zürich MS service.

Synthesis of AX-35 and analogs. AX-35 (originally **GW861072X** in Ballell *et al.*, 2013) was synthesized in two steps. EDC-mediated amide coupling of diethylphosphonoacetic acid (**1**) with 1-piperonylpiperazine (**2**) provided phosphonate **3** in 96% yield. Subsequent HWE-reaction with thiophen-2-carbaldehyde (**4i**) afforded **AX-35** in 90% yield (scheme 1). Using intermediate **3** with the corresponding aldehyde in the HWE-reaction, four different analogs, **AX-36** - **AX-39**, were synthesized for initial SAR investigation (scheme 1).



Scheme 1. Reagents and conditions: (a) EDC, HOBT, Et₃N, DCM, 80 °C (MW), 3 h, 96%; (b) Aldehydes **4i-v**, NaH, THF, rt, 18 h, 86-98%.

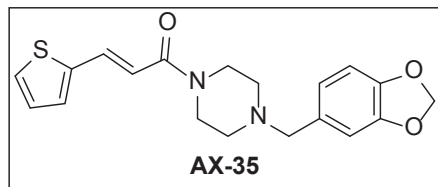
Diethyl (2-(4-(benzo[d][1,3]dioxol-5-ylmethyl)piperazin-1-yl)-2-oxoethyl)phosphonate (3)



Diethylphosphonoacetic acid (**1**) (434.6 μ L, 2.70 mmol, 1.20 eq.), HOBt (365.3 mg, 2.70 mmol, 1.20 eq.), EDC (476.9 μ L, 2.70 mmol, 1.20 eq.), Et₃N (374.6 μ L, 2.70 mmol, 1.20 eq.), and 1-piperonylpiperazine (**2**) (496.2 mg, 2.25 mmol, 1.00 eq.) were dissolved in DCM (5.0 mL). The mixture was heated in the microwave at 80 °C for 3 h, quenched with saturated NaHCO₃ (10 mL) and extracted with DCM (3 x 10 mL). The combined organic layers dried over MgSO₄, filtered and concentrated in *vacuo*. Flash chromatography (DCM/MeOH 98:2 to 95:5 to 9:1) provided phosphonate **3** (864.1 mg, 2.17 mmol, 96%) as a yellow oil.

TLC (SiO₂; DCM/MeOH 95:5, UV): R_f = 0.16. **¹H-NMR** (400 MHz, CDCl₃): δ (ppm) = 6.69 (s, 1H), 6.60 – 6.55 (m, 2H), 5.78 (s, 2H), 4.01 (dq, J = 8.2, 7.1 Hz, 4H), 3.52 – 3.39 (m, 4H), 3.27 (s, 2H), 2.91 (d, J = 22.0 Hz, 2H), 2.29 (dt, J = 31.6, 5.1 Hz, 4H), 1.19 (t, J = 7.1 Hz, 6H). **¹³C-NMR** (101 MHz, CDCl₃): δ (ppm) = 162.8 (d, $^2J_{C-P}$ = 7.0 Hz), 147.4, 146.5, 131.2, 121.9, 109.0, 107.6, 100.7, 62.3, 62.2 (d, $^2J_{C-P}$ = 7.2 Hz), 52.6, 52.2, 46.7, 41.7, 33.0 (d, $^1J_{C-P}$ = 132.8 Hz), 16.1 (d, $^3J_{C-P}$ = 8.7 Hz). **³¹P-NMR** (162 MHz, CDCl₃): δ (ppm) = 21.1 (m). **IR** (thin film): ν = 2980, 2924, 2813, 1641, 1502, 1489, 1441, 1394, 1367, 1341, 1247, 1139, 1095, 1028, 966, 867, 810, 789, 720, 676, 591, 576 cm⁻¹. **HR-MS** (ESI): Calcd for C₁₈H₂₈N₂O₆P [M+H]⁺, 399.1679 m/z ; Found, 399.1676 m/z .

(E)-1-(4-(Benzo[d][1,3]dioxol-5-ylmethyl)piperazin-1-yl)-3-(thiophen-2-yl)prop-2-en-1-one
(AX-35)

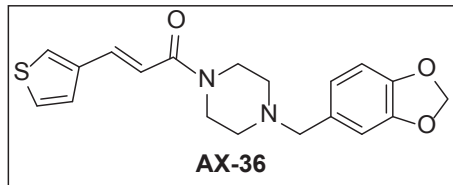


To a solution of **3** (753.1 mg, 1.89 mmol, 1.00 eq.) in THF (25.0 mL) were added NaH (54.4 mg, 2.27 mmol, 1.20 eq.) and thiophen-2-carbaldehyde (**4i**) (210.1 μ L, 2.27 mmol, 1.20 eq.). The reaction mixture was stirred at rt for 18 h, filtered through celite, then concentrated in *vacuo*. Flash chromatography (DCM/MeOH 98:2 to 95:5) provided **AX-35** (608.5 mg, 1.71 mmol, 90%) as a yellow oil.

TLC (SiO₂; DCM/MeOH 98:2, UV): R_f = 0.22. **¹H-NMR** (400 MHz, CDCl₃): δ (ppm) = 7.76 (dt, J = 15.1, 0.8 Hz, 1H), 7.25 (dt, J = 5.1, 1.0 Hz, 1H), 7.15 (dt, J = 3.5, 0.8 Hz, 1H), 6.97 (dd, J = 5.1, 3.6 Hz, 1H), 6.83 – 6.80 (m, 1H), 6.72 – 6.67 (m, 2H), 6.63 (d, J = 15.1 Hz, 1H), 5.88 (s, 2H), 3.62 (d, J = 46.2 Hz, 4H), 3.38 (s, 2H), 2.42 – 2.36 (m, 4H). **¹³C-NMR** (101 MHz, CDCl₃): δ (ppm) = 165.1, 147.9, 146.9, 140.6, 135.6, 131.7, 130.3, 128.1, 127.2, 122.32, 116.0, 109.5, 108.0, 101.1, 62.7, 62.6, 53.3, 52.7, 45.9, 42.3. **IR** (thin film): ν = 3069, 3005, 2895, 2810, 2772, 1638, 1597, 1501, 1488, 1439, 1416, 1367, 1335, 1298, 1282, 1269, 1238, 1205, 1145, 1114, 1096, 1037, 1000, 966, 932, 922, 864, 822, 810, 791, 703, 651, 575, 534, 518, 490 cm^{-1} . **HR-MS** (ESI): Calcd for C₁₉H₂₁N₂O₃S [M+H]⁺, 357.1267 m/z ; Found, 357.1264 m/z .

(E)-1-(4-(Benzo[d][1,3]dioxol-5-ylmethyl)piperazin-1-yl)-3-(thiophen-3-yl)prop-2-en-1-one

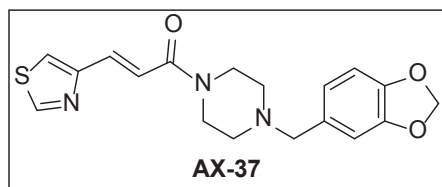
(AX-36)



To a solution of **3** (1.51 g, 3.79 mmol, 1.00 eq.) in THF (50.0 mL) were added NaH (109.0 mg, 4.54 mmol, 1.20 eq.) and thiophen-3-carbaldehyde (**4ii**) (415.0 μ L, 4.54 mmol, 1.20 eq.). The reaction mixture was stirred at rt for 18 h, filtered through celite, then concentrated in *vacuo*. Flash chromatography (DCM/MeOH 98:2 to 95:5) provided **AX-36** (1.30 g, 3.64 mmol, 96%) as a yellow oil.

TLC (SiO₂; DCM/MeOH 95:5, UV): R_f = 0.17. **¹H-NMR** (400 MHz, CDCl₃): δ (ppm) = 8.18 (d, J = 15.3 Hz, 1H), 7.94 (dd, J = 2.8, 1.3 Hz, 1H), 7.83 – 7.78 (m, 2H), 7.37 (d, J = 1.3 Hz, 1H), 7.29 – 7.17 (m, 3H), 6.45 (s, 2H), 4.28 – 4.09 (m, 4H), 3.94 (s, 2H), 2.99 – 2.92 (m, 4H). **¹³C-NMR** (101 MHz, CDCl₃): δ (ppm) = 165.4, 147.7, 146.7, 138.2, 136.3, 131.5, 126.8, 126.7, 125.1, 122.1, 116.7, 109.3, 107.9, 100.9, 62.5, 53.1, 52.6, 45.8, 42.1. **IR** (thin film): ν = 3675, 3077, 2987, 2971, 2900, 2811, 2772, 2238, 1731, 1645, 1599, 1502, 1488, 1439, 1412, 1368, 1335, 1298, 1283, 1270, 1239, 1146, 1114, 1094, 1038, 1000, 975, 908, 867, 809, 781, 727, 645, 606, 573, 524, 425 cm⁻¹. **HR-MS** (ESI): Calcd for C₁₉H₂₁N₂O₃S [M+H]⁺, 357.1267 m/z ; Found, 357.1271 m/z .

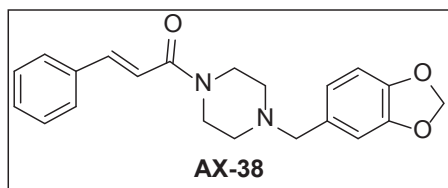
(*E*)-1-(4-(Benzo[d][1,3]dioxol-5-ylmethyl)piperazin-1-yl)-3-(1 λ^3 ,3 λ^2 -thiazol-4-yl)prop-2-en-1-one (**AX-37**)



To a solution of **3** (1.51 g, 3.79 mmol, 1.00 eq.) in THF (50.0 mL) were added NaH (109.2 mg, 4.55 mmol, 1.20 eq.) and thiazole-4-carbaldehyde (**4iii**) (515.0 mg, 4.55 mmol, 1.20 eq.). The reaction mixture was stirred at rt for 18 h, filtered through celite, then concentrated in *vacuo*. Flash chromatography (DCM/MeOH 98:2 to 95:5) provided **AX-37** (1.32 g, 3.70 mmol, 98%) as a yellow oil.

TLC (SiO₂; DCM/MeOH 95:5, UV): *R_f* = 0.14. **¹H-NMR** (400 MHz, CDCl₃): δ (ppm) = 8.83 – 8.74 (m, 1H), 7.64 (dd, *J* = 14.9, 0.8 Hz, 1H), 7.40 (d, *J* = 2.0 Hz, 1H), 7.30 (d, *J* = 15.0 Hz, 1H), 6.84 (d, *J* = 1.3 Hz, 1H), 6.76 – 6.68 (m, 2H), 5.93 (s, 2H), 3.69 (dt, *J* = 28.2, 4.8 Hz, 4H), 3.41 (s, 2H), 2.46 – 2.40 (m, 4H). **¹³C-NMR** (101 MHz, CDCl₃): δ (ppm) = 165.2, 153.7, 153.6, 153.2, 153.1, 147.7, 146.8, 134.2, 131.5, 122.2, 120.2, 119.8, 109.4, 107.9, 100.9, 62.6, 53.2, 52.6, 45.9, 42.2. **IR** (thin film): ν = 3078, 2891, 2811, 2772, 2236, 1646, 1604, 1501, 1488, 1439, 1367, 1334, 1267, 1248, 1238, 1204, 1145, 1114, 1095, 1038, 999, 973, 909, 879, 819, 791, 726, 645, 594, 574, 528, 486 cm⁻¹. **HR-MS** (ESI): Calcd for C₁₈H₂₀N₃O₃S [M+H]⁺, 358.1220 *m/z*; Found, 358.1223 *m/z*.

(*E*)-1-(4-(Benzo[d][1,3]dioxol-5-ylmethyl)piperazin-1-yl)-3-phenylprop-2-en-1-one (**AX-38**)

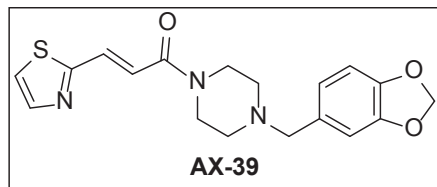


To a solution of **3** (1.50 g, 3.77 mmol, 1.00 eq.) in THF (50.0 mL) were added NaH (108.4 mg, 4.52 mmol, 1.20 eq.) and benzaldehyde (**4iv**) (459.0 μ L, 4.52 mmol, 1.20 eq.). The reaction mixture was stirred at rt for 18 h, filtered through celite, then concentrated in *vacuo*. Flash chromatography (DCM/MeOH 98:2 to 95:5) provided **AX-38** (1.24 g, 3.53 mmol, 94%) as a yellow oil.

TLC (SiO₂; DCM/MeOH 95:5, UV): R_f = 0.26. **¹H-NMR** (400 MHz, CDCl₃): δ (ppm) = 7.65 (d, J = 15.4 Hz, 1H), 7.54 – 7.46 (m, 2H), 7.40 – 7.28 (m, 3H), 6.92 – 6.81 (m, 2H), 6.79 – 6.64 (m, 2H), 5.92 (s, 2H), 3.68 (d, J = 39.6 Hz, 4H), 3.42 (s, 2H), 2.53 – 2.36 (m, 4H). **¹³C-NMR** (101 MHz, CDCl₃): δ (ppm) = 165.4, 147.8, 146.8, 142.7, 135.3, 131.6, 129.6, 128.8, 127.8, 122.2, 117.2, 109.4, 107.9, 101.0, 62.6, 53.2, 52.6, 52.6, 45.9, 42.2. **IR** (thin film): ν = 3060, 2810, 2772, 2236, 1646, 1603, 1500, 1488, 1438, 1366, 1334, 1301, 1238, 1205, 1145, 1115, 1096, 1038, 999, 976, 920, 863, 810, 762, 727, 705, 685, 645, 565, 530, 482 cm⁻¹. **HR-MS** (ESI): Calcd for C₂₁H₂₃N₂O₃ [M+H]⁺, 351.1703 m/z ; Found, 351.1707 m/z .

(E)-1-(4-(Benzo[d][1,3]dioxol-5-ylmethyl)piperazin-1-yl)-3-(thiazol-2-yl)prop-2-en-1-one

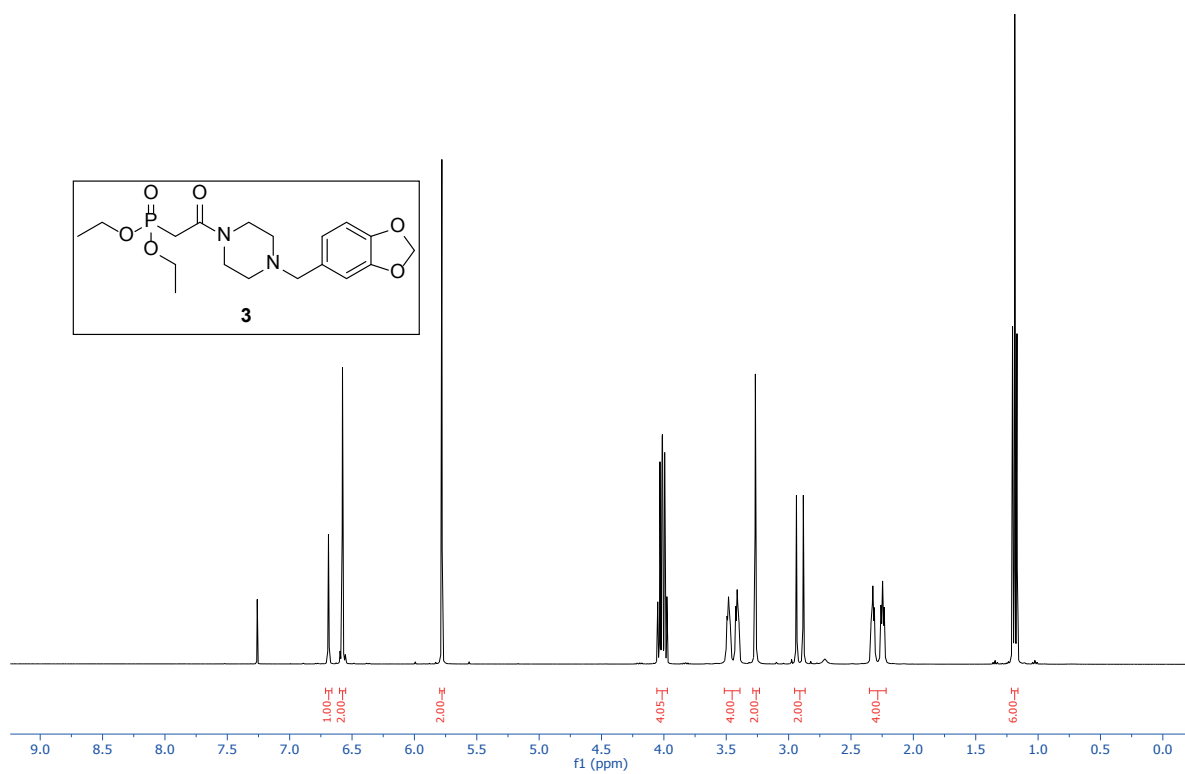
(AX-39)

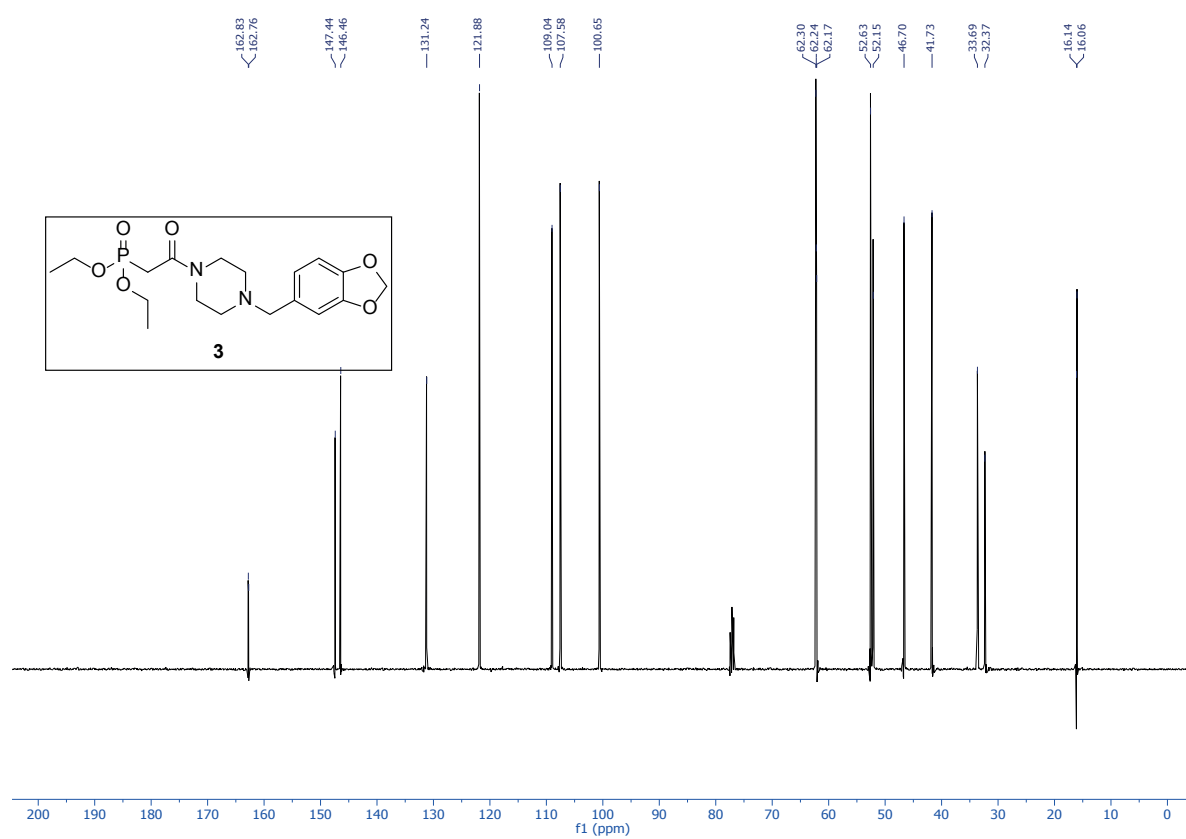


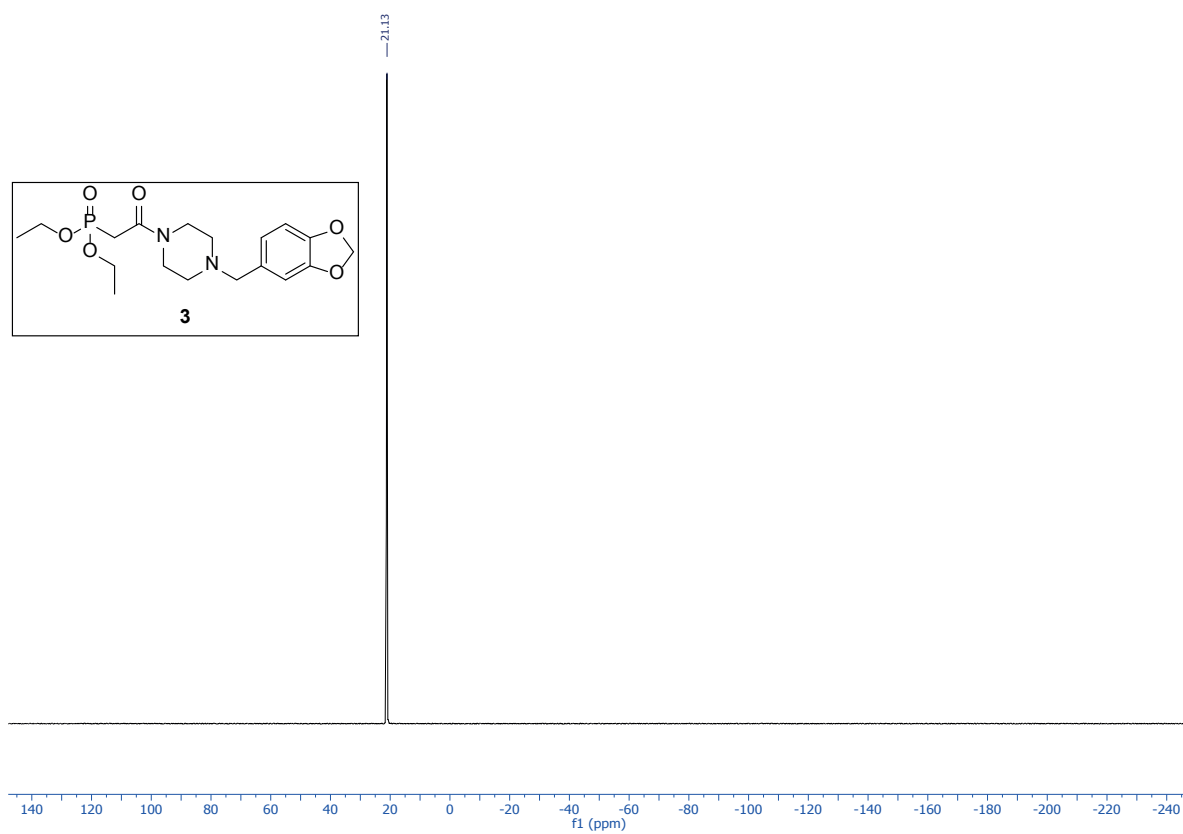
To a solution of **3** (1.76 g, 4.42 mmol, 1.00 eq.) in THF (50.0 mL) were added NaH (127.2 mg, 5.30 mmol, 1.20 eq.) and thiazole-2-carbaldehyde (**4v**) (465.6 μ L, 5.30 mmol, 1.20 eq.). The reaction mixture was stirred at rt for 18 h, filtered through celite, then concentrated in *vacuo*. Flash chromatography (DCM/MeOH 98:2 to 95:5) provided **AX-39** (1.35 g, 3.78 mmol, 86%) as an orange oil.

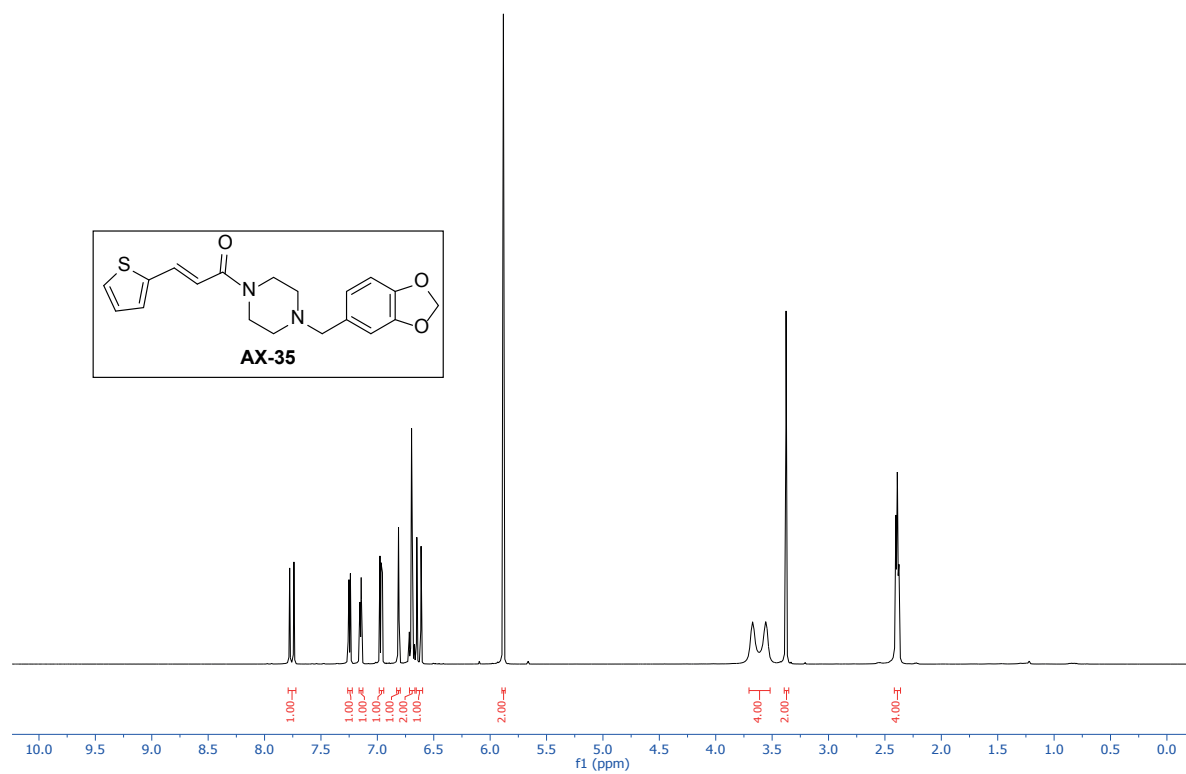
TLC (SiO₂; DCM/MeOH 95:5, UV): R_f = 0.38. **¹H-NMR** (400 MHz, CDCl₃): δ (ppm) = 7.83 (d, J = 3.2 Hz, 1H), 7.69 (d, J = 15.1 Hz, 1H), 7.36 (d, J = 3.2 Hz, 1H), 7.26 (d, J = 15.1 Hz, 1H), 6.81 (d, J = 1.3 Hz, 1H), 6.72 – 6.67 (m, 2H), 5.90 (s, 2H), 3.65 (dt, J = 33.7, 4.9 Hz, 4H), 3.39 (s, 2H), 2.44 – 2.38 (m, 4H). **¹³C-NMR** (101 MHz, CDCl₃): δ (ppm) = 164.2, 147.9, 146.9, 144.5, 133.5, 131.6, 122.3, 121.7, 121.1, 109.5, 108.1, 101.1, 62.7, 53.3, 52.6, 46.1, 42.5. **IR** (thin film): ν = 3448, 3075, 2900, 2811, 2773, 1733, 1643, 1605, 1501, 1487, 1439, 1397, 1367, 1334, 1289, 1238, 1137, 1114, 1094, 1037, 999, 966, 932, 875, 810, 791, 768, 733, 707, 656, 617, 590, 577, 519 cm⁻¹. **HR-MS** (ESI): Calcd for C₁₈H₂₀N₃O₃S [M+H]⁺, 358.1220 m/z ; Found, 358.1227 m/z .

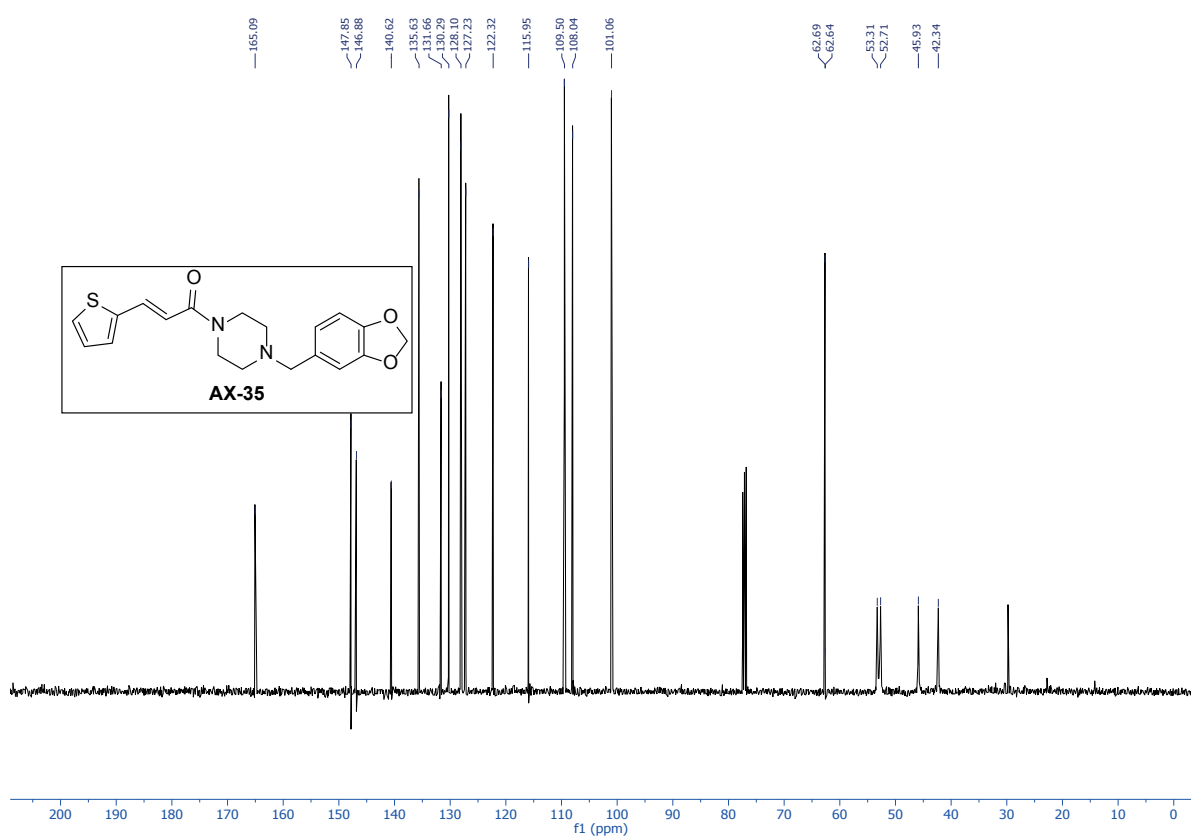
¹H-, ¹³C- AND ³¹P-NMR SPECTRA

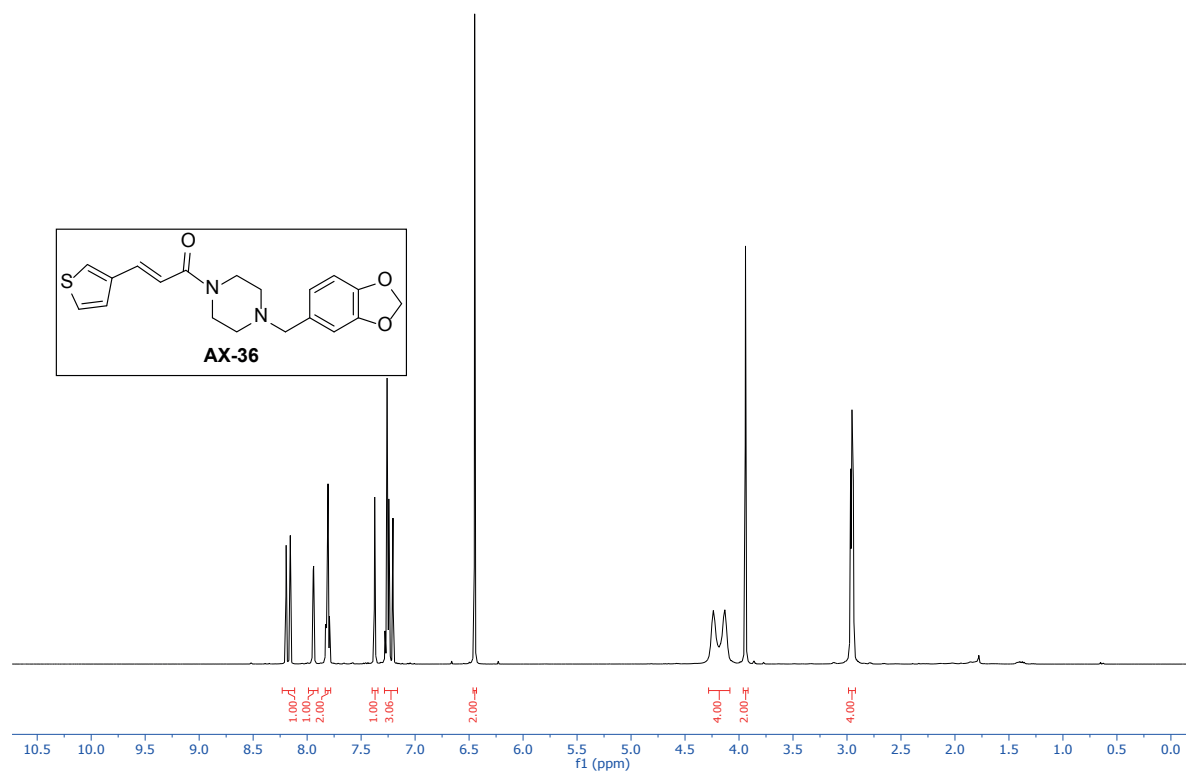


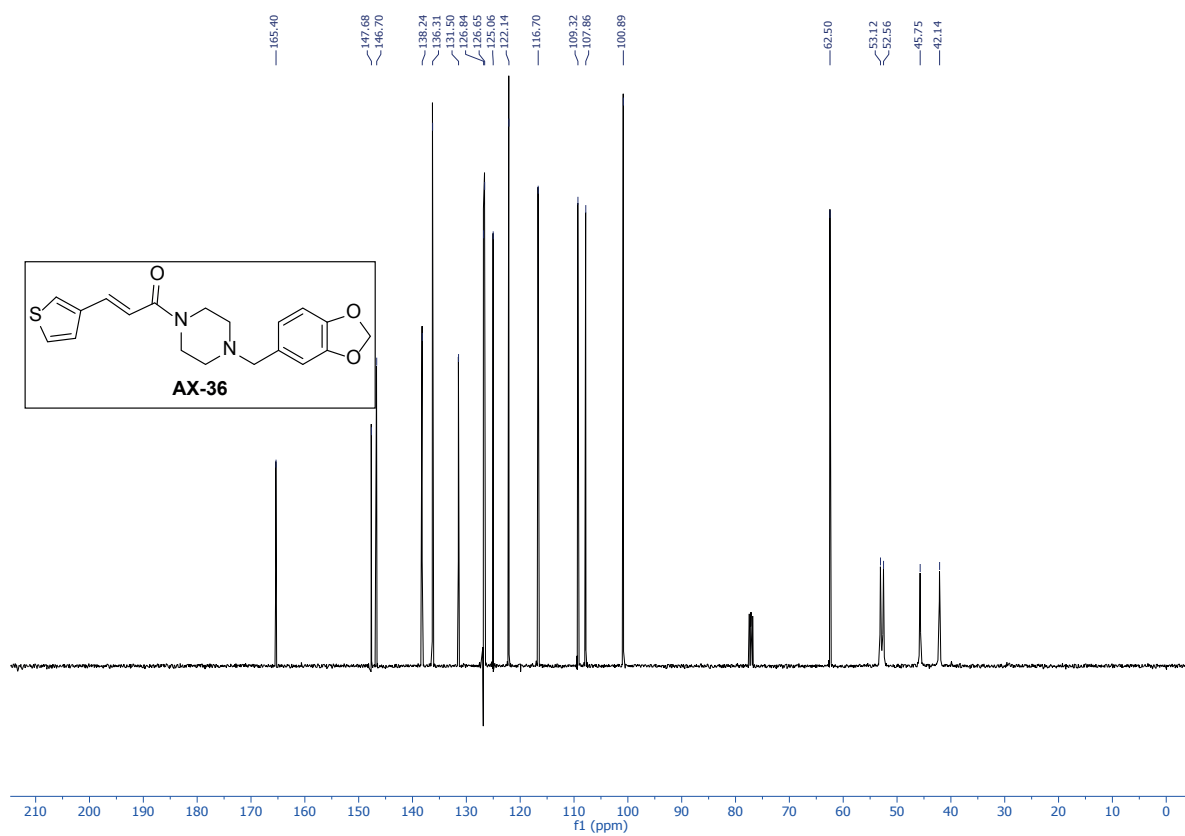


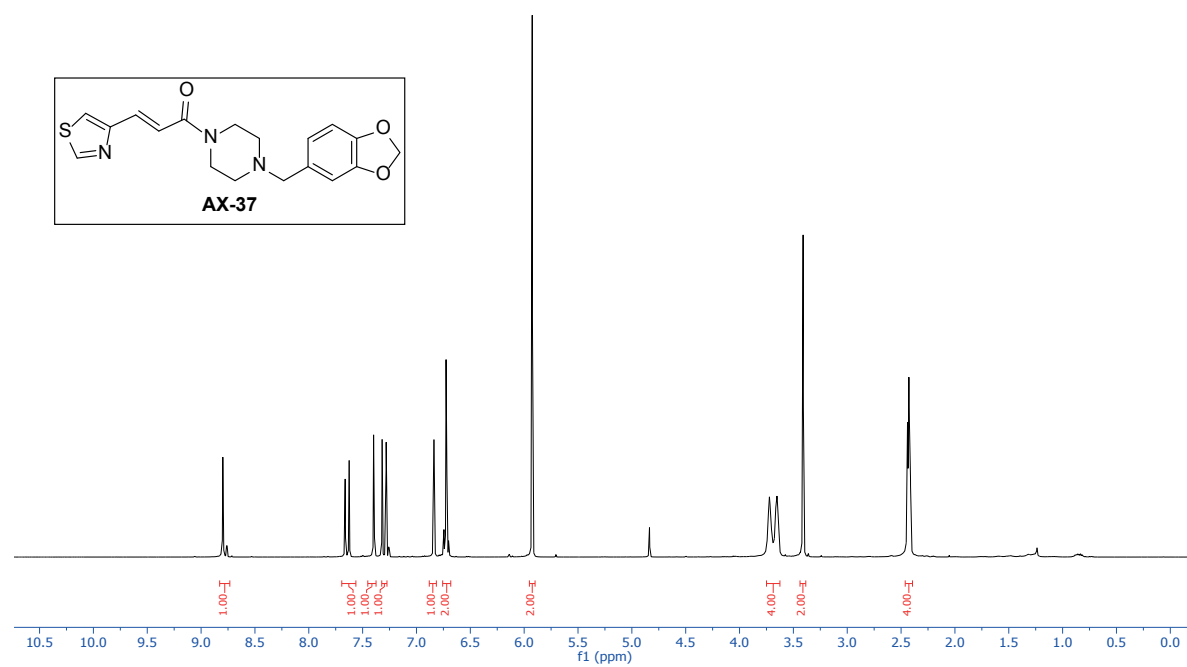


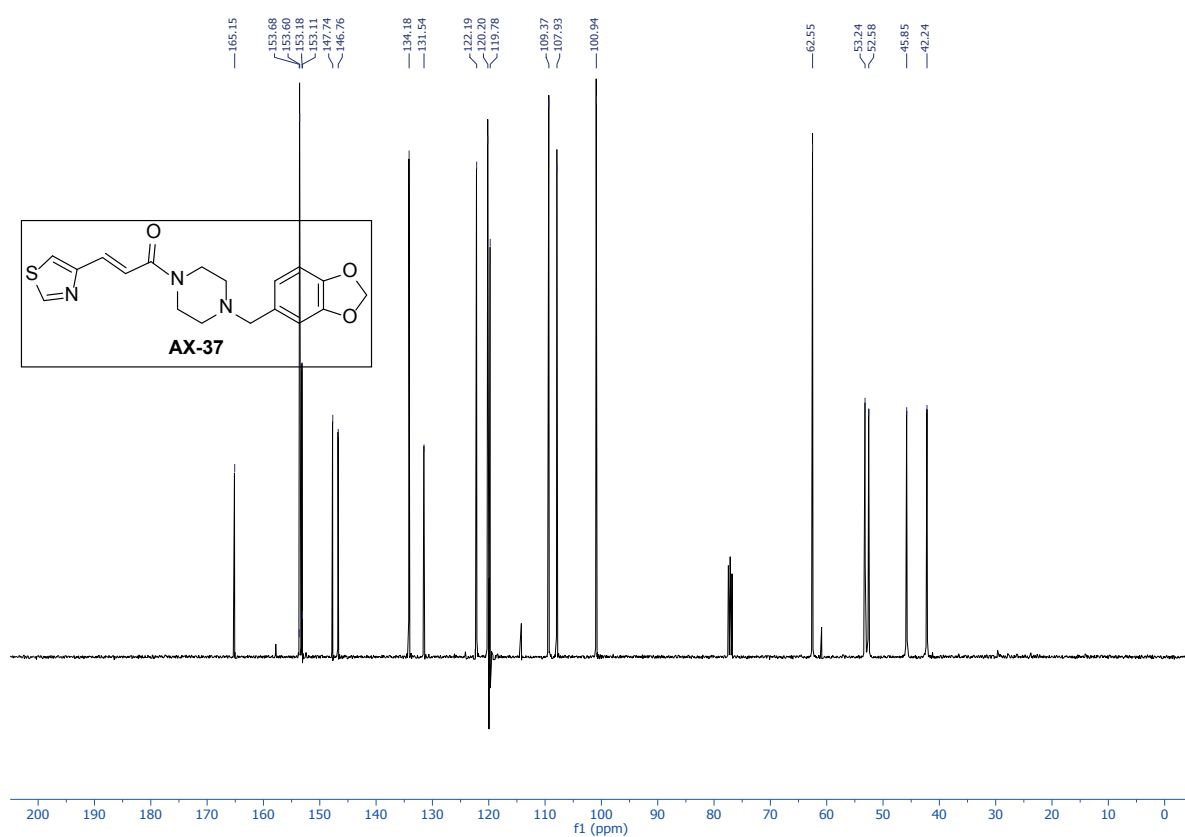


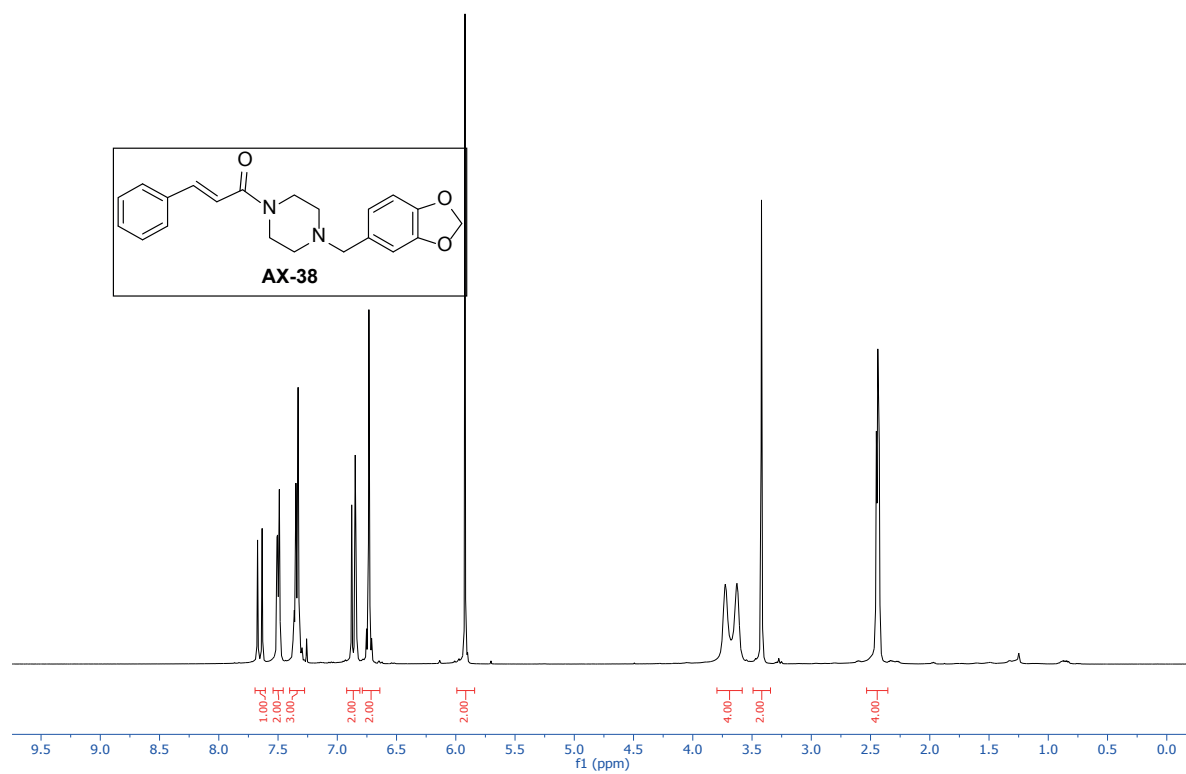


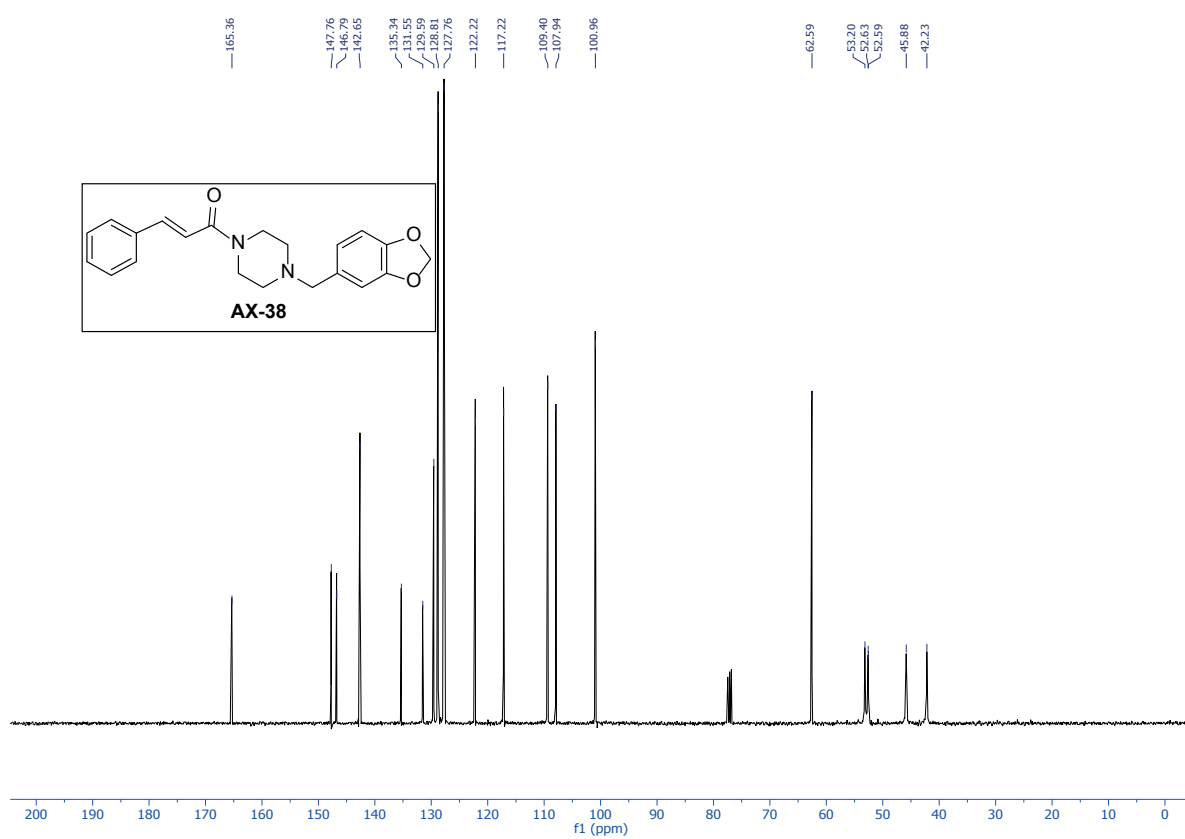


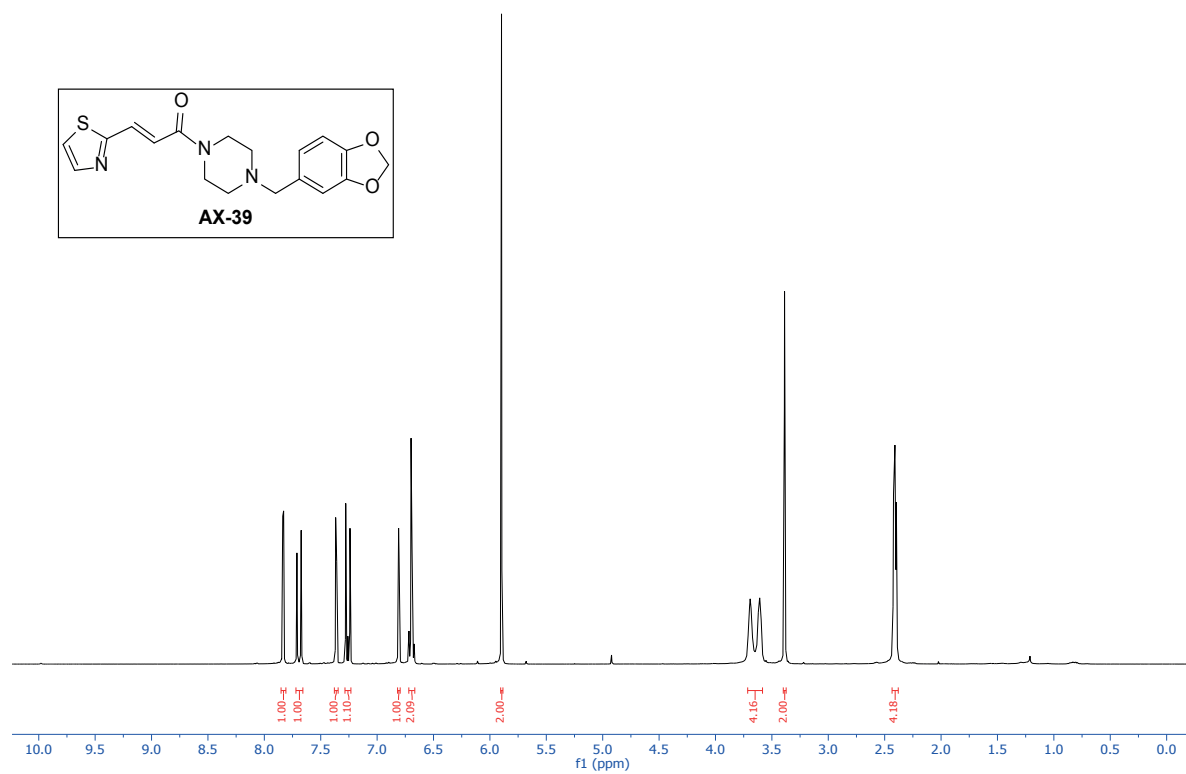


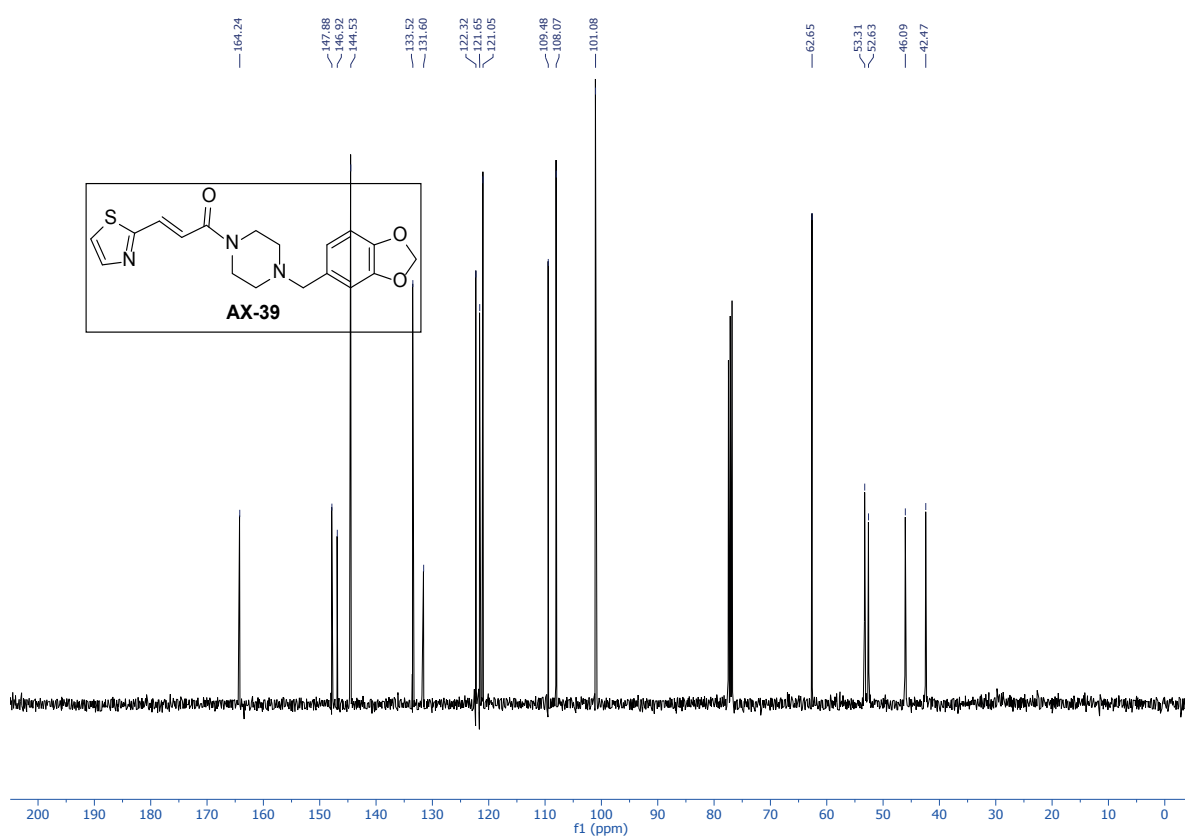












SUPPLEMENTARY METHODS

Assessment of efficacy in a chronic mouse model of TB. Female BALB/c mice (5-6 weeks old, 20g) from Charles River Laboratories were infected with a low-dose aerosol of *M. tuberculosis* H37Rv. Treatment was initiated 4 weeks after the infection by oral gavage 5 days a week over 4 weeks. INH was prepared at 25 mg/kg in ddH₂O, Q203 at 10 mg/kg in TPGS 20% (as described in (1) and AX derivatives at 10 mg/kg in TPGS 20%. The non-treated group received the vehicle TPGS 20% alone. Compounds were ground with a pestle and mortar followed by sonication at room temperature for 30 min. Compound solutions were stored at 4°C and freshly prepared at the start of each week. The day after the final treatment, all groups were sacrificed and serial dilutions of lung and spleen homogenates were plated on 7H10 agar containing 10 µg/ml cyclohexamide and 25 µg/ml ampicillin. Experiments were approved by the Swiss Cantonal Veterinary Authority (authorisation number 3082).

Checkerboard assays for two-drug combinations containing AX-35. Interactions between AX-35 and PBTZ169, BDQ or CFM were determined using the checkerboard assay (2, 3). *M. tuberculosis* H37Rv was grown to log-phase in 7H9 media and diluted to an OD₆₀₀ of 0.0001. 75 µl of bacterial suspension (about 10³ cells) was added per well of a 96-well plate. PBTZ169, BDQ or CFM were two-fold serially diluted column-wise (1st compound). AX-35 was prepared in 7H9 medium starting at 8x MIC and serial dilutions were made to 0.125x. 25 µl of diluted compound at each concentration was added to a row of the 96-well plate. After incubation of the plates for 6 days at 37°C, 10 µl of 0.025% resazurin was added. The fluorescence intensity was read after 24 h incubation using an Infinite F200 Tecan plate reader. For rows where an MIC value could be determined, the fractional inhibitory concentration index (ΣFIC index) was calculated using the equation $\Sigma\text{FIC index} = \text{FIC}_{1\text{st compound}} + \text{FIC}_{\text{AX-35}} = (\text{MIC of } 1^{\text{st}} \text{ compound, tested in combination}) / (\text{MIC of } 1^{\text{st}} \text{ compound, alone}) + (\text{MIC of AX-35, tested$

in combination)/(MIC of AX-35, alone). Σ FIC index ≤ 0.5 indicates synergism, $0.5 < \Sigma$ FIC index ≤ 4 additivity, and Σ FIC index > 4 antagonism.

REFERENCES

1. Pethe K, Bifani P, Jang J, Kang S, Park S, Ahn S, Jiricek J, Jung J, Jeon HK, Cechetto J, Christophe T, Lee H, Kempf M, Jackson M, Lenaerts AJ, Pham H, Jones V, Seo MJ, Kim YM, Seo M, Seo JJ, Park D, Ko Y, Choi I, Kim R, Kim SY, Lim S, Yim S-A, Nam J, Kang H, Kwon H, Oh C-T, Cho Y, Jang Y, Kim J, Chua A, Tan BH, Nanjundappa MB, Rao SPS, Barnes WS, Wintjens R, Walker JR, Alonso S, Lee S, Kim J, Oh S, Oh T, Nehrbass U, Han S-J, No Z, Lee J, Brodin P, Cho S-N, Nam K, Kim J. 2013. Discovery of Q203, a potent clinical candidate for the treatment of tuberculosis. *Nat Med* 19:1157.
2. Reddy VM, Einck L, Andries K, Nacy CA. 2010. In Vitro Interactions between New Antitubercular Drug Candidates SQ109 and TMC207. *Antimicrob Agents Chemother* 54:2840–2846.
3. Lechartier B, Hartkoorn RC, Cole ST. 2012. In Vitro Combination Studies of Benzothiazinone Lead Compound BTZ043 against *Mycobacterium tuberculosis*. *Antimicrob Agents Chemother* 56:5790–5793.

SUPPLEMENTARY TABLES

Table S1 Intrinsic clearance (Cl_{int}) and clearance category of AX derivatives in mouse and human liver microsomes

	Mouse microsomes		Human microsomes	
	Clearance Category	Clint ($\mu\text{l}/\text{min}/\text{mg}$)	Clearance Category	Clint ($\mu\text{l}/\text{min}/\text{mg}$)
AX-35	high	119.6	medium	21.7
AX-36	high	116.8	medium	16.8
AX-37	N.D.	N.D.	N.D.	N.D.
AX-38	high	63.8	medium	13.3
AX-39	N.D.	N.D.	N.D.	N.D.
Carbamazepine	low	0.6	low	0.4
Nifedipine	high	104.6	high	121.1

N.D. = not determined

Table S2 Interactions of AX-35 with PBTZ169, BDQ or CFM in *M. tuberculosis* H37Rv. Data obtained are mean Σ FIC indices \pm SD from two independent experiments.

fold MIC of AX-35	AX-35 with PBTZ169		AX-35 with BDQ		AX-35 with CFM	
	Mean Σ FIC Index	SD	Mean Σ FIC Index	SD	Mean Σ FIC Index	SD
0.5	1.63	0.08	1.06	0.13	0.79	0.07
0.25	1.31	0.04	1.33	0.00	0.80	0.15
0.125	1.03	0.24	1.17	0.00	0.92	0.29
0.0625	0.83	0.28	1.00	0.17	1.02	0.13

Table S3 List of primers used in this study

Primer name	Sequence
RvQcrB_S182P_For (recombineering)	5'-CTGTCGGGACTCGGTCTGCGCGCGGCACTCTCG <u>CCG</u> ATCACGCTGGGTATGCCGGTAATCGGGACCTGGC-3'
RvQcrB_M342V_For (recombineering)	5'-ACCATTCCCGCCCCGGTCTGGGTGCGCGTGATC <u>G</u> TGGGCCTGGTTTCGTCCTGCTACCCGCCTACCCAT-3'
QcrB_full_01F	5'-AATCCTGTGCCCTTGTCACC-3'
QcrB_full_01R	5'-AAAATGCGCCGGAATTGAAC-3'
QcrB_full_02F	5'-CCATCTTGATCCCCAGGCTC-3'
QcrB_full_02R	5'-AGAAAAGTGCCTACTACCCGG-3'
QcrB_full_03F	5'-TGGTTTTCGTCCTGCTACCC-3'
QcrB_full_03R	5'-GGTGATCGAGTGGCTATACG-3'
cydB_F	5'-GACGATGCCTACCGATTCGC-3'
cydB_R	5'-CCAGCCACGTCCAGTCTTTG-3'
lipU_F	5'-CAAAGGAACACAAGCAGGCG-3'
lipU_R	5'-GTCTACCTGGTTCCTCGCTG-3'
tgs4_F	5'-GTCACCTTCGCCAGCATCAA-3'
tgs4_R	5'-GGTTTGAGCTCGGTGAATG-3'

SUPPLEMENTARY FIGURES

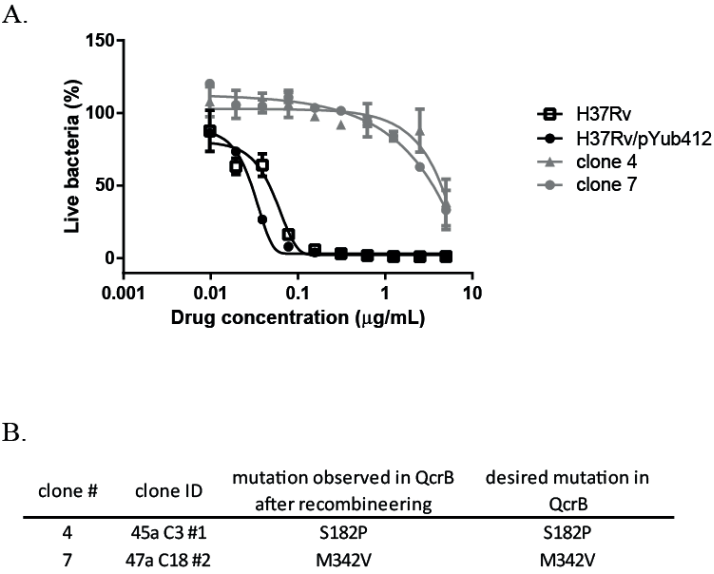


FIG S1 Recombineering of mutations associated with AX resistance in chromosomal *M. tuberculosis* H37Rv *qcrB*. (A) Two recombinant clones with strong resistance phenotype to AX compared to wild-type H37Rv or H37Rv containing co-transformed vector pYUB412. (B) Sanger sequencing across *qcrB* confirms insertion of desired base changes in recombinant clones resulting in missense mutations S182P and M342V. The absence of other mutations was confirmed by WGS.

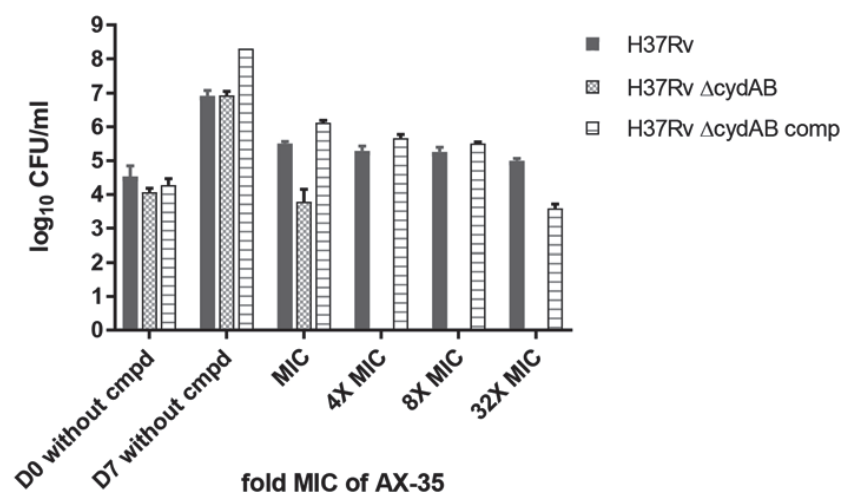


FIG S2 Mode of action of AX-35. MBCs (representing 99.9% killed bacteria compared to D0) of AX-35 were measured in *M. tuberculosis* H37Rv, H37Rv Δ cydAB, and H37Rv Δ cydAB::cydAB complemented strains by exposing mycobacteria to varying concentrations of AX-35 (fold MICs respective to each strain) over a duration of 7 days in liquid 7H9 complete media followed by plating on 7H10 solid medium. CFUs were counted after 4 weeks of incubation at 37°C.

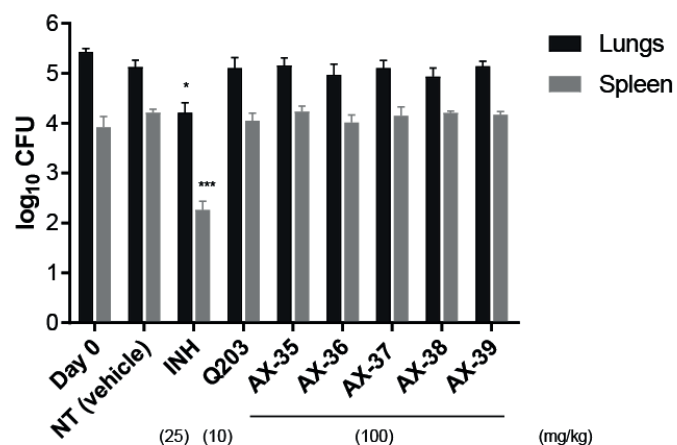


FIG S3 Activity of AX compounds in a chronic mouse model of TB. Bacterial burden (CFU) was determined in the lungs (black columns) and spleens (grey columns) of five mice treated with vehicle control (TPGS 20%) or compounds treated with doses as indicated brackets (mg/kg) by oral gavage. Day 0 indicates the start of treatment, whereas the rest of the data are obtained from Day 28 when treatment ended. Data from one experiment is presented as mean \pm SD. Statistical analysis was performed using one-way ANOVA, Dunnett's Multiple Comparison Test compared to non-treated vehicle condition (* p <0.05, *** p <0.001).

Chapter 3: Discovery of new plant-derived inhibitors with potent F420-dependent activity against *Mycobacterium tuberculosis*

Caroline S. Foo¹, Tobias Brütsch², Patrick Eisenring², Anthony Vocat¹, Andrej Benjak¹,
Andréanne Lupien¹, Jérémie Piton¹, Karl-Heinz Altmann², Stewart T. Cole¹

¹Global Health Institute, École Polytechnique Fédérale de Lausanne, Switzerland

²Institute of Pharmaceutical Sciences, Department of Chemistry and Applied Biosciences, ETH
Zürich, Switzerland

Manuscript in preparation, 2018

Contributions: design and execution of experiments, data analysis, manuscript preparation

ABSTRACT

As Tuberculosis (TB) continues to be a global pandemic, new drugs are urgently needed against its etiological agent, *Mycobacterium tuberculosis*. Herein, we report on our work with a new, promising series of anti-tuberculars, PB compounds, which have been derived from naturally-occurring lapachol. PB analogs have substantially improved activity against replicating *M. tuberculosis* *in vitro* compared to lapachol, and demonstrate activity against non-replicating *M. tuberculosis* SS18b as well as in infected THP-1 macrophages. The activity of PB analogs is selective and not associated with cytotoxicity. Isolation and characterization of mutants of *M. tuberculosis* resistant to PB compounds revealed mutations in the *fgdI* gene encoding the F₄₂₀-dependent glucose-6-phosphate dehydrogenase, a likely primary determinant of PB-resistance. Cross-resistance studies further identified the lack of F₄₂₀ biosynthesis in mediating resistance to PB analogs. Interestingly, a *M. tuberculosis* strain without a functional deazaflavin-dependent nitroreductase Ddn, which relies on reduced F₄₂₀ for enzymatic activity, remained susceptible to PB compounds. This presents a different mechanism of action compared to the prodrugs Delamanid and PA-824, both of which require reduced F₄₂₀ and Ddn for activation via nitro-reduction. PB compounds therefore act through a novel mechanism of action and are likely prodrugs which require bioactivation by a different reduced- F₄₂₀-dependent enzyme to highly active species. Our findings highlight the potential of these lapachol-derived PB analogs as new, promising, potent anti-tuberculars with a novel F₄₂₀-dependent activity and will guide future lead optimisation and target identification.

INTRODUCTION

Tuberculosis (TB) is one of the top ten most deadly diseases globally and the leading cause of death due to an infectious disease (1), with *Mycobacterium tuberculosis* (*M. tuberculosis*) as its etiological agent. The current front-line treatment for drug-susceptible TB (DS-TB) emerged in the 1980s, and is a six-month, directly-observed therapy (DOT) comprising isoniazid, rifampicin, pyrazinamide and ethambutol. The treatment for drug-resistant TB (DR-TB) is more complex (consisting of at least five drugs), lasts even longer (between 9 and 20 months), and is costly (between US\$2000 and 5000 per individual) with low cure rates (at around 50% or less) (2). Within an infected host, *M. tuberculosis* is thought to exist in a spectrum of metabolic states (3). Non-replicating bacilli, in particular, persist against conventional anti-TB drugs, which are highly effective against replicating bacilli (4), and explain the lengthy TB treatment durations required to achieve cure. Adherence to prolonged treatment regimens is often poor and this contributes towards the emergence of drug-resistant *M. tuberculosis* strains. As part of new regimens, new anti-TB drugs should thus be potent with novel mechanisms of action to reduce treatment durations, target different bacillary sub-populations including persisters, and kill drug-resistant strains more effectively (5).

Instances of new anti-TB drugs are Bedaquiline (BDQ, Sirturo) and Delamanid (Deltiya), whose approvals in 2012 by the U.S. Food and Drug Administration (FDA) (6) and 2014 by the European Commission (7), respectively, were important milestones in the context of contemporary TB drug development after a dry spell of new TB drugs for more than 40 years. While BDQ targets the *atpE* subunit of the ATP synthase (8), Delamanid has a more pleiotropic mechanism of action. Delamanid is a bicyclic nitroimidazole that shares a similar mechanism of action to PA-824 (Pretomanid), another related nitroimidazole, which is currently in Phase 3 clinical trials (Fig. 1a, b) (9). Both compounds are active against replicating and non-replicating *M. tuberculosis* (10, 11). Their aerobic activity has been attributed to the inhibition of mycolic acid synthesis, whereas their anaerobic activity stems from their bioactivation by a reduced F₄₂₀-dependent enzyme, a deazaflavin-dependent nitroreductase

(Ddn), to highly active intermediates that kill *M. tuberculosis* non-specifically through the release of nitric oxide, which causes respiratory poisoning and cellular damage of the pathogen (10–13). Resistance to these compounds is mediated by mutations in *fbiA*, *fbiB*, and *fbiC*, three genes involved in biosynthesis of the 5-deazaflavin F₄₂₀ cofactor, and *fgdI* whose product generates the reduced form of F₄₂₀, and Ddn (11, 14, 15).

As with Delamanid and PA-824, most compounds in the global TB drug pipeline are small, synthetic, drug-like molecules. Another strategy to generate new chemical entities is to exploit natural products for their potential as anti-tuberculars. A historical example is the front-line TB drug rifampicin, which was generated from semisynthetic modifications of rifamycins, a class of naturally-occurring antibiotics isolated from *Streptomyces mediterranei* (18). Similar approaches have been adopted in contemporary TB drug discovery, for instance based on *Streptomyces*-derived spectinomycin (19), griselimycin (20), capuramycin (21), and pyridomycin (22). Analogs generated from these natural products are being optimised for improved potency against *M. tuberculosis* and to enhance their pharmacological properties.

Apart from bacteria, another important source of natural medicinal compounds comes from plants. Lapachol, a naturally-occurring naphthaquinone (Fig. 1c), is extracted from trees of the Bignoniaceae family, including those from the *Tabebuia* genus which are native to Central and South America (23). Like other quinones, a wide spectrum of medicinal properties have been attributed to lapachol, including anti-cancer, anti-microbial, anti-malarial, and anti-fungal activity (24, 25). Due to its availability and simple structure which is suitable for SAR studies, we considered lapachol as an attractive starting scaffold for lead optimisation against *M. tuberculosis*.

In this study, we describe the characterisation of four lapachol-derived analogs, the PB compounds, which are active against *M. tuberculosis in vitro* and in infected macrophages. PB analogs have markedly improved activity which is selective against *M. tuberculosis* compared to the parent

compound, lapachol, and also demonstrate *ex vivo* activity in infected macrophages. Isolation of *M. tuberculosis* strains resistant to PB compounds revealed a dependence on the reduced form of the F₄₂₀ cofactor for their activity.

RESULTS

Characterization of lapachol-derived PB compounds. The activity of the naturally-occurring compound lapachol against *M. tuberculosis* H37Rv *in vitro* was initially measured. Since lapachol is active against replicating *M. tuberculosis* H37Rv *in vitro* with a MIC of 13.9 µg/ml (Fig. 1, Table 1), an SAR study was initiated and several lapachol-derived analogs, named PB, were generated. All PB analogs have substantially improved activity against *M. tuberculosis* H37Rv compared to lapachol, with MIC values ranging from 0.4 µg/ml (Table 1) to 0.05 µg/ml, with PB-117 and PB-118 being the most active analogs. To determine whether PB compounds were also active against non-replicating *M. tuberculosis*, the percentage of maximum inhibition (I_{\max}) at 10 µg/ml of these molecules was measured *in vitro* using the streptomycin-starved *M. tuberculosis* 18b strain as a latency model (26). As shown in Table 1, I_{\max} values of these compounds range from 35% and 96%, indicating some activity of the PB family in this model of non-replicating *M. tuberculosis*.

To further characterise the antimicrobial activity of the PB series, two analogs, namely PB-089 and PB-116, were tested against a panel of bacteria and fungi. Intriguingly, their activity was found to be highly specific to certain mycobacteria of the *M. tuberculosis* complex (MTBC), namely *M. tuberculosis*, *M. canettii*, *M. bovis*, and *M. bovis* BCG (Table 2), implying that the mechanism of action of PB compounds is related to specific properties of these strains from the MTBC complex.

Since *M. tuberculosis* is an intracellular pathogen, the anti-microbial activity of the compounds were measured in an *ex vivo* model of *M. tuberculosis*-infected THP-1 macrophages and IC₅₀ values were measured to determine intracellular activity. IC₅₀ ranged from 1.4 to 3.2 µg/ml for PB-089, PB-117, and PB-118 (Table 1), reflecting their potent *ex vivo* activity. However, no *ex vivo* activity for PB-116

was observed in this model. Cytotoxicity was measured in human HepG2 cells, and no to moderate cytotoxicity was observed for these compounds, as evident from the TD₅₀ values obtained (Table 1). This results in acceptable selectivity of all PB analogs, with selective indices (HepG2 TD₅₀/ MIC) above 250, and PB-089 and PB-117 being the two most selective analogs (Table 1). To obtain insight into the metabolic stability of PB compounds, the intrinsic clearance (Cl_{int}) was determined in mouse and human liver microsomes. As evident from Table 3, PB analogs have only low metabolic stability in both cases.

Altogether, structural modifications to lapachol led to substantially improved anti-tubercular activity of the PB compounds, with PB-117 and PB-118 as leads of this series.

Deleterious mutations in *fgdI* are associated with resistance to PB compounds.

Spontaneous resistant mutants were isolated in *M. tuberculosis* H37Rv on 7H10 complete solid medium containing compounds at concentrations of either 10x MIC (for PB-089) or 20x MIC (for PB-116, PB-117, and PB-118). MIC values for isolated resistant clones were determined in 7H9 liquid medium using the resazurin microtiter assay plate (REMA) method, and PB-resistant clones were found to have a 10- to 40-fold increase in MIC compared to wild-type H37Rv. Resistance frequencies of *M. tuberculosis* H37Rv to PB compounds *in vitro* are estimated at between 1×10^{-6} and 8×10^{-7} . Whole-genome sequencing (WGS) of PB-resistant strains revealed two mutations in each strain, one occurring in *fgdI* and the other in a *pps* gene, resulting in missense mutations, premature polypeptide termination or frameshifts (Table 4). In *M. tuberculosis*, *fgdI* encodes the F₄₂₀-dependent glucose-6-phosphate dehydrogenase, Fgd1, which catalyses the oxidation of glucose-6-phosphate to 6-phosphogluconolactone with the concomitant reduction of the F₄₂₀ cofactor while *pps* genes are involved in the biosynthesis of the cell wall lipid phthiocerol dimycocerosate (PDIM), which is involved in the virulence of the bacillus (27). All identified mutations associated with resistance to PB are functionally deleterious for their respective gene functions, including Ser54Leu in *fgdI* as predicted

by the Provean web server (28, 29), which is in line with the non-essentiality of both *fgd1* and *pps* genes for *in vitro* growth of *M. tuberculosis* (30).

Cross-resistance studies of PB compounds and PB-resistant strains. To investigate if all analogs in the PB series share the same mechanism of action, the susceptibility of PB-resistant mutants to all PB compounds were determined. From dose-response curves of the two PB-resistant strains to all PB analogs, an increase in MIC by 20- to 100-fold compared to that in wild-type H37Rv was observed (Fig. 2), indicating that all analogs share the same mechanism of action.

Since deleterious mutations in Fgd1 and in the enzymes involved in the F₄₂₀ biosynthesis pathway are also known to mediate resistance to Delamanid and PA-824, cross-resistance studies to Delamanid and PA-824 were also conducted to gain further insight into the mechanism of action of PB compounds. As expected, PB-resistant mutants also demonstrate complete resistance to Delamanid and PA-824 (Fig. 2), further validating the absence of a functional Fgd1 in these strains. The activity of PB compounds was additionally determined in two Delamanid/PA-824 resistant mutants, namely an FbiC mutant strain, which has a transposon insertion in *fbiC*, and a Ddn mutant harbouring a transposon in *ddn*, with defective FbiC and Ddn gene products, respectively. Interestingly, while the *fbiC* mutant strain is highly resistant to all PB analogs (Fig. 2), which would imply that the F₄₂₀ cofactor is necessary for PB activity as with Delamanid and PA-824, the *ddn* mutant strain has no or only very low resistance to PB compounds (Fig. 2), indicating that the mechanism of action of this family does not largely depend on Ddn, unlike Delamanid and PA-824.

Altogether, the cross-resistance studies indicate that all PB analogs share the same mechanism of action against *M. tuberculosis in vitro* and confirm the presence of *fgd1* mutations in PB-resistant strains. Furthermore, the mechanism of action of PB compounds differs from that of Delamanid and PA-824, despite their activation requiring the F₄₂₀ cofactor, as the nitroreductase Ddn is not involved.

DISCUSSION

In this study, we describe the characterisation of four lapachol-derived PB analogs with substantially improved activity against replicating *M. tuberculosis* *in vitro* compared to the parent scaffold. The potent micromolar activity of these compounds is selective against *M. tuberculosis* and not due to cytotoxicity, and limited to mycobacterial species of the MTBC tested. PB compounds demonstrate activity against non-replicating *M. tuberculosis* in the SS18b model, and most analogs have activity in *M. tuberculosis*-infected macrophages. A potential liability of these compounds that will need addressing during further optimisation, is their low metabolic stability, as observed in mouse and human microsomes, which could reduce their efficacy against *M. tuberculosis* *in vivo*.

Similar to PA-824-resistance, mutations in *fgd1* and *pps* were identified in *M. tuberculosis* strains spontaneously resistant to PB compounds (11, 12). Although not validated in this study, it is unlikely that *pps* genes are primary determinants of PB resistance. *pps* genes are required for the biosynthesis of PDIM, in which mutations have often been observed in *in vitro* experiments (31). This is probably attributed to the large coding capacity necessary for the production of PDIM and its *in vitro* redundancy as a virulence factor (27, 31, 32). Furthermore, it was demonstrated that PDIM mutations were not associated with PA-824 resistance as validated by genetic complementation (12).

It is interesting to note that PDIM synthesis in mycobacteria relies on the reduced form of the 5-deazaflavin electron carrier, F₄₂₀-H₂ (33). F₄₂₀ production is uncommon and restricted to certain archaea and bacteria (34, 35), including universally in mycobacteria (36). *M. tuberculosis* is predicted to carry at least 33 F₄₂₀-dependent enzymes (28, 34), including F₄₂₀-dependent glucose 6-phosphate dehydrogenase Fgd1 and deazaflavin-dependent nitroreductase Ddn, both of which have been experimentally validated (37, 38). Fgd1 is an unusual glucose-6-phosphate dehydrogenase in that it catalyses the oxidation of glucose-6-phosphate to 6-phosphogluconolactone via F₄₂₀ instead of NADP

(37, 39) and is a main enzyme for the generation of reduced F_{420} (40, 41), while the proposed physiological role of Ddn is that of a F_{420} -H₂-dependent quinone reductase (38).

Fgd1, together with Ddn and the F_{420} biosynthetic enzymes FbiA, FbiB, and FbiC, are necessary components for the bioactivation of the prodrugs Delamanid and PA-824. Mutations in any of these enzymes render *M. tuberculosis* resistant to these compounds (11, 14, 15). In the case of PB analogs, only non-functional Fgd1 and FbiC enzymes result in PB resistance, indicating that activity of these compounds relies on F_{420} and its reduced form, without the involvement of Ddn. This is consistent with the absence of available nitro groups on PB compounds for nitro-reduction (Table 1). It is highly likely that PB compounds are also prodrugs, activated by another hitherto unidentified F_{420} -H₂-dependent enzyme, which is common to *M. tuberculosis*, *M. bovis* and *M. canettii*, members of the MTBC, and absent in other mycobacteria, to highly reactive species and causing pleiotropic damage to the bacillus without acting on a specific target, in a similar manner to Delamanid and PA-824 (Fig. 3).

Since nitroreductases are uninvolved in the activation of PB compounds, 26 F_{420} -dependent enzymes identified up until now could act as potential activators, among which two are Fgd enzymes and the others are monooxygenases and oxidoreductases. From comparative mycobacterial genomics, the involvement of Rv3618 and Rv2074 can be ruled out as although these genes have been deleted from the *M. bovis* genome, this bacterium remains susceptible to PB analogs. An additional 14 genes are unlikely to be involved as well, as they are present in *M. smegmatis*, against which PB compounds are inactive. This leaves 8 possible candidates that could serve as the activator and investigating them further should help us to understand the activation mechanism and to identify the active form of the PB compounds.

A pertinent issue with the use of quinones as therapeutics is their associated cytotoxicity (25). As PB compounds require F_{420} -H₂-dependent activation, it is unlikely that they retain broad-spectrum activity

as F₄₂₀ and Fgd1 production is restricted to certain bacteria (39), thus likely reducing perturbations of the host microbiota. Furthermore, since mammalian enzymes are incapable of F₄₂₀ biosynthesis, cross-activation of these compounds leading to unspecific toxic side effects on the host could be avoided as well, thus mitigating the risk of quinone cytotoxicity.

Since a variety of mutations in seemingly inessential genes, *fgd1*, *fbiA*, *fbiB*, and *fbiC* mediate *in vitro* resistance to PB, the *in vitro* resistance frequency of *M. tuberculosis* to PB compounds is high and estimated at 10⁻⁶ to 10⁻⁷. This is comparable to the ranges reported for Delamanid, PA-824, and INH at 10⁻⁵ to 10⁻⁶, 10⁻⁵ to 10⁻⁷, and 10⁻⁶ respectively (12, 14, 15, 42). Notably, as mutations in *ddn* are not associated with resistance to PB compounds, PB analogs have the potential to be backup molecules for Delamanid and PA-824 for strains of *M. tuberculosis* resistant to these compounds due to mutations in *ddn*.

The clinical relevance of these mutations, however, remain to be determined as Delamanid and PA-824 advance in Phase 3 clinical trials (9). In a case of a clinical isolate, mutations in *fbiA* and *fgd1* have been associated with phenotypic resistance to Delamanid (43). Since F₄₂₀-H₂ possibly contributes to low-redox potential reactions for the anaerobic survival of *M. tuberculosis* (44), and *fgd1* and F₄₂₀-H₂ have roles in protecting the bacillus against nitrosative and oxidative stress (40, 41), it is tempting to speculate that mutations in *fgd1* and/or F₄₂₀ biosynthetic enzymes would occur at a higher fitness cost for certain bacillary populations, and therefore the *in vivo* emergence of resistance might be reduced or the transmission of such resistant strains be impaired.

In conclusion, it is evident from our SAR data that structural changes to the natural product, lapachol, can markedly improve activity against *M. tuberculosis* and generate a promising new family of anti-tuberculars. It is likely that PB compounds act through a novel mechanism of action against *M. tuberculosis*. Altogether, considering the profiling performed in this study, the PB analogs merit

further optimisation and characterisation studies, and ongoing work is also being undertaken to identify their activator and the active species.

TABLES AND FIGURES

Table 1 Characterization of PB series: activity against *M. tuberculosis* H37Rv and SS18b; cytotoxicity and selective index

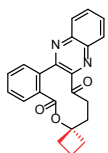
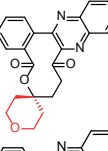
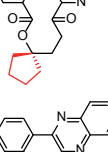
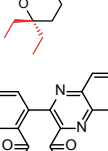
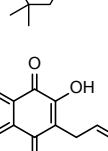
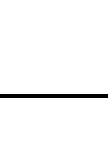
Compound ID	Structure	Anti-mycobacterial activity against <i>M. tuberculosis</i> H37Rv		Anti-mycobacterial activity against <i>M. tuberculosis</i> SS18b	Cytotoxicity in HepG2 cells	Selective Index
		<i>in vitro</i>	<i>ex vivo</i> in THP-1 macrophages	<i>in vitro</i>		
		MIC (µg/ml)	IC ₅₀ (µg/ml)	I _{max} (%)	TD50 (µg/ml)	(TD ₅₀ /MIC)
PB-089		0.2	~3.2	35	>100	500
PB-116		0.1	no activity	47	28	280
PB-117		0.05	~2.5	96	21	420
PB-118		0.05	1.4	96	13	260
PB-001 (TB-189)		0.4	N.D.	75	>100	250
Lapachol		13.9	N.D.	N.D.	N.D.	N.D.
Rifampicin		0.001	0.1	71	50	50000

Table 2 Activity of PB-089 and PB-116 against selected microorganisms

<i>Microorganisms</i>	MIC (µg/ml)		
	PB-089	PB-116	RIF
<i>Bacillus subtilis</i>	>100	>100	0.3
<i>Candida albicans</i>	>100	>100	1.5
<i>Corynebacterium diphtheriae</i>	>100	>100	0.0004
<i>Corynebacterium glutamicum</i>	>100	>100	0.004
<i>Enterococcus faecalis</i>	>100	>100	0.6
<i>Escherichia coli</i>	>100	>100	6.7
<i>Listeria monocytogenes</i>	>100	>100	0.8
<i>Micrococcus luteus</i>	>100	>100	0.7
<i>Mycobacterium abscessus</i>	>100	>100	22.5
<i>Mycobacterium avium</i>	>100	>100	25
<i>Mycobacterium bolletii</i>	>100	>100	47
<i>Mycobacterium bovis</i> AF2122/97	0.2	0.7	0.0008
<i>Mycobacterium bovis</i> BCG	0.3	0.4	0.0008
<i>Mycobacterium canettii</i> STB-L	0.1	0.3	0.01
<i>Mycobacterium marinum</i>	>100	>100	0.5
<i>Mycobacterium massiliense</i>	>100	>100	26.9
<i>Mycobacterium smegmatis</i>	>100	>100	1.7
<i>Mycobacterium tuberculosis</i>	0.2	0.1	0.001
<i>Mycobacterium ulcerans</i>	>100	>100	0.01
<i>Mycobacterium vaccae</i>	>100	>100	2.5
<i>Pseudomonas aeruginosa</i>	>100	>100	1
<i>Pseudomonas putida</i>	>100	>100	0.2
<i>Salmonella typhimurium</i>	>100	>100	0.7
<i>Staphylococcus aureus</i>	>100	>100	3.8

Table 3 Intrinsic clearance (Cl_{int}) and clearance category of AX derivatives in mouse and human liver microsomes

	Mouse microsomes		Human microsomes	
	Clearance Category	Cl_{int} ($\mu\text{l}/\text{min}/\text{mg}$)	Clearance Category	Cl_{int} ($\mu\text{l}/\text{min}/\text{mg}$)
PB-089	high	462.9	high	63.8
PB-116	high	105.7	high	115.9
PB-117	high	N.D.	high	471.1
PB-118	high	64.9	high	220.1
Carbamazepine	low	2.9	low	0.4
Nifedipine	high	116.2	high	116.2

N.D. = could not be determined

Table 4 Whole-genome sequencing (WGS) of *M. tuberculosis* H37Rv PB-resistant strains

Compound	Selected on 7H10 plates + compound (fold MIC)	Clone	Gene	Codon change	Amino acid change
PB 089	10x	A4	<i>fgdI</i> <i>ppsA</i>	161C>T 2871dupC	Ser54Leu Glu958fs
PB 089	10x	A6	<i>fgdI</i> <i>ppsA</i>	161C>T 2871dupC	Ser54Leu Glu958fs
PB 117	20x	1	<i>fgdI</i> <i>ppsA</i>	161C>T 2871dupC	Ser54Leu Glu958fs
PB 117	20x	5	<i>fgdI</i> <i>ppsA</i>	161C>T 2871dupC	Ser54Leu Glu958fs
PB 116	20x	B1	<i>fgdI</i> <i>ppsA</i>	161C>T 2871dupC	Ser54Leu Glu958fs
PB 116	20x	B4	<i>fgdI</i> <i>ppsA</i>	161C>T 2871dupC	Ser54Leu Glu958fs
PB 118	20x	C4	<i>fgdI</i> <i>ppsA</i>	161C>T 2871dupC	Ser54Leu Glu958fs
PB 118	20x	C3	<i>fgdI</i> <i>ppsD</i>	55G>T 4743dupG	Glu19* Gln1582fs

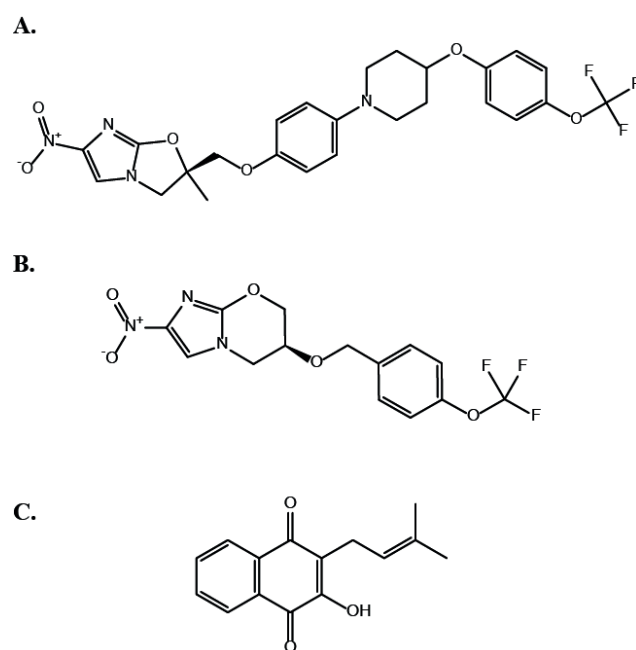


FIG 1 Chemical structures of (A) Delamanid, (B) PA-824 (Pretomanid), and (C) lapachol, from which PB analogs are derived

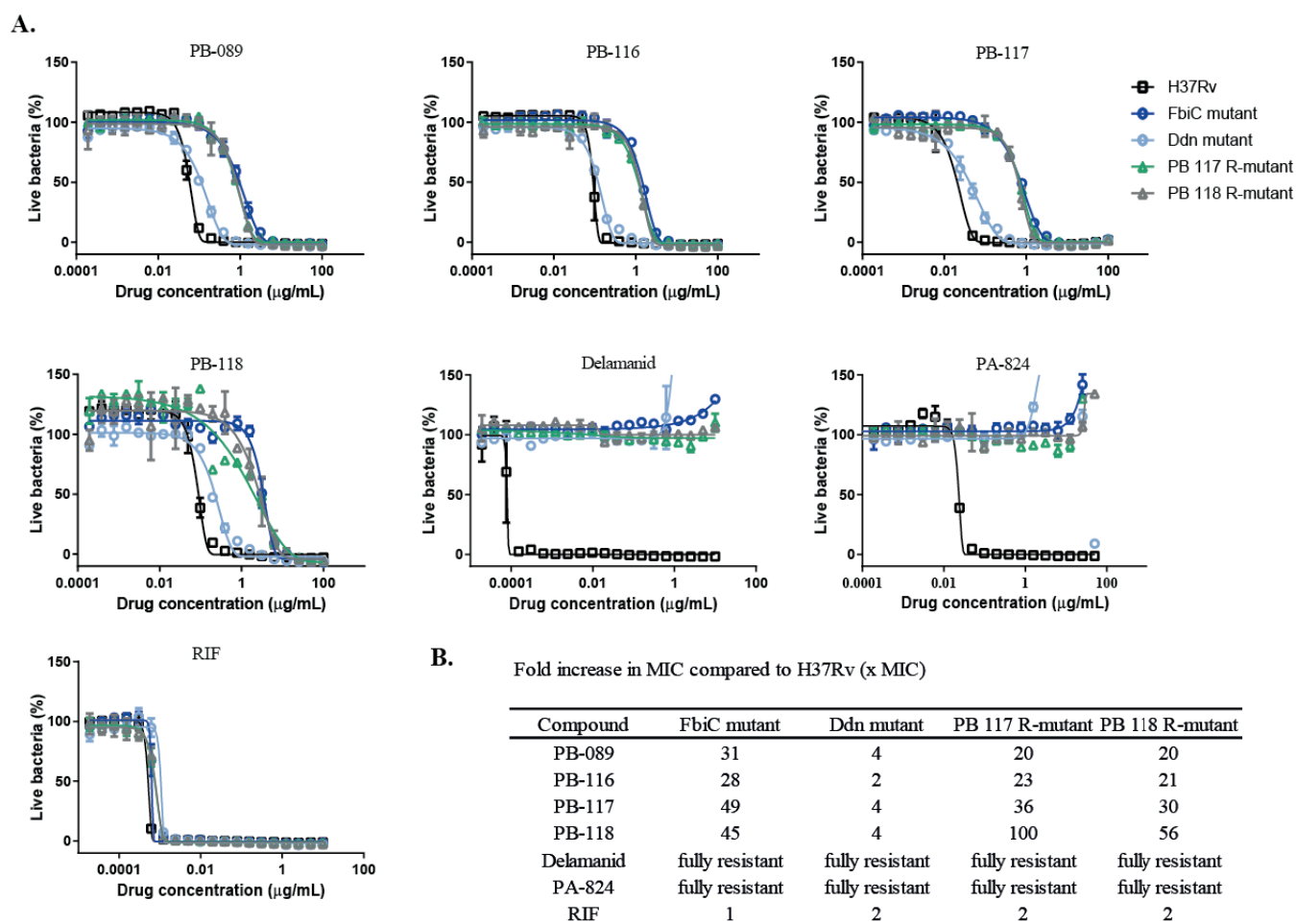


FIG 2 Cross-resistance studies of PB compounds. (A) Dose-response curves of *M. tuberculosis* wild-type H37Rv, FbiC mutant, Ddn mutant, and two PB-resistant mutant strains to PB compounds, Delamanid, PA-824, and RIF. Data are presented as technical duplicates of mean \pm SD; graphs are representative of two independent experiments. (B) Overview of the fold increase in MIC for each compound in each strain as a ratio to the MIC obtained for *M. tuberculosis* H37Rv.

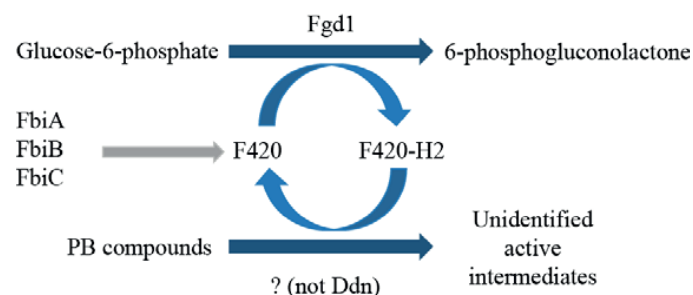


FIG 3 Proposed mechanism of F₄₂₀-dependent action of PB compounds. The biosynthesis of the 5-deazaflavin hydride carrier F₄₂₀ involves FbiA, FbiB, and FbiC, a process restricted to certain species of bacteria, including mycobacteria. Fgd1 reduces F₄₂₀ with the oxidation of glucose-6-phosphate to 6-phosphogluconolactone. Reduced F₄₂₀, F₄₂₀-H₂, is utilised by an unidentified F₄₂₀-dependent enzyme (not Ddn) to activate PB compounds to highly active intermediates which are detrimental for *M. tuberculosis*, either killing or inhibiting the growth of the bacillus. Adapted from (15).

MATERIALS AND METHODS

Drugs used in this study. Lapachol and RIF were from Sigma Aldrich.

Culture conditions of *M. tuberculosis* strains, other bacteria and eukaryotic cell lines.

Mycobacterial strains were grown at 37°C in Middlebrook 7H9 broth (Difco) supplemented with 0.2% glycerol, 0.05% Tween-80 and 10% albumin dextrose catalase (ADC) (7H9 complete) or on 7H10 agar plates supplemented with 0.5% glycerol and 10% oleic ADC. *Bacillus subtilis*, *Candida albicans*, *Corynebacterium diphtheriae*, *Corynebacterium glutamicum*, *Escherichia coli*, *Micrococcus luteus*, *Pseudomonas putida*, *Salmonella typhimurium*, and *Staphylococcus aureus* were grown in LB broth. *Enterococcus faecalis*, *Listeria monocytogenes*, and *Pseudomonas aeruginosa* were grown in brain heart infusion (BHI) broth. HepG2 cells were grown in DMEM (Gibco) media supplemented with 10% fetal bovine serum at 37°C with 5% CO₂. THP-1 macrophages were grown in RPMI medium supplemented with 10% fetal bovine serum and 1 mM sodium pyruvate at 37°C with 5% CO₂.

Determination of MICs. MICs were determined using the resazurin reduction microplate assay (REMA) as previously described (45). Strains were grown to log-phase (OD₆₀₀ 0.4 to 0.8) and diluted to an OD₆₀₀ of 0.0001. Two-fold serial dilutions of each test compound were prepared in 96-well plates containing 100 µl of bacteria per well (3 x 10³ cells per well). Plates were incubated either at 30°C or 37°C as required with appropriate incubation times (e.g. for *M. tuberculosis* at 37°C, 6 days). 10 µl of resazurin (0.0025% w/v) was added to each well, after which the fluorescence intensity of the resorufin metabolite (excitation/emission: 560/590 nm) was read using an Infinite F200 Tecan plate reader. MIC values representing 90% growth inhibition were determined by a non-linear fitting of the data to the Gompertz equation using GraphPad Prism. Drug-testing against streptomycin-starved 18b (SS18b) was performed as described above for REMA assays using an SS18b culture maintained in 7H9 medium without streptomycin for 2 weeks and a final OD₆₀₀ of 0.1 as previously reported (46).

Cytotoxicity for HepG2 cells. Human HepG2 cells (4,000 cells/well) were incubated for 3 days with two-fold serially diluted compounds at 37°C, under an atmosphere of 5% CO₂. Cell viability was determined by the addition of resazurin (0.0025% w/v) for 4 h at 37°C and the fluorescence intensity measured as in REMA.

Assessment of drug activity *ex vivo* in THP-1 macrophages. 1×10^5 THP-1 human monocytic cells/well were seeded in 96-well plates and incubated with 4 nM phorbol-12-myristate-13-acetate (PMA) overnight to stimulate macrophage differentiation. Differentiated macrophages were infected with *M. tuberculosis* H37Rv grown to log phase (OD₆₀₀ 0.4 to 0.8) at MOI 5. Extracellular bacteria were removed after 3-4 h incubation at 37°C with 5% CO₂ by removing the RPMI medium and washing with PBS. Compounds to be tested were prepared in separate 96-well plates by two-fold serial dilutions in a final volume of 100 µl RPMI which was then transferred to the plates of infected THP-1 macrophages. Plates were sealed and incubated for 48 h at 37°C with 5% CO₂. 10 µl of PrestoBlue® (ThermoFischer Scientific) was added and plates were incubated for up to 1 h at 37°C with 5% CO₂ before the fluorescence intensity (excitation/emission: 560/590 nm) was measured using Infinite F200 Tecan plate reader. Dose-response curves were plotted and IC₅₀ values obtained using a non-linear regression fit equation (log[inhibitor] vs response, variable slope) in GraphPad Prism.

Microsomal stability studies. Metabolic stability of the compounds was measured based on intrinsic clearance (Cl_{int}) in mouse and human liver microsomes as previously described (47). Final compound concentration in the mixture of microsomes and NADPH-regeneration system was 2 µg/ml, and a mixture without NADPH-regeneration was also prepared for each compound as a control of the stability of the compound with time. Carbamazepine and nifedipine at 2 µg/ml were used as low and high intrinsic clearance controls, respectively.

Isolation and characterization of PB-resistant mutants. PB-resistant mutants of *M. tuberculosis* H37Rv were isolated on 7H10 complete solid agar plates containing compound

concentrations at 10x MIC for PB-089 and 20x MIC for PB-116, PB-117, and PB-118, with 2.4×10^8 bacteria exposed per condition. REMA assays were performed on isolated colonies after re-streaking on 7H10 complete solid medium. Genomic DNA extraction was performed using the QiaAMP UCP Pathogen Minikit (Qiagen) as per manufacturer's instructions. Whole-genome sequencing was performed using Illumina technology with sequencing libraries prepared using the KAPA HyperPrep kit (Roche) and sequenced on Illumina HiSeq 2500 instrument. All raw reads were adapter- and quality-trimmed with Trimmomatic v0.33 (48) and mapped onto the *M. tuberculosis* H37Rv reference genome (RefSeq NC_000962.3) using Bowtie2 v2.2.5 (49). The bamleftalign program from the FreeBayes package v0.9.20-18 (50) was used to left-align indels. Reads with mapping quality below 8 and duplicate reads were omitted.

Variant analysis. Variant calling was done using VarScan v2.3.9 (51) using the following cut-offs: minimum overall coverage of ten non-duplicated reads, minimum of five non-duplicated reads supporting the SNP, base quality score >15 , and a SNP frequency above 30%. The rather low thresholds, especially the SNP frequency, were deliberately chosen to avoid missing potential variants in alignment-difficult regions, or in case of mixed population. All putative variants unique to the mutant strains were manually checked by inspecting the alignments.

ACKNOWLEDGEMENTS

We would like to thank Prof. Cliff Barry and Dr. Neeraj Dhar for providing *M. tuberculosis* Ddn and FbiC transposon mutant strains, and Dr. Jaroslav Roh for the synthesis of PA-824 used in this study. We also appreciate the technical expertise of Dr. Charlotte Avanzi for the library preparation. The research leading to these results received funding from the European Community's Seventh Framework Programme (MM4TB, Grant 260872).

REFERENCES

1. 2017. The top 10 causes of death. WHO.
2. World Health Organization. 2017. Global Tuberculosis Report 2017. S.l.
3. Mitchison DA. 1979. Basic Mechanisms of Chemotherapy. *Chest* 76:771–780.
4. McKinney JD. 2000. *In vivo veritas*: The search for TB drug targets goes live. *Nat Med* 6:1330–1333.
5. Zumla A, Nahid P, Cole ST. 2013. Advances in the development of new tuberculosis drugs and treatment regimens. *Nat Rev Drug Discov* 12:388–404.
6. Sirturo (bedaquiline) product insert. Silver Spring, MD: Food and Drug Administration.
7. European Medicines Agency - Find medicine - Deltyba.
8. Koul A, Dendouga N, Vergauwen K, Molenberghs B, Vranckx L, Willebrords R, Ristic Z, Lill H, Dorange I, Guillemont J, Bald D, Andries K. 2007. Diarylquinolines target subunit c of mycobacterial ATP synthase. *Nat Chem Biol* 3:323.
9. Working Group for New TB Drugs |.
10. Matsumoto M, Hashizume H, Tomishige T, Kawasaki M, Tsubouchi H, Sasaki H, Shimokawa Y, Komatsu M. 2006. OPC-67683, a Nitro-Dihydro-Imidazooxazole Derivative with Promising Action against Tuberculosis In Vitro and In Mice. *PLOS Med* 3:e466.
11. Stover CK, Warren P, VanDevanter DR, Sherman DR, Arain TM, Langhorne MH, Anderson SW, Towell JA, Yuan Y, McMurray DN, Kreiswirth BN, Barry CE, Baker WR. 2000. A small-molecule nitroimidazopyran drug candidate for the treatment of tuberculosis. *Nature* 405:962–966.

12. Manjunatha UH, Boshoff H, Dowd CS, Zhang L, Albert TJ, Norton JE, Daniels L, Dick T, Pang SS, Barry CE. 2006. Identification of a nitroimidazo-oxazine-specific protein involved in PA-824 resistance in *Mycobacterium tuberculosis*. *Proc Natl Acad Sci U S A* 103:431–436.
13. Manjunatha U, Boshoff HI, Barry CE. 2009. The mechanism of action of PA-824. *Commun Integr Biol* 2:215–218.
14. Haver HL, Chua A, Ghode P, Lakshminarayana SB, Singhal A, Mathema B, Wintjens R, Bifani P. 2015. Mutations in Genes for the F420 Biosynthetic Pathway and a Nitroreductase Enzyme Are the Primary Resistance Determinants in Spontaneous In Vitro-Selected PA-824-Resistant Mutants of *Mycobacterium tuberculosis*. *Antimicrob Agents Chemother* 59:5316–5323.
15. Fujiwara M, Kawasaki M, Hariguchi N, Liu Y, Matsumoto M. 2018. Mechanisms of resistance to delamanid, a drug for *Mycobacterium tuberculosis*. *Tuberculosis* 108:186–194.
16. Schatz A, Bugle E, Waksman SA. 1944. Streptomycin, a Substance Exhibiting Antibiotic Activity Against Gram-Positive and Gram-Negative Bacteria.*†. *Proc Soc Exp Biol Med* 55:66–69.
17. Hoagland DT, Liu J, Lee RB, Lee RE. 2016. New agents for the treatment of drug-resistant *Mycobacterium tuberculosis*. *Adv Drug Deliv Rev* 102:55–72.
18. Sensi P. 1983. History of the development of rifampin. *Rev Infect Dis* 5 Suppl 3:S402-406.
19. Lee RE, Hurdle JG, Liu J, Bruhn DF, Matt T, Scherman MS, Vaddady PK, Zheng Z, Qi J, Akbergenov R, Das S, Madhura DB, Rathi C, Trivedi A, Villellas C, Lee RB, Rakesh, Waidyarachchi SL, Sun D, McNeil MR, Ainsa JA, Boshoff HI, Gonzalez-Juarrero M, Meibohm B, Böttger EC, Lenaerts AJ. 2014. Spectinamides: a new class of semisynthetic antituberculosis agents that overcome native drug efflux. *Nat Med* 20:152–158.

20. Kling A, Lukat P, Almeida DV, Bauer A, Fontaine E, Sordello S, Zaburannyi N, Herrmann J, Wenzel SC, König C, Ammerman NC, Barrio MB, Borchers K, Bordon-Pallier F, Brönstrup M, Courtemanche G, Gerlitz M, Geslin M, Hammann P, Heinz DW, Hoffmann H, Klieber S, Kohlmann M, Kurz M, Lair C, Matter H, Nuermberger E, Tyagi S, Fraisse L, Grosset JH, Lagrange S, Müller R. 2015. Targeting DnaN for tuberculosis therapy using novel griselimycins. *Science* 348:1106–1112.
21. Koga T, Fukuoka T, Doi N, Harasaki T, Inoue H, Hotoda H, Kakuta M, Muramatsu Y, Yamamura N, Hoshi M, Hirota T. 2004. Activity of capuramycin analogues against *Mycobacterium tuberculosis*, *Mycobacterium avium* and *Mycobacterium intracellulare* in vitro and in vivo. *J Antimicrob Chemother* 54:755–760.
22. Hartkoorn RC, Sala C, Neres J, Pojer F, Magnet S, Mukherjee R, Uplekar S, Boy-Röttger S, Altmann K-H, Cole ST. 2012. Towards a new tuberculosis drug: pyridomycin – nature’s isoniazid. *EMBO Mol Med* 4:1032–1042.
23. Gottlieb O R, Mors WB. 1980. Potential Utilization of Brazilian Wood Extractives. *J Agric Food Chem* 28:188–196.
24. Hussain H, Krohn K, Ahmad VU, Miana GA, Green IR. 2007. Lapachol: an overview. *Arkivoc* 2:145–171.
25. O’Brien PJ. 1991. Molecular Mechanisms of Quinone Toxicity. *Chem-Biol Interactions*.
26. Sala C, Dhar N, Hartkoorn RC, Zhang M, Ha YH, Schneider P, Cole ST. 2010. Simple Model for Testing Drugs against Nonreplicating *Mycobacterium tuberculosis*. *Antimicrob Agents Chemother* 54:4150–4158.

27. Cox JS, Chen B, McNeil M, Jr WRJ. 1999. Complex lipid determines tissue-specific replication of *Mycobacterium tuberculosis* in mice. *Nature* 402:79–83.
28. Choi Y, Sims GE, Murphy S, Miller JR, Chan AP. 2012. Predicting the Functional Effect of Amino Acid Substitutions and Indels. *PLoS ONE* 7:e46688.
29. Choi Y, Chan AP. 2015. PROVEAN web server: a tool to predict the functional effect of amino acid substitutions and indels. *Bioinformatics* 31:2745–2747.
30. Kapopoulou A, Lew JM, Cole ST. 2011. The MycoBrowser portal: A comprehensive and manually annotated resource for mycobacterial genomes. *Tuberculosis* 91:8–13.
31. Domenech P, Reed MB. 2009. Rapid and spontaneous loss of phthiocerol dimycocerosate (PDIM) from *Mycobacterium tuberculosis* grown in vitro: implications for virulence studies. *Microbiol Read Engl* 155:3532–3543.
32. Camacho LR, Ensergueix D, Perez E, Gicquel B, Guilhot C. Identification of a virulence gene cluster of *Mycobacterium tuberculosis* by signature-tagged transposon mutagenesis. *Mol Microbiol* 34:257–267.
33. Purwantini E, Daniels L, Mukhopadhyay B. 2016. F420H2 Is Required for Phthiocerol Dimycocerosate Synthesis in *Mycobacteria*. *J Bacteriol* 198:2020–2028.
34. Eirich LD, Vogels GD, Wolfe RS. 1978. Proposed Structure for Coenzyme F420 from *Methanobacterium*. *American Chemical Society* 17.
35. Daniels L, Bakhiet N, Harmon K. 1985. Widespread Distribution of a 5-deazaflavin Cofactor in *Actinomyces* and Related Bacteria. *Syst Appl Microbiol* 6:12–17.

36. Selengut JD, Haft DH. 2010. Unexpected Abundance of Coenzyme F420-Dependent Enzymes in *Mycobacterium tuberculosis* and Other Actinobacteria. *J Bacteriol* 192:5788–5798.
37. Purwantini E, Daniels L. 1996. Purification of a novel coenzyme F420-dependent glucose-6-phosphate dehydrogenase from *Mycobacterium smegmatis*. *J Bacteriol* 178:2861–2866.
38. Gurumurthy M, Rao M, Mukherjee T, Rao SPS, Boshoff HI, Dick T, Barry CE, Manjunatha UH. 2013. A novel F420-dependent anti-oxidant mechanism protects *Mycobacterium tuberculosis* against oxidative stress and bactericidal agents. *Mol Microbiol* 87:744–755.
39. Purwantini E, Gillis TP, Daniels L. 1997. Presence of F420-dependent glucose-6-phosphate dehydrogenase in *Mycobacterium* and *Nocardia* species, but absence from *Streptomyces* and *Corynebacterium* species and methanogenic Archaea. *FEMS Microbiol Lett* 146:129–134.
40. Hasan MR, Rahman M, Jaques S, Purwantini E, Daniels L. 2010. Glucose 6-Phosphate Accumulation in *Mycobacteria* IMPLICATIONS FOR A NOVEL F420-DEPENDENT ANTI-OXIDANT DEFENSE SYSTEM. *J Biol Chem* 285:19135–19144.
41. Purwantini E, Mukhopadhyay B. 2009. Conversion of NO₂ to NO by reduced coenzyme F420 protects mycobacteria from nitrosative damage. *Proc Natl Acad Sci* 106:6333–6338.
42. Johnson R, Streicher EM, Louw GE, Warren RM, van Helden PD, Victor TC. 2006. Drug resistance in *Mycobacterium tuberculosis*. *Curr Issues Mol Biol* 8:97–111.
43. Bloemberg GV, Keller PM, Stucki D, Trauner A, Borrell S, Latshang T, Coscolla M, Rothe T, Hömke R, Ritter C, Feldmann J, Schulthess B, Gagneux S, Böttger EC. 2015. Acquired Resistance to Bedaquiline and Delamanid in Therapy for Tuberculosis. *N Engl J Med* 373:1986–1988.

44. Boshoff HIM, Barry 3rd CE. 2005. Tuberculosis — metabolism and respiration in the absence of growth. *Nat Rev Microbiol* 3:70–80.
45. Palomino J-C, Martin A, Camacho M, Guerra H, Swings J, Portaels F. 2002. Resazurin Microtiter Assay Plate: Simple and Inexpensive Method for Detection of Drug Resistance in *Mycobacterium tuberculosis*. *Antimicrob Agents Chemother* 46:2720–2722.
46. Zhang M, Sala C, Hartkoorn RC, Dhar N, Mendoza-Losana A, Cole ST. 2012. Streptomycin-Starved *Mycobacterium tuberculosis* 18b, a Drug Discovery Tool for Latent Tuberculosis. *Antimicrob Agents Chemother* 56:5782–5789.
47. Makarov V, Neres J, Hartkoorn RC, Ryabova OB, Kazakova E, Šarkan M, Huszár S, Piton J, Kolly GS, Vocat A, Conroy TM, Mikušová K, Cole ST. 2015. The 8-Pyrrole-Benzothiazinones Are Noncovalent Inhibitors of DprE1 from *Mycobacterium tuberculosis*. *Antimicrob Agents Chemother* 59:4446–4452.
48. Bolger AM, Lohse M, Usadel B. 2014. Trimmomatic: a flexible trimmer for Illumina sequence data. *Bioinformatics* 30:2114–2120.
49. Langmead B, Salzberg SL. 2012. Fast gapped-read alignment with Bowtie 2. *Nat Methods* 9:357–359.
50. Garrison E, Marth G. 2012. Haplotype-based variant detection from short-read sequencing. *ArXiv12073907 Q-Bio*.
51. Koboldt DC, Zhang Q, Larson DE, Shen D, McLellan MD, Lin L, Miller CA, Mardis ER, Ding L, Wilson RK. 2012. VarScan 2: Somatic mutation and copy number alteration discovery in cancer by exome sequencing. *Genome Res* 22:568–576.

Chapter 4: Characterization of DprE1-mediated Benzothiazinone Resistance in *Mycobacterium tuberculosis*

Caroline Shi-Yan Foo¹, Benoit Lechartier^{1,2}, Gaëlle S. Kolly¹, Stefanie Boy-Röttger¹, João Neres^{1,3}, Jan Rybníček^{1,4}, Andréanne Lupien¹, Claudia Sala¹, Jérémie Piton¹, Stewart T. Cole¹

¹Global Health Institute, École Polytechnique Fédérale de Lausanne, CH-1015 Lausanne, Switzerland

²Centre hospitalier universitaire vaudois (CHUV), CH-1011 Lausanne, Switzerland

³UCB Biopharma, Chemin du Foriest, 1420 Braine L'Alleud, Belgium

⁴1st Department of Internal Medicine, University of Cologne, D-50937 Cologne, Germany

Antimicrobial Agents and Chemotherapy, 2016, doi:10.1128/AAC.01523-16

Contributions: design and execution of experiments, data analysis, manuscript preparation

Characterization of DprE1-Mediated Benzothiazinone Resistance in *Mycobacterium tuberculosis*

Caroline Shi-Yan Foo,^a Benoit Lechartier,^{a,b} Gaëlle S. Kolly,^a Stefanie Boy-Röttger,^a João Neres,^{a,c} Jan Rybníček,^{a,d} Andréanne Lupien,^a Claudia Sala,^a Jérémie Piton,^a Stewart T. Cole^a

Global Health Institute, École Polytechnique Fédérale de Lausanne, Lausanne, Switzerland^a; Centre Hospitalier Universitaire Vaudois, Lausanne, Switzerland^b; UCB Biopharma, Braine L'Alleud, Belgium^c; 1st Department of Internal Medicine, University of Cologne, Cologne, Germany^d

Benzothiazinones (BTZs) are a class of compounds found to be extremely potent against both drug-susceptible and drug-resistant *Mycobacterium tuberculosis* strains. The potency of BTZs is explained by their specificity for their target decaprenylphosphoryl-D-ribose oxidase (DprE1), in particular by covalent binding of the activated form of the compound to the critical cysteine 387 residue of the enzyme. To probe the role of C387, we used promiscuous site-directed mutagenesis to introduce other codons at this position into *dprE1* of *M. tuberculosis*. The resultant viable BTZ-resistant mutants were characterized *in vitro*, *ex vivo*, and biochemically to gain insight into the effects of these mutations on DprE1 function and on *M. tuberculosis*. Five different mutations (C387G, C387A, C387S, C387N, and C387T) conferred various levels of resistance to BTZ and exhibited different phenotypes. The C387G and C387N mutations resulted in a lower growth rate of the mycobacterium on solid medium, which could be attributed to the significant decrease in the catalytic efficiency of the DprE1 enzyme. All five mutations rendered the mycobacterium less cytotoxic to macrophages. Finally, differences in the potencies of covalent and noncovalent DprE1 inhibitors in the presence of C387 mutations were revealed by enzymatic assays. As expected from the mechanism of action, the covalent inhibitor PBTZ169 only partially inhibited the mutant DprE1 enzymes compared to the near-complete inhibition with a noncovalent DprE1 inhibitor, Ty38c. This study emphasizes the importance of the C387 residue for DprE1 activity and for the killing action of covalent inhibitors such as BTZs and other recently identified nitroaromatic inhibitors.

Mycobacterium tuberculosis is the etiological agent of tuberculosis (TB), an infectious disease which is a leading cause of death worldwide and poses a major threat to global health. The World Health Organization estimates that in 2014, 9.6 million people contracted TB, and 1.5 million people died (1). In addition, the emergence and worldwide spread of multidrug-resistant TB (MDR-TB) and extensively drug-resistant TB (XDR-TB) are alarming. With MDR-TB strains being resistant to the frontline drugs isoniazid and rifampin and XDR-TB strains being resistant to frontline and additionally second-line drugs, there is an urgent need for new drugs for TB.

1,3-Benzothiazin-4-ones (BTZs) were discovered in 2009, with the lead compound BTZ043 having high potency (MIC of 1 ng/μl) against *M. tuberculosis* strain H37Rv (2) and demonstrating efficacy against MDR and XDR clinical isolates (3). Piperazine-containing BTZ (PBTZ) derivatives were then designed with improved pharmacological properties (4), and the optimized lead compound PBTZ169 is currently in clinical trials (5).

Genetic analysis of resistant mutants and enzymology have identified the target of BTZs as decaprenylphosphoryl-β-D-ribose oxidase (DprE1), an essential flavoenzyme in *M. tuberculosis* involved in cell wall synthesis (2). DprE1 acts in concert with DprE2 to catalyze the epimerization of decaprenyl-phosphoribose (DPR) to decaprenyl-phospho-D-arabinofuranose (DPA), which is the sole precursor for the synthesis of arabinogalactan and lipoarabinomannan (LAM) in the mycobacterium cell wall (6).

BTZ behaves as a suicide substrate for the reduced form of DprE1 by undergoing nitroreduction to form a nitroso derivative, which specifically forms a covalent adduct with C387 in the DprE1 active site (7–10). The C387 residue of DprE1 is highly conserved in orthologous enzymes in actinobacteria, except in *Mycobacterium avium* and *M. aurum*, where cysteine is replaced by alanine

and serine, respectively. These mutations confer natural resistance to BTZ (2). Spontaneous mutants resistant to BTZ that were raised in *Mycobacterium smegmatis* and *M. tuberculosis* revealed that glycine or serine substitutions at C387 increased the MIC by at least 1,000-fold (2). The clinical importance of the C387 residue of DprE1 was confirmed as well when 240 *M. tuberculosis* clinical isolates were tested, since all these isolates were found to be BTZ sensitive and had the conserved cysteine codon.

The vulnerability of DprE1 lies in its essentiality in mycobacteria and its localization in the cell wall (11), accounting for the fact that DprE1 has been identified as the target of several structurally distinct compounds in recent drug screens. These compounds can be classified as covalent or noncovalent DprE1 inhibitors. Covalent inhibitors such as BTZ, the nitroquinoxaline VI-9376 (12), and the nitroimidazole 377790 (13) are nitroaromatic compounds possessing the necessary nitro group required for covalent adduct formation at C387 on DprE1. Noncovalent inhibitors such as TCA1 (14), 1,4-azaindoles (15), pyrazolopyridones (16), 4-aminoquinolone piperidine amides (17), and Ty38c

Received 14 July 2016 Returned for modification 22 July 2016

Accepted 7 August 2016

Accepted manuscript posted online 15 August 2016

Citation Foo CS-Y, Lechartier B, Kolly GS, Boy-Röttger S, Neres J, Rybníček J, Lupien A, Sala C, Piton J, Cole ST. 2016. Characterization of DprE1-mediated benzothiazinone resistance in *Mycobacterium tuberculosis*. Antimicrob Agents Chemother 60:6451–6459. doi:10.1128/AAC.01523-16.

Address correspondence to Stewart T. Cole, stewart.cole@epfl.ch.

Supplemental material for this article may be found at <http://dx.doi.org/10.1128/AAC.01523-16>.

Copyright © 2016, American Society for Microbiology. All Rights Reserved.

(18) block enzyme activity by forming hydrophobic, electrostatic, and van der Waals interactions with particular residues in the DprE1 active site.

Given the pivotal role played by the C387 residue of DprE1 in the efficacy of nitroaromatic compounds, the aim of this study was to identify mutations at C387 that are tolerated and confer resistance to (P)BTZ in order to understand the underlying mechanisms of resistance involved as well as the overall influence of these mutations on the DprE1 enzyme and on the pathogen *M. tuberculosis*.

MATERIALS AND METHODS

Bacterial strains, culture conditions, and chemicals. *M. tuberculosis* H37Rv, *M. smegmatis* mc²155, and merodiploid strains were grown at 37°C in Middlebrook 7H9 broth (Difco) supplemented with 0.2% glycerol, 0.05% Tween 80, and 10% albumin-dextrose-catalase (ADC) or on Middlebrook 7H10 agar (Difco) supplemented with 0.2% glycerol and 10% oleic acid-albumin-dextrose-catalase (OADC). For cloning procedures, One Shot TOP10 chemically competent *Escherichia coli* cells (Invitrogen) were grown in Luria-Bertani (LB) broth or on LB agar containing kanamycin (50 µg/ml) or hygromycin (200 µg/ml). All chemicals were purchased from Sigma-Aldrich unless otherwise stated.

Generation of randomly mutated *dprE1* in merodiploid *M. tuberculosis* strains. The *dprE1* gene under the control of its natural promoter, located upstream of Rv3789, was amplified together with Rv3789 by using primers rv3790-fwd and rv3790-rev and cloned in the pCR-Blunt II-TOPO vector (Invitrogen). The resulting plasmid was used to generate random mutations in the TGC codon encoding Cys387. Site-directed mutagenesis was carried out by using the Stratagene QuikChange II site-directed mutagenesis kit with primers containing random bases at the site of interest. The mutated fragments were ligated into the pND255 vector, kindly provided by N. Dhar, École Polytechnique Fédérale de Lausanne (EPFL), Lausanne, Switzerland, which harbors a hygromycin resistance cassette. Six pools of randomly mutated plasmids were obtained (pBLX 1 to pBLX 6), and each pool was screened independently. The resulting integrative vectors were then transformed and integrated at the L5-attB site of *M. smegmatis* mc²155 and *M. tuberculosis* H37Rv. Transformants were selected on 7H10 agar plates with or without BTZ043 at 400 ng/ml. A specific primer was used to repeat the site-directed mutagenesis to obtain the DprE1^{C387G} mutant, which was selected on BTZ043-containing medium. All primers are listed in Table S1 in the supplemental material.

Determination of MICs. MICs were determined by using the resazurin reduction microplate assay (REMA) as previously described (19). *M. tuberculosis* strains were grown in 7H9 medium to log phase (optical density at 600 nm [OD₆₀₀] of 0.4 to 0.8) and diluted to an OD₆₀₀ of 0.0001. One hundred microliters of the bacterial suspension (3 × 10³ cells) was pipetted into wells of a 96-well plate. Compounds (BTZ043, PBTZ169, Ty38c, moxifloxacin, and rifampin) were added to the first column, and subsequently, 2-fold serial dilutions were made. After 6 days of incubation at 37°C, 10 µl of 0.025% (wt/vol) resazurin was added to each well. The fluorescence intensity was read after 24 h of incubation by using an Infinite F200 Tecan plate reader, and MIC values were determined by non-linear fitting of the data to the Gompertz equation (35) using GraphPad Prism.

Site-directed mutagenesis of *dprE1* at C387 in *M. tuberculosis* H37Rv. Generation of point mutations in *M. tuberculosis* H37Rv was done by a recombinering method (20, 21). H37Rv/pJV53 was grown to log phase (OD₆₀₀ of 0.5) in 7H9 medium containing 25 µg/ml of kanamycin before being induced with 0.2% acetamide overnight. Competent cells were transformed with 100 ng of 70-bp single-stranded oligonucleotides (leading and lagging strands) (see Table S1 in the supplemental material) containing the desired mutations, and transformants were selected on 7H10 agar plates either with or without 400 ng/ml BTZ043. Single-nucleotide polymorphisms (SNPs) in resistant colonies were confirmed by colony PCR.

Fitness assessment of *dprE1* mutant strains in liquid culture. All strains were diluted to an initial OD₆₀₀ of 0.05, and OD₆₀₀ measurements were taken every 24 h to monitor growth over a period of 2 weeks. The generation time for each strain was calculated by using the equation $G = t/[3.3 \times \log_{10}(b/B)]$, where G is the generation time, t is the time interval of two measurements in the exponential phase, b is the final OD₆₀₀, and B is the initial OD₆₀₀. Two independent cultures for each strain were used for growth rate measurements.

Expression and purification of wild-type and mutant *M. tuberculosis* DprE1. *M. tuberculosis* *dprE1* was cloned into plasmid pET28a, and the recombinant protein was coexpressed in *E. coli* BL21 (DE3) along with the *M. tuberculosis* GroEL2 (Rv0440) and *E. coli* GroES chaperones in a modified version of the pGro7 plasmid (TaKaRa Bio Inc.). DprE1 was purified as described previously (4) to obtain pure protein with bound flavin adenine dinucleotide (FAD). BTZ-resistant C387G, C387S, C387A, C387T, and C387N mutants were obtained by site-directed mutagenesis with the pET28a-*dprE1* plasmid by using the Stratagene QuikChange II site-directed mutagenesis kit. Expression and purification of the mutant proteins were carried out as described above for the wild-type (WT) protein. Protein concentrations were determined by using the bicinchoninic acid (BCA) assay (Pierce BCA protein assay kit; Thermo Scientific).

DprE1 enzymatic activity assays. Enzyme activities of wild-type and mutant DprE1 proteins were determined in a two-step coupled assay (9). Reactions were carried out in black 96-well half-area plates (catalog number 3686; Corning) in a final volume of 25 µl per well. The reaction mixture consisted of the DprE1 protein (protein concentrations were adapted to obtain similar fluorescence signals [1.5 µM for the WT, 1.5 µM for the C387S mutant, 7.5 µM for C387G, 3 µM for C387A, 10.5 µM for C387T, and 10.5 µM for C387N]), FAD (1 µM), horseradish peroxidase (HRP) (0.2 µM), Amplex Red (50 µM) (Life Technologies), and farnesyl-phosphoryl-β-D-ribofuranose (FPR) (0 µM, 0.2 µM, 0.4 µM, 0.6 µM, or 0.8 µM) in assay buffer (50 mM glycyl glycine [pH 8.0], 200 mM potassium glutamate, 0.002% Brij 35). A standard curve was obtained with a serial dilution of resorufin sodium salt. FPR was used to start the reaction, and the conversion of Amplex Red to resorufin was immediately monitored by fluorescence measurement (excitation/emission wavelength of 560/590 nm) in the kinetic mode on a Tecan M200 instrument at 30°C. To determine 50% inhibitory concentrations (IC₅₀s), the reaction mixture consisting of DprE1, FAD, HRP, and Amplex Red was first incubated with the test compound (with 2-fold serial dilution starting with dimethyl sulfoxide [DMSO] [1% final DMSO concentration]) for 10 min at 30°C before the addition of FPR (0.3 µM). The background fluorescence intensity from the reaction mixture without FPR was subtracted from the values for all reactions. Fluorescence units were converted to resorufin concentrations by using a standard curve. Reaction rates at each FPR concentration or compound concentration were determined and fitted to either the Hill equation for non-Michaelis-Menten kinetics to obtain steady-state kinetic constants or a log[inhibitor]-versus-normalized response (with 100% activity of each enzyme being defined under steady-state conditions in the absence of the inhibitor and 0% activity being defined as the full inhibition of WT DprE1 in the presence of 40 µM the inhibitor) to obtain IC₅₀s by using GraphPad Prism.

Infection of THP-1 macrophages. Human monocytic THP-1 cells were grown in RPMI medium supplemented with 10% FBS. A total of 2 × 10⁴ cells/well of a 96-well plate in 50 µl RPMI medium were differentiated by using phorbol-12-myristate-13-acetate (PMA) (final concentration of 4 nM). Plates were sealed with gas-permeable sealing films and incubated at 37°C with 5% CO₂. Cells were infected the following day. RPMI medium containing PMA was removed from the wells, and cells were washed and incubated with RPMI medium alone. H37Rv, *dprE1* mutant strains, and H37RvΔRD1 were grown to log phase (OD₆₀₀ of between 0.4 and 0.8), washed in 7H9 medium, and resuspended to an OD₆₀₀ of 1 (3 × 10⁸ bacteria/ml). THP-1 cells were infected at a multiplicity of infection (MOI) of 5 in 50 µl RPMI medium and incubated for 3 days before the addition of 5 µl PrestoBlue cell viability reagent (Life Technologies). After

TABLE 1 DprE1 C387 mutations conferring resistance to BTZ043 in *M. tuberculosis*

Residue or mutation	Source or organism in which mutation was previously identified	No. of isolates ^b	BTZ043 MIC (μg/ml)	MXF ^c MIC (μg/ml)	Codon(s) identified by sequencing
C387 (WT)	Wild type		0.002	0.031	TGC
C387G	<i>M. tuberculosis</i> , <i>M. smegmatis</i> ^a	3	12.5	0.063	GGA, GGC
C387S	<i>M. tuberculosis</i> , <i>M. smegmatis</i> , <i>M. aurum</i> ^a	28	>100	0.031	TCA, TCC, TCG, TCT, AGC
C387A	<i>M. avium</i> ^a	5	>100	0.031	GCC, GCG
C387T	This study	18	>100	0.031	ACA, ACC, ACT
C387N	This study	7	6.25	0.031	AAT

^a See reference 2.^b Colonies were isolated on plates containing 400 ng/ml of BTZ043.^c MXF, moxifloxacin.

1 h of incubation at room temperature (RT), fluorescence was measured by using a Tecan M200 instrument (excitation/emission wavelength of 560/590 nm).

Structural studies of WT and mutant DprE1 proteins. DprE1 mutants were modeled based on the *M. tuberculosis* DprE1 structure (PDB accession number 4NCR) (9), using the “Position Scan” function in the FoldX plug-in (22) implemented in YASARA View molecular graphics software (23). Illustrations were made by using PyMOL (24), and the prediction of the functional effect of amino acid substitutions was computed by using the Provean Web server (25, 26).

RESULTS

Five DprE1 mutations confer resistance to BTZ043 in *M. tuberculosis*. In an initial screen to determine which mutations at the C387 residue of DprE1 confer resistance to BTZ043, the gene with a randomly mutated codon at position 387 was expressed under the control of its natural promoter in *M. tuberculosis* H37Rv. Since previous reports described BTZ-resistant substitutions at C387 as being dominant (2), a partially diploid strain was used. The promoter of the Rv3789-*dprE1*-*dprE2* operon (27) was exploited for the construction of partially diploid strains carrying random mutations at the C387 residue of DprE1. In doing so, potential artifacts derived from any unbalanced expression of the wild-type and mutant alleles were avoided.

After selection on 400 ng/ml BTZ043, transformants were screened by PCR to identify mutations associated with resistance, and their MICs for BTZ043 were determined. Various mutations were identified in colonies from BTZ043-containing plates, of which 28 were serine (C387S), 18 were threonine (C387T), 5 were alanine (C387A), 3 were glycine (C387G), and 7 were asparagine (C387N) substitutions. Random mutagenesis proved successful, as several different codons for each mutation were found, and BTZ043 MIC values of the colonies established their resistance

levels (Table 1). Out of 9 possible codons that can be derived from single mutations at C387, which are most likely to occur clinically, only codon TCT coding for C387S appeared in the screen. The C387G mutation resulted in slower-growing colonies on solid medium, although this effect was not observed in liquid culture (see Fig. S1 and S2 in the supplemental material). The finding that the observed phenotype was not due to additional spontaneous mutations was confirmed by growing *M. tuberculosis* cells transformed with a plasmid (pBLG) (see Table S2 in the supplemental material) harboring the C387G substitution, suggesting that the growth defect of *M. tuberculosis* on solid medium was attributed to the glycine mutation. Although the same strategy was adopted to select for BTZ-resistant mutants in *M. smegmatis* expressing the *M. tuberculosis* *dprE1* locus, this was unsuccessful (data not shown).

To further exclude any effects of having two copies of *dprE1* due to the partially diploid strain used in the initial screen, site-directed mutagenesis was performed directly on chromosomal *dprE1* of H37Rv at the C387 residue. C387S, C387A, and C387T mutations were successfully introduced into *dprE1* without additional undesired mutations, and normal-sized colonies were selected on BTZ043-containing plates (Table 2). The introduction of C387G and C387N substitutions gave rise to two different colony sizes, both of which occurred in the absence of BTZ043. Small colonies were found to harbor solely the desired mutation (either C387G or C387N), whereas normal-sized colonies were found to have either a C387G V388I double mutation or C387T instead of the desired C387N mutation (Table 2). Resistance of these strains with *dprE1* C387 mutations to BTZ043 was confirmed by REMA (Table 2).

Fitness assessment of *dprE1* mutant strains. The growth of H37Rv and *dprE1* mutant strains was monitored in liquid 7H9

TABLE 2 Characterization of different H37Rv *dprE1* mutants^a

Mutation	Codon	Colony size	Presence of BTZ in plate from which colonies were picked	Mutation(s) identified by sequencing	BTZ043 MIC (μg/ml)	RIF MIC (μg/ml)
C387	TGC (WT)				0.0008	0.0016
C387S	TCC	Normal	BTZ043	C387S	≥10	0.0016
C387A	GCC	Normal	BTZ043	C387A	>10	0.0016
C387T	AAT	Normal	BTZ043	C387T	>10	0.0016
C387G	GGC	Small		C387G	Undet.	Undet.
		Normal		C387G V388I	5	0.0008
C387N	ACC	Small		C387N	1.25	0.0008
		Normal		C387T*	>10	0.0016

^a RIF, rifampin; Undet., undetermined. * indicates the C387T mutation with an ACT codon.

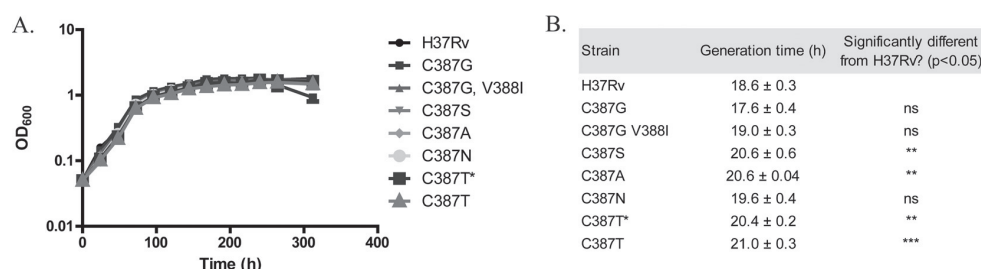


FIG 1 Fitness of H37Rv and *dprE1* mutant strains in 7H9 medium. (A) Growth curves of H37Rv and *dprE1* mutant strains obtained by measuring the OD₆₀₀ of bacterial cultures at 24-h intervals over a period of 14 days, with an initial OD₆₀₀ of 0.05. (B) The generation time for each strain was calculated by using the equation $G = t/[3.3 \times \log_{10}(b/B)]$, where G is the generation time; t is the time interval between two measurements within the exponential phase, here 0 to 48 h; b is the final OD₆₀₀; and B is the initial OD₆₀₀. Data from two independent experiments are presented as means ± standard deviations. Statistical analysis was performed by using one-way analysis of variance with Dunnett's posttest (**, $P < 0.01$; ***, $P < 0.001$). C387T* indicates a mutation containing the ACT codon, compared to C387T, which has the AAT codon instead. "ns" indicates no significance.

medium in the absence of BTZ043 over 2 weeks. Growth curves did not reflect any striking differences in fitness between H37Rv and mutant strains during the exponential or the stationary phase (Fig. 1A). The generation time for each strain was calculated in the exponential phase of growth. For certain mutants (C387S, C387A, and C387T), their generation times significantly differ from that of H37Rv (Fig. 1B), although these differences appear to be too small to be reflected in the growth curves of the mutant strains. Notably, the growth defect of the C387G and C387N mutants on solid medium was not observed in liquid medium.

Effect of DprE1 C387 mutations on *M. tuberculosis* cytotoxicity. The influence of C387 mutations on the cytotoxicity of the mycobacterium was examined *ex vivo* by infecting THP-1 macrophages with the H37Rv and H37Rv *dprE1* C387 mutant strains. As a control, an attenuated strain with reduced virulence, H37RvΔRD1 (28), was used, and this showed decreased cytotoxicity, with macrophage viability being around 60% of that of non-infected macrophages. About 40% of macrophages remained viable after infection with each of the five *dprE1* mutants, compared to about 25% of macrophages remaining viable after being infected with H37Rv (Fig. 2), indicating that the C387 mutations decrease the cytotoxicity of *M. tuberculosis*.

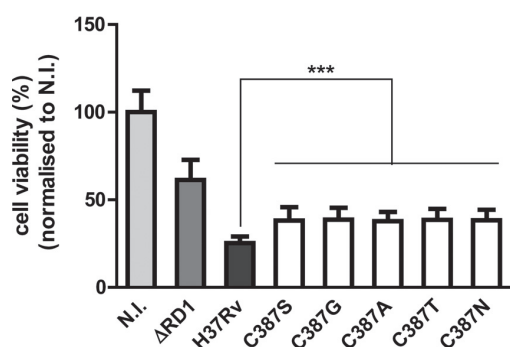


FIG 2 DprE1 C387 mutations affect the cytotoxicity of *M. tuberculosis*. THP-1 cells were infected with H37Rv, H37RvΔRD1, and H37Rv *dprE1* C387 mutant strains at an MOI of 5 or left untreated (not infected [N.I.]). Macrophage viability was measured at 3 days postinfection. Data from two independent experiments were normalized to data under noninfected conditions and are presented as means ± standard deviations. Statistical analysis was performed by using one-way analysis of variance with Dunnett's posttest (***, $P < 0.001$).

Steady-state enzymatic activity of DprE1 mutants. To investigate whether DprE1 C387 mutations could affect the proper functioning of the enzyme, the steady-state enzymatic activity of purified WT and mutant DprE1 proteins was measured by using a two-step coupled enzymatic assay. For each protein, reaction rates at four substrate concentrations were fitted to the Hill equation for non-Michaelis-Menten kinetics to obtain parameters of substrate binding affinity ($K_{0.5}$), turnover number (k_{cat}), and catalytic efficiency ($k_{cat}/K_{0.5}$). None of the mutations at C387 of DprE1 affected the binding affinity of the substrate for the enzyme, as seen from their $K_{0.5}$ values, which were similar to that of the WT enzyme (Fig. 3A). C387G and C387N mutations significantly decreased the turnover rate of the enzyme (Fig. 3B), and consequently, these two mutations reduced the overall catalytic efficiency of DprE1 by about 4-fold (Fig. 3C).

Effect of DprE1 C387 mutations on the potency of DprE1 inhibitors. IC₅₀ values of covalent (PBTZ169) and noncovalent (Ty38c) DprE1 inhibitors (Fig. 4A) were determined for WT and DprE1 mutant proteins. As BTZ043 showed behavior similar to that of PBTZ169 in this assay (data not shown), and the MIC of PBTZ169 was 3-fold lower than that of BTZ043 in *M. tuberculosis*, PBTZ169 was used in this study. Unlike the wild-type enzyme, whose activity is completely inhibited at high PBTZ169 concentrations, mutant enzymes are only partially inhibited at the highest PBTZ169 concentration (40 μM), apparently reaching a plateau at 30 to 40% activity (Fig. 4B). In contrast, this concentration of the noncovalent inhibitor Ty38c was sufficient to inhibit almost all activity of both WT and mutant enzymes (Fig. 4B and C).

This finding confirms the importance of the C387 residue of DprE1 in the mode of inhibition of the covalent inhibitor PBTZ169 and indicates that the replacement of the Cys residue hardly affects the binding of noncovalent inhibitors to DprE1. This can be further seen from the IC₅₀ values of PBTZ169 and Ty38c obtained for WT and mutant enzymes (Fig. 4C). All mutant enzymes showed increased PBTZ169 IC₅₀ values compared to that for the WT, thus accounting for the BTZ resistance of the mutants. Ty38c IC₅₀ values for the C387S and C387A mutants were identical to that for the WT, while the C387G, C387T, and C387N mutants had slightly higher values than that for the WT (Fig. 4C), indicating that substitutions at C387 have a more modest effect on Ty38c activity. PBTZ169 and Ty38c MIC values were also determined for H37Rv and *dprE1* mutant strains (Table 3). C387 mu-

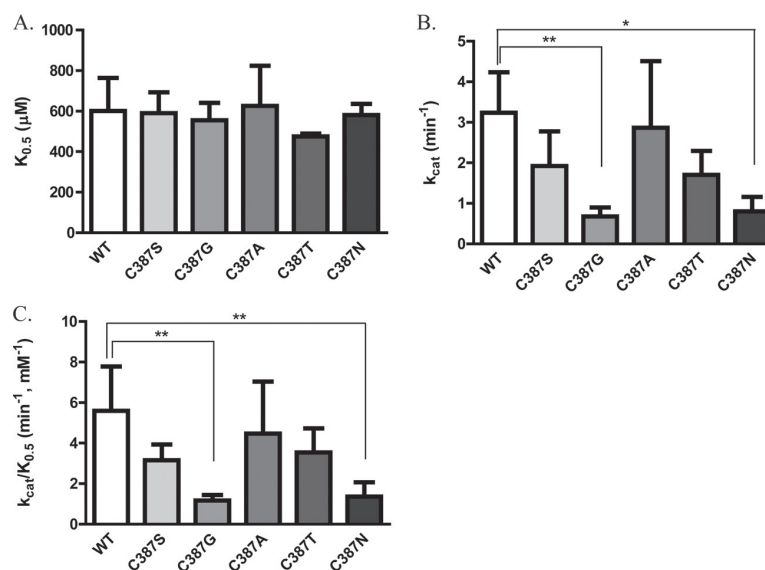


FIG 3 Steady-state enzymatic activity of WT and DprE1 mutants. Shown are substrate binding affinity ($K_{0.5}$) (A), turnover number (k_{cat}) (B), and catalytic efficiency ($k_{\text{cat}}/K_{0.5}$) (C) steady-state parameters obtained for the WT and DprE1 mutants by fitting enzyme activity at various FPR concentrations (0.2 to 0.8 mM) to the equation $Y = V_{\text{max}} \times X^h / (K_{\text{prime}} + X^h)$, where Y is enzyme activity, X is the substrate concentration, K_{prime} equals $(K_{0.5})^h$, and h is the Hill coefficient, by using GraphPad Prism. Data from at least three independent experiments are presented as means \pm standard deviations. Statistical analysis was performed by using one-way analysis of variance with Dunnett's posttest (*, $P < 0.05$; **, $P < 0.01$).

tations cause an increase in the PBTZ169 MIC compared to H37Rv, with strains harboring C387S, C387A, and C387T mutations having higher levels of resistance (MIC of $>1 \mu\text{g/ml}$) and those with C387G and C387N mutations having lower levels of resistance (MIC of 0.5 to 0.6 $\mu\text{g/ml}$) to PBTZ169. In the case of Ty38c, mutant strains had MIC values ranging from 0.1 to 0.8 $\mu\text{g/ml}$, and the trend was similar to that seen with PBTZ169.

Taken together, these data demonstrate that C387 mutations decrease the potency of covalently binding DprE1 inhibitors such as PBTZ169 to a much greater extent than noncovalent DprE1 inhibitors, represented here by Ty38c. As the MICs of lower-resistance mutants could be measured, one of the mutants (C387N) was used to investigate the effect of a C387 mutation on the interaction between BTZ and bedaquiline (BDQ), as synergism between these two classes of compounds *in vitro* (29) and *in vivo* (4) was previously described. Using a checkerboard assay, the partial synergism of PBTZ169 and BDQ observed in H37Rv at $0.5 \times \text{MIC}$ was not significantly altered by the DprE1 C387N mutation (see Fig. S3 in the supplemental material).

Modeling the effect of C387 mutations on the active site of DprE1. To gain further insight into the mechanism of resistance of DprE1 mutants to BTZ and to predict the effect of each mutation on the functionality of DprE1, substitution at C387 with every amino acid was modeled *in silico* based on the structure of *M. tuberculosis* DprE1.

Modeling showed that all the substitutions are tolerated in terms of steric hindrance. Indeed, amino acid 387 is localized on a beta sheet where the side chain could easily be accommodated since it is exposed to the solvent toward the substrate binding pocket (Fig. 5A). Substitutions at this position will lead to a modification of the shape and volume of the substrate binding pocket (Fig. 5B). It is evident from these models that some substitutions

will lead to nonfunctional proteins. More precisely, only substitutions by small and/or polar residues such as asparagine, aspartate, serine, threonine, alanine, and glycine would lead to functional enzymes, whereas amino acids with larger side chains (arginine, tryptophan, phenylalanine, glutamate, glutamine, tyrosine, methionine, lysine, and histidine) would block access to the substrate, resulting in nonfunctional enzymes. Furthermore, exposure of the side chain to the solvent excludes the possibility of a hydrophobic residue occupying this position (leucine, isoleucine, and valine), and the proline substitution is not favored in beta sheet structures, as it cannot complete the hydrogen-bonding network.

To confirm these observations, a prediction of the functional effects of amino acid substitutions was computed by using the Provan Web server (25, 26). Interestingly, only alanine, serine, and threonine were found to be nondeleterious. Altogether, these results are in agreement with the data obtained from the screen.

The superposition of crystal structures of WT DprE1 and the C387A, C387S, C387G, C387T, and C387N mutants in complex with PBTZ169 or Ty38c revealed that these five substitutions do not block the access of both inhibitors to the binding pocket (see Fig. S4 in the supplemental material). As expected, the five mutants are not able to form the critical covalent adduct with PBTZ169. In these cases, PBTZ169 is stabilized only unspecifically by van der Waals interactions in the binding pocket and behaves as an inefficient noncovalent inhibitor, resulting in a dramatic reduction of PBTZ169 potency. On the other hand, C387 is not directly implicated in the binding of the noncovalent inhibitor Ty38c. Although C387 mutations do not influence the main interaction with Ty38c, they could still affect the environment in the substrate binding pocket, leading to a modest impairment of the inhibitor activity.

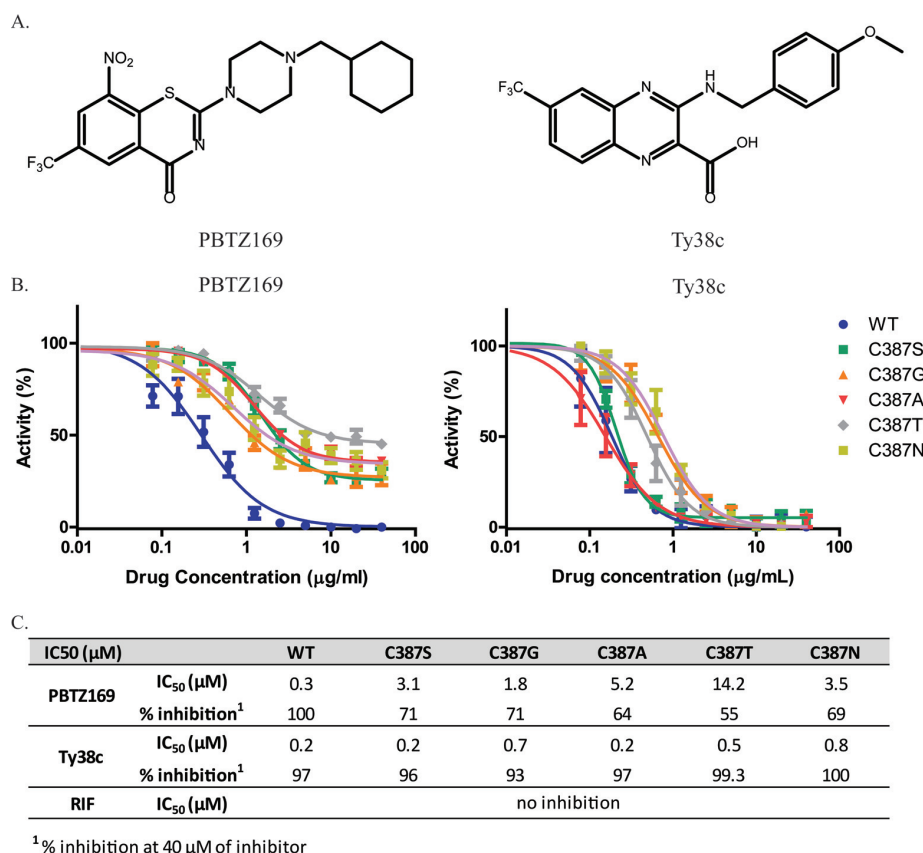


FIG 4 Effects of DprE1 C387 mutations on potency of DprE1 inhibitor activity. (A) Structures of the DprE1 inhibitors PBTZ169 and Ty38c. PBTZ169 inhibits DprE1 via a covalent bond between the reduced form of its nitro group and the C387 residue of DprE1, whereas Ty38c, which lacks the nitro group, is a noncovalent inhibitor of DprE1. (B) Curves of enzyme activity with increasing inhibitor (PBTZ169 or Ty38c) concentrations for WT and mutant enzymes. A total of 40 μM the inhibitor was used for the highest concentration, with subsequent 2-fold serial dilutions. Enzymatic activities at each inhibitor concentration were normalized to steady-state enzymatic activity in the absence of any inhibitor. (C) PBTZ169 and Ty38c IC₅₀ values and maximum inhibition for WT and mutant enzymes. IC₅₀ values were obtained by fitting the curves in panel B to the log[inhibitor]-versus-normalized response by using GraphPad Prism. Maximum percent inhibition of the WT or mutant enzyme was determined with 40 μM the inhibitor. Data from at least two independent experiments are presented as means ± standard deviations.

DISCUSSION

DprE1 plays an essential role in the DPA pathway for cell wall synthesis in *M. tuberculosis*. Having been identified as the target of at least five structurally distinct inhibitors in recent years, DprE1 is an extremely vulnerable target of the pathogen (30, 31). Among

the inhibitors, PBTZ169 is a highly potent covalent inhibitor of DprE1 and is currently in phase I trials. We have studied the critical C387 residue of DprE1 required for the covalent interaction with PBTZ169 and with other nitroaromatic inhibitors by identifying and characterizing substitutions at this residue that are tolerated and confer resistance to BTZs.

The data obtained confirmed the dominant nature of the mutations introduced (2) and identified C387S, C387A, C387T, C387G, and C387N as DprE1 mutations viable for the bacteria while conferring various levels of resistance to BTZ043 and PBTZ169. The C387S, C387A, and C387T mutations confer high levels of resistance of H37Rv to BTZs, while C387G and C387N confer intermediate levels of resistance. As previously reported, C387S and C387A substitutions are naturally occurring mutations found in *M. aurum* and *M. avium*, and C387G and C387S were found in colonies spontaneously resistant to BTZ043 (2). C387N and C387T are novel mutations identified here from this screen. To our knowledge, these mutations have hitherto remained unidentified in DprE1 in mutants spontaneously resistant to

TABLE 3 PBTZ169 and Ty38c MICs for H37Rv and H37Rv *dprE1* C387 mutant strains

Strain	PBTZ169 MIC (μg/ml)	Ty38c MIC (μg/ml)	RIF ^a MIC (μg/ml)
H37Rv	0.0001	0.1	0.001
C387S	>1	0.5	0.001
C387G	0.5	0.04	0.0005
C387A	>1	0.1	0.001
C387T	>1	0.8	0.001
C387N	0.6	0.1	0.001
NTB1 ^b	>1	0.7	0.001

^a RIF, rifampin.

^b BTZ-resistant strain with a C387S mutation (control).

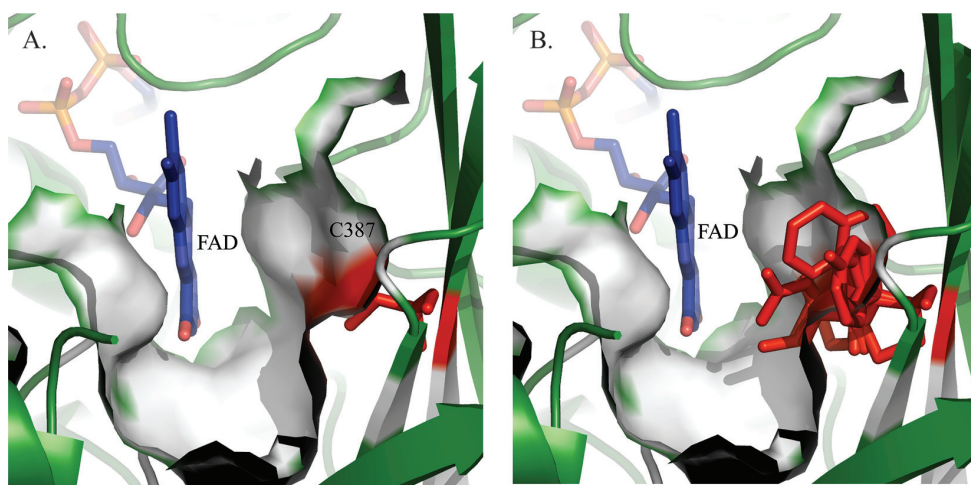


FIG 5 Closeup views of the substrate binding pocket of *M. tuberculosis* WT DprE1 compared to mutant models. (A) Substrate binding pocket in the crystal structure of *M. tuberculosis* DprE1 (PDB accession number 4NCR). FAD is represented in blue, and cysteine 387 is presented in red. The solvent-accessible surface is represented by the white surface. (B) Superposition of crystal structures of *M. tuberculosis* WT DprE1 and 19 substitution models at residue 387 (represented by sticks in red). The side chains of some amino acids likely block the substrate binding site, leading to a nonfunctional enzyme.

BTZ043, likely because two or three bases of the cysteine codon (TGC) need to be mutated to generate a threonine (ACA, ACC, and ACT) or an asparagine (AAT) codon.

The fact that C387S and C387A mutations do not result in *M. tuberculosis* growth defects or in reduced enzymatic capabilities and are predicted to be nondeleterious mutations that do not block the access of the substrate to the binding pocket are consistent with their occurrence in nature. Although C387G and C387N mutations appear to allow substrate access in structural models, it appears that the nonoptimal size of their side chains (i.e., either too small or too large) strongly impacts the resulting shape of the substrate binding pocket and would affect the stability and binding of the substrate, resulting in reduced enzymatic activity. Furthermore, these mutations are also predicted to be deleterious and would have a detrimental impact on the biological function of DprE1. As seen experimentally, growth defects were observed on solid medium in the presence of these mutations. This could be a consequence of the impaired catalytic capability of DprE1, which would imply that the epimerization of DPR to DPA and, by extension, the formation of the arabinogalactan layer in the mycobacterium cell wall occur at lower rates.

DprE1 C387 mutations are less cytotoxic than the WT in macrophages. Regardless of the substitution at C387, there is an impaired ability of *M. tuberculosis* to induce host cell death. The exact mechanism remains unclear; however, one might speculate that these mutations result in slower replication of the mycobacterium in an *ex vivo* context. Another possibility is that the *M. tuberculosis* cell wall component LAM is formed at a reduced rate as a result of decreased DPA synthesis. Since LAM has been found to inhibit phagosome maturation within macrophages (32), this capability could be reduced in the presence of C387 mutations, with a consequent decrease in the survival of the pathogen in the host cell.

The importance of the C387 residue in the binding of covalent DprE1 inhibitors is illustrated biochemically by the increase in PBTZ169 IC_{50} values in the presence of C387 substitutions and the fact that even at high concentrations of PBTZ169, there is no full

inhibition in all the mutant enzymes. This residual enzymatic activity explains the ability of the mutant to survive *in vitro* even in the presence of the compound at concentrations much higher than the MIC. In the case of the noncovalent DprE1 inhibitor, C387G and C387N mutations modestly affect its activity although to a considerably lesser extent than that of PBTZ169. These findings are further supported by WT and mutant DprE1 structures docked with either PTBZ169 or Ty38c, where the effects of C387 mutations on the covalent and noncovalent mechanisms of inhibition are modeled at the atomic level.

With the initial BTZ-resistant mutant selection procedure, mutants conferring lower-level resistance may have been missed due to growth defects. An explanation for the unsuccessful selection of BTZ-resistant mutants in *M. smegmatis* may be due to the differences in the regulation of arabinogalactan or lipoarabinomannan biosynthesis in the two species or to the different genomic organization of *M. smegmatis*. Furthermore, it was reported previously that the level of activity of the *M. tuberculosis* *embA* promoter was markedly lower in *M. smegmatis* (33), suggesting that control of gene expression may be organized differently in this nonpathogenic mycobacterium. Therefore, it appears that *M. smegmatis* may not be the best model for studying genes implicated in arabinan-derived cell wall components expressed under the control of *M. tuberculosis* promoters.

In conclusion, we have identified five mutations in DprE1 that do not affect the viability of *M. tuberculosis*, which give rise to a functional enzyme and generate BTZ resistance. As these five BTZ-resistant mutants appear less cytotoxic in macrophages, they may also be less fit should these mutations arise in humans. From a clinical standpoint, an understanding of DprE1-mediated BTZ resistance will facilitate clinical trials of the drug candidate PBTZ169 by screening *M. tuberculosis* for C387 mutations over the course of treatment. In the case of the C387N mutant with an intermediate level of resistance to PBTZ169, it appears that the synergy between PBTZ169 and BDQ does not depend on the covalent bond of C387 with PBTZ169. This is consistent with the

finding that noncovalent DprE1 inhibitors, the 1,4-azaindoles, also display synergism with BDQ (34). The lack of cross-resistance of BTZ-resistant mutants to Ty38c as reported in this work would also be an important consideration when deciding which and how many DprE1 inhibitors to develop clinically, as a noncovalent DprE1 inhibitor could be used after resistance to the covalent one develops, or vice versa. Altogether, this work provides timely insight into the mechanisms of resistance of *M. tuberculosis* to DprE1 inhibitors as PBTZ169 progresses into clinical trials.

ACKNOWLEDGMENTS

We thank Neeraj Dhar for providing plasmid pND255, Vadim Makarov for BTZ043 and PBTZ169, Maria-Paola Costi for Ty38c, and Anthony Vocat for his technical assistance in REMAs.

FUNDING INFORMATION

This work was supported by the European Community's Seventh Framework Program FP7/2007-2013 under grant agreement 260872. Benoit Lechartier was a recipient of a grant from the Fondation Jacqueline Beytout. João Neres was awarded a Marie Curie fellowship.

REFERENCES

1. WHO. 2015. Global tuberculosis report 2015. WHO, Geneva, Switzerland.
2. Makarov V, Manina G, Mikusova K, Mollmann U, Ryabova O, Saint-Joanis B, Dhar N, Pasca MR, Buroni S, Lucarelli AP, Milano A, De Rossi E, Belanova M, Bobovska A, Dianiskova P, Kordulakova J, Sala C, Fullam E, Schneider P, McKinney JD, Brodin P, Christophe T, Waddell S, Butcher P, Albrethsen J, Rosenkrands I, Brosch R, Nandi V, Bharath S, Gaonkar S, Shandil RK, Balasubramanian V, Balganesht T, Tyagi S, Grosset J, Riccardi G, Cole ST. 2009. Benzothiazinones kill Mycobacterium tuberculosis by blocking arabinan synthesis. *Science* 324:801–804. <http://dx.doi.org/10.1126/science.1171583>.
3. Pasca MR, Degiacomi G, de Jesus Lopes Ribeiro AL, Zara F, De Mori P, Heym B, Mirrione M, Brerra R, Pagani L, Pucillo L, Troupioti P, Makarov V, Cole ST, Riccardi G. 2010. Clinical isolates of Mycobacterium tuberculosis in four European hospitals are uniformly susceptible to benzothiazinones. *Antimicrob Agents Chemother* 54:1616–1618. <http://dx.doi.org/10.1128/AAC.01676-09>.
4. Makarov V, Lechartier B, Zhang M, Neres J, van der Sar AM, Raadsen SA, Hartkoorn RC, Ryabova OB, Vocat A, Decosterd LA, Widmer N, Budin T, Bitter W, Andries K, Pojer F, Dyson PJ, Cole ST. 2014. Towards a new combination therapy for tuberculosis with next generation benzothiazinones. *EMBO Mol Med* 6:372–383. <http://dx.doi.org/10.1002/emmm.201303575>.
5. Working Group on New TB Drugs. 2015. Drug pipeline. Stop TB Partnership, Geneva, Switzerland. <http://www.newtbdrugs.org/pipeline.php>. Accessed 22 November 2015.
6. Mikusova K, Huang H, Yagi T, Holsters M, Vereecke D, D'Haese W, Scherman MS, Brennan PJ, McNeil MR, Crick DC. 2005. Decaprenylphosphoryl arabinofuranose, the donor of the D-arabinofuranosyl residues of mycobacterial arabinan, is formed via a two-step epimerization of decaprenylphosphoryl ribose. *J Bacteriol* 187:8020–8025. <http://dx.doi.org/10.1128/JB.187.23.8020-8025.2005>.
7. Trefzer C, Rengifo-Gonzalez M, Hinner MJ, Schneider P, Makarov V, Cole ST, Johnsson K. 2010. Benzothiazinones: prodrugs that covalently modify the decaprenylphosphoryl-β-D-ribose 2'-epimerase DprE1 of Mycobacterium tuberculosis. *J Am Chem Soc* 132:13663–13665. <http://dx.doi.org/10.1021/ja106357w>.
8. Trefzer C, Škovicová H, Buroni S, Bobovská A, Nenci S, Molteni E, Pojer F, Pasca MR, Makarov V, Cole ST, Riccardi G, Mikusová K, Johnsson K. 2012. Benzothiazinones are suicide inhibitors of mycobacterial decaprenylphosphoryl-β-D-ribose 2'-oxidase DprE1. *J Am Chem Soc* 134:912–915. <http://dx.doi.org/10.1021/ja211042r>.
9. Neres J, Pojer F, Molteni E, Chiarelli LR, Dhar N, Boy-Rottger S, Buroni S, Fullam E, Degiacomi G, Lucarelli AP, Read RJ, Zanonni G, Edmondson DE, De Rossi E, Pasca MR, McKinney JD, Dyson PJ, Riccardi G, Mattevi A, Cole ST, Binda C. 2012. Structural basis for

benzothiazinone-mediated killing of Mycobacterium tuberculosis. *Sci Transl Med* 4:150ra121. <http://dx.doi.org/10.1126/scitranslmed.3004395>.

10. Batt SM, Jabeen T, Bhowruth V, Quill L, Lund PA, Eggeling L, Alderwick LJ, Futterer K, Besra GS. 2012. Structural basis of inhibition of Mycobacterium tuberculosis DprE1 by benzothiazinone inhibitors. *Proc Natl Acad Sci U S A* 109:11354–11359. <http://dx.doi.org/10.1073/pnas.1205735109>.
11. Brecik M, Centárová I, Mukherjee R, Kolly GS, Huszár S, Bobovská A, Kilacsková E, Mokošová V, Svetlikova Z, Šarkan M, Neres J, Korduláková J, Cole ST, Mikusová K. 29 April 2015. DprE1 is a vulnerable tuberculosis drug target due to its cell wall localization. *ACS Chem Biol* <http://dx.doi.org/10.1021/acscchembio.5b00237>.
12. Magnet S, Hartkoorn RC, Székely R, Pató J, Triccas JA, Schneider P, Szántai-Kis C, Örfi L, Chambon M, Banfi D, Bueno M, Turcatti G, Kéri G, Cole ST. 2010. Leads for antitubercular compounds from kinase inhibitor library screens. *Tuberculosis* 90:354–360. <http://dx.doi.org/10.1016/j.tube.2010.09.001>.
13. Stanley SA, Grant SS, Kawate T, Iwase N, Shimizu M, Wivagg C, Silvis M, Kazvanskaya E, Aquadro J, Golas A, Fitzgerald M, Dai H, Zhang L, Hung DT. 2012. Identification of novel inhibitors of M. tuberculosis growth using whole cell based high-throughput screening. *ACS Chem Biol* 7:1377–1384. <http://dx.doi.org/10.1021/cb300151m>.
14. Wang F, Sambandan D, Halder R, Wang J, Batt SM, Weinrick B, Ahmad I, Yang P, Zhang Y, Kim J, Hassani M, Huszar S, Trefzer C, Ma Z, Kaneko T, Mdululi KE, Franzblau S, Chatterjee AK, Johnsson K, Mikusova K, Besra GS, Futterer K, Robbins SH, Barnes SW, Walker JR, Jacobs WR, Schultz PG. 2013. Identification of a small molecule with activity against drug-resistant and persistent tuberculosis. *Proc Natl Acad Sci U S A* 110:E2510–E2517. <http://dx.doi.org/10.1073/pnas.1309171110>.
15. Shirude PS, Shandil R, Sadler C, Naik M, Hosagrahara V, Hameed S, Shinde V, Bathula C, Humnabadkar V, Kumar N, Reddy J, Panduga V, Sharma S, Ambady A, Hegde N, Whiteaker J, McLaughlin RE, Gardner H, Madhavapeddi P, Ramachandran V, Kaur P, Narayan A, Guptha S, Awasthy D, Narayan C, Mahadevaswamy J, Vishwas KG, Ahuja V, Srivastava A, Prabhakar K, Bharath S, Kale R, Ramaiah M, Choudhury NR, Sambandamurthy VK, Solapure S, Iyer PS, Narayanan S, Chatterji M. 2013. Azaindoles: noncovalent DprE1 inhibitors from scaffold morphing efforts, kill Mycobacterium tuberculosis and are efficacious in vivo. *J Med Chem* 56:9701–9708. <http://dx.doi.org/10.1021/jm401382v>.
16. Panda M, Ramachandran S, Ramachandran V, Shirude PS, Humnabadkar V, Nagalapuri K, Sharma S, Kaur P, Guptha S, Narayan A, Mahadevaswamy J, Ambady A, Hegde N, Rudrapatna SS, Hosagrahara VP, Sambandamurthy VK, Raichurkar A. 2014. Discovery of pyrazolopyridones as a novel class of non-covalent dprE1 inhibitor with potent anti-mycobacterial activity. *J Med Chem* 57:4761–4771. <http://dx.doi.org/10.1021/jm5002937>.
17. Naik M, Humnabadkar V, Tantry SJ, Panda M, Narayan A, Guptha S, Panduga V, Manjrekar P, Jena LK, Koushik K, Shanbhag G, Jatheendranath S, Manjunatha MR, Gorai G, Bathula C, Rudrapatna S, Achar V, Sharma S, Ambady A, Hegde N, Mahadevaswamy J, Kaur P, Sambandamurthy VK, Awasthy D, Narayan C, Ravishanker S, Madhavapeddi P, Reddy J, Prabhakar K, Saralaya R, Chatterji M, Whiteaker J, McLaughlin B, Chiarelli LR, Riccardi G, Pasca MR, Binda C, Neres J, Dhar N, Signorino-Gelo F, McKinney JD, Ramachandran V, Shandil R, Tommasi R, Iyer PS, Narayanan S, Hosagrahara V, Kavanagh S, Dinesh N, Ghorpade SR. 2014. 4-Aminoquinolone piperidine amides: noncovalent inhibitors of DprE1 with long residence time and potent antimycobacterial activity. *J Med Chem* 57:5419–5434. <http://dx.doi.org/10.1021/jm5005978>.
18. Neres J, Hartkoorn RC, Chiarelli LR, Gadupudi R, Pasca MR, Mori G, Venturelli A, Savina S, Makarov V, Kolly GS, Molteni E, Binda C, Dhar N, Ferrari S, Brodin P, Delorme V, Landry V, de Jesus Lopes Ribeiro AL, Farina D, Saxena P, Pojer F, Carta A, Luciani R, Porta A, Zanonni G, De Rossi E, Costi MP, Riccardi G, Cole ST. 2015. 2-Carboxyquinoloxalines kill Mycobacterium tuberculosis through noncovalent inhibition of DprE1. *ACS Chem Biol* 10:705–714. <http://dx.doi.org/10.1021/cb5007163>.
19. Palomino J-C, Martin A, Camacho M, Guerra H, Swings J, Portaels F. 2002. Resazurin microtiter assay plate: simple and inexpensive method for detection of drug resistance in Mycobacterium tuberculosis. *Antimicrob Agents Chemother* 46:2720–2722. <http://dx.doi.org/10.1128/AAC.46.8.2720-2722.2002>.
20. van Kessel JC, Marinelli LJ, Hatfull GF. 2008. Recombineering myco-

- bacteria and their phages. *Nat Rev Microbiol* 6:851–857. <http://dx.doi.org/10.1038/nrmicro2014>.
21. Rybníček J, Vocat A, Sala C, Busso P, Pojer F, Benjak A, Cole ST. 2015. Lansoprazole is an antituberculous prodrug targeting cytochrome bc1. *Nat Commun* 6:7659. <http://dx.doi.org/10.1038/ncomms8659>.
 22. Van Durme J, Delgado J, Stricher F, Serrano L, Schymkowitz J, Rousseau F. 2011. A graphical interface for the FoldX forcefield. *Bioinformatics* 27:1711–1712. <http://dx.doi.org/10.1093/bioinformatics/btr254>.
 23. Krieger E, Vriend G. 2014. YASARA View—molecular graphics for all devices—from smartphones to workstations. *Bioinformatics* 30:2981–2982. <http://dx.doi.org/10.1093/bioinformatics/btu426>.
 24. Schrödinger LLC. 2015. The PyMOL molecular graphics system, version 1.8. Schrödinger, LLC, Cambridge, MA.
 25. Choi Y, Sims GE, Murphy S, Miller JR, Chan AP. 2012. Predicting the functional effect of amino acid substitutions and indels. *PLoS One* 7:e46688. <http://dx.doi.org/10.1371/journal.pone.0046688>.
 26. Choi Y, Chan AP. 2015. PROVEAN Web server: a tool to predict the functional effect of amino acid substitutions and indels. *Bioinformatics* 31:2745–2747. <http://dx.doi.org/10.1093/bioinformatics/btv195>.
 27. Kolly GS, Mukherjee R, Kilacsková E, Abriata LA, Raccaud M, Blaško J, Sala C, Dal Peraro M, Mikušová K, Cole ST. 2015. GtrA protein Rv3789 is required for arabinosylation of arabinogalactan in *Mycobacterium tuberculosis*. *J Bacteriol* 197:3686–3697. <http://dx.doi.org/10.1128/JB.00628-15>.
 28. Hsu T, Hingley-Wilson SM, Chen B, Chen M, Dai AZ, Morin PM, Marks CB, Padiyar J, Goulding C, Gingery M. 2003. The primary mechanism of attenuation of bacillus Calmette-Guerin is a loss of secreted lytic function required for invasion of lung interstitial tissue. *Proc Natl Acad Sci U S A* 100:12420–12425. <http://dx.doi.org/10.1073/pnas.1635213100>.
 29. Lechartier B, Hartkoorn RC, Cole ST. 2012. In vitro combination studies of benzothiazinone lead compound BTZ043 against *Mycobacterium tuberculosis*. *Antimicrob Agents Chemother* 56:5790–5793. <http://dx.doi.org/10.1128/AAC.01476-12>.
 30. Riccardi G, Pasca MR, Chiarelli LR, Manina G, Mattevi A, Binda C. 2013. The DprE1 enzyme, one of the most vulnerable targets of *Mycobacterium tuberculosis*. *Appl Microbiol Biotechnol* 97:8841–8848. <http://dx.doi.org/10.1007/s00253-013-5218-x>.
 31. Mikusova K, Makarov V, Neres J. 2013. DprE1—from the discovery to the promising tuberculosis drug target. *Curr Pharm Des* 20:4379–4403. <http://dx.doi.org/10.2174/138161282027140630122724>.
 32. Vergne I, Fratti RA, Hill PJ, Chua J, Belisle J, Deretic V. 2004. *Mycobacterium tuberculosis* phagosome maturation arrest: mycobacterial phosphatidylinositol analog phosphatidylinositol mannoside stimulates early endosomal fusion. *Mol Biol Cell* 15:751–760. <http://dx.doi.org/10.1091/mbc.E03-05-0307>.
 33. Amin AG, Goude R, Shi L, Zhang J, Chatterjee D, Parish T. 2008. EmbA is an essential arabinosyltransferase in *Mycobacterium tuberculosis*. *Microbiology* 154:240–248. <http://dx.doi.org/10.1099/mic.0.2007/012153-0>.
 34. Chatterji M, Shandil R, Manjunatha MR, Solapure S, Ramachandran V, Kumar N, Saralaya R, Panduga V, Reddy J, Prabhakar KR, Sharma S, Sadler C, Cooper CB, Mdluli K, Iyer PS, Narayanan S, Shirude PS. 2014. 1,4-Azaindole, a potential drug candidate for treatment of tuberculosis. *Antimicrob Agents Chemother* 58:5325–5331. <http://dx.doi.org/10.1128/AAC.03233-14>.
 35. Lambert RJW, Pearson J. 2000. Susceptibility testing: accurate and reproducible minimum inhibitory concentration (MIC) and noninhibitory concentration (NIC) values. *Journal of Applied Microbiology* 88:784–790. <http://dx.doi.org/10.1046/j.1365-2672.2000.01017.x>.

SUPPLEMENTAL MATERIAL

SUPPLEMENTARY METHODS

Determination of PBTZ169 and BDQ interaction in H37Rv and C387N mutant. Drug interactions between PBTZ169 and BDQ were determined using the checkerboard assay [1, 2]. *M. tuberculosis* strains were grown in 7H9 medium to log- phase (OD₆₀₀ 0.4 - 0.8) and diluted to an OD₆₀₀ of 0.0001. 75 µl of bacterial suspension (2.25×10^3 cells) was added per well of a 96-well plate. The first compound was added to the first column and two-fold serial dilutions were made column-wise. The second compound was prepared in 7H9 at a concentration 8x MIC and serial dilutions were made to 0.125x MIC. 25 µl of diluted compound at each concentration was added to a row of the 96-well plate. Various combinations of PBTZ169 and BDQ were thus obtained in a final volume of 100 µl per well. Plates were incubated for 6 days at 37°C, 10 µl of 0.025% w/v resazurin was added to each well. The fluorescence intensity was read after 24 h incubation using an Infinite F200 Tecan plate reader.

For rows where an MIC value could be determined, the fractional inhibitory concentration index (Σ FICI) was calculated using the equation Σ FIC index = $FIC_{PBTZ} + FIC_{BDQ} = (MIC \text{ of PBTZ, tested in combination}) / (MIC \text{ of PBTZ, alone}) + (MIC \text{ of BDQ, tested in combination}) / (MIC \text{ of BDQ, alone})$. Σ FIC ≤ 0.5 is considered as synergism, $0.5 < \Sigma$ FIC ≤ 4 additivity, and Σ FIC > 4 antagonism.

SUPPLEMENTARY FIGURES

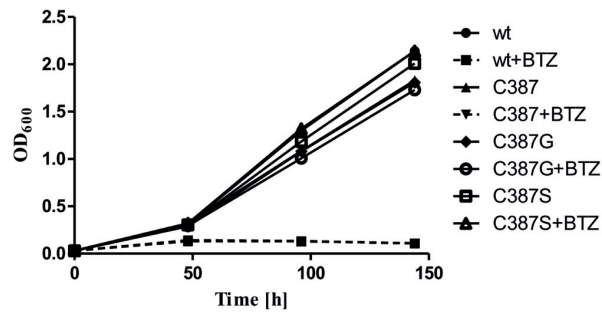


FIG S1 Growth comparison of H37Rv and mutant strains in liquid medium with or without BTZ043. *M. tuberculosis* H37Rv (wt) was grown with (+BTZ) or without 400 ng/ml BTZ043. Wild-type growth was compared to the merodiploid strain harbouring the cysteine codon (C387), which behaves like the wild-type strain, and the glycine or serine mutants (C387G and C387S), which are both fully resistant to BTZ. The C387A, C387N and C387T mutants behaved like the other mutants (not shown in the graph).

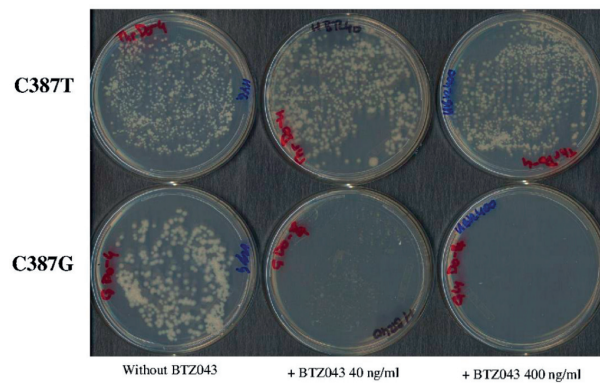


FIG S2 Growth comparison between C387T and C387G mutant strains on solid media with or without BTZ043. The mutants DprE1^{C387G} and DprE1^{C387T} were plated with or without 40 or 400 ng/ml BTZ on the same day. The picture was taken after 21 days of incubation at 37°C. The C387G mutant CFUs on BTZ-containing plates were hardly detectable after 3 weeks of incubation but were countable after 6 weeks.

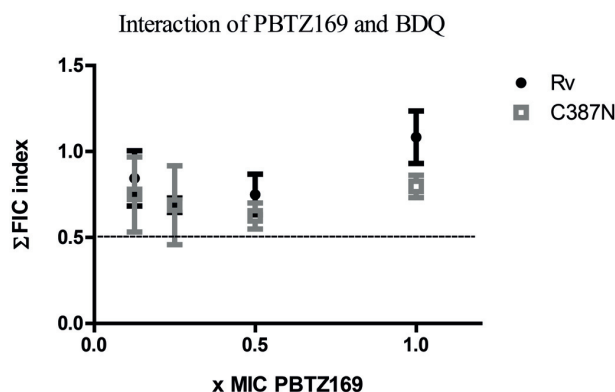


FIG S3 Interactions of PBTZ169 and BDQ in H37Rv and C387N mutant. The sum of fractional inhibitory concentration (FIC) of PBTZ169 and of BDQ were calculated with the equation $\Sigma\text{FIC index} = \text{FIC}_{\text{PBTZ169}} + \text{FIC}_{\text{BDQ}} = (\text{MIC of PBTZ169, tested in combination})/(\text{MIC of PBTZ169, alone}) + (\text{MIC of BDQ, tested in combination})/(\text{MIC of BDQ, alone})$. ΣFIC indices were calculated for drug concentrations where an MIC could be determined using a checkerboard assay with REMA as a viability marker. Black circles represent H37Rv, grey squares represent C387N mutant strain. The dotted line indicates the threshold for synergism. Data from two independent experiments are presented as mean \pm SD.

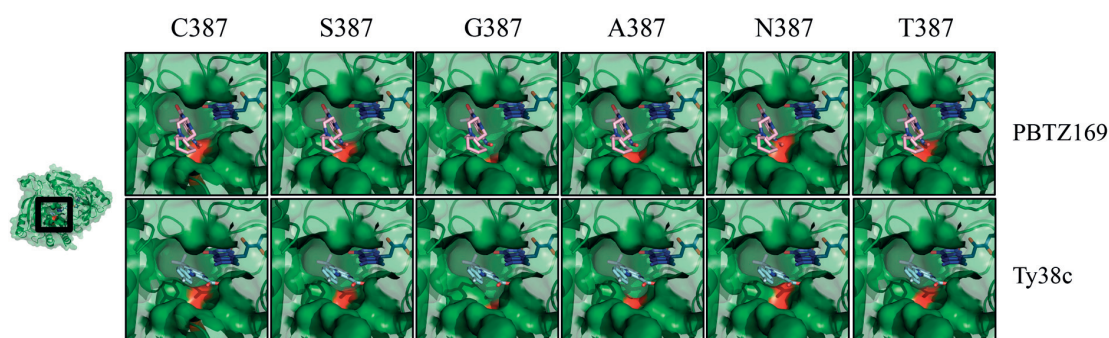


FIG S4 Models of binding of PBTZ169 and Ty38c in the binding pocket of the five DprE1 mutants. The 387 position of DprE1 is represented in red, FAD in blue. PBTZ169 and Ty38c are shown docked into the binding pocket of DprE1 WT and mutant crystal structures. Both compounds are able to bind to the 5 mutants.

TABLE S1 Primers used in this study

Primer name	Sequence
Mut90_fwd	CCATCCCGGGCTGGAACATC>NNNGTCGACTTCCCCATCAAGGACG [§]
Mut90_rev	CGTCCTTGATGGGGAAGTCGACNNNGATGTTCCAGCCCGGGATGG
90C387G_fwd	CCATCCCGGGCTGGAACATCGGGCGTCGACTTCCCCATCAAGGACG
90C387G_rev	CGTCCTTGATGGGGAAGTCGACGCCGATGTTCCAGCCCGGGATGG
Rv3790_fwd	AATACTCCATGGCCATCCTGACGGATGGCCTTGACAGCCCACTAGGTCAGGC*
Rv3790_rev	AATGCAAGTACTCTACAGCAGCTCCAAGCGTC*
JN C387S_fwd	GGCTGGAACATCAGCGTCGACTTCCCC
JN C387S_rev	CCGACCTTGATAGTCGACGCTGAAGGGG
JN C387G_fwd	GGCTGGAACATCGGGCGTCGACTTCCCC
JN C387G_rev	CCGACCTTGATAGCCGACGCTGAAGGGG
Rv3790c387G_For	gccgctcagctccccatccgggctggaacatcgcgctcagctccccatcaaggacgggctggggaag
Rv3790c387G_Rev	cttccccagccgctccttgatggggaagtcgacgccgatgtccagccgggatggggaagctgagcggc
Rv3790c387S_For	gccgctcagctccccatccgggctggaacatcctcgctcagctccccatcaaggacgggctggggaag
Rv3790c387S_Rev	cttccccagccgctccttgatggggaagtcgacgggatgtccagccgggatggggaagctgagcggc
Rv3790c387A_For	gccgctcagctccccatccgggctggaacatcgccgctcagctccccatcaaggacgggctggggaag
Rv3790c387A_Rev	cttccccagccgctccttgatggggaagtcgacggcgatgtccagccgggatggggaagctgagcggc
Rv3790c387T_For	gccgctcagctccccatccgggctggaacatcacgctcagctccccatcaaggacgggctggggaag
Rv3790c387T_Rev	cttccccagccgctccttgatggggaagtcgacgggatgtccagccgggatggggaagctgagcggc
Rv3790c387N_For	gccgctcagctccccatccgggctggaacatcaatgctcagctccccatcaaggacgggctggggaag
Rv3790c387N_Rev	cttccccagccgctccttgatggggaagtcgacattgatgtccagccgggatggggaagctgagcggc
Rv3790C387N_F	CGGGCTGGAACATCAACGTCGACTTCCCCATC
Rv3790C387N_R	GATGGGGAAGTCGACGTTGATGTTCCAGCCCCG
Rv3790C387A_F	CGGGCTGGAACATCGCCGTCGACTTCCCCATC
Rv3790C387A_R	GATGGGGAAGTCGACGGCGATGTTCCAGCCCCG
Rv3790C387T_F	CGGGCTGGAACATCACCGTCGACTTCCCCATC
Rv3790C387T_R	GATGGGGAAGTCGACGGTGATGTTCCAGCCCCG

* Restriction sites are indicated in italics in the primer sequence

[§] NNN: random bases used for C387 mutagenesis

TABLE S2 Plasmids used in this study

Name	Description and features	Resistance marker	References
pND255	L5-integrative vector	Hyg ^R	N. Dhar, unpublished
pBL2	<i>wild-type promoter –rv3789-dprE1</i> cloned into pCR [®] – Blunt II – TOPO [®] Vector (Invitrogen)	Kan ^R	this study
pET28a-dprE1	Expression vector for DprE1 protein production	Kan ^R , Cam ^R	[3]
pND255-derivative plasmid			
pBLX1-6	Pools of vectors carrying randomly mutated <i>dprE1</i> and expressed under the natural promoter located upstream of <i>rv3789</i>	Hyg ^R	this study
pBLG	Mutated <i>dprE1</i> (C387G) and expressed under the natural promoter located upstream of <i>rv3789</i>	Hyg ^R	this study

TABLE S3 Strains used in this study

Strain	Plasmid	Genotype	Reference
H37Rv	-	Wild-type	[4]
H37Rv:: <i>dprE1</i> (C387X)	pBLX1-6*	wt promoter-rv3789- <i>dprE1</i> (C387X) at the L5-attB site	this study
H37Rv:: <i>dprE1</i> (C387G)	pBLG	wt promoter-rv3789- <i>dprE1</i> (C387G) at the L5-attB site	this study
H37Rv/pJV53	pJV53	Expression of Che9c gene products 60 and 61 to facilitate double-stranded DNA re-combination in mycobacteria	[5]
H37Rv Δ RD1	-	Deletion of RD1 region of H37Rv	[6]
<i>dprE1</i> (C387S)	-	H37Rv strain carrying C387S mutation in <i>dprE1</i>	this study
<i>dprE1</i> (C387A)	-	H37Rv strain carrying C387A mutation in <i>dprE1</i>	this study
<i>dprE1</i> (C387T)	-	H37Rv strain carrying C387T mutation in <i>dprE1</i>	this study
<i>dprE1</i> (C387G)	-	H37Rv strain carrying C387G mutation in <i>dprE1</i>	this study
<i>dprE1</i> (C387N)	-	H37Rv strain carrying C387N mutation in <i>dprE1</i>	this study

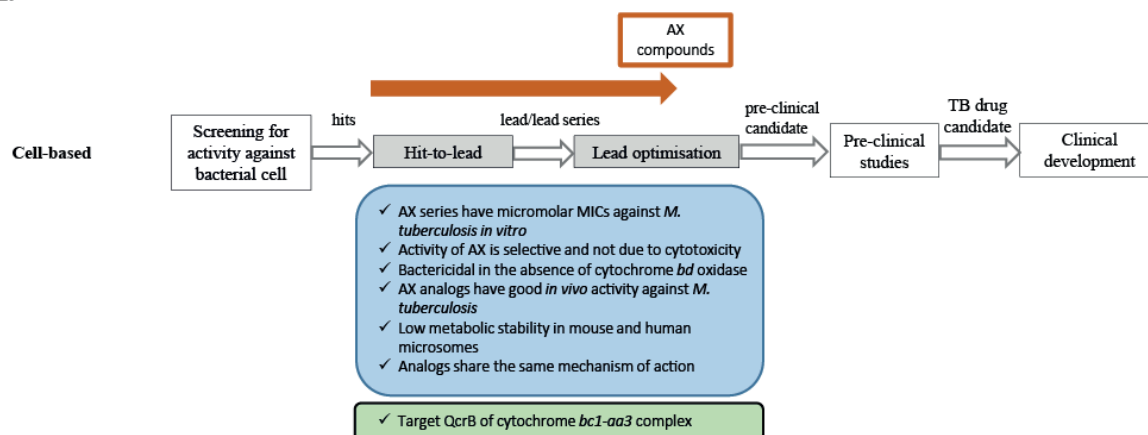
REFERENCES

1. **Reddy, V. M., Einck, L., Andries, K., and Nacy, C. A.** 2010. In Vitro Interactions between New Antitubercular Drug Candidates SQ109 and TMC207. *Antimicrobial Agents and Chemotherapy*, 54(7):2840–2846. doi:10.1128/AAC.01601-09.
2. **Lechartier, B., Hartkoorn, R. C., and Cole, S. T.** 2012. In Vitro Combination Studies of Benzothiazinone Lead Compound BTZ043 against *Mycobacterium tuberculosis*. *Antimicrobial Agents and Chemotherapy*, 56(11):5790–5793. doi:10.1128/AAC.01476-12.
3. **Makarov, V., Lechartier, B., Zhang, M., Neres, J., van der Sar, A. M., Raadsen, S. A., Hartkoorn, R. C., Ryabova, O. B., Vocat, A., Decosterd, L. A., Widmer, N., Buclin, T., Bitter, W., Andries, K., Pojer, F., Dyson, P. J., and Cole, S. T.** 2014. Towards a new combination therapy for tuberculosis with next generation benzothiazinones. *EMBO Molecular Medicine*, 6(3):372–383. doi:10.1002/emmm.201303575.
4. **Cole, S. T., Brosch, R., Parkhill, J., Garnier, T., Churcher, C., Harris, D., Gordon, S. V., Eiglmeier, K., Gas, S., Barry, C. E., Tekaia, F., Badcock, K., Basham, D., Brown, D., Chillingworth, T., Connor, R., Davies, R., Devlin, K., Feltwell, T., Gentles, S., Hamlin, N., Holroyd, S., Hornsby, T., Jagels, K., Krogh, A., McLean, J., Moule, S., Murphy, L., Oliver, K., Osborne, J., Quail, M. A., Rajandream, M.-A., Rogers, J., Rutter, S., Seeger, K., Skelton, J., Squares, R., Squares, S., Sulston, J. E., Taylor, K., Whitehead, S., and Barrell, B. G.** 1998. Deciphering the biology of *Mycobacterium tuberculosis* from the complete genome sequence. *Nature*, 393(6685):537–544. doi:10.1038/31159.

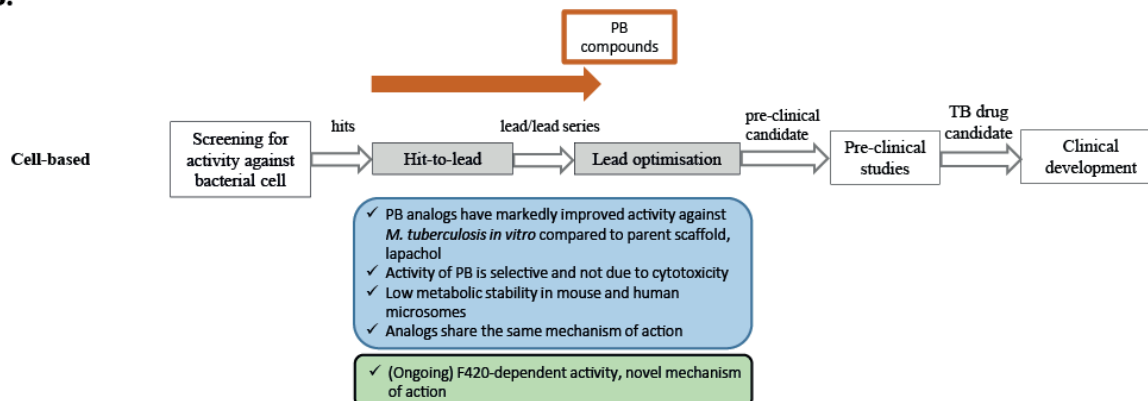
5. **van Kessel, J. C., Marinelli, L. J., and Hatfull, G. F.** 2008. Recombineering mycobacteria and their phages. *Nature Reviews Microbiology*, 6(11):851–857.
6. **Hsu, T., Hingley-Wilson, S. M., Chen, B., Chen, M., Dai, A. Z., Morin, P. M., Marks, C. B., Padiyar, J., Goulding, C., and Gingery, M.** 2003. The primary mechanism of attenuation of bacillus Calmette–Guerin is a loss of secreted lytic function required for invasion of lung interstitial tissue. *Proceedings of the National Academy of Sciences*, 100(21):12420–12425.

Chapter 5: Conclusions and Perspectives

A.



B.



C.

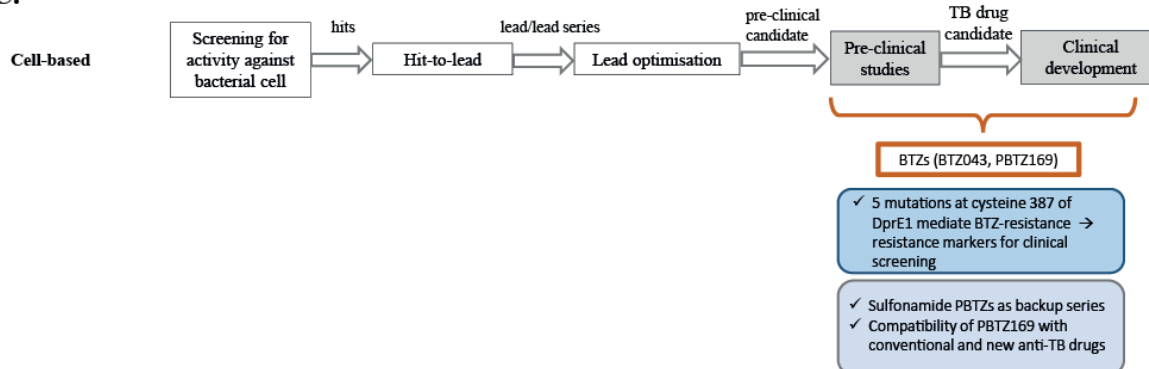


Figure 1: Overview of the main contributions of this thesis. Discovery of (A) AX compounds (Chapter 2), (B) PB compounds (Chapter 3), and (C) clinical development support of BTZs (Chapter 4, Annex Chapter A1, A2, and A3).

To fulfil the aim of this thesis, which has been to enhance the global TB drug pipeline in order to contribute to new drugs active against *M. tuberculosis*, the discovery of two new, highly promising families of anti-tuberculars, the arylvinylpiperazine amides AX in Chapter 2 and the lapachol-derived PB compounds in Chapter 3, as well as the elucidation of the underlying mechanisms of resistance to BTZs in Chapter 4, have been presented in the earlier chapters of this thesis.

Chapter 2 details the characterisation and extensive profiling of the AX compounds from a whole cell-based approach through activities associated with hit-to-lead generation and lead optimisation (Fig. 1a). This family remains interesting due to their potent activity against *M. tuberculosis* and their ease of chemical synthesis. While AX-35 is the lead compound *in vitro*, structural modifications to this parent molecule improved activity of two analogs tested *in vivo*. Future work should therefore be focused on advancing this family, or at least these three more potent analogs, further in the lead optimisation phase. This would imply improving liabilities of these compounds, one of which identified in this study is their metabolic stability, which is likely to influence their *in vivo* efficacy and should be confirmed by future pharmacokinetics studies in mice. In this respect, biochemical information obtained in this work with regards to important residues for target binding could guide future structure-based SAR studies.

The target of AX compounds was identified in this thesis as the QcrB subunit of the cytochrome *bc1-aa3* complex. Since AX compounds have a different mode of interaction in the same binding site in QcrB as Q203, these compounds could be further developed as backup QcrB inhibitors, in particular in the event of emergence of resistance to Q203. That QcrB is the target of several structurally diverse chemical entities may be attributed to its localisation in the mycobacterial membrane, similar to other promiscuous targets such as DprE1 and MmpL3,

where its active site is exposed to the periplasm (1). As it often occurs with membrane proteins, the expression and purification of functional enzymes is challenging and to date, a purified, functional QcrB has yet to be reported. Without the purified enzyme, biochemical validation of the target and target-based SAR studies are both limited. In the case of AX compounds, this study has validated the target as QcrB through alternative, multi-faceted approaches of genetics, transcriptomics, and bioenergetic flux assays. Gene expression profiling studies have also reaffirmed the compensatory respiratory role of the alternate terminal oxidase, cytochrome *bd*. With inhibition of QcrB and in the absence of cytochrome *bd* oxidase, AX compounds become bactericidal. Therefore, future work on AX compounds should also encompass combination studies with potential small-molecule inhibitors of cytochrome *bd* oxidase, as demonstrated with aurachin D (2).

Ironically, this respiratory flexibility between the two terminal oxidases can also be used to the disadvantage of the bacillus, as demonstrated by the potent killing of *M. tuberculosis* with a combination of BDQ, Q203, and CFM, whereby activation of cytochrome *bd* oxidase upon inhibition of cytochrome *bc1-aa3* potentiates CFM activity (3). Therefore, dysregulation of the terminal oxidases represents a novel strategy against the bacillus, and could be incorporated into a new anti-TB regimen mainly targeting oxidative phosphorylation. Such a regimen would extensively perturb respiratory flux and ATP production, and theoretically would be able to target the spectrum of metabolic states of *M. tuberculosis* physiologically and shorten treatment duration, particularly as ATP homeostasis is critical for sustaining all states of the bacillus (4). For such a regimen to be effectively implemented however, these drugs must be highly specific for the mycobacterial respiratory components without affecting those of the human mitochondrial counterparts. However, it is highly likely that a mutation in any of the targets would threaten the efficacy of the other compounds within the regimen, and therefore such a

combination may be more suited for MDR- and XDR-TB cases rather than as a front-line treatment.

In Chapter 3, the characterisation and profiling of lapachol-derived PB compounds through a whole cell-based approach with mainly hit-to-lead generation activities are elaborated (Fig. 1b). PB analogs are interesting as anti-tuberculars in that they derive from a naturally-occurring, readily-available source, are easily synthesised, and have substantially improved activity against *M. tuberculosis* compared to the parent scaffold, lapachol. Furthermore, these molecules demonstrate activity against non-replicating *M. tuberculosis*. Future work should focus on advancing this family further through lead optimisation activities, and prioritising PB-089, PB-117, and PB-118 analogs in particular, since PB-116 does not demonstrate intracellular activity in infected macrophages. A liability of this family identified in this study is their metabolic instability, which can be addressed through more medicinal chemistry studies. Additional key activities should include pharmacokinetics studies *in vivo*, as well as determining the *in vivo* efficacy of these compounds in both replicating and non-replicating models of TB.

This study establishes the reliance on the F₄₂₀ cofactor for activity of PB analogs against *M. tuberculosis*. While the F₄₂₀-dependent mechanism of activity is similar to Delamanid and PA-824, what is different in the case of the PB compounds is that Ddn is not required for activity, and therefore the prospect of a novel, mainly MTBC-specific mechanism of action for this family is exciting. The discovery program of PB compounds should continue independently, and these molecules could additionally serve as alternatives for Delamanid and PA-824 should phenotypic resistance, mediated by mutations in Ddn, arise to both these agents. To obtain more insight into the mechanism of action of PB compounds, the next steps would be to identify the F₄₂₀-dependent activator and the highly active species to which PB analogs are activated to. The

possibility of different mechanisms being attributed to the activity of PB compounds against replicating and non-replicating *M. tuberculosis* should also be explored, as with Delamanid and PA-824.

Since there is an unusually high dependency of *M. tuberculosis* on the F₄₂₀ cofactor (5), which may be required for its survival under anaerobic conditions (6), the F₄₂₀ biosynthesis pathway could be a novel, attractive target against non-replicating *M. tuberculosis* for shortening TB treatment durations. The relevance of this pathway as a drug target remains to be validated *in vivo*, and should it prove essential, a target-based, whole-cell screening approach could be undertaken to identify hits targeting F₄₂₀ biosynthesis by measuring the resistance of *M. tuberculosis* to PB, Delamanid, or PA-824.

Lastly, this thesis provides support to the ongoing pre-clinical and clinical development of BTZs. The underlying resistance mechanisms of *M. tuberculosis* to these highly potent compounds is elucidated in Chapter 4 (Fig. 1c). This study identifies 5 out of 19 possible mutations occurring at the cysteine 387 residue of DprE1 mediating resistance to BTZs, two of which are reported for the first time here. Apart from the identification of BTZ-resistance markers, profiling of the levels of resistance for these mutations is also important clinically as it can guide decisions in the inclusion and dosage of BTZs as part of a regimen. This study also reveals that all five mutations impose fitness costs on *M. tuberculosis* intracellularly, indicating that these mutations, and consequently, BTZ-resistance, may have a lower tendency to emerge clinically. This hypothesis needs to be verified by monitoring the frequency of phenotypic resistance to PBTZ169 in patients and screening for the five C387 mutations of DprE1 over the course of clinical trials. The lack of cross-resistance between covalent and non-covalent DprE1 inhibitors biochemically is further highlighted in this study. Differences between these two

classes in interactions within the binding pocket of DprE1 can further inspire and rationally guide structure-based design to generate potential backup molecules and series of BTZs to overcome the emergence of BTZ-resistance, as demonstrated by the generation of sulfonamide PBTZs (Annex A1, A2). In addition, since combination therapy is required for TB treatment to reduce the emergence of antibiotic resistance and to target multiple sub-populations of bacilli, new TB drug candidates need to be evaluated as part of regimens. As demonstrated in Annex A3, MCZ does not display antagonistic interactions with conventional and new TB drugs, demonstrating its compatibility as a component of a novel anti-TB regimen.

In a broader context, several observations and considerations related to TB drug discovery and development can be made from the course of this thesis and other encountered works. Firstly, it is important to extensively characterise new molecules for their anti-tubercular activity across different systems and models, since the susceptibility of the bacillus to compounds and the physiological relevance of the targets are highly influenced by the metabolic state of *M. tuberculosis*. Secondly, natural product entities and human-targeted drugs represent promising alternatives to current small, synthetic molecule libraries for expanding and diversifying chemical space of anti-tuberculars with novel mechanisms of action (7). Since large, complex natural product entities often pose challenges for downstream SAR studies and optimisation, those with simpler scaffolds such as lapachol could be prioritised for TB drug discovery. With regards to re-purposing human-targeted drugs for TB, a case in point is lansoprazole (LPZ), a proton pump inhibitor requiring activation by host cells to LPZ sulfide for potent activity against *M. tuberculosis* (8). Thirdly, while the focus of the compounds described in this thesis has been mainly on their activity against *M. tuberculosis*, the therapeutic potential of these molecules (and others being developed for TB) may be expanded to other mycobacterial diseases, such as Buruli ulcer and leprosy, leading to alternative avenues for their development.

Another important consideration is that since anti-TB drugs are preferably orally dosed, interactions between the gut microbiome should be taken into account for therapy and drug development. As gut bacteria are capable of modulating drug efficacy and toxicity (9), characterising such drug-microbiome interactions would aid in maximising efficacy of a drug. A further point of consideration is the risk of acquired antibiotic resistance through the consumption of human-targeted, non-antimicrobial drugs (7), and thus monitoring such events would be important for guiding implementation of TB regimens, such as in the context of the co-disease burden of TB and diabetes. Lastly, having several different anti-TB drugs with the same mechanism of action would be advantageous in addressing possibilities of undesired drug interactions, thus ensuring the compatibility of therapies within and without, such as in cases of TB-HIV co-infection.

Naturally, much work still remains to fully realise the antibiotic potential of the compounds presented in this thesis. TB drug discovery and development typically spans over 10 to 20 years, inadvertently leading to high costs associated with this long and risky process. An estimated US\$2 billion a year is required to fund TB research and development for new drugs, vaccines, and improved diagnostics, however this amount falls woefully short of the US\$0.7 billion available per year (10). This lack of financial support is an important factor impeding the progress towards eradicating TB.

As a disease associated with low socio-economic status, tackling TB in today's context necessitates the emphasis on the affordability, accessibility, and ease of use for the effective implementation of available and novel tools. Nevertheless, TB remains a disease which does not recognise political nor geographical boundaries. Overcoming this global pandemic therefore requires a combined, concerted, international effort from all levels, from governments

introducing effective public health policies and robust healthcare infrastructure, public and private organisations actively involved in providing financing support, researchers contributing to the improvement and generation of novel tools, to medical and healthcare workers on the front-line with TB patients. Altogether, motivated by common goals and guided by bold visions, such as, to quote Bill Gates, “Why can’t we treat TB in two weeks?”, it is through these borderless co-operations that we can envision and work towards a TB-free world.

References

1. Cole ST. 2016. Inhibiting *Mycobacterium tuberculosis* within and without. *Philos Trans R Soc B Biol Sci* 371.
2. Lu P, Asseri AH, Kremer M, Maaskant J, Ummels R, Lill H, Bald D. 2018. The anti-mycobacterial activity of the cytochrome bcc inhibitor Q203 can be enhanced by small-molecule inhibition of cytochrome bd. *Sci Rep* 8:2625.
3. Lamprecht DA, Finin PM, Rahman MA, Cumming BM, Russell SL, Jonnala SR, Adamson JH, Steyn AJC. 2016. Turning the respiratory flexibility of *Mycobacterium tuberculosis* against itself. *Nat Commun* 7:12393.
4. Rao SPS, Alonso S, Rand L, Dick T, Pethe K. 2008. The protonmotive force is required for maintaining ATP homeostasis and viability of hypoxic, nonreplicating *Mycobacterium tuberculosis*. *Proc Natl Acad Sci* 105:11945–11950.
5. Selengut JD, Haft DH. 2010. Unexpected Abundance of Coenzyme F420-Dependent Enzymes in *Mycobacterium tuberculosis* and Other Actinobacteria. *J Bacteriol* 192:5788–5798.
6. Boshoff HIM, Barry 3rd CE. 2005. Tuberculosis — metabolism and respiration in the absence of growth. *Nat Rev Microbiol* 3:70–80.
7. Maier L, Pruteanu M, Kuhn M, Zeller G, Telzerow A, Anderson EE, Brochado AR, Fernandez KC, Dose H, Mori H, Patil KR, Bork P, Typas A. 2018. Extensive impact of non-antibiotic drugs on human gut bacteria. *Nature* 555:623–628.
8. Rybníček J, Vocat A, Sala C, Busso P, Pojer F, Benjak A, Cole ST. 2015. Lansoprazole is an antituberculous prodrug targeting cytochrome *bc₁*. *Nat Commun* 6:7659.

9. Spanogiannopoulos P, Bess EN, Carmody RN, Turnbaugh PJ. 2016. The microbial pharmacists within us: a metagenomic view of xenobiotic metabolism. *Nat Rev Microbiol* 14:273–287.
10. World Health Organization. 2017. Global Tuberculosis Report 2017. S.l.

**Appendix Chapter A1: Structural studies of *Mycobacterium tuberculosis* DprE1
interacting with its inhibitors**

Jérémie Piton, Caroline S.Y. Foo and Stewart T. Cole

Global Health Institute, École Polytechnique Fédérale de Lausanne, CH-1015 Lausanne, Switzerland

Drug Discovery Today, 2017, doi.org/10.1016/j.drudis.2016.09.014

Contributions: manuscript preparation



Structural studies of *Mycobacterium tuberculosis* DprE1 interacting with its inhibitors

Jérémie Piton, Caroline S.-Y. Foo and Stewart T. Cole



Global Health Institute, Ecole Polytechnique Fédérale de Lausanne, Station 19, 1015 Lausanne, Switzerland

The flavoenzyme DprE1 catalyses a crucial step in arabinan production for cell wall biosynthesis in *Mycobacterium tuberculosis* and is a highly vulnerable drug target. It was first discovered using benzothiazinones (BTZ): exquisitely potent bactericidal agents that are being developed as drugs to treat tuberculosis. Subsequently, many compounds with diverse scaffolds were found to act as either covalent or noncovalent DprE1 inhibitors. Covalent inhibitors, like the BTZ, are all nitroaromatic compounds that serve as suicide substrates after DprE1-mediated nitroreduction. Here, we describe how high-resolution structures of DprE1, alone and in complex with various ligands, explain enzyme activity and inhibition.

Introduction

Mycobacteria, including *Mycobacterium tuberculosis*, possess a remarkably elaborate cell wall structure. In addition to the peptidoglycan layer, the mycobacterial cell wall is composed of two other major components, namely arabinogalactan and mycolic acids, which are noncovalently linked to an outer capsule of proteins and polysaccharides [1]. Some of the most effective antibiotics against tuberculosis (TB) to date are those targeting enzymes involved in synthesising cell wall components. Frontline TB drugs isoniazid (INH) and ethambutol (EMB) inhibit key enzymes involved in the biosynthesis of mycolic acids and arabinan respectively [2–6]. In the past decade, whole-cell screens have enabled the identification of several new classes of compounds that target proteins such as MmpL3 or DprE1, which are required for the biosynthesis of cell wall components [7,8]. These enzymes have been described as promising targets for new clinical candidates to fight TB.

DprE1, encoded by the gene *dprE1* (*rv3790*), is an essential flavoenzyme of *M. tuberculosis* involved in cell wall synthesis and serves as a decaprenylphosphoryl-beta-D-ribose 2'-oxidase [9]. DprE1 acts in concert with DprE2 to catalyse the two-step epimerisation of decaprenyl-phospho-ribose (DPR) to decaprenyl-phospho-arabinose (DPA), which is the sole precursor for the synthesis of arabinogalactan and lipoarabinomannan [10]. DprE1

catalyses the first step of epimerisation, namely oxidation of DPR to an intermediary decaprenyl-phospho-2'-keto-D-arabinose (DPX) with reduction of the FAD cofactor to FADH₂. DPX is then reduced to DPA by the NADH-dependent decaprenylphosphoryl-D-2-keto erythro pentose reductase (DprE2) [10]. DprE1 and DprE2 are both essential for cell growth and the survival of *M. tuberculosis* [11,12]. Recently, it was found that the epimerisation process occurs in the periplasmic space, thereby explaining the vulnerability of DprE1 as a target [13].

Inhibitors of DprE1

BTZ043, the lead compound of the benzothiazinone (BTZ) series, was the first DprE1 inhibitor described and is exceptionally potent with an *in vitro* or *ex vivo* minimal inhibitory concentration (MIC) in the nanomolar range [14]. The mode of action of BTZ043 explains its extraordinary potency because it behaves as a suicide substrate for the reduced form of DprE1. BTZ043 and other BTZ derivatives undergo nitroreduction to form a nitroso derivative, which specifically forms a covalent adduct with cysteine 387 (C387) in the active site of DprE1, irreversibly inhibiting the enzyme [15–17]. C387 is highly conserved in orthologous DprE1 enzymes in actinobacteria, except in *Mycobacterium avium* and *Mycobacterium aurum* where cysteine is replaced by alanine and serine respectively. These mutations confer natural BTZ resistance [14].

Corresponding author: Cole, S.T. (stewart.cole@epfl.ch)

TABLE 1

Known compounds targeting DprE1 and their inhibition properties

Covalent inhibitors				Noncovalent inhibitors			
Molecule	Structure	MIC (μM)	Refs	Molecule	Structure	MIC (μM)	Refs
BTZ043		0.002	[14]	TCAI		0.51	[27]
PBTZ169		0.0006	[18]	TBA-7371 (1–4 azaindoles)		0.39	[31,32]
DNB1		0.69	[19]	Ty38c (2-carboxyquinoxalines)		3.1	[34]
VI-9376		3.1	[20]	4-AQs (cmp-3)		0.8	[38]
377790		^a	[21]	PyrBTZ02 (8-pyrrole-BTZ)		0.34	[25]
BTO		0.07	[22]	1,2,4-Triazole containing 1,4-BTZ derivatives (cmp-6c)		30	[35]
cBT		4.2	[23]	1,3-BTZ azide		0.47	[26]
				Benzothiazolylpyrimidine-5-carboxamides (cmp-7a)		0.08	[28]
				Pyrazolopyridones (cmp-19)		0.1	[33]

^a The IC_{50} in *M. tuberculosis* for this compound is 0.48 μM .

To date, 15 new classes of DprE1 inhibitors with antimycobacterial activity have been described (Table 1). These inhibitors are categorised into two families according to their mode of action. Six are known to inhibit DprE1 irreversibly by forming a covalent adduct with C387 of DprE1 in the same manner as BTZ, whereas nine act as competitive noncovalent inhibitors. This review will focus on the most recent inhibitors and structural studies of DprE1 in complex with its inhibitors.

Common characteristics of the covalent inhibitors are the presence of a nitro group and their inactivity against C387A and C387S DprE1 mutants. PBTZ169 has one of the lowest MICs against *M. tuberculosis* (0.6 nM) and resulted from a lead optimisation campaign [14,18]. PBTZ169 has completed Phase I clinical trials and acts in synergy with pyrazinamide and bedaquiline, making this combination a potential new TB drug regimen [18]. DprE1 has also been identified as the target of the dinitrobenzamides (DNBs), nitroquinoxalines (with the lead molecule VI-9376)

and nitroimidazoles (with the lead molecule 377790), all of which behave as covalent inhibitors [19–21].

Recently, a new scaffold was found from a whole-cell screen against *Mycobacterium bovis* BCG which resulted in the identification of benzothiazole-*N*-oxide (BTO) targeting DprE1 [22]. Unfortunately, several toxicity and mutagenicity issues were associated with this molecule. However, modulating the stereoelectronic properties of the benzothiazole ring in SAR studies led to the discovery of a novel class of antitubercular agents called cBT [6-methyl-7-nitro-5-(trifluoromethyl)-1,3-benzothiazoles] [22,23]. Although less potent, cBT are non-mutagenic and exhibit an improved safety profile.

Genotoxicity is a potential concern for covalent inhibitors because nitro-aromatic compounds generally carry a risk of mutagenicity [24]; PBTZ169 has been found to be non-mutagenic in preclinical tests. Two studies have demonstrated that the nitro group present on BTZ can be replaced with a pyrrole ring or an

azide group while retaining significant antimycobacterial activity [25,26]. These non-nitro BTZ analogues then behave as noncovalent inhibitors and are considerably less potent than their covalent counterparts.

Within the past three years, a considerable number of noncovalent DprE1 inhibitors have been found. In a cell-based screen, a new compound, TCA1, was identified that has activity against replicating and nonreplicating *M. tuberculosis*. It is also effective *in vivo* alone or in combination with frontline TB drugs in acute and chronic mouse models of TB. TCA1 targets two different enzymes: DprE1 and MoeW [27]. Lacking a nitro group, it is unable to bind covalently to C387. TCA1-resistant mutants harbour a Y314C substitution in DprE1. Interestingly, the Y314C mutant strain, which is resistant to TCA1, remains sensitive to BTZ suggesting that the binding mechanism of TCA1 to DprE1 is different from that of BTZ. Recently, new molecules based on the structure of TCA1, benzothiazolylpyrimidine-5-carboxamides, were designed by structure-based drug design approaches. [28]. These new molecules are more active than TCA1 with an MIC of 80 nM (seven-fold lower than that of TCA1) in *M. tuberculosis* and have better oral bioavailability than TCA1 and BTZ043.

The 1,4-azaindole series is another class of noncovalent inhibitors that target DprE1, and was identified during a scaffold-morphing approach starting from a published anti-TB, non-DprE1 imidazo-pyridine scaffold [29–31]. Spontaneous resistant mutants contain a single Y314H mutation in DprE1, which is the same mutation found in TCA1-resistant mutants. In contrast, no cross-resistance was observed between BTZ and azaindole-resistant strains, suggesting that TCA1 and 1,4-azaindoles behave similarly to noncovalent inhibitors. Like TCA1, 1,4-azaindoles have good oral exposure, are active *in vivo* and are promising candidates for the development of a novel anti-TB drug [32].

Pyrazolopyridones, which originated from a whole-cell screen, were also found to inhibit DprE1 in a noncovalent manner with an MIC of 0.1 μ M [33]. As with 1,4-azaindoles, the Y314H mutation confers resistance to pyrazolopyridones. Interestingly, pyrazolopyridones showed enhanced potency against the BTZ-resistant strains carrying C387S and C387G mutations in DprE1 as compared with the wild-type strain. This series has not been tested *in vivo* because the pharmacodynamic properties require further optimisation.

2-Carboxyquinoxalines have also been identified as noncovalent DprE1 inhibitors in a phenotypic screening of a quinoxaline library [34]. Spontaneous resistant mutants have G17C and L368P substitutions in DprE1. Interestingly, although the authors have indicated that no cross-resistance was observed between either of these *dprE1* mutants and BTZ043, the BTZ-resistant C387S mutant strain conferred some cross-resistance to Ty38c by increasing the MIC four-fold. These observations suggest that G17, L368 and C387 are involved in the binding of 2-carboxyquinoxalines to DprE1. Unfortunately, these compounds are inactivated by decarboxylation in *M. tuberculosis* by the protein encoded by *rv3406*. The lead compound of 2-carboxyquinoxalines is Ty38c which has an MIC of 3.1 μ M.

4-Aminoquinolone piperidine amides (AQs) are novel scaffolds identified from a whole-cell screen with an MIC of 800 nM [35]. Again, the Y314H mutation leading to azaindole, pyrazolopyridone and TCA1 resistance has a strong impact on the efficacy of

AQs. This series has excellent drug-like properties, including good solubility and an attractive pharmacological profile. A new strategy to find novel inhibitors involves forming hybrids between moieties of two different molecules. Examples include 1,2,4-triazole-containing 1,4-benzothiazinone derivatives [35] and a pyrazine-thiazolidinone hybrid scaffold [36], showing relatively low activity against *M. tuberculosis*.

Structural studies of DprE1

There are currently 22 entries in the Protein Data Bank corresponding to DprE1 structures (Table 2). Three structures of *Mycobacterium smegmatis* DprE1 have been solved in two different space groups and one structure contains BTZ043. The 19 other structures are *M. tuberculosis* DprE1 crystallised in two crystal forms, namely hexagonal and orthorhombic, in complex with or without inhibitors.

The structures of the *M. smegmatis* and *M. tuberculosis* DprE1 enzymes are similar (83% sequence identity; RMSD of 0.464 Å for 340 C α) [16,17,37]. DprE1 is characterised by the two-domain topology of the vanillyl-alcohol oxidase family of oxidoreductases including a FAD-binding domain (residues 7–196, 413–461) and the substrate-binding domain (residues 197–412). The monoclinic and hexagonal crystal forms display an apparent dimer of DprE1. However, Batt *et al.* suggest that DprE1 does not dimerise in solution [16].

The cofactor is deeply buried in the FAD-binding domain, with the isalloxazine positioned at the interface of the substrate-binding domain in front of the substrate-binding pocket [16,17]. In contrast to the homologous structure of alditol oxidase, DprE1 does not covalently bind the prosthetic group. Interestingly, the *M. smegmatis* DprE1 structure has also been solved in the absence of the FAD cofactor, indicating that FAD is inessential for the folding of the protein. [37].

Electron density in all crystal forms obtained for *M. tuberculosis* or *M. smegmatis* DprE1 reveals disorder of two surface loops in the substrate-binding domain (Fig. 1) [16–18,27,34,37]. These loops can be involved in interactions with the cell membrane, with other protein partners involved in the DPA biosynthesis pathway or with the substrate DPR [16]. Interestingly, disordered loop I (amino acids 269–303) and disordered loop II (316–330) are located just above the substrate-binding pocket, leaving the active site wide open in the ligand-free form and thus could act as a gate for the substrate. The extent of disorder depends on the contact with the symmetry-related molecule of the crystal form. In all the monoclinic crystal forms (P2₁) where there are two molecules in the asymmetric unit, disorder of the two loops is higher in monomer B than in monomer A owing to symmetric contact. Furthermore, it is clear from structural studies that the disordered loops can behave differently depending on the inhibitor. Some inhibitors can such as Ty38c, QN118, QN127 and Ty21c stabilise loop I, whereas CT319 stabilises loop II. Ty36c and QN129 stabilise both loops (Table 2).

Structural studies of DprE1 in complex with covalent inhibitors

M. smegmatis DprE1 was crystallised in complex with BTZ043 [17], shedding light on the structural basis of the inhibition mechanisms of covalent inhibitors. BTZ043 is a mechanism-based covalent inhibitor, which requires the enzymatic activity of the protein with the substrate to convert the nitro group of BTZ043 to the

TABLE 2

Solved structure of DprE1 present in PDB

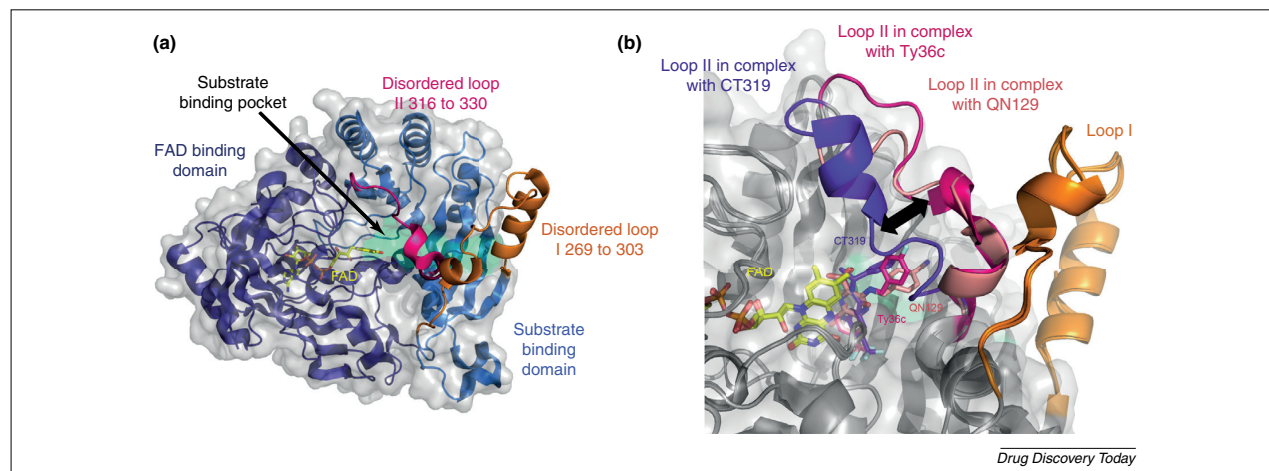
PDB ID	Space group	Resolution	Mol/ASU ^a	Disordered regions (loop I/loop II)	Species	Inhibitor	Inhibition mechanism	Refs
4G3T	<i>P</i> ₃ ₂ ₁	2.35	1	(275–307)/(323–337)	<i>M. smegmatis</i>			[37]
4G3U	<i>P</i> ₂ ₁	2.69	1	(275–307)/(323–337)	<i>M. smegmatis</i>			[37]
4FDP	<i>P</i> ₂ ₁	2.23	2	Chain A: (269–283)/(316–330) Chain B: (269–293)/(316–330)	<i>M. tuberculosis</i>			[16]
4FEH	<i>P</i> ₆ ₄	2.04	1	(269–297)/(316–322)	<i>M. tuberculosis</i>			[16]
4AUT	<i>P</i> ₃ ₂ ₁	2.1	1	(275–303)/(330–336)	<i>M. smegmatis</i>			[17]
4F4Q	<i>P</i> ₂ ₁ ₂ ₁	2.62	1	(275–302)/(324–337)	<i>M. smegmatis</i>	BTZ043	Covalent	[17]
4NCR	<i>P</i> ₂ ₁	1.88	2	Chain A: (272–283)/(315–330) Chain B: (271–295)/(315–330)	<i>M. tuberculosis</i>	PBTZ169	Covalent	[18]
4FDN	<i>P</i> ₆ ₄	2.4	1	(269–297)/(315–322)	<i>M. tuberculosis</i>	CT325	Covalent	[16]
4FF6	<i>P</i> ₂ ₁	2.6	2	Chain A: (269–283)/(316–330) Chain B: (269–292)/(316–330)	<i>M. tuberculosis</i>	CT325	Covalent	[16]
4P8H	<i>P</i> ₂ ₁	3	2	Chain A: (269–293)/(315–330) Chain B: (269–290)/(314–330)	<i>M. tuberculosis</i>	cBT6a	Covalent	[23]
4PFA	<i>P</i> ₂ ₁	2.56	2	Chain A: (271–284)/(317–329) Chain B: (269–292)/(317–330)	<i>M. tuberculosis</i>	BTO	Covalent	[22]
4FDO	<i>P</i> ₆ ₄	2.4	1	(269–297)/–	<i>M. tuberculosis</i>	CT319	Noncovalent	[16]
4KW5	<i>P</i> ₂ ₁	2.61	2	Chain A: (269–287)/(317–330) Chain B: (268–293)/(317–330)	<i>M. tuberculosis</i>	TCA1	Noncovalent	[27]
4P8C	<i>P</i> ₂ ₁	1.95	2	Chain A: (269–273)/(324–325) Chain B: (271–293)/(317–330)	<i>M. tuberculosis</i>	QN127	Noncovalent	[34]
4P8K	<i>P</i> ₂ ₁	2.49	2	Chain A: –/(317–325) Chain B: (271–292)/(317–330)	<i>M. tuberculosis</i>	Ty38c	Noncovalent	[34]
4P8L	<i>P</i> ₂ ₁	2.02	2	Chain A: –/– Chain B: (271–292)/(317–330)	<i>M. tuberculosis</i>	Ty36c	Noncovalent	[34]
4P8M	<i>P</i> ₂ ₁	2.09	2	Chain A: (271–289)/(318–325) Chain B: (268–300)/(314–329)	<i>M. tuberculosis</i>	QN114	Noncovalent	[34]
4P8N	<i>P</i> ₂ ₁	1.79	2	Chain A: –/(327–330) Chain B: (270–290)/(317–330)	<i>M. tuberculosis</i>	QN118	Noncovalent	[34]
4P8P	<i>P</i> ₂ ₁	2.2	2	Chain A: –/(324–329) Chain B: (271–290)/(317–330)	<i>M. tuberculosis</i>	QN127	Noncovalent	[34]
4P8T	<i>P</i> ₂ ₁	2.55	2	Chain A: –/– Chain B: (271–290)/(316–330)	<i>M. tuberculosis</i>	QN129	Noncovalent	[34]
4P8Y	<i>P</i> ₂ ₁	2.01	2	Chain A: –/(327–329) Chain B: (271–293)/(315–330)	<i>M. tuberculosis</i>	Ty21c	Noncovalent	[34]
4PFD	<i>P</i> ₂ ₁	2.3	2	Chain A: (268–289)/(320–325) Chain B: (268–298)/(316–329)	<i>M. tuberculosis</i>	cBT	Noncovalent	[22]

^a Mol/ASU corresponds to the number of molecules per asymmetric unit.

active nitroso form. To generate the DprE1–BTZ043 adduct and to obtain the structure of the covalent complex, DprE1 was incubated with BTZ043 and farnesylphosphoryl-D-ribofuranose (FPR; an analogue of DPR with a shorter polyprenyl chain serving as a suitable enzyme substrate) before performing crystallisation trials [17]. BTZ043 is located in the substrate-binding pocket in front of the isoalloxazine ring of FAD and binds covalently to C394 (equivalent to C387 in *M. tuberculosis*). There are no major structural changes between the native complexed forms of DprE1. The trifluoromethyl group of BTZ043 is situated in a hydrophobic pocket formed by side chains of H132, G133, K134, K367, F369 and N385. The piperidine ring of BTZ043 is maintained on each side by the isoalloxazine ring of FAD, and by G117 and V365. The spirocyclic moiety of BTZ043 is located

at the protein surface and lacks full electron density, resulting in the flexibility of this region of the molecule. Indeed, there is only one van der Waals interaction between L363 and the spirocyclic moiety (Fig. 2a). The two disordered regions are not visible in the density map, suggesting that BTZ043 does not interact with these loops.

M. tuberculosis DprE1 was also crystallised in the presence of PBTZ169 [18], which binds DprE1 in the same manner as BTZ043, with the exception of an extra van der Waals interaction with W230 (Fig. 2b). As with BTZ043, the electron density map does not account fully for the cyclohexyl moiety of PBTZ169, suggesting that this moiety is not stabilised by the protein. Furthermore, loops I and II are also disordered as in the BTZ043–DprE1 complex suggesting that there are no interactions in these regions.

**FIGURE 1**

Structure of DprE1 and conformations of the two disordered loops. **(a)** Overall structure of DprE1 (PDB code 4P8L). FAD-binding domain is in deep blue and substrate-binding domain in light blue. Substrate-binding pocket is represented as a lime green surface. The two disordered loops are represented in orange for loop I (residues from 269 to 303) and hot pink for loop II (316 to 330). **(b)** Superimposition of the three structures where loop II is stabilised in the crystal structure. Conformations of loop II in the presence of CT329 (violet), QN129 (salmon) or Ty36c (hot pink) are different, suggesting that inhibitors induced the conformational change and are implicated in the stabilisation of the loop.

Recently, Lange *et al.* reported the structures of covalent complexes between DprE1 and BTO derivatives and showed that these compounds also have the same binding mode as BTZ (Fig. 2c). The trifluoromethyl group occupies the same hydrophobic groove and the covalent bond with C387 remains the main determinant of interaction (Fig. 2c). DprE1 was crystallised in complex with cBT, which still binds in the same pocket as the original BTO, but curiously the methyl group creates an unfavourable interaction with neighbouring polar residues (N385, Q336), which affects its ability to bind covalently to the protein, and could explain the decreased activity for this compound (Fig. 2d). A structure of a complex with cBT binding to DprE1 as a noncovalent inhibitor has been solved (Fig. 2e). Obviously, cBT binds differently to the protein compared with covalent inhibitors. The methyl group of cBT is situated in the hydrophobic pocket whereas the trifluoromethyl group is shifted towards another hydrophobic groove. The nitro group, which appears not to have been transformed into a nitroso, is stabilised by H-bonds formed with residues N365 and Q336. Finally, C387 and K418 stabilise the complex by the formation of additional H-bonds. The structure is not linked to any publication in the Protein Data Bank and there is no information about the relevance of this complex. Nevertheless, this structure could represent the pre-complex before the nitro-reduction of the nitro group, suggesting that there is a conformational change of the inhibitor before and after nitroreduction by FADH₂. Finally, loops I and II are not modelled in the three complexes with BTO or cBT derivatives, suggesting that there are no interactions between these inhibitors and loop II (Table 2).

M. tuberculosis DprE1 was also crystallised in complex with CT319, which is from a class of BTZ-inspired inhibitors [16]. In this study, complexes were obtained in different space groups, providing crystallographically independent views of the binding mode of inhibitors. CT319 has the nitro-aromatic ring moiety and the trifluoromethyl functional group of BTZ043, whereas the other

part of the molecule is more similar to DNB compounds. The compound is located in the BTZ-binding pocket, with the trifluoromethyl group in the hydrophobic groove. Surprisingly, the phenyl group of CT319 stabilises the disordered loop II with van der Waals interactions. However, this complex was made with a nonactivated enzyme (without prior incubation) and so the nitro group of CT319 does not bind covalently to C387. To circumvent the need for inhibitor activation for crystallisation studies, CT325 was synthesised. It is a nitroso derivative of CT319 that can covalently react with the cysteine of the active site without the need for prior enzymatic activation. CT325 binds in the same manner as CT319 except that it forms a covalent complex with C387. Interestingly, although the terminal phenylethyl group of CT319 and loop II of DprE1 interact and are ordered in the noncovalent complex, they are disordered in the case of the CT325 in the covalent complex.

Structural studies of DprE1 in complex with noncovalent inhibitors

Structural characterisation of TCA1 in complex with *M. tuberculosis* DprE1 revealed that TCA1 is located in the central cavity of DprE1 in a boomerang-like conformation as in the case of the covalent inhibitors, with the thiophene moiety situated deep in the hydrophobic pocket at the bottom of the active site [27]. As with the covalent inhibitors, this interaction appears to be very important for the binding. Furthermore, TCA1 is maintained by polar contacts between the carboxamido group and thiazole nitrogen of TCA1 and K418 of *M. tuberculosis* DprE1. Also, the carbamate moiety forms van der Waals interactions important for the stabilisation of the compound with the phenyl ring of Y314. The significance of this interaction was proven when Y314 was replaced by alanine, leading to a TCA1-resistant mutant [27].

Structures with eight different 2-quinoxalines have been solved [34]. Interestingly, disordered loops I and II are visible in the electronic density map to different extents, depending on the

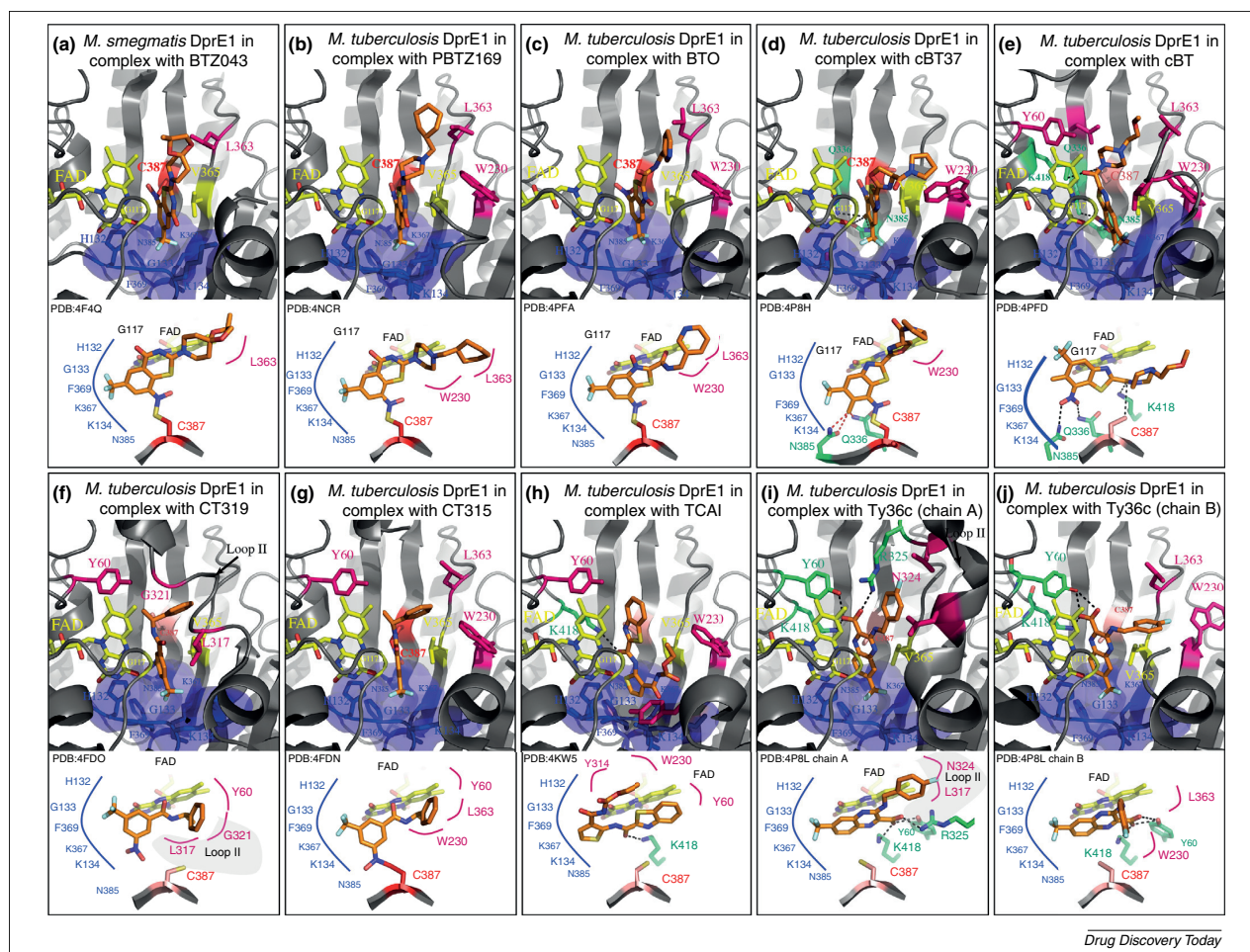


FIGURE 2

Structural and interaction map of DprE1 with inhibitors. Carbon α trace atom is represented in grey and inhibitors by orange sticks. Except for the structure of *Mycobacterium smegmatis* DprE1 in complex with BTZ043 (4F4Q), all the complexes were crystallised with the *Mycobacterium tuberculosis* DprE1 enzyme. To facilitate description, the *M. tuberculosis* numbering is used. The hydrophobic groove is represented by sticks and surface is blue. FAD, G117 and V365 (yellow sticks) form the middle part of the binding cavity and the side of the pocket. In hot pink are amino acids implicated in the stabilisation of inhibitors in the pocket with van der Waals contacts. Amino acids involved in H-bonding with inhibitors are represented in lime green and the H-bonds by black dots. Cysteine 387 is represented as a red stick when it forms a covalent bond with the inhibitors and in salmon pink when it is not involved in inhibitor binding.

complex (Table 2). Whereas loop I is complete in chain A of almost all structures, electron density was observed for the whole of loop II in only two cases (chain A with Ty36c and QN129), providing important information regarding the flexibility and potential interactions of this loop with the 2-carboxyquinoxalines.

In all complexes, the common 2-carboxy-6-trifluoromethylquinoxaline core is observed in the same position as with covalent and noncovalent inhibitors, located close to the FAD. The trifluoromethyl group occupies the same hydrophobic pocket as was observed for the covalent inhibitors BTZ043 or PBTZ169. The carboxylate group of the quinoxaline forms a H-bond with K418, an essential catalytic residue, and Y60, which is essential for binding the 2-quinoxalines. Interestingly, in the Ty36c and QN129 complexes, there is an extra H-bond between the carboxylate group of the quinoxaline and the side chain of R325, which is located in disordered loop II. There are also two van der Waals interactions with L317 and N324 that are involved in stabilisation and these

might explain the stabilisation of loop II in these two complexes. The two quinoxaline-resistant mutants with G17C and L368P mutations do not directly interact with any of the quinoxaline inhibitors, indicating that these mutations could induce a conformational change leading to a modification of the binding pocket. Intriguingly, there are two different configurations of the compounds in the structures. Quinoxaline is able to adopt a planar conformation (benzyl and quinoxaline rings approximately coplanar) as in the Ty36c monomer A complex structure (Fig. 2i) or a bent conformation (benzyl and quinoxaline rings approximately perpendicular) as in monomer B of the same crystal structure (Fig. 2j).

Concluding remarks and future perspectives

DprE1 is present only in actinobacteria, and its druggability is linked to its essentiality in mycobacteria because it is required for the formation of the mycobacterial cell wall, and to its location in the periplasm. These properties account for the vulnerability of

this target. To our knowledge, DprE1 is the only FAD-dependent enzyme belonging to the vanillyl-alcohol oxidase family of oxidoreductases that possesses a cysteine in the active site, and therefore is able to activate and bind nitro-inhibitors.

Since the discovery of BTZ043 in 2009, 15 new classes of inhibitors were found to be active against *M. tuberculosis* and target DprE1. Currently, the most potent of all DprE1 inhibitors, PBTZ169, is nearing Phase II trials as a result of its high efficacy against *M. tuberculosis* MDR strains and its synergism with BDQ. We believe that this compound could greatly increase the chances of survival of patients affected by multidrug-resistant TB.

From the comparative analysis of the 22 structures in PDB, it is clear that the binding sites of covalent and noncovalent inhibitors overlap significantly and all the inhibitors target the same binding pocket. The interaction of a hydrophobic group with the hydrophobic groove is common to all the inhibitors. This interaction appears to be the first key determinant for binding. C387 clearly plays a crucial part for the binding of covalent inhibitors, and also remains an important residue in the binding of noncovalent inhibitors such as 2-quinoxalines and pyrazolopyridones. Nevertheless, the covalent link with DprE1 might be dispensable for the binding as was observed for CT319 or cBT, which could bind to DprE1 without forming a covalent bond. Interestingly, some inhibitors such as Ty36c, CT319 or QN129 are stabilised by the disordered loop II. Altogether, these structures provide interesting information on potential contacts such as R325 with the disordered loop II, which could be exploited to enhance the affinity of new inhibitors for DprE1. Inhibitors are mainly stabilised in the pocket by van der

Waals interactions. In certain cases, amino acids in the substrate-binding pocket form H-bonds with inhibitors, for instance Y60 and K418 with the 2-quinoxalines, K418 with TCA1 and N386, Q336 and K418 with the cBT series.

It is important to note that several docking studies on DprE1 in complex with inhibitors such as benzothiazolopyrimidine-5-carboxamides [28], 4-aminoquinolone piperidine amides [38], 1,2,4-triazole-containing 1,4-benzothiazinone derivatives [35], pyrazolopyridones, 8-pyrrole-benzothiazinones [25] and 1,3-benzothiazinone azide [26] have been conducted. The results of these studies were not extensively developed in this review but it seems that the same, aforementioned regions contribute to the stabilisation of all the inhibitors. Up until now, the majority of the inhibitory scaffolds have arisen from whole-cell screening campaigns. Nowadays, attempts are underway to use more-rational design to increase compound activity using the available structural information, not only to guide drug design and SAR but also to improve pharmacodynamic properties and bioavailability. Our review will aid the design of such new inhibitors.

Conflicts of interest

S.T.C. is a named inventor on patents related to this article.

Acknowledgement

This work was supported by the European Community's Seventh Framework Programme FP7/2007–2013 under grant agreement 260872.

References

- Kieser, K.J. and Rubin, E.J. (2014) How sisters grow apart: mycobacterial growth and division. *Nat. Rev. Microbiol.* 12, 550–562
- Takayama, K. and Kilburn, J.O. (1989) Inhibition of synthesis of arabinogalactan by ethambutol in *Mycobacterium smegmatis*. *Antimicrob. Agents Chemother.* 33, 1493–1499
- Quemard, A. *et al.* (1991) Isoniazid inhibition of mycolic acid synthesis by cell extracts of sensitive and resistant strains of *Mycobacterium aurum*. *Antimicrob. Agents Chemother.* 35, 1035–1039
- Mikusova, K. *et al.* (1995) Biogenesis of the mycobacterial cell wall and the site of action of ethambutol. *Antimicrob. Agents Chemother.* 39, 2484–2489
- Belanger, A.E. *et al.* (1996) The embAB genes of *Mycobacterium avium* encode an arabinosyl transferase involved in cell wall arabinan biosynthesis that is the target for the antimycobacterial drug ethambutol. *Proc. Natl. Acad. Sci. U. S. A.* 93, 11919–11924
- Vilcheze, C. *et al.* (2006) Transfer of a point mutation in *Mycobacterium tuberculosis* inhA resolves the target of isoniazid. *Nat. Med.* 12, 1027–1029
- Li, W. *et al.* (2016) Therapeutic potential of the *Mycobacterium tuberculosis* mycolic acid transporter, MmpL3. *Antimicrob. Agents Chemother.* 60, 5198–5207
- Riccardi, G. *et al.* (2013) The DprE1 enzyme, one of the most vulnerable targets of *Mycobacterium tuberculosis*. *Appl. Microbiol. Biotechnol.* 97, 8841–8848
- Wolucka, B.A. (2008) Biosynthesis of D-arabinose in mycobacteria – a novel bacterial pathway with implications for antimycobacterial therapy. *FEBS J.* 275, 2691–2711
- Mikusova, K. *et al.* (2005) Decaprenylphosphoryl arabinofuranose, the donor of the D-arabinofuranosyl residues of mycobacterial arabinan, is formed via a two-step epimerization of decaprenylphosphoryl ribose. *J. Bacteriol.* 187, 8020–8025
- Crellin, P.K. *et al.* (2011) Decaprenylphosphoryl-beta-D-ribose 2'-epimerase, the target of benzothiazinones and dinitrobenzamides, is an essential enzyme in *Mycobacterium smegmatis*. *PLoS ONE* 6, e16869
- Kolly, G.S. *et al.* (2014) Assessing the essentiality of the decaprenyl-phospho-D-arabinofuranose pathway in *Mycobacterium tuberculosis* using conditional mutants. *Mol. Microbiol.* 92, 194–211
- Breck, M. *et al.* (2015) DprE1 is a vulnerable tuberculosis drug target due to its cell wall localization. *ACS Chem. Biol.* 10, 1631–1636
- Makarov, V. *et al.* (2009) Benzothiazinones kill *Mycobacterium tuberculosis* by blocking arabinan synthesis. *Science* 324, 801–804
- Trefzer, C. *et al.* (2012) Benzothiazinones are suicide inhibitors of mycobacterial decaprenylphosphoryl-beta-D-ribofuranose 2'-oxidase DprE1. *J. Am. Chem. Soc.* 134, 912–915
- Batt, S.M. *et al.* (2012) Structural basis of inhibition of *Mycobacterium tuberculosis* DprE1 by benzothiazinone inhibitors. *Proc. Natl. Acad. Sci. U. S. A.* 109, 11354–11359
- Neres, J. *et al.* (2012) Structural basis for benzothiazinone-mediated killing of *Mycobacterium tuberculosis*. *Sci. Transl. Med.* 4, 150ra121
- Makarov, V. *et al.* (2014) Towards a new combination therapy for tuberculosis with next generation benzothiazinones. *EMBO Mol. Med.* 6, 372–383
- Christophe, T. *et al.* (2009) High content screening identifies decaprenylphosphoribose 2' epimerase as a target for intracellular antimycobacterial inhibitors. *PLoS Pathog.* 5, e1000645
- Magnet, S. *et al.* (2010) Leads for antitubercular compounds from kinase inhibitor library screens. *Tuberculosis* 90, 354–360
- Stanley, S.A. *et al.* (2012) Identification of novel inhibitors of *M. tuberculosis* growth using whole cell based high-throughput screening. *ACS Chem. Biol.* 7, 1377–1384
- Landge, S. *et al.* (2015) Discovery of benzothiazoles as antimycobacterial agents: synthesis, structure–activity relationships and binding studies with *Mycobacterium tuberculosis* decaprenylphosphoryl-beta-D-ribose 2'-oxidase. *Bioorg. Med. Chem.* 23, 7694–7710
- Landge, S. *et al.* (2016) Nitroarenes as antitubercular agents: stereoelectronic modulation to mitigate mutagenicity. *ChemMedChem* 11, 331–339
- Purohit, V. and Basu, A.K. (2000) Mutagenicity of nitroaromatic compounds. *Chem. Res. Toxicol.* 13, 673–692
- Makarov, V. *et al.* (2015) The 8-pyrrole-benzothiazinones are noncovalent inhibitors of DprE1 from *Mycobacterium tuberculosis*. *Antimicrob. Agents Chemother.* 59, 4446–4452
- Tiwari, R. *et al.* (2016) Design, syntheses, and anti-TB activity of 1,3-benzothiazinone azide and click chemistry products inspired by BTZ043. *ACS Med. Chem. Lett.* 7, 266–270
- Wang, F. *et al.* (2013) Identification of a small molecule with activity against drug-resistant and persistent tuberculosis. *Proc. Natl. Acad. Sci. U. S. A.* 110, E2510–E2517

- 28 Chikhale, R. *et al.* (2015) Development of selective DprE1 inhibitors: design, synthesis, crystal structure and antitubercular activity of benzothiazolylpyrimidine-5-carboxamides. *Eur. J. Med. Chem.* 96, 30–46
- 29 No, Z. *et al.* (2011) Anti-infective compounds. WO 2011/113606 A1
- 30 No, Z. *et al.* (2011) Anti-infective pyrido(1,2-a)pyrimidines. WO 2011/085990 A1
- 31 Shirude, P.S. *et al.* (2013) Azaindoles: noncovalent DprE1 inhibitors from scaffold morphing efforts, kill *Mycobacterium tuberculosis* and are efficacious *in vivo*. *J. Med. Chem.* 56, 9701–9708
- 32 Chatterji, M. *et al.* (2014) 1,4-Azaindole, a potential drug candidate for treatment of tuberculosis. *Antimicrob. Agents Chemother.* 58, 5325–5331
- 33 Panda, M. *et al.* (2014) Discovery of pyrazolopyridones as a novel class of noncovalent DprE1 inhibitor with potent anti-mycobacterial activity. *J. Med. Chem.* 57, 4761–4771
- 34 Neres, J. *et al.* (2015) 2-Carboxyquinoxalines kill *Mycobacterium tuberculosis* through noncovalent inhibition of DprE1. *ACS Chem. Biol.* 10, 705–714
- 35 Shaikh, M.H. *et al.* (2016) Synthesis and bioactivity of novel triazole incorporated benzothiazinone derivatives as antitubercular and antioxidant agent. *Bioorg. Med. Chem. Lett.* 26, 561–569
- 36 Chitre, T.S. *et al.* (2016) Synthesis and docking studies of pyrazine-thiazolidinone hybrid scaffold targeting dormant tuberculosis. *Bioorg. Med. Chem. Lett.* 26, 2224–2228
- 37 Li, H. and Jogl, G. (2013) Crystal structure of decaprenylphosphoryl-beta-D-ribose 2'-epimerase from *Mycobacterium smegmatis*. *Proteins* 81, 538–543
- 38 Naik, M. *et al.* (2014) 4-Aminoquinolone piperidine amides: noncovalent inhibitors of DprE1 with long residence time and potent antimycobacterial activity. *J. Med. Chem.* 57, 5419–5434

Appendix Chapter A2: Structure-based drug design and characterization of sulfonyl-piperazine benzothiazinone inhibitors of DprE1 from *Mycobacterium tuberculosis*

Jérémie Piton¹, Anthony Vocat¹, Andréanne Lupien¹, Caroline Foo¹, Olga Riabova², Vadim Makarov², Stewart T. Cole^{1*}

¹Global Health Institute, École Polytechnique Fédérale de Lausanne, CH-1015 Lausanne, Switzerland

²FRC Fundamentals of Biotechnology RAS, Leninsky prospekt 33-2, Moscow, 119071, Russian Federation

Antimicrobial Agents and Chemotherapy, 2018, doi: 10.1128/AAC.00681-18

Contributions: execution of microsomal and enzymatic assays, manuscript preparation

ABSTRACT

Macozinone (MCZ) is a tuberculosis (TB) drug candidate that specifically targets the essential flavoenzyme DprE1 thereby blocking synthesis of the cell wall precursor decaprenyl phosphoarabinose (DPA) and provoking lysis of *Mycobacterium tuberculosis*. As part of the MCZ back-up program we exploited structure-guided drug design to produce a new series of sulfone-containing derivatives, 2-sulphonylpiperazin 8-nitro 6-trifluoromethyl 1,3-benzothiazin-4-one, or sPBTZ. These compounds are less active than MCZ but have a better solubility profile and some derivatives display enhanced stability in microsomal assays. DprE1 was efficiently inhibited by sPBTZ and covalent adducts with the active site cysteine residue (C387) were formed. However, despite the H-bonding potential of the sulfone group no additional bonds were seen in the crystal structure of the sPBTZ-DprE1 complex with compound 11326127 as compared to MCZ. Compound 11626091, the most advanced sPBTZ, displayed good antitubercular activity in the murine model of chronic TB but was less effective than MCZ. Nonetheless, further testing of this MCZ backup compound is warranted as part of combination treatment with other TB drugs.

INTRODUCTION

DprE1 is an essential flavoprotein of *Mycobacterium tuberculosis* involved in decaprenylphosphoryl-beta-D-arabinose (DPA) synthesis. DPA is the sole precursor of arabinose for production of both arabinogalactan and lipoarabinomannan (1), important components of the mycobacterial cell wall. DprE1, together with its counterpart DprE2, catalyses the epimerization of decaprenylphosphoryl- β -D-ribose (DPR) to DPA in a two-step mechanism. In the last decade, many inhibitors were discovered to target DprE1, which is considered nowadays as the Achilles' heel of *M. tuberculosis* due to its essentiality and especially to its localization in the periplasm (2). DprE1 inhibitors can be classified into two families according to their mode of action: some of them inhibit DprE1 irreversibly by forming a covalent adduct with cysteine 387 (C387) of DprE1, whereas others act as competitive non-covalent inhibitors (3).

The first covalent DprE1 inhibitors discovered were benzothiazinones (BTZ), exemplified by the lead compound, BTZ043, which is exceptionally potent with *in vitro* and *ex vivo* minimal inhibitory concentration (MIC) values in the nanomolar range (4). A lead optimization campaign gave rise to PBTZ169, now known as Macozinone (MCZ). It is currently the most potent BTZ compound against *M. tuberculosis* with an MIC of 0.3 nM (5), has completed preclinical development successfully and is now undergoing Phase I and phase II clinical trials (<https://www.newtbdrugs.org/pipeline/clinical>). A common characteristic of the covalent DprE1 inhibitors is the presence of a nitro group on the molecule, which is essential for the mechanism of inhibition. Indeed, this nitro group is converted by DprE1 containing FADH₂ into an extremely reactive nitroso group which specifically targets the cysteine residue at position 387 (C387) in the active site of DprE1, to form a covalent adduct and thereby irreversibly inhibits the enzyme (4-7, 8, 9-13). It has been demonstrated that the presence of C387 is essential for the activity of covalent DprE1 inhibitors (4, 14).

Apart from the covalent bond with C387, covalent DprE1 inhibitors are otherwise only maintained in the pocket by steric hindrance and Van Der Waals interactions, which explains why a simple substitution at C387 results in complete resistance of the enzyme to these compounds (3). As part of the MCZ-back-up program, this observation prompted us to revisit the Structure Activity Relationship (SAR) in order to obtain derivatives with other anchor points in the active site of DprE1, since such compounds might retain activity against C387 mutants should these arise.

Several non-covalent DprE1 inhibitors have also been found (15-24). Similar to the covalent DprE1 inhibitors, these non-covalent compounds sit in the substrate-binding pocket of DprE1 and act as competitive inhibitors. Interestingly, a class of non-covalent inhibitors, 2-carboxyquinoxalines, are active against BTZ-resistant *M. tuberculosis* strains with substitutions at C387 of DprE1 (14). Molecules from this family possess an essential 2-carboxylate moiety that forms key hydrogen bonds with the side-chain of Lysine 418 and the hydroxyl group of Tyrosine 60 (18). Hence, it can be hypothesised that a composite molecule between 2-carboxyquinoxalines and MCZ could overcome resistance issues and increase specificity to the target.

Revisiting the SAR of MCZ further provides the opportunity to improve pharmacodynamics properties of MCZ such as aqueous solubility to increase its oral bioavailability, metabolic stability, and *in vivo* activity (25). It has been observed that the potency of BTZ derivatives is inversely proportional to their solubility (4, 5). Therefore, the solubility and bioavailability of the most active benzothiazinones are parameters for improvement. Factors controlling the aqueous solubility of organic molecules are complex and drug solubility issues are usually solved by a combination of empirical and rational drug design strategies. More than twenty crystal structures of DprE1 with or without inhibitors were reviewed recently to identify the structural determinants for activity and to guide rational drug design (3).

Based on our prior observations, the aim of this study was to design a new structure-guided series of MCZ derivatives with increased activity against either wild-type *M. tuberculosis* or its BTZ-resistant mutants, and with improved solubility, absorption, bioavailability and metabolic stability of the compound *in vivo*. Therefore, a new series of MCZ derivatives, harbouring a sulfonylpiperazine group, was designed (2-sulphonylpiperazin 8-nitro 6-trifluoromethyl 1,3-benzothiazin-4-one or sPBTZ), synthesized and characterized. This study identifies 11626091 as the best sPBTZ and demonstrates that this compound has a promising combination of antitubercular activity and ADME/T (Absorption, Distribution, Metabolism, and Excretion – Toxicity) properties.

RESULTS

Rationale. When BTZ inhibitors bind to their target, DprE1, the sole bond formed is a covalent semimercaptal bond with the active site cysteine residue, C387. We reasoned first that introducing a sulfonyl group into the MCZ scaffold might offer a second anchor by mimicking the carboxylate moiety of the 2-carboxyquinoxalines that acts as a H-bond acceptor with DprE1 and increases affinity of the inhibitor for the target. Secondly, sulfonyl groups are well characterized and present in many FDA-approved drugs, in particular anti-mycobacterial agents, such as dapson. Based on these observations, sulfonyl groups might increase both the solubility and bioavailability of the inhibitor *in vivo*. Lastly, the geometry imposed by sulfonyl groups opens new directions for investigation of the SAR.

Synthesis of sPBTZ. The synthesis of 17 sulfanyl-piperazino BTZ (sPBTZ) derivatives was performed in a two-step procedure from 2-(methylthio)-8-nitro-6-(trifluoromethyl)-4*H*-1,3-benzothiazin-4-one, as described previously (5). Its reaction with a 5-molar excess of free piperazine generated the corresponding piperazine derivative with a high yield. This scaffold was

used in the reactions with different alkyl-, aryl- or heteryl-sulfochlorides to form sulfanyl-piperazino BTZs. The compounds synthesized have different types of sulfonyl substitutions thus allowing the structure-activity relationship to be studied. It is clear that compounds with alkyl substitutions have much better antitubercular activity and aryl derivatives have much lower activity, consistent with our previous data for piperazine-containing BTZ (PBTZ) derivatives (5)

Hydrophilicity. The octanol-water partition coefficient, logP, which is regarded as a suitable indicator of molecular hydrophobicity and bioavailability, was calculated for all derivatives to measure the effects of introducing a sulfonyl group on the PBTZ backbone. Interestingly, the addition of the sulfonyl group between the benzothiazinone and piperazine moieties has the tendency to decrease the clogP coefficient and therefore hydrophobicity (Table 1). The sulfonylated derivative of MCZ, sPBTZ169 (11326127) that carries a sulfonyl group between the piperazine and cyclohexyl moieties, has a clogP of 3.28 whereas MCZ has a clogP of 4.31. This implies that the introduction of a sulfonyl group decreases hydrophobicity, and may thus increase solubility in physiological conditions and subsequently could have an important impact on bioavailability.

Antitubercular activity. The activity of all sPBTZ derivatives was tested *in vitro* against *M. tuberculosis* H37Rv and MIC₉₉ values were determined (Table 1). Most sPBTZ were active *in vitro* in the sub-micromolar range, proving that that addition of the sulfonyl group does not abolish activity. However, none has a better activity than MCZ. 11626093, which has a butyl group, has the highest activity of MIC 1 ng/μL corresponding to 5 times the MIC₉₉ of MCZ. The introduction of a sulfone between the piperazine and the cyclohexyl negatively affected the activity of the compound, reducing activity by 30 fold, as observed with sPBTZ169 (11326127), which has an MIC₉₉ of 6 nM. It was previously shown that substituting the methylecyclohexyl in MCZ with small radicals such as methyl or ethyl decreases the activity of compounds, with MIC of 250 ng/mL and

60 ng/mL, respectively (5). Interestingly, when methylcyclohexyl is substituted by sulfonylmethyl (11626095) or sulfonylethyl (11626092), the activity decreases less and the compounds are 10-times more active than the non-sulfonated derivatives (MIC of 20 ng/mL and 3 ng/mL, respectively). Substitution with a butyl leads to the same activity independent of the sulfonyl group. This observation indicates that the presence of the sulfonyl group positively affects activity when the radical is small (methyl or ethyl) whereas it negatively influences activity when the substituent is long and hydrophobic.

Similarly to the other BTZ derivatives, the activities of the sulfonyl derivatives are inversely proportional to the logP (4), suggesting that activity could be related to solubility in lipids (Figure S1). Seven molecules were selected based on their activity/logP profile for further characterisation (Figure S1).

Target engagement and structural studies. To ensure that sPBTZs specifically target DprE1, selected sulfonyl derivatives were tested against *M. tuberculosis* NTB1, a DprE1 mutant that carries a cysteine 387 serine (C387S) substitution and is thus resistant to BTZ. As expected, none of the sBTZs are active against NTB1, indicating that DprE1 is their primary target (Table 2). Furthermore, it is unlikely that the sulfonyl group is able to mimic the carboxylate moiety of 2-carboxyquinoxalines in stabilizing the compound in the pocket as a non-covalent inhibitor.

To investigate whether the introduction of the sulfonyl group could influence the position of the inhibitor and allow more contact within the binding pocket, a crystal structure of DprE1 in complex with sPBTZ169 was solved and compared to the crystal structure of DprE1 with MCZ. sPBTZ169 is located in the same pocket as MCZ and other BTZ derivatives. It sits in an hydrophobic pocket *via* the trifluoromethyl group and is covalently bound to C387 (Figure 1). The compound is maintained by Van der Waals interaction on each side by V365, Y314, W230 and FAD, and a hydrogen bond between K418 and the oxygen atom of the nitro group of sPBTZ169.

Unfortunately, the orientation of sPBTZ does not favor the formation of a new anchor to the protein for instance interaction between the sulfonyl function and Y60. Furthermore as MCZ, the electron density map does not account fully for the sulfonyl-cyclohexyl moiety of sPBTZ169 likely due to its higher flexibility demonstrating that sulfonyl is not stabilized in the pocket (5).

To determine whether the sulfonyl group could affect the activity at the protein level and even help to stabilize the inhibitor in the active site of a BTZ-resistant C387S DprE1 variant, the inhibition of DprE1 activity was measured *in vitro*. IC₅₀ values were determined for the wild type and the BTZ-resistant C387S mutant enzyme for MCZ and sPBTZ169 (Table S2). sPBTZ169 has an IC₅₀ of 1.1 and 12 μ M against wild type and BTZ-resistant DprE1, respectively, whereas the corresponding IC₅₀ values for MCZ are 0.3 and 3.6 μ M. That introducing the sulfonyl group on the MCZ scaffold leads to 4-fold less activity suggests that even if the environment of the protein is favorable for an H-bond acceptor, the presence of a hydrophobic group, such as a cyclohexyl in MCZ, is still preferable for activity of the drug. On the other hand, the higher IC₅₀ against C387S compared to the WT enzyme validates the structural studies in that the sulfonyl group does not help to stabilize the molecule in the pocket of the BTZ-resistant mutant C387S.

ADME/T. To assess potential cytotoxic effects of the sulfonyl group on the sPBTZ derivatives, viability of HepG2 cells was monitored after exposure to different concentrations of the compounds. The concentration for half-maximal cytotoxicity (TD₅₀) was determined for each compound. Four of the seven compounds were not cytotoxic (11326059, 11326127, 11626093, 11626094) while three of them showed mild cytotoxicity at concentrations of around 10 μ g/mL (11626091, 11626092, 11626095). Taken together, the selective index representing the ratio of the antitubercular activity of compounds (MIC₉₉ against H37Rv) to cytotoxicity (TD₅₀ against HepG2 cells) is more than acceptable for the chosen seven compounds (Table 2).

Since solubility issues are often encountered in drug development, which would consequently impact bioavailability, activity *in vitro*, ADMET results and activity *in vivo*, the solubility of these derivatives was calculated by the shake flask method in equilibrium in water. Experimental solubility constants measured were then compared to theoretical solubility constants calculated using the SwissADME webserver (26). sPBTZ are predicted to have increased solubility compared to MCZ in water (Table 3) and experimental solubility constants measured in water for all sPBTZ derivatives are consistent with theoretical constants calculated by SwissADME using different algorithms (Table 3). As expected, 11626095, 11626092 and 11626091, harboring methyl, ethyl and cyclopropyl groups, respectively, are the most soluble sPBTZ derivatives. In contrast, 11326059, 11326127, 11626093, and 11626094 that carry bigger hydrophobic groups are at least 100-times less soluble in water. Interestingly, there is a good correlation between water solubility and clogP. However, a discrepancy between the predicted and experimental solubility for MCZ was observed. In fact, MCZ is 400 times more soluble in water than calculated with different algorithms.

Another possible issue in the development of MCZ might be metabolic instability (5). In order to test if the sulfonyl group could improve metabolic stability effected by mouse CD-1 or human liver enzymes, microsomal stability experiments were conducted. Intrinsic clearance (Cl_{int}) values were then calculated for each compound and compared to the Cl_{int} of Carbamazepine and Nifedipine, used as controls for low and high intrinsic clearance respectively. It is important to note that the Compounds 11626095, 11626091 and 11626092 harbouring the smallest radical chains methyl, ethyl and cyclopropyl, respectively, have the lowest clearances in both mouse and human microsomes, indicative of their stability. 11626093 carrying a butyl radical is metabolically stable in human but highly unstable in mouse microsomes, suggesting that it could be a good substrate for mouse but not human microsomal enzymes. Compounds 11326059 and 11326127 have

medium clearances in both mouse and human microsomes, similar to MCZ and BTZ043. Of note, 11626094 is highly unstable in the presence of human microsomes. These results reveal a strong correlation between the length of the substituent after the piperazine moiety and instability in microsomes.

Activity in the murine model of chronic TB. Finally, the *in vivo* efficacy of 11626091 was assessed in the murine model of chronic TB following low-dose aerosol infection of BALB/cByJ mice with *M. tuberculosis* and treatment at 50 mg/kg (Figure 2). Compound 11626091 was selected as it is the most promising taking into account its activity (“only” 15 times less active than MCZ), cytotoxicity, solubility, and metabolic stability properties. *In vivo* activity of 11626091 was tested at 50 mg/kg and compared to activity of MCZ at standard dose of 25 mg/kg and INH at standard dose of 10 mg/kg.

Compared to the untreated control group, the bacterial burden in the lungs and spleens of 11626091-treated mice was 0.46 ($P<0.05$) and 1.03 ($P<0.0001$) \log_{10} CFU lower, respectively (Fig 2), whereas the values for those organs from MCZ-treated mice were 1.03 ($P<0.0001$) and 1.47 ($P<0.0001$) \log_{10} CFU. These results indicate that 11626091 is highly active *in vivo* in the murine model of chronic TB, although it is less able to reduce the bacterial load in the lungs than treatment with MCZ.

DISCUSSION

Lead compounds for new anti-TB drugs should possess not only potent sterilizing activity but also good pharmacokinetic profiles to facilitate their co-administration with other anti-TB and anti-HIV (human immunodeficiency virus) agents. New drugs should also be appropriate for once daily oral dosing and be relatively inexpensive to produce to ensure that all high-burden countries have

access. Structure-based rational drug design supports drug development and has the potential to increase the activity and pharmacokinetic properties of lead compounds.

The new sPBTZ series was designed as part of the MCZ back-up program. MCZ is a BCS (biopharmaceutical classification system) class 2 drug with a low dissolution rate but excellent absorption (5). Structural studies indicate that the environment of the binding pocket in the protein can accommodate a polar group at the cyclohexyl position of MCZ (3). A sulfonyl group was deemed to be a good candidate because it is well characterized and present in many soluble and metabolically stable FDA-approved drugs including those for treating mycobacterial infections. For instance, sulfamethoxazole is a sulfonamide drug used in co-trimoxazole prophylaxis for HIV-infected patients, demonstrating that it is compatible with anti-retroviral treatment (27).

It was previously shown that there is a strong correlation between logP and BTZ activity (4). We found that introduction of a sulfonyl group into the MCZ scaffold to form the sPBTZ series decreases both logP and activity *in vitro* (Table 1). However, sPBTZ still retain potency and the presence of the sulfonyl group improved aqueous solubility for those derivatives which harbour small side chains, such as methyl, ethyl or cyclopropyl, as compared to MCZ (5). Interestingly, aqueous solubility and metabolic stability measured in microsomes indicate a better profile for sPBTZ with small groups rather than those with long hydrophobic chains or MCZ. Despite being less active than MCZ our sulfonylated PBTZ with long hydrophobic chains, methyl (11626095), ethyl (11626092) or cyclopropyl (11626091) derivatives are considered as good candidates in terms of their solubility and metabolic stability profiles. The efficacy of the most active derivative of the three, 11626091, was assessed *in vivo* in the murine model of chronic TB, where relatively good activity was measured in the lungs and particularly in the spleens (Figure 2). It is also important to note that dissolution of 11626091 was considerably easier than MCZ in methylcellulose, the solvent used for the *in vivo* studies (technical observation, data not shown).

One of the objectives of inserting a sulfonyl group into the PBTZ backbone was to mitigate potential BTZ-resistance by increasing the number of hydrogen bonds with DprE1. Indeed, a sulfonyl could act as an H-bond acceptor in order to anchor the protein to the H-bond donors, for example the hydroxyl group of Tyrosine 60 localized in the binding pocket. This group was identified as a key player in the stabilization of 2-carboxyquinoxalines, molecules that remain active against BTZ-resistant DprE1. Unfortunately, as was observed in the crystal structure and enzymatic inhibition assays, the sulfonyl group of sPBTZ is not implicated in the binding and stabilization of the drug in the pocket as originally hypothesized. This explains the resistance of the BTZ-resistant *M. tuberculosis* mutant NTB1 to sPBTZ.

To conclude, our study identifies 11626091 as an active, metabolically stable and moderately soluble molecule that is less active than MCZ *in vitro* and *in vivo*. However, given its better solubility, compound 11626091 represents an attractive back-up to MCZ, that should now be tested in combination with other TB drug candidates such as bedaquiline in order to assess its potential to contribute to a new regimen.

MATERIALS AND METHODS

Synthesis. The synthetic route used to produce sPBTZ and related procedures are described in the supporting materials.

Octanol-water partition coefficient logP calculation. The log P values were calculated using the program Hyperchem 7.5 (Hypercube Inc., <http://www.hyper.com>).

Bacterial strains and culture conditions. *M. tuberculosis* strain H37Rv and its BTZ-resistant mutant (C387S) NTB1 were grown at 37°C with shaking in Middlebrook 7H9 broth (Difco) supplemented with 10% albumin-dextrose-catalase (ADC) enrichment, 0.2% glycerol, and 0.05% Tween 80. The *in vitro* activities against all mycobacterial strains were measured with the resazurin reduction microplate assay (REMA), by 2-fold serial dilutions of the compounds in the working bacterial culture in 96-well plates (final volume of 100 μ l). Following incubation for 6 days at 37°C bacterial viability was determined by adding resazurin for 24 h at 37°C and measuring the fluorescence of the resorufin metabolite (excitation wavelength, 560 nm; emission wavelength, 590 nm) using a Tecan Infinite M200 microplate reader. Briefly, the noise signal obtained in the blank control wells was subtracted from the fluorescence values of test samples and mycobacterial viability in each well were proportionally calculated compared to 100% growth in control wells. Bacterial viability curves and MIC₉₉ value were calculated with GraphPad Prism software version 7.0, using “Gompertz equation for MIC determination” analysis (GraphPad Software, Inc., La Jolla, CA, USA).

Cytotoxicity studies. The cytotoxicity of the compounds was measured as described previously against the human hepatic cell line, HepG2 (20). Briefly, cells were incubated (4,000 cells/well) with serial dilutions of compounds (2-fold dilutions; 100 to 0.1 μ g/ml) in a 96-well microplate. Following incubation for 3 days at 37°C cell viability was determined by adding resazurin for 4 h at 37°C and measuring the fluorescence of the resorufin metabolite (excitation

wavelength, 560 nm; emission wavelength, 590 nm) using a Tecan Infinite M200 microplate reader. Data were corrected for background (no-cell control) and expressed as a percentage of the value for untreated cells (cells only).

Data were fitted to obtain IC₅₀ values, using “Log(inhibitor) vs. response – Variable slope” function implemented in GraphPad Prism software version 7.0 (GraphPad Software, Inc., La Jolla, CA, USA). Selective index refers to the ratio of the dose of drug that causes toxicity effects (TD₅₀) to the dose that leads to the desired pharmacological effect (MIC₉₉).

Water Solubility. Water solubility measurements were performed using the shake flask method (28). Approximately 1 mL of water was added to 1 mg of compound in an Eppendorf tube and incubated for 3 days at 25°C with shaking at 800 rpm. Suspensions were centrifuged at 16,100 x g for 10 min and the supernatant filtered using 0.22 μ filters. Filtrates were injected onto a high-performance liquid chromatography (HPLC) column (Dionex) and the amount of compound quantified using a calibration curve.

Inhibition assays, crystallography and structural studies of DprE1 complexed with sPBTZ. Recombinant *M. tuberculosis* DprE1 was overexpressed and purified as described previously (5) to obtain highly concentrated and pure protein with bound flavin adenine dinucleotide (FAD). Enzyme activities in the presence of MCZ, Ty38c and 11326127 were measured as described previously to determine IC₅₀ (50% inhibitory concentrations) values for both wild-type and C131S mutant DprE1 proteins (14).

For crystallization purposes, *M. tuberculosis* DprE1 (approximately 40 μ M) was incubated for 3h at 30 °C, with 200 μ M sulfonyl-BTZ 11326127 and 200 μ M FPR (farnesyl phosphoribose), in 20 mM Tris pH 8.5, 50 mM NaCl. The protein was concentrated to approximately 15 mg/mL on an Amicon centrifugal device (30,000 MWCO, Millipore). Crystals were obtained by the hanging-

drop vapor diffusion method at 18 °C. Experiments were set up by mixing 1 μ l of the protein sample with 1 μ l of the reservoir solution containing 100 mM imidazole, pH 7.2-7.5, 18-24 % polypropyleneglycol 400. Yellow crystals grew in approximately 1-3 days and were transferred to a cryo-protectant (reservoir solution with 25% glycerol) prior to flash-cooling in liquid nitrogen.

X-ray data were collected at SLS, beamline PROXIMA 3. Data were integrated with the program XDS (29) and processed using PHENIX (30). Structure was solved by molecular replacement using PHENIX (31) and the structure of *M. tuberculosis* DprE1 (PDB code : 4NCR, (5)) as a template. Molecular replacement was subjected to iterative rounds of refinement and rebuilding in coot (32) and PHENIX. The coordinates and structure factors have been deposited in the Brookhaven Protein Data Bank (accession numbers 6G83).

Metabolic stability *in vitro*. The intrinsic clearance (CL_{int}) of compounds was measured in both mouse and human liver microsomes. Briefly, 100 μ g of mouse (CD-1) or human liver microsomes (both from Invitrogen) were mixed in 0.1M phosphate buffer (pH 7.4) containing 0.01 μ l of compound dissolved in DMSO at 10 mg/ml, in a final volume of 50 μ l. In parallel, a NADPH-regenerating system (Promega) was prepared in 0.1 M phosphate buffer (pH 7.4). The solutions were pre-incubated at 37°C for 10 min before the intrinsic clearance assessment was initiated by mixing the two solutions (50 μ l of each; final compound concentration, 1 μ g/ml) at 37°C. After 0, 5, 15, 30, and 60 min, the reactions were terminated by transferring 100 μ l of the reaction mixture into 100 μ l of acetonitrile and placing the mixture on ice for 30 min for full protein precipitation. Samples were then centrifuged at 12,000 x g for 10 min, and the supernatant was injected onto a high-performance liquid chromatography (HPLC) column (Dionex) to quantify the amount of parent compound remaining over time. To control that the clearance is due to the enzyme activity of the microsomes and not to unspecific microsomal protein binding, mouse (CD-1) or human liver

microsomes (both from Invitrogen) were mixed in 0.1M phosphate buffer (pH 7.4) containing 0.01 µl of compound dissolved in DMSO at 10 mg/ml and incubated without NADPH-regenerating system. After 0 and 60 min the reactions were terminated, prepared and analyzed as previously described. Carbamazepine and Nifedipine at the same concentrations were used as controls for low and high intrinsic clearances respectively.

Anti-mycobacterial activity of 11626091 against chronic TB in mice. Female BALB/cByJ mice, aged 5 to 6 weeks, were purchased from Charles River Laboratories (France). Mice were infected with a low dose aerosol (100 – 200 CFU/lung) of logarithmic-phase *M. tuberculosis* H37Rv bacilli, then were allocated to experimental groups and returned to their cages. Five mice were used per time point for each regimen. Treatment was initiated 4 weeks after infection.

Macozinone (MCZ), 11626091, and isoniazid (INH) were prepared weekly in 0.5% methylcellulose and administered at 25, 50, and 10 mg/kg, respectively, by gavage 5 days a week for 4 weeks. *In vivo* efficacy of each treatment was assessed by CFU enumeration after plating dilutions of the lung and spleen homogenates on 7H10 agar plates containing 10% OADC, cycloheximide (10 µg/ml), and ampicillin (50 µg/ml). Plates were incubated for 4 weeks at 37°C before CFU were enumerated. CFU counts were log10 transformed before analysis as mean log10 CFU ± standard deviation (SD), and were compared by Student's t-test using GraphPad Prism® version 7.0 software (GraphPad Software, Inc., La Jolla, CA, USA). P values less than 0.05 were considered as statistically significant.

Experiments were approved by the Swiss Cantonal Veterinary Authority (authorization no. 3082) and performed between June-August 2017.

ACKNOWLEDGMENTS

The research leading to these results was performed as part of the More Medicines for Tuberculosis (MM4TB) project and received funding from the European Community's Seventh Framework Programme ([FP7/ 2007-2013]) under grant agreement no. 260872. We thank Aline Reynaud and Florence Pojer from the Ppscf facility at EPFL for their technical support.

REFERENCES

1. Mikusova K, Huang H, Yagi T, Holsters M, Vereecke D, D'Haese W, Scherman MS, Brennan PJ, McNeil MR, Crick DC. 2005. Decaprenylphosphoryl arabinofuranose, the donor of the D-arabinofuranosyl residues of mycobacterial arabinan, is formed via a two-step epimerization of decaprenylphosphoryl ribose. *Journal of bacteriology* 187:8020-5.
2. Brecik M, Centarova I, Mukherjee R, Kolly GS, Huszar S, Bobovska A, Kilacsikova E, Mokosova V, Svetlikova Z, Sarkan M, Neres J, Kordulakova J, Cole ST, Mikusova K. 2015. DprE1 Is a Vulnerable Tuberculosis Drug Target Due to Its Cell Wall Localization. *ACS Chem Biol* 10:1631-6.
3. Piton J, Foo CS, Cole ST. 2016. Structural studies of *Mycobacterium tuberculosis* DprE1 interacting with its inhibitors. *Drug Discov Today* doi:10.1016/j.drudis.2016.09.014.
4. Makarov V, Manina G, Mikusova K, Mollmann U, Ryabova O, Saint-Joanis B, Dhar N, Pasca MR, Buroni S, Lucarelli AP, Milano A, De Rossi E, Belanova M, Bobovska A, Dianiskova P, Kordulakova J, Sala C, Fullam E, Schneider P, McKinney JD, Brodin P, Christophe T, Waddell S, Butcher P, Albrethsen J, Rosenkrands I, Brosch R, Nandi V, Bharath S, Gaonkar S, Shandil RK, Balasubramanian V, Balganesch T, Tyagi S, Grosset J, Riccardi G, Cole ST. 2009. Benzothiazinones kill *Mycobacterium tuberculosis* by blocking arabinan synthesis. *Science* 324:801-4.
5. Makarov V, Lechartier B, Zhang M, Neres J, van der Sar AM, Raadsen SA, Hartkoorn RC, Ryabova OB, Vocat A, Decosterd LA, Widmer N, Buclin T, Bitter W, Andries K, Pojer F, Dyson PJ, Cole ST. 2014. Towards a new combination therapy for tuberculosis with next generation benzothiazinones. *EMBO Mol Med* 6:372-83.
6. Batt SM, Jabeen T, Bhowruth V, Quill L, Lund PA, Eggeling L, Alderwick LJ, Futterer K, Besra GS. 2012. Structural basis of inhibition of *Mycobacterium tuberculosis* DprE1 by benzothiazinone inhibitors. *Proc Natl Acad Sci U S A* 109:11354-9.
7. Trefzer C, Rengifo-Gonzalez M, Hinner MJ, Schneider P, Makarov V, Cole ST, Johnsson K. 2010. Benzothiazinones: prodrugs that covalently modify the decaprenylphosphoryl-beta-D-ribose 2'-epimerase DprE1 of *Mycobacterium tuberculosis*. *J Am Chem Soc* 132:13663-5.
8. Neres J, Pojer F, Molteni E, Chiarelli LR, Dhar N, Boy-Rottger S, Buroni S, Fullam E, Degiacomi G, Lucarelli AP, Read RJ, Zanoni G, Edmondson DE, De Rossi E, Pasca MR,

- McKinney JD, Dyson PJ, Riccardi G, Mattevi A, Cole ST, Binda C. 2012. Structural basis for benzothiazinone-mediated killing of *Mycobacterium tuberculosis*. *Science translational medicine* 4:150ra121.
9. Christophe T, Jackson M, Jeon HK, Fenistein D, Contreras-Dominguez M, Kim J, Genovesio A, Carralot JP, Ewann F, Kim EH, Lee SY, Kang S, Seo MJ, Park EJ, Skovierova H, Pham H, Riccardi G, Nam JY, Marsollier L, Kempf M, Joly-Guillou ML, Oh T, Shin WK, No Z, Nehrbass U, Brosch R, Cole ST, Brodin P. 2009. High content screening identifies decaprenyl-phosphoribose 2' epimerase as a target for intracellular antimycobacterial inhibitors. *PLoS Pathog* 5:e1000645.
 10. Magnet S, Hartkoorn RC, Szekely R, Pato J, Triccas JA, Schneider P, Szantai-Kis C, Orfi L, Chambon M, Banfi D, Bueno M, Turcatti G, Keri G, Cole ST. 2010. Leads for antitubercular compounds from kinase inhibitor library screens. *Tuberculosis (Edinb)* 90:354-60.
 11. Stanley SA, Grant SS, Kawate T, Iwase N, Shimizu M, Wivagg C, Silvis M, Kazyanskaya E, Aquadro J, Golas A, Fitzgerald M, Dai H, Zhang L, Hung DT. 2012. Identification of novel inhibitors of *M. tuberculosis* growth using whole cell based high-throughput screening. *ACS Chem Biol* 7:1377-84.
 12. Landge S, Mullick AB, Nagalapur K, Neres J, Subbulakshmi V, Murugan K, Ghosh A, Sadler C, Fellows MD, Humnabadkar V, Mahadevaswamy J, Vachaspati P, Sharma S, Kaur P, Mallya M, Rudrapatna S, Awasthy D, Sambandamurthy VK, Pojer F, Cole ST, Balganeshts, Ugarkar BG, Balasubramanian V, Bandodkar BS, Panda M, Ramachandran V. 2015. Discovery of benzothiazoles as antimycobacterial agents: Synthesis, structure-activity relationships and binding studies with *Mycobacterium tuberculosis* decaprenylphosphoryl-beta-D-ribose 2'-oxidase. *Bioorg Med Chem* 23:7694-710.
 13. Landge S, Ramachandran V, Kumar A, Neres J, Murugan K, Sadler C, Fellows MD, Humnabadkar V, Vachaspati P, Raichurkar A, Sharma S, Ravishankar S, Guptha S, Sambandamurthy VK, Balganeshts, Ugarkar BG, Balasubramanian V, Bandodkar BS, Panda M. 2016. Nitroarenes as Antitubercular Agents: Stereoelectronic Modulation to Mitigate Mutagenicity. *ChemMedChem* 11:331-9.

14. Foo CS, Lechartier B, Kolly GS, Boy-Rottger S, Neres J, Rybniker J, Lupien A, Sala C, Piton J, Cole ST. 2016. Characterization of DprE1-Mediated Benzothiazinone Resistance in *Mycobacterium tuberculosis*. *Antimicrob Agents Chemother* 60:6451-6459.
15. Wang F, Sambandan D, Halder R, Wang J, Batt SM, Weinrick B, Ahmad I, Yang P, Zhang Y, Kim J, Hassani M, Huszar S, Trefzer C, Ma Z, Kaneko T, Mdluli KE, Franzblau S, Chatterjee AK, Johnsson K, Mikusova K, Besra GS, Futterer K, Robbins SH, Barnes SW, Walker JR, Jacobs WR, Jr., Schultz PG. 2013. Identification of a small molecule with activity against drug-resistant and persistent tuberculosis. *Proc Natl Acad Sci U S A* 110:E2510-7.
16. Shirude PS, Shandil R, Sadler C, Naik M, Hosagrahara V, Hameed S, Shinde V, Bathula C, Humnabadkar V, Kumar N, Reddy J, Panduga V, Sharma S, Ambady A, Hegde N, Whiteaker J, McLaughlin RE, Gardner H, Madhavapeddi P, Ramachandran V, Kaur P, Narayan A, Guptha S, Awasthy D, Narayan C, Mahadevaswamy J, Vishwas KG, Ahuja V, Srivastava A, Prabhakar KR, Bharath S, Kale R, Ramaiah M, Choudhury NR, Sambandamurthy VK, Solapure S, Iyer PS, Narayanan S, Chatterji M. 2013. Azaindoles: noncovalent DprE1 inhibitors from scaffold morphing efforts, kill *Mycobacterium tuberculosis* and are efficacious in vivo. *J Med Chem* 56:9701-8.
17. Chatterji M, Shandil R, Manjunatha MR, Solapure S, Ramachandran V, Kumar N, Saralaya R, Panduga V, Reddy J, Prabhakar KR, Sharma S, Sadler C, Cooper CB, Mdluli K, Iyer PS, Narayanan S, Shirude PS. 2014. 1,4-azaindole, a potential drug candidate for treatment of tuberculosis. *Antimicrob Agents Chemother* 58:5325-31.
18. Neres J, Hartkoorn RC, Chiarelli LR, Gadupudi R, Pasca MR, Mori G, Venturelli A, Savina S, Makarov V, Kolly GS, Molteni E, Binda C, Dhar N, Ferrari S, Brodin P, Delorme V, Landry V, de Jesus Lopes Ribeiro AL, Farina D, Saxena P, Pojer F, Carta A, Luciani R, Porta A, Zanoni G, De Rossi E, Costi MP, Riccardi G, Cole ST. 2015. 2-Carboxyquinoxalines kill *mycobacterium tuberculosis* through noncovalent inhibition of DprE1. *ACS Chem Biol* 10:705-14.
19. Naik M, Humnabadkar V, Tantry SJ, Panda M, Narayan A, Guptha S, Panduga V, Manjrekar P, Jena LK, Koushik K, Shanbhag G, Jatheendranath S, Manjunatha MR, Gorai G, Bathula C, Rudrapatna S, Achar V, Sharma S, Ambady A, Hegde N, Mahadevaswamy J, Kaur P, Sambandamurthy VK, Awasthy D, Narayan C, Ravishankar S, Madhavapeddi

- P, Reddy J, Prabhakar K, Saralaya R, Chatterji M, Whiteaker J, McLaughlin B, Chiarelli LR, Riccardi G, Pasca MR, Binda C, Neres J, Dhar N, Signorino-Gelo F, McKinney JD, Ramachandran V, Shandil R, Tommasi R, Iyer PS, Narayanan S, Hosagrahara V, Kavanagh S, Dinesh N, Ghorpade SR. 2014. 4-aminoquinolone piperidine amides: noncovalent inhibitors of DprE1 with long residence time and potent antimycobacterial activity. *J Med Chem* 57:5419-34.
20. Makarov V, Neres J, Hartkoorn RC, Ryabova OB, Kazakova E, Sarkan M, Huszar S, Piton J, Kolly GS, Vocat A, Conroy TM, Mikusova K, Cole ST. 2015. The 8-Pyrrole-Benzothiazinones Are Noncovalent Inhibitors of DprE1 from *Mycobacterium tuberculosis*. *Antimicrob Agents Chemother* 59:4446-52.
 21. Shaikh MH, Subhedar DD, Arkile M, Khedkar VM, Jadhav N, Sarkar D, Shingate BB. 2016. Synthesis and bioactivity of novel triazole incorporated benzothiazinone derivatives as antitubercular and antioxidant agent. *Bioorg Med Chem Lett* 26:561-9.
 22. Tiwari R, Miller PA, Chiarelli LR, Mori G, Sarkan M, Centarova I, Cho S, Mikusova K, Franzblau SG, Oliver AG, Miller MJ. 2016. Design, Syntheses, and Anti-TB Activity of 1,3-Benzothiazinone Azide and Click Chemistry Products Inspired by BTZ043. *ACS Med Chem Lett* 7:266-70.
 23. Panda M, Ramachandran S, Ramachandran V, Shirude PS, Humnabadkar V, Nagalapur K, Sharma S, Kaur P, Guptha S, Narayan A, Mahadevaswamy J, Ambady A, Hegde N, Rudrapatna SS, Hosagrahara VP, Sambandamurthy VK, Raichurkar A. 2014. Discovery of pyrazolopyridones as a novel class of noncovalent DprE1 inhibitor with potent anti-mycobacterial activity. *J Med Chem* 57:4761-71.
 24. Chikhale R, Menghani S, Babu R, Bansode R, Bhargavi G, Karodia N, Rajasekharan MV, Paradkar A, Khedekar P. 2015. Development of selective DprE1 inhibitors: Design, synthesis, crystal structure and antitubercular activity of benzothiazolylpyrimidine-5-carboxamides. *Eur J Med Chem* 96:30-46.
 25. Amidon GL, Lennernas H, Shah VP, Crison JR. 1995. A theoretical basis for a biopharmaceutic drug classification: the correlation of in vitro drug product dissolution and in vivo bioavailability. *Pharm Res* 12:413-20.

26. Daina A, Michielin O, Zoete V. 2017. SwissADME: a free web tool to evaluate pharmacokinetics, drug-likeness and medicinal chemistry friendliness of small molecules. *Sci Rep* 7:42717.
27. Guidelines W. 2014. Guidelines on Post-Exposure Prophylaxis for HIV and the Use of Co-Trimoxazole Prophylaxis for HIV-Related Infections Among Adults, Adolescents and Children: Recommendations for a Public Health Approach: December 2014 supplement to the 2013 consolidated guidelines on the use of antiretroviral drugs for treating and preventing HIV infection, Geneva.
28. Bergstrom CA, Wassvik CM, Johansson K, Hubatsch I. 2007. Poorly soluble marketed drugs display solvation limited solubility. *J Med Chem* 50:5858-62.
29. Kabsch W. 2010. Integration, scaling, space-group assignment and post-refinement. *Acta Crystallogr D Biol Crystallogr* 66:133-44.
30. Adams PD, Afonine PV, Bunkoczi G, Chen VB, Davis IW, Echols N, Headd JJ, Hung LW, Kapral GJ, Grosse-Kunstleve RW, McCoy AJ, Moriarty NW, Oeffner R, Read RJ, Richardson DC, Richardson JS, Terwilliger TC, Zwart PH. 2010. PHENIX: a comprehensive Python-based system for macromolecular structure solution. *Acta Crystallogr D Biol Crystallogr* 66:213-21.
31. McCoy AJ, Grosse-Kunstleve RW, Adams PD, Winn MD, Storoni LC, Read RJ. 2007. Phaser crystallographic software. *J Appl Crystallogr* 40:658-674.
32. Emsley P, Cowtan K. 2004. Coot: model-building tools for molecular graphics. *Acta Crystallogr D Biol Crystallogr* 60:2126-32.

Table 1: Structure activity relationship of the different 2-sulphonylpiperazin 8-nitro 6-trifluoromethyl 1,3-benzothiazin-4-ones derivatives (sulfonyl PBTZ derivatives) in *M. tuberculosis* H37Rv

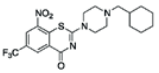
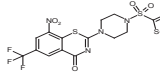
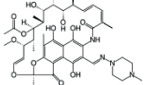
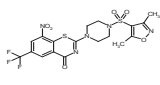
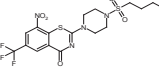
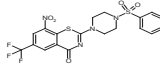
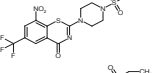
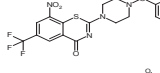
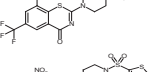
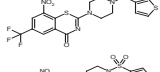
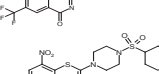
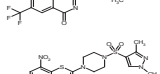
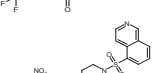
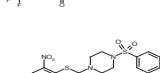
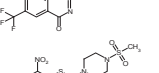
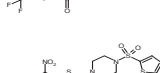
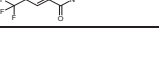
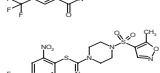
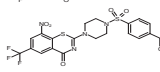
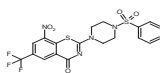

Compound Name	Molecular structure	clogP	MIC ₉₉ H37Rv (µg/mL)	Compound Name	Molecular structure	clogP	MIC ₉₉ H37Rv (µg/mL)
PBTZ169		4.31	0.0002	11326121		3.62	0.03
Rifampicin		3.7	0.0008	11326056		1.79	0.06
11626093		2.69	0.001	11326120		4.56	0.1
11626091		2	0.003	11326123		3.98	0.1
11626092		1.82	0.003	11326128		2.59	0.1
11326059		2.6	0.004	11326058		2.35	0.4
11326127		3.28	0.006	11326061		1.81	0.4
11626094		3.1	0.01	11326125		5.23	0.5
11626095		1.36	0.02	11326122		4.51	0.8
				11326126		1.33	1.6
				11326119		0.15	50
				11326124		5.06	800

Table 2: *In vitro* activity of selected sPBTZ derivatives against *M. tuberculosis* H37Rv and its BTZ-resistant mutant (NTB1) and cytotoxicity for HepG2 cells

Compound Name	H37Rv MIC ₉₉ (µg/mL)	NTB1 MIC ₉₉ (µg/mL)	TD50 (µg/mL)	Selective index
11326059	0.004	>100	100	25000
11326127	0.006	>100	>100	>16666
11626091	0.003	14.7	8.10	2700
11626092	0.003	25.1	8.90	2967
11626093	0.001	>100	>100	>100000
11626094	0.01	>100	100.00	10000
11626095	0.02	75	7.80	390
PBTZ169	0.0002	>100	44.00	220000
Rifampicin	0.0008	0.0008	100.00	125000

Table 3: Water solubility of selected sPBTZ derivatives measured by shake flask method compared to solubility calculated on SwissAdme ((26))

Compound Name	Solubility measured in water (µg/mL)	Solubility calculated in water (µg/ml)	clogP
11326059	<0.01	0.12	2.6
11326127	<0.01	0.26	3.28
11626091	8.6 ± 3.8	4.69	1.91
11626092	10.7 ± 4.6	7.2	2
11626093	0.105 ± 0.05	0.93	2.69
11626094	0.088 ± 0.04	0.18	3.1
11626095	10.6 ± 1.8	16.9	1.36
PBTZ169	31.1 ± 6.4	0.0795	4.31

Table 4: Metabolic stability of sPBTZ derivatives measured in mouse and human microsomes

Compound Name	Cl_{int} mouse microsome (μl/min/mg protein)	Cl_{int} human microsome (μl/min/mg protein)	References
11326059	18.6	16.8	This study
11326127	19	21.5	This study
11626091	2.7	9.7	This study
11626092	3	1.4	This study
11626093	42	6.4	This study
11626094	24	277	This study
11626095	0.9	1.0	This study
Carbamazepine	0.6	0.4	This study
Nifedipine	105	121.1	This study
PBTZ169	36.7	28	(5)
BTZ043	16.5	4.20	(5)

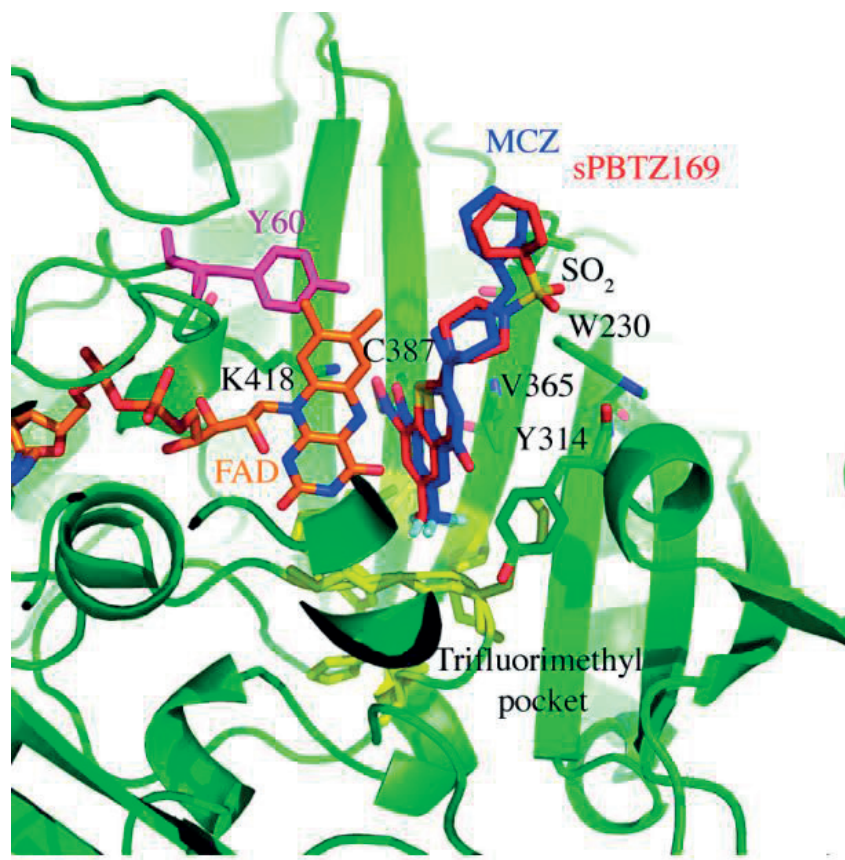


Figure 1: Structural comparison between the crystal structure of DprE1 in complex with sulfonyl derivative sPBTZ169 (11326127) and the structure in complex with MCZ (PDB code : 4NCR (5)). DprE1 is represented in green in the cartoon. sPBTZ169 (in red) sits in the trifluoromethyl hydrophobic pocket (in yellow) and binds covalently to C387. It is maintained by FAD (orange) and some lateral chains represented in sticks. Y60, a key residue in the binding of 2-Carboxyquinoxalines, is represented in pink.

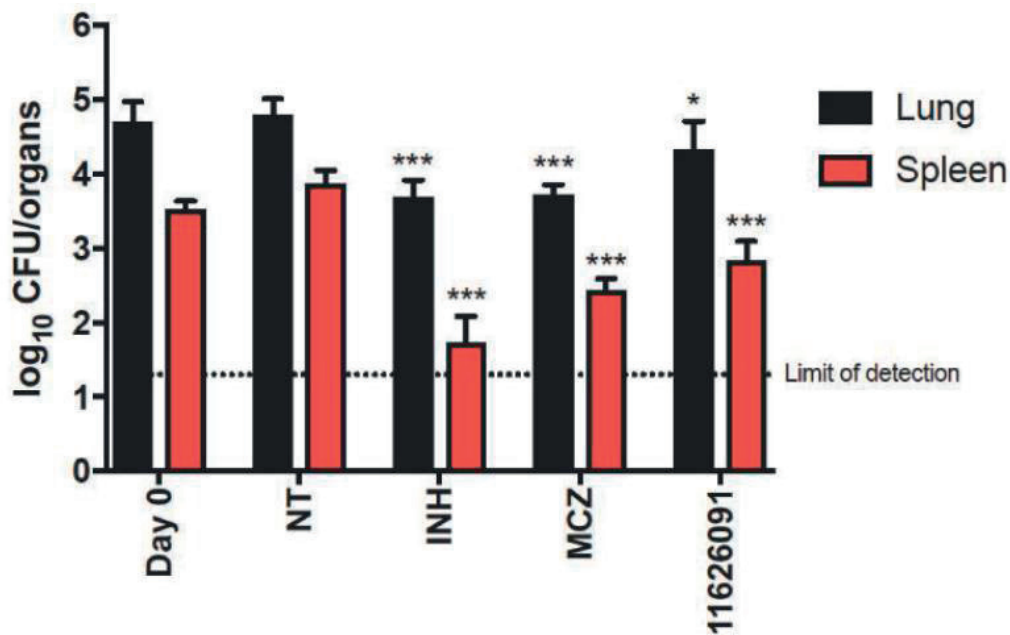
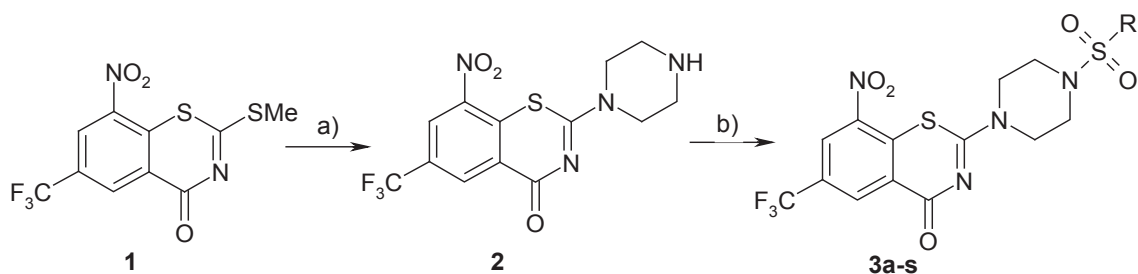
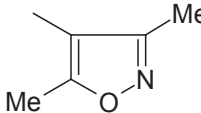
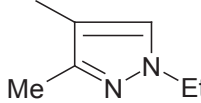
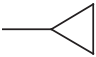
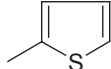
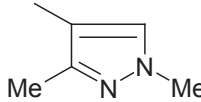
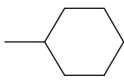
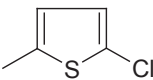
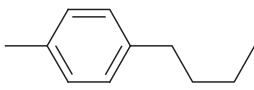
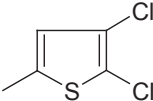
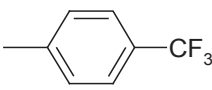
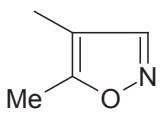
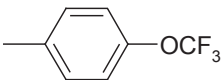
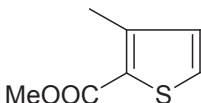
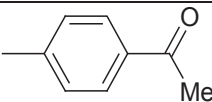
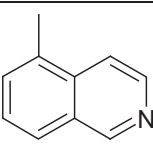
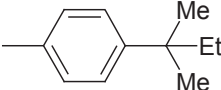


Figure 2: Activity of the sPBTZ derivative 11626091 (50 mg/kg) compared to *in vivo* activity of INH (10 mg/kg) or MCZ (25 mg/kg) in the mouse model of chronic TB. Black columns correspond to the bacterial burden in lungs and red columns correspond to the bacterial burden in the spleens, at day 0 (D0) when treatment was initiated, or day 28 (NT) when treatment ended. Bars represent the mean \pm s.d. of CFUs from 5 mice per group. NT: untreated control. Limit of detection: 20 CFU/organ. The significance of difference was calculated using the Student t-test. * $P < 0.05$. ** $P < 0.005$. *** $P < 0.0001$ compared to NT.

SUPPLEMENTAL MATERIAL

Synthetic route for 2-[4-(R-sulfonyl)piperazin-1-yl]-8-nitro-6-(trifluoromethyl)-4*H*-1,3-benzothiazin-4-one derivatives



3	R	3	R
a	Me	k	
b	Et	l	
c		m	
d	n-butyl	n	
e		o	
f		p	
g		q	
h		r	
i		s	
j			

General Procedure for the synthesis of 2-[4-(R-sulfonyl)piperazin-1-yl]-8-nitro-6-(trifluoromethyl)-4*H*-1,3-benzothiazin-4-one derivatives.

Step a). At 20 °C, finely ground solid 2-(methylthio)-8-nitro-6-(trifluoromethyl)-4*H*-1,3-benzothiazin-4-one (25 mmol) (Makarov, EMBO Mol Med, 2014) was added in one portion under intensive mixing to solution of piperazine hexahydrate (125 mmol) in 15 ml of ethanol. After 5 min reaction mixture was diluted by water, yellow solid was filtered off and recrystallised from ethyl acetate twice. The yield of 8-nitro-2-piperazin-1-yl-6-(trifluoromethyl)-4*H*-1,3-benzothiazin-4-one is 74%, mp 151-5 °C. Mass (EI), m/z ($I_{\text{relat.}}$ (%)): 359.3126 $[M]^+$ (45). $C_{11}H_{13}F_3N_4O_3S$. 1H NMR (DMSO- d_6): 3.16 (4H, br s, $N(CH_2)_2$), 3.98 (4H, br s, $N(CH_2)_2$), 8.73 (1H, s, CH), 8.87 (1H, s, CH) ppm.

Step b). Solution of 8-nitro-2-piperazin-1-yl-6-(trifluoromethyl)-4*H*-1,3-benzothiazin-4-one (10 mmol) in 5 mL of pyridine was treated by corresponding sulfonyl chloride (10 mmol) at 20 °C. After 1 hour the reaction mixture was diluted by water and acidified by concentrated hydrochloride solution in water till pH 1. Formed solid of 2-[4-(R-sulfonyl)piperazin-1-yl]-8-nitro-6-(trifluoromethyl)-4*H*-1,3-benzothiazin-4-one was filtered off and washed by water.

2-[4-(Methylsulfonyl)piperazin-1-yl]-8-nitro-6-(trifluoromethyl)-4*H*-1,3-benzothiazin-4-one **3a** (11626095) Yield 61%. Mp. 186-8 °C (EtOH). Mass (EI), m/z ($I_{\text{relat.}}$ (%)): 437.4042 $[M]^+$ (49). $C_{14}H_{13}F_3N_4O_5S_2$. 1H NMR (DMSO- d_6): 2.93 (3H, s, CH_3), 3.24 (4H, br s, $N(CH_2)_2$), 4.05 (4H, br s, $N(CH_2)_2$), 8.76 (1H, s, CH), 8.88 (1H, s, CH) ppm.

2-[4-(Ethylsulfonyl)piperazin-1-yl]-8-nitro-6-(trifluoromethyl)-4*H*-1,3-benzothiazin-4-one **3b** (11626092) Yield 74%. Mp. 204-7 °C (EtOH). Mass (EI), m/z ($I_{\text{relat.}}$ (%)): 451.4208 $[M]^+$ (86). $C_{15}H_{15}F_3N_4O_5S_2$. 1H NMR (DMSO- d_6): 1.34 (3H, t, $J = 7.4$ Hz, CH_3), 2.75 (2H, q, $J = 7.4$ Hz, CH_2), 3.26 (4H, br s, $N(CH_2)_2$), 4.06 (4H, br s, $N(CH_2)_2$), 8.77 (1H, s, CH), 8.85 (1H, s, CH) ppm.

2-[4-(Cyclopropylsulfonyl)piperazin-1-yl]-8-nitro-6-(trifluoromethyl)-4*H*-1,3-benzothiazin-4-one **3c** (11626091) Yield 57%. Mp. 201-4 °C (EtOH). Mass (EI), m/z ($I_{\text{relat.}}$ (%)): 463.4415 $[M]^+$ (52). $C_{16}H_{15}F_3N_4O_5S_2$. 1H NMR (DMSO- d_6): 1.48 (4H, m, CH_2CH_2), 3.26 (4H, br s, $N(CH_2)_2$), 3.81 (1H, m, CH), 4.09 (4H, br s, $N(CH_2)_2$), 8.73 (1H, s, CH), 8.86 (1H, s, CH) ppm.

2-[4-(*n*-butylsulfonyl)piperazin-1-yl]-8-nitro-6-(trifluoromethyl)-4*H*-1,3-benzothiazin-4-one **3d** (11626093) Yield 64%. Mp. 215-9 °C (H_2O /EtOH). Mass (EI), m/z ($I_{\text{relat.}}$ (%)): 479.4839 $[M]^+$ (89). $C_{17}H_{19}F_3N_4O_5S_2$. 1H NMR (DMSO- d_6): 0.85 (3H,

t, $J = 7.2$ Hz, CH₃), 1.23 (2H, m, CH₂), 1.66 (2H, m, CH₂), 2.64 (2H, t, $J = 7.2$ Hz, CH₂), 3.21 (4H, br s, N(CH₂)₂), 4.06 (4H, br s, N(CH₂)₂), 8.75 (1H, s, CH), 8.84 (1H, s, CH) ppm.

2-[4-(Cyclohexylsulfonyl)piperazin-1-yl]-8-nitro-6-(trifluoromethyl)-4H-1,3-benzothiazin-4-one **3e** (11326127) Yield 47%. Mp. 283-5 °C (EtOH). Mass (EI), m/z ($I_{\text{relat.}}(\%)$): 463.4415 [M]⁺ (72). C₁₉H₂₁F₃N₄O₅S₂. ¹H NMR (DMSO-*d*₆): 1.52 (6H, m, (CH₂)₃), 2.42 (4H, m, 2CH₂), 2.64 (2H, t, $J = 7.2$ Hz, CH₂), 3.21 (4H, br s, N(CH₂)₂), 4.06 (4H, br s, N(CH₂)₂), 8.75 (1H, s, CH), 8.84 (1H, s, CH) ppm.

2-{4-[(4-butylphenyl)sulfonyl]piperazin-1-yl}-8-nitro-6-(trifluoromethyl)-4H-1,3-benzothiazin-4-one **3f** (11326124) Yield 37%. Mp. 226-9 °C (EtOH). Mass (EI), m/z ($I_{\text{relat.}}(\%)$): 555.5799 [M]⁺ (69). C₂₃H₂₃F₃N₄O₅S₂. ¹H NMR (DMSO-*d*₆): 0.88 (3H, t, $J = 7.2$ Hz, CH₃), 1.23 (2H, m, CH₂), 1.66 (2H, m, CH₂), 2.66 (2H, m, CH₂), 3.21 (4H, br s, N(CH₂)₂), 4.06 (4H, br s, N(CH₂)₂), 7.03 (2H, d, $J = 8.7$ Hz, 2CH), 7.66 (2H, d, $J = 8.7$ Hz, 2CH), 8.77 (1H, s, CH), 8.86 (1H, s, CH) ppm.

2-{4-[(4-trifluoromethylphenyl)sulfonyl]piperazin-1-yl}-8-nitro-6-(trifluoromethyl)-4H-1,3-benzothiazin-4-one **3g** (11326123) Yield 46%. Mp. 222-5 °C (EtOH). Mass (EI), m/z ($I_{\text{relat.}}(\%)$): 567.4715 [M]⁺ (50). C₂₀H₁₄F₆N₄O₅S₂. ¹H NMR (DMSO-*d*₆): 3.22 (4H, br s, N(CH₂)₂), 4.05 (4H, br s, N(CH₂)₂), 7.82 (2H, d, $J = 6.3$ Hz, 2CH), 8.04 (2H, d, $J = 6.3$ Hz, 2CH), 8.72 (1H, s, CH), 8.88 (1H, s, CH) ppm.

2-{4-[(4-trifluoromethoxyphenyl)sulfonyl]piperazin-1-yl}-8-nitro-6-(trifluoromethyl)-4H-1,3-benzothiazin-4-one **3h** (11326120) Yield 52%. Mp. 207-9 °C (EtOH). Mass (EI), m/z ($I_{\text{relat.}}(\%)$): 583.4709 [M]⁺ (36). C₂₀H₁₄F₆N₄O₇S₂. ¹H NMR (DMSO-*d*₆): 3.20 (4H, br s, N(CH₂)₂), 4.01 (4H, br s, N(CH₂)₂), 7.62 (2H, d, $J = 6.3$ Hz, 2CH), 7.90 (2H, d, $J = 6.3$ Hz, 2CH), 8.71 (1H, s, CH), 8.83 (1H, s, CH) ppm.

2-{4-[(4-acetylphenyl)sulfonyl]piperazin-1-yl}-8-nitro-6-(trifluoromethyl)-4H-1,3-benzothiazin-4-one **3i** (11326119) Yield 64%. Mp. 280-2 °C (CH₃CN). Mass (EI), m/z ($I_{\text{relat.}}(\%)$): 541.5102 [M]⁺ (59). C₂₁H₁₇F₃N₄O₆S₂. ¹H NMR (DMSO-*d*₆): 2.48 (3H, s, CH₃), 3.26 (4H, br s, N(CH₂)₂), 4.03 (4H, br s, N(CH₂)₂), 7.97 (4H, m, 4CH), 8.71 (1H, s, CH), 8.83 (1H, s, CH) ppm.

2-(4-{4-[(1,1-dimethylpropyl)phenyl]sulfonyl}piperazin-1-yl)-8-nitro-6-(trifluoromethyl)-4H-1,3-benzothiazin-4-one **3j** (11326125) Yield 37%. Mp. 231-3 °C (EtOH). Mass (EI), m/z ($I_{\text{relat.}}(\%)$): 569.6065 [M]⁺ (33). C₂₄H₂₅F₃N₄O₆S₂. ¹H NMR (DMSO-*d*₆): 0.76 (3H, t, $J = 7.2$ Hz, CH₃), 1.31 (6H, s, 2CH₃), 1.69 (2H, m, CH₂), 3.23

(4H, br s, N(CH₂)₂), 4.06 (4H, br s, N(CH₂)₂), 7.33 (2H, d, *J* = 8.7 Hz, 2CH), 7.47 (2H, d, *J* = 8.7 Hz, 2CH), 8.73 (1H, s, CH), 8.87 (1H, s, CH) ppm.

2-{4-[(3,5-dimethylisoxazol-4-yl)sulfonyl]piperazin-1-yl}-8-nitro-6-(trifluoromethyl)-4*H*-1,3-benzothiazin-4-one **3k** (11326056) Yield 79%. Mp. 265-7 °C (EtOH/DMF). Mass (EI), *m/z* (*I*_{relat.}(%)): 518.4813 [M]⁺ (31). C₁₈H₁₆F₃N₅O₆S₂. ¹H NMR (DMSO-d₆): 2.31 (3H, s, CH₃), 2.64 (3H, s, CH₃), 3.26 (4H, br s, N(CH₂)₂), 4.05 (4H, br s, N(CH₂)₂), 8.77 (1H, s, CH), 8.85 (1H, s, CH) ppm.

2-{4-[(1-ethyl-3-methyl-1*H*-pyrazol-4-yl)sulfonyl]piperazin-1-yl}-8-nitro-6-(trifluoromethyl)-4*H*-1,3-benzothiazin-4-one **3l** (11326058) Yield 73%. Mp. 218-20 °C (EtOH). Mass (EI), *m/z* (*I*_{relat.}(%)): 531.5237 [M]⁺ (44). C₁₉H₁₉F₃N₆O₅S₂. ¹H NMR (DMSO-d₆): 1.31 (3H, t, *J* = 5.9 Hz, CH₃), 2.28 (3H, s, CH₃), 3.18 (4H, br s, N(CH₂)₂), 4.06 (4H, br s, N(CH₂)₂), 4.09 (2H, q, *J* = 6.6 Hz, CH₂), 8.27 (1H, s, CH), 8.78 (1H, s, CH), 8.86 (1H, s, CH) ppm.

8-nitro-2-[4-(2-thienylsulfonyl)piperazin-1-yl]-6-(trifluoromethyl)-4*H*-1,3-benzothiazin-4-one **3m** (11326059) Yield 80%. Mp. 210-4 °C (EtOH). Mass (EI), *m/z* (*I*_{relat.}(%)): 505.5042 [M]⁺ (67). C₁₇H₁₃F₃N₄O₅S₃. ¹H NMR (DMSO-d₆): 3.20 (4H, br s, N(CH₂)₂), 4.05 (4H, br s, N(CH₂)₂), 7.25 (1H, br s, CH), 7.68 (1H, br s, CH), 8.03 (1H, br s, CH), 8.73 (1H, s, CH), 8.83 (1H, s, CH) ppm.

2-{4-[(1,3-dimethyl-1*H*-pyrazol-4-yl)sulfonyl]piperazin-1-yl}-8-nitro-6-(trifluoromethyl)-4*H*-1,3-benzothiazin-4-one **3n** (11326061) Yield 64%. Mp. 200-3 °C (EtOH). Mass (EI), *m/z* (*I*_{relat.}(%)): 517.4966 [M]⁺ (74). C₁₈H₁₇F₃N₆O₅S₂. ¹H NMR (DMSO-d₆): 2.41 (3H, s, CH₃), 3.17 (4H, br s, N(CH₂)₂), 3.72 (3H, s, NCH₃), 4.03 (4H, br s, N(CH₂)₂), 7.63 (s, 1H, CH), 8.75 (1H, s, CH), 8.86 (1H, s, CH) ppm.

2-{4-[(5-chloro-2-thienyl)sulfonyl]piperazin-1-yl}-8-nitro-6-(trifluoromethyl)-4*H*-1,3-benzothiazin-4-one **3o** (11326121) Yield 39%. Mp. 210-3 °C (EtOH/DMF). Mass (EI), *m/z* (*I*_{relat.}(%)): 539.9492 [M]⁺ (53). C₁₇H₁₂F₃ClN₄O₅S₃. ¹H NMR (DMSO-d₆): 3.24 (4H, br s, N(CH₂)₂), 4.06 (4H, br s, N(CH₂)₂), 7.39 (1H, d, *J* = 5.1 Hz, CH), 7.58 (1H, d, *J* = 5.1 Hz, CH), 8.78 (1H, s, CH), 8.85 (1H, s, CH) ppm.

2-{4-[(4,5-dichloro-2-thienyl)sulfonyl]piperazin-1-yl}-8-nitro-6-(trifluoromethyl)-4*H*-1,3-benzothiazin-4-one **3p** (11326122) Yield 46%. Mp. 265-7 °C (EtOH/DMF). Mass (EI), *m/z* (*I*_{relat.}(%)): 574.3942 [M]⁺ (58). C₁₇H₁₁F₃Cl₂N₄O₅S₃. ¹H NMR (DMSO-d₆): 3.26 (4H, br s, N(CH₂)₂), 4.07 (4H, br s, N(CH₂)₂), 7.83 (1H, s, CH), 8.77 (1H, s, CH), 8.86 (1H, s, CH) ppm.

2-{4-[(3-methylisoxazol-4-yl)sulfonyl]piperazin-1-yl}-8-nitro-6-(trifluoromethyl)-4H-1,3-benzothiazin-4-one **3q** (11326126) Yield 86%. Mp. 281-3 °C (EtOH/DMF). Mass (EI), m/z ($I_{\text{relat.}}(\%)$): 504.4542 $[M]^+$ (61). $C_{17}H_{14}F_3N_5O_6S_2$. 1H NMR (DMSO- d_6): 2.33 (3H, s, CH_3), 3.26 (4H, br s, $N(CH_2)_2$), 4.04 (4H, br s, $N(CH_2)_2$), 7.69 (1H, s, CH), 8.75 (1H, s, CH), 8.86 (1H, s, CH) ppm.

Methyl 3-({4-[8-nitro-4-oxo-6-(trifluoromethyl)-4H-1,3-benzothiazin-2-yl]piperazin-1-yl}sulfonyl)thiophene-2-carboxylate **3r** (11326128) Yield 74%. Mp. 127-9 °C (EtOH/DMF). Mass (EI), m/z ($I_{\text{relat.}}(\%)$): 563.5412 $[M]^+$ (68). $C_{19}H_{15}F_3N_4O_7S_3$. 1H NMR (DMSO- d_6): 3.20 (4H, br s, $N(CH_2)_2$), 3.83 (3H, s, OCH_3), 4.07 (4H, br s, $N(CH_2)_2$), 6.81 (1H, d, $J = 5.3$ Hz, CH), 7.67 (1H, d, $J = 5.3$ Hz, CH), 8.70 (1H, s, CH), 8.84 (1H, s, CH) ppm.

2-[4-(isoquinolin-5-ylsulfonyl)piperazin-1-yl]-8-nitro-6-(trifluoromethyl)-4H-1,3-benzothiazin-4-one **3s** (11626094) Yield 85%. Mp. 243-5 °C (EtOH/DMF). Mass (EI), m/z ($I_{\text{relat.}}(\%)$): 550.5265 $[M]^+$ (36). $C_{22}H_{16}F_3N_5O_5S_2$. 1H NMR (DMSO- d_6): 3.24 (4H, br s, $N(CH_2)_2$), 4.06 (4H, br s, $N(CH_2)_2$), 7.80 (1H, t, $J = 7.9$ Hz, CH), 7.99 (1H, d, $J = 5.6$ Hz, CH), 8.38 (2H, m, 2CH), 8.73 (1H, s, CH), 8.85 (1H, s, CH), 8.93 (1H, d, $J = 5.6$ Hz, CH), 9.57 (1H, s, CH) ppm.

Table S1 : IC₅₀ values measured for Ty38c, PBTZ169 and sPBTZ169 (11326127) against wild-type and BTZ-resistant *M. tuberculosis* C387S DprE1

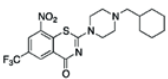
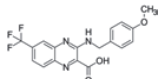
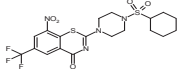
compound	structure	IC ₅₀ (μM)		References
		WT	C387S	
PBTZ169		0.3	3.6	This study
Ty38c		0.2	0.2	(1)
sPBTZ169		1.1	12	This study

Table S2. Data collection and refinement statistics

	DprE1-sPBTZ169
Beamline	SLS X06DA (PXIII)
Wavelength (Å)	1
Resolution range (Å)	49.15- 2.40 (2.48-2.40)
Space group	P 1 2 ₁ 1
Unit cell (Å, °)	78.164 84.024 81.666 90 103.983 90
Total reflections	79124 (7781)
Unique reflections	39831 (3914)
Multiplicity	2.0 (2.0)
Completeness (%)	98.81 (98.19)
Mean I/sigma(I)	16.42 (2.56)
R-merge	0.03362 (0.3709)
R-meas	0.04754 (0.5245)
CC1/2	0.999 (0.85)
CC*	1 (0.959)
R-work	0.1978
R-free	0.2248
Number of non-hydrogen atoms	6512
Ramachandran favored (%)	97.58
Ramachandran allowed (%)	2.42
Ramachandran outliers (%)	0.00
Rotamer outliers (%)	1.92
Clashscore	4.47
Average B-factor	60.34

Statistics for the highest-resolution shell are shown in parentheses.

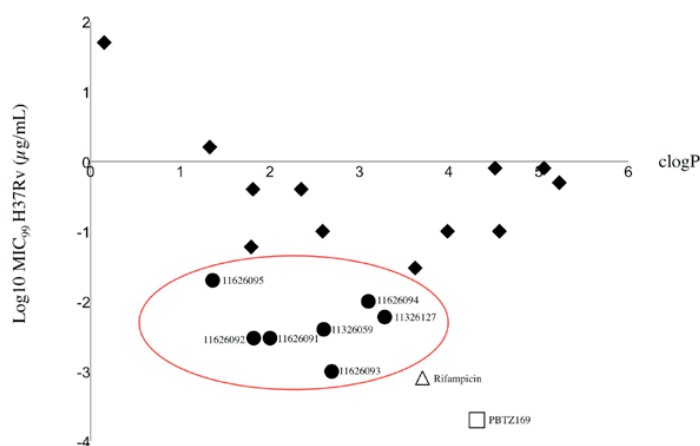


Fig S1: Antitubercular activity versus hydrophobicity. Distribution and activity of 2-sulphonylpiperazin 8-nitro 6-trifluoromethyl 1,3-benzothiazin-4-ones derivatives as a function of clogP. Surrounded in red, the 7 chosen compounds with a good activity/logP profile. Lozenges indicate other compounds not discussed in the text.

References

1. Foo CS, Lechartier B, Kolly GS, Boy-Rottger S, Neres J, Rybniker J, Lupien A, Sala C, Piton J, Cole ST. 2016. Characterization of DprE1-Mediated Benzothiazinone Resistance in *Mycobacterium tuberculosis*. *Antimicrob Agents Chemother* 60:6451-6459.

Appendix Chapter A3: An optimized background regimen for treatment of active tuberculosis with the next-generation benzothiazinone Macozinone (PBTZ169)

Andréanne Lupien¹, Anthony Vocat¹, Caroline Shi-Yan Foo, Emilyne Blattes², Jean-Yves Gillon^{2*}, Vadim Makarov³, Stewart T. Cole^{1,†}

¹Global Health Institute, Ecole Polytechnique Fédérale de Lausanne, CH-1015 Lausanne, Switzerland

²Innovative Medicines for Tuberculosis (iM4TB), Innovation Park, Building I, CH-1015 Lausanne, Switzerland

³Dept. of Stresses of Microorganisms, A.N. Bach Institute of Biochemistry, Moscow, Russian Federation

*Present address: Drugs for Neglected Diseases *initiative*, 15 Chemin Louis-Dunant, 1202 Geneva, Switzerland

Antimicrobial Agents and Chemotherapy, 2018, doi: 10.1128/AAC.00840-18

Contributions: execution of viability assays, manuscript preparation

ABSTRACT

The efficacy of the standardized four-drug regimen (comprising isoniazid, rifampicin, pyrazinamide and ethambutol) for the treatment of tuberculosis (TB) is menaced by the emergence of multidrug (MDR) and extensively drug-resistant (XDR) strains of *Mycobacterium tuberculosis*. Intensive efforts have been made to develop new antibiotics or to repurpose old drugs and several of these are currently being evaluated in clinical trials for their anti-tubercular activity. Among the new candidate drugs is macozinone (MCZ), the piperazine-containing benzothiazinone, PBTZ169, which is currently being evaluated in phase I/II clinical trials.

Here, we determined the *in vitro* and *in vivo* activity of MCZ in combination with a range of anti-TB drugs in order to design a new regimen against active TB. Two-drug combinations with MCZ were tested against *M. tuberculosis* using checkerboard and CFU enumeration after drug exposure assays. MCZ was observed to have no interactions with all first- and second-line anti-TB drugs. At the MIC of each drug, MCZ with either bedaquiline (BDQ), clofazimine (CLO), delamanid (DMD) or sutezolid (STZ) reduced the bacterial burden by two logs compared to the drugs alone, indicating synergism. MCZ also displays synergism with clomiphene (CLM), a potential inhibitor of the undecaprenyl pyrophosphate synthase (UppS) in mycobacteria. For all the other drugs tested in combination with MCZ, no synergistic activity was observed. Neither antagonism nor increased cytotoxicity were found for most combinations, suggesting that MCZ could be added to different TB regimens without any significant adverse effects.

INTRODUCTION

With more than 9 million people infected worldwide, tuberculosis (TB) is the major cause of death due to a bacterial pathogen (1). As recommended by the WHO, the mainstay regimen for drug-susceptible TB relies on a multi-drug therapy which consists of isoniazid (INH), rifampicin (RIF), pyrazinamide (PZA) and ethambutol (EMB) (1). The increasing number of multi-drug resistant TB (MDR-TB) and extensively resistant TB (XDR-TB) cases challenge the reliability of this regimen to treat active TB. MDR-TB strains are resistant to both isoniazid (INH) and rifampicin (RIF), the two most active drugs for drug-susceptible TB (DS-TB). MDR-TB treatment involves second-line injectable aminoglycosides (e.g. amikacin and capreomycin) and fluoroquinolones. In the case of XDR-TB, resistance to RIF, INH, aminoglycosides, and fluoroquinolones is observed. With more than 480 000 reported cases of MDR-TB and 9.5% of MDR-TB cases worldwide classified as XDR-TB, drugs active against new *Mycobacterium tuberculosis* pharmacological targets are indeed in need (1).

An effective regimen for the treatment of TB consists of multiple drugs that inhibit several distinct essential cellular activities in the bacterium. The effectiveness of a regimen is further enhanced if synergism is present between the constituents. Recently, studying the combinatory effect of anti-TB agents has become of interest to the TB community in order to find more efficacious treatments. Several combinations of anti-TB drugs have demonstrated potentiation of the individual drug activity *in vitro* when combined. Interestingly, drugs such as cephalosporins, which have limited activity in *M. tuberculosis* due to the presence of the BlaC β -lactamase, were shown to be synergistic with drugs of the rifamycin family, bedaquiline (BDQ) and delamanid (DMD) (2, 3). Furthermore, the β -lactamase inhibitor, clavulanate as a component of triple combinations including cephalosporins (and other beta-lactams) proved to be a key synergistic

partner due to its ability to rescue the activity of RIF against a RIF-resistant strain (2). A combination of amoxicillin/clavulanate with first-line anti-TB drugs has also been explored and showed potent synergism against MDR isolates (4). Repurposing drugs such as spectinomycin was also studied to test the concept that clinically available antibiotics with limited efficacy against *M. tuberculosis* might be used for TB treatment when co-administered with macrolides and azoles (5). The combinatory effect of new drugs has also been assessed, whereby MmpL3 inhibitors act synergistically with RIF, BDQ, clofazimine (CLO), and β -lactams (6). Altogether, these studies demonstrate the potential of anti-TB drugs to act synergistically and the possibility to optimize treatment regimens against DS-TB, MDR-TB, and XDR-TB or even to develop a pan-TB regimen (7).

A potential component of such regimens is the clinical candidate macozinone (MCZ) previously known as PBTZ169 (<https://www.newtbdrugs.org/>). MCZ is a bactericidal benzothiazinone that inhibits the essential flavoprotein DprE1 by forming a covalent bond with the active site Cys387 residue (8) thus preventing synthesis of decaprenyl phosphoryl ribose. Despite its lack of activity against non-replicating bacteria, MCZ is highly potent against *M. tuberculosis* *in vitro* (9), *ex vivo* and *in vivo*, where, alone, it significantly reduces the bacterial burden in the lungs and spleens of chronically infected mice (10). A new regimen including MCZ, BDQ, and PZA was found to be more efficacious than the standard three-drug treatment in a murine model of chronic disease (10). MCZ was also shown to act synergistically with BDQ and CLO (10, 11). BDQ is an inhibitor of the F1/F0 ATP synthase and CLO is thought to be reduced by the mycobacterial type 2 NADH:quinone oxidoreductase, NDH-2, leading to a CLO-mediated increase in NADH oxidation and production of reactive oxygen species (ROS) (12, 13). Other studies have

also reported that CLO may act on the lipids of the bacterial cell wall, as observed in macrophages infected with *M. leprae* (14). However, the mechanism of action of this drug is far from understood.

As part of a new regimen, further studies are needed to evaluate the potential activity of MCZ when combined with other anti-TB agents. Although several new or repurposed drugs have been evaluated for their potential to be used with MCZ in combination against active TB, there has been no comprehensive work performed to optimize MCZ-containing regimens. In this study, we embarked on a thorough characterization and evaluation of the potential activity of MCZ in combination with other TB drugs using a combination of checkerboard and CFU enumeration after drug exposure assays.

RESULTS

Activity of MCZ when combined with first- and second-line anti-TB drugs against strain H37Rv.

The MIC of all compounds used in this study against the H37Rv strain of *M. tuberculosis* is shown in Table 1 and was determined by a resazurin-based microtiter assay (REMA) (15). All drugs tested are active against the bacterium under these conditions except PZA. The activity of MCZ was then determined in combination with the first-line drugs RIF, INH and EMB using checkerboard assay. At concentrations ranging from 0.5X MIC to 0.0625X MIC, the combination of MCZ with first-line drugs resulted in minimal fractional inhibitory index (FICI_m) and maximal fractional inhibitory index (FICI_M) values ranging from 0.75 to 2.0, respectively (Table 2). MCZ was also tested in combination with the second-line injectable agent amikacin (AMK), the fluoroquinolones, levofloxacin (LVX) and moxifloxacin (MFX), the bacteriostatic agents, D-cycloserine (DCS), ethionamide (ETO), and *para*-aminosalicylic acid (PAS). For all combinations, FICI_m and FICI_M range from 1.125 to 3, respectively (Table 2). Taken together, these results show that MCZ has neither synergistic nor antagonistic interactions with the first- and second-line anti-TB drugs.

Activity of MCZ with repurposed or new anti-TB drugs.

In cases of MDR-and XDR-TB disease, the use of new anti-TB drugs or repurposed drugs is required (16). Several repurposed drugs, including the anti-leprosy agent CLO, the macrolide clarithromycin (CLR), the carbapenem meropenem (MEM) and the oxazolidinone linezolid (LZD) are now in trials for the treatment of MDR-TB (17–20). In addition, new anti-TB compounds are available. These drugs include the diarylquinoline BDQ, the dihydro-nitroimidazole DMD, the

oxazolidinone STZ and the QcrB inhibitor lansoprazole sulfide LPZs. CLR, DMD, LPZs, LZD, MEM, and STZ are not synergistic when individually combined with MCZ, with $FICI_m$ and $FICI_M$ ranging between 1.033 and 2.5 (Table 3). As previously reported, benzothiazinones have a synergistic effect when combined with CLO and BDQ (10, 11). In the checkerboard assay, synergism was observed at concentrations close to the MIC *in vitro* (0.25X MIC and above) suggesting that MCZ synergism with CLO and BDQ is dependent on the concentration of MCZ. Interestingly, both BDQ and CLO were reported to act on *M. tuberculosis* by disrupting the proton motive force of the mycobacterial membrane (21). To assess the activity of MCZ with other uncouplers, we tested pairwise combinations of clomiphene (CLM) and tamoxifen (TMX), using the H37Rv-lux strain for TMX, due to a high fluorescence background at concentrations higher than the MIC when TMX susceptibility was determined by REMA (data not shown) (21). SQ109, although reported to act as an uncoupler, was not included in the study as its activity was previously shown to be indifferent in the presence of benzothiazinones (10, 21, 22). CLM and TMX alone are both active against H37Rv with a MIC of 24.8 μ g/mL and 14.22 μ g/mL respectively (Table 1). Synergism was observed when MCZ was combined *in vitro* with CLM (Table 3) whereas no combinatory effect was found with TMX (Table 3).

CFU enumeration after drug exposure.

MCZ is a bactericidal drug that inhibits the DprE1 enzyme (10, 23). To assess the cidal activity of MCZ in two-drug combinations *in vitro*, CFU enumeration was performed on H37Rv in the presence of BDQ, CLO, MFX, DMD and STZ (Fig. 1B and Table S1). First, the activity of the drugs was assessed at 2X MIC, 1X MIC, 0.5X MIC and 0.25X MIC of each compound. The activity of INH and RIF was also determined at 1X MIC and 0.25X MIC, as controls (Fig. 1A). RIF and

INH decreased significantly the bacterial burden, by 2.2 log₁₀ CFU/mL and below the detection limit, respectively (Fig. 1A), when compared to the non-treated control at D7. MCZ, BDQ, CLO, DMD, and MFX showed dose-dependent bactericidal activity (Fig. 1B). No dose-dependency was observed when H37Rv was exposed to STZ (Fig. 1B). At the MIC of each drug, the combination of MCZ with BDQ, CLO, MOX, DMD, and STZ significantly decreased the number of CFU compared to each drug alone (Fig. 1C). In combination, MCZ significantly increased the bactericidal activity reducing the number of CFU below that seen before treatment (D0, Fig. 1C). In the absence of MCZ, only the combination of CLO and BDQ had this effect (data not shown). At 0.25X MIC of each drug, a significant decrease in the bacterial viability was only observed when MCZ was combined with CLO (Fig. 1C). Also, a decrease of 1.08 log₁₀ CFU/mL was observed when MCZ was combined with BDQ at 0.25X MIC of each drug (Fig. 1C). This result suggests that despite the lack of synergism at 0.25X MIC, MCZ and BDQ can potentiate their bactericidal action *in vitro*. Interestingly, these results imply that at optimal concentrations of each drug, either combination of MCZ with BDQ, CLO, DEL, MFX or with STZ can increase the bactericidal activity *in vitro* compared to the drugs used alone.

Cytotoxicity of potent synergistic combinations containing MCZ.

Cytotoxicity of the synergistic combinations was determined against HepG2 cells. All drugs alone, except CLO, had TD50 and TD99 higher than 20 µg/mL (Table 4). The toxicity of two-drug combinations was similar to that of the more toxic drug in the combination except for MCZ-DMD and DMD-STZ (Table 4). The TD50 and TD99 of the MCZ-DMD combination were 7.7-fold and 7.8-fold higher than MCZ and DMD alone, respectively. In the case of DMD-STZ,

the combination was 2.1-fold more toxic than STZ alone. Interestingly, the three-drug combination MCZ-BDQ-DMD has similar toxicity to that of the MCZ-DMD combination.

***In vivo* activity of MCZ in combination with DMD and STZ.**

Despite the lack of synergism in the checkerboard assay (Table 3), both MCZ-DMD and MCZ-STZ combinations were able to decrease bacterial viability *in vitro* by more than 2 log₁₀ CFU when added at a concentration equal to the MIC of each drug (Fig. 1C). Thus, the *in vivo* activity of these two drugs was evaluated in a TB mouse model (Fig. 2). At the concentrations tested, all drugs alone and in combinations significantly decreased the bacterial burden, by more than 2.18 log₁₀ in the lungs and 1.71 log₁₀ in the spleens, as compared to the D0 level, thus indicating a bactericidal effect. Although no combinatory effect was observed in these organs when MCZ, DMD, and STZ were combined in two-drug combinations, the triple combination, MCZ-DMD-STZ, was more active in the lungs of *M. tuberculosis*-infected mice than DMD-STZ (the most active of the two-drug combinations) with cidal activity of more than 0.69 log₁₀ CFU (*p*-value = 0.014 (*)). Moreover, MCZ-DMD-STZ was also more active than the mainstay regimen (RIF-INH-PZA-RHZ) in this model, reducing the burden by 1.17 log₁₀ CFU compared to RHZ (*p*-value = 0.004 (**)). In the spleen, the most active two-drug combination was MCZ-DMD although no significant decrease ($\leq 0.5\log_{10}$ CFU) in the bacterial burden could be observed in the case of the triple combination of MCZ-DMD-STZ. These results suggest that in spite of the lack of synergism observed between MCZ, DMD, and STZ in this model, under the conditions tested, the MCZ-DMD-STZ combination is efficacious in treating TB infection in the mouse, comparable to the mainstay regimen of RHZ.

DISCUSSION

In this study, we determined the combinatory effects of MCZ with not only first- and second-line TB drugs, but also with new and repurposed drugs with anti-tubercular activity. Synergism is indeed of interest for the optimization of a multi-drug regimen, as the activity of the drugs would be potentiated by the presence of another compound. More importantly, antagonistic interactions between drugs should be avoided, so as not to impair the activity of the regimen. We demonstrated that MCZ has no antagonistic effects with the first-line anti-TB drugs RIF, INH and EMB (Table 2) as well as the second-line drugs (Table 2). This is consistent with previously published results obtained *in vitro* with combinations containing BTZ043, the lead compound from the benzothiazinone chemical class (23). MCZ was previously shown to be synergistic with BDQ and CLO *in vitro* and *in vivo* (10, 11). In this study, we observed similar synergism between MCZ, BDQ, and CLO in the checkerboard assay and enhanced bactericidal activity of MCZ in the CFU enumeration after drug exposure assay *in vitro* (Table 3 and Fig. 1).

Interestingly, MCZ is also synergistic with CLM in the *in vitro* checkerboard assay. CLM is a nonsteroidal, ovulatory stimulant that acts as a selective estrogen receptor modulator (24). Little is known about the mechanism of action of CLM in *M. tuberculosis*. However, a previous study in *Staphylococcus aureus* showed that CLM targets the undecaprenyl diphosphate synthase (UppS), an enzyme, which catalyzes the condensation of isopentenyl diphosphate with allylic pyrophosphates (25) and acts in the same pathway as DprE1 in actinobacteria. In *Corynebacterium glutamicum*, overexpression of UppS was able to rescue the wild-type strain and induce BTZ043 resistance by providing sufficient decaprenyl phosphate for cell wall biosynthesis. The 2.15 Å crystal structure (PDB: 5CQJ) of *Escherichia coli* UppS in the presence of CLM has already been determined (25). Despite the low identity between the *M. tuberculosis* and *E. coli* UppS sequences

(39.02%), 10 of the 16 amino acids reported to interact with CLM are conserved (M25, N28, H43, G46, V50, A69, L93, L100, L107 and L139 according to *E. coli* numbering), suggesting that in *M. tuberculosis* CLM is also an inhibitor of UppS (Fig. S2). CLM may thus be used as a booster of MCZ activity by further inhibiting the decaprenyl phosphate pathway of actinobacteria.

CLM, BDQ and CLO have all been reported to act as protonophore uncouplers which disrupt mycobacterial membrane potential (21). BDQ and CLO similarly demonstrated synergism with MCZ, as with CLM, in our study, although no synergism was observed with other uncouplers such as SQ109 and TMX (Table 3; (10)). SQ109 was reported to dissipate the transmembrane proton concentration gradient (ΔpH), membrane potential ($\Delta\psi$), or both components of the proton motive force simultaneously, mainly due to its inhibitory effect on MmpL3 and other MmpL-driven processes (22). Little is known about the mechanism of action of TMX against *M. tuberculosis*. It was previously hypothesized that TMX may cause a loss of transmembrane potential and ultimately cell death by a significant efflux of K^+ and Na^+ ions from bacterial cells (26) and this may also occur in *M. tuberculosis*. Interestingly, BDQ and CLO, which synergize with MCZ, act on components of the electron-transport chain (ETC) in the bacterial membrane. BDQ is an inhibitor of the F_1/F_0 ATP synthase and CLO is thought to be reduced by the mycobacterial type 2 NADH:quinone oxidoreductase, NDH-2 enzyme, leading to a CLO-mediated increase in NADH oxidation and reactive oxygen species (ROS) production (12, 13). Other studies have also reported that CLO may act on the lipids of the bacterial cell wall, as observed in macrophages infected with *M. leprae* (14). On the other hand, there are compounds targeting the ETC such as LPZs, which are not synergistic when combined with MCZ *in vitro* (Table 3). LPZs targets the QcrB component of the cytochrome *bc₁* oxidase, loss of which is thought to be compensated for by the other terminal

oxidase in *M. tuberculosis*, cytochrome *bd* (27). Further studies will be needed to fully understand the mechanism underlying the two-drug synergism of MCZ with BDQ, CLO, and CLM.

As observed from the CFU enumeration after drug exposure assay at certain optimal concentrations, the bactericidal activity of MCZ is enhanced by BDQ, CLO, DMD, MFX, and STZ (Fig. 1). In addition, BDQ and CLO potentiate their activity. Interestingly, all drugs tested were reported to have bactericidal activity against *M. tuberculosis* *in vitro* or *in vivo* (28–32). Background regimens with MCZ and BDQ, CLO, DMD, MFX, or STZ would thus be promising alternatives to decrease the bacterial burden *in vivo*. In this study, MCZ in combination with DMD and STZ was assessed in a murine infection model. Despite the lack of synergism between the drugs *in vivo*, this regimen was able to decrease the bacterial burden in the lungs and spleens of infected mice over one month of treatment to a level lower than that of RHZ (Fig. 2). DMD and STZ are suitable candidates for the treatment of TB as they have low toxicity in preclinical species and are well-tolerated in humans (28, 33). However, further studies on their potential cytotoxicity when combined with MCZ should be performed before use in humans, as increased HepG2 cytotoxicity was observed with this combination (Table 4).

In conclusion, MCZ enhances the activity of several potential partner drugs *in vitro* and *in vivo*. According to the results obtained in this study, BDQ, CLO, DMD and STZ are indeed good candidates to elaborate a new MCZ-containing regimen active against all forms of TB. Moreover, boosting MCZ activity by the addition of CLM is also of interest but further studies will be needed to determine the efficacy of this specific combination *in vivo*.

MATERIALS AND METHODS

Strain and culture methods.

M. tuberculosis H37Rv (Institut Pasteur) was used for the in vitro assessment of drug activity against replicating H37Rv (9). Bacteria were cultured in 7H9 complete (Middlebrook 7H9 [Difco] broth supplemented with 10% albumin-dextrose-catalase (ADC) enrichment, 0.2% glycerol, 0.05% Tween 80) at 37°C when needed.

Drug preparation.

Amikacin (AMK, Sigma), bedaquiline (BDQ, Janssen Pharmaceutica NV), clofazimine (CLO, Sigma), clomiphene (CLM, Sigma), clarithromycin (CLR, Sigma), D-cycloserine (DCS, Sigma), delamanid (DMD, Otsuka Co.), ethambutol (EMB, Sigma), ethionamide (ETO, Sigma), isoniazid (INH, Sigma), levofloxacin (LVX, Sigma), linezolid (LZD, AstraZeneca), lansoprazol sulfide (LPZs, Toronto Research Chemicals), meropenem (MEM, Sigma), moxifloxacin (MFX, Sigma), *para*-aminosalicylic acid (PAS, Sigma), MCZ HCl salt (called MCZ throughout, was obtained from iM4TB), pyrazinamide (PZA, Fluka), rifampicin (RIF, Sigma), sutezolid (STZ, Sequella) and tamoxifen (TMX, Sigma) were dissolved in DMSO to obtain stock concentrations of 10 mg/mL. Aliquots were stored at -20°C. When needed, the drugs were diluted in DMSO to the desired concentration. Stocks were thawed a maximum of 5 times to avoid potential loss of drug potency.

Antimycobacterial assays.

Drugs were tested against *M. tuberculosis* H37Rv strain using the resazurin microtiter assay (REMA) in 96-well plates as previously described (15). Briefly, a mid-logarithmic phase culture of H37Rv (OD_{600nm} approx. 0.5) was diluted in 7H9 complete medium to an OD_{600nm} of 0.0001 (approximately 3X10⁴ CFU/mL). Bacteria (100 µL) were then dispensed in transparent flat-bottom 96 well plates. Two-fold serial dilutions of each drug (resuspended in DMSO) were then prepared. On each plate, controls without drug and media alone were included. Plates were incubated for six days at 37°C before addition of resazurin (0.025% [wt/vol] to 1/10 of the well volume). After overnight incubation, the fluorescence of the resazurin metabolite, resorufin, was determined with excitation at 560 nm and emission at 590 nm, measured using a TECAN Infinite M200 microplate reader. The MIC was calculated using GraphPad Prism software (version 7) and the Gompertz equation for MIC determination. All drugs were tested at least in duplicate.

Checkerboard assay.

To assess if compounds in two-drug combinations acted synergistically, antagonistically, or indifferently, a checkerboard assay was employed using REMA. The assay was performed in 96 well plates as sketched in Fig. S1. Fractional inhibitory concentrations (FICs) were calculated using the following formula:

$$\text{FIC (X + Y)} = [\text{MIC of compound X in combination with compound Y}] / [\text{MIC of X alone}].$$

The fractional inhibitory index (FICI) was calculated as FICI of compound X + FICI of compound Y to evaluate interaction profiles. FICI values ≤ 0.5 are indicative of synergistic activity, ΣFICI values ≥ 4.0 are indicative of antagonism. The MIC in this assay is defined by the lowest

concentration that inhibits at least 90% of the bacterial growth (MIC_{90}). Values in between correspond to additivity (indifferent). $FICI_m$ and $FICI_M$ were also determined and reported as the lowest FICI ($FICI_m$) and the highest FICI ($FICI_M$) observed out of all assays performed. Also, the mean FICI was calculated for all drug combinations between the 0.5X MIC and 0.0625X MIC. In the table, $\Sigma FICI$ represents the mean $\Sigma FICI$ of all FICI obtained between the 0.5X MIC and 0.0625X MIC of MCZ HCl. The experiments were performed in biological duplicates.

When mentioned, the interaction between MCZ and drugs was also assessed using the luminescent H37Rv-pEG200 strain, as previously described (34). A mid-logarithmic phase culture of H37Rv-PEG200 (OD_{600nm} approx. 0.5) was diluted in 7H9 complete to an OD_{600nm} of 0.001 (approximately 3×10^5 CFU/mL). Luminescence was measured by using a TECAN Infinite M200 microplate reader after 6 days incubation at 37°C. The MIC was calculated using GraphPad Prism software (version 7) and the Gompertz equation for MIC determination. All combinations were tested at least in duplicate.

CFU enumeration after drug exposure *in vitro*.

To assess the activity of anti-TB drugs on bacterial viability, H37Rv was diluted to an OD_{600nm} of 0.0001 and exposed to the drugs using the same protocol as for REMA. After seven days incubation, 50 μ L of bacteria were 10-fold serially-diluted in PBS containing 0.05% Tween80 and plated on 7H10 agar plates containing 10% OADC (Gibco). CFUs were counted after four weeks incubation at 37°C. D0 (the day the bacteria were exposed to the drugs) and D7 (after seven days incubation with the drugs) were also plated as a control to determine the bacterial growth. For each experiment, a REMA assay was performed in addition to determine the MIC of the drugs tested. Significant results for drugs tested alone were reported as a decrease of at least 2 \log_{10}

CFU/mL compared to the mean CFU/mL of the non-treated control (NT) at D7. For combinations, significant effects were reported as a decrease of at least 2 log₁₀ CFU/mL compared to the mean CFU/mL of drugs tested alone.

Cytotoxicity assay.

Drugs were tested individually in duplicate for their cytotoxicity against human hepatic HepG2 cells (ATCC® HB-8065™) by REMA (10). Drugs were prepared in DMSO to a final concentration of 100 µg/mL and were then added to 96-well plates containing 4.0 X10⁴ cells/well in a final volume of 100 µL. The drugs were then serially diluted two-fold. The plates were incubated for three days at 37°C and fluorescence, after addition of resazurin, was determined using a TECAN M200 microplate reader. Cytotoxic effect was expressed as TD50 and TD99, which correspond to the toxic doses inhibiting growth of 50% and 99% of the HepG2 cells, respectively.

To assess the potential cytotoxic effect of two-drug regimens combining MCZ with another drug in HepG2 cells, a mixture of MCZ (final concentration in the plate: 50 µg/mL) and each of the other drugs (final concentration 50 µg/mL) was added to the plates containing HepG2 cells. The mixture was then two-fold serially diluted and incubated three days at 37°C before resazurin was added to the plates.

***In vivo* assessment of MCZ in combination with DMD and STZ.**

Female BALB/c mice (5-6 week-old) were obtained from Charles River Laboratories. Mice were subjected to a low-dose aerosol infection of *M. tuberculosis* H37Rv. Treatment began 4 weeks

after infection and compounds were administered by gavage 5 days a week for 4 weeks to infected mice, so as to determine the *in vivo* efficacy of single drugs and combinations.

DMD and STZ activity were first assessed in combination with MCZ at the following doses (mg/kg): STZ: 100; MCZ 25; DMD 5; PZA, 150; RIF, 10; INH, 25. In this experiment, 5% Arabic gum in distilled water was used as the vehicle. At the end of the experiment, all mice were sacrificed and the bacterial load in the lungs and spleen was determined by plating dilutions of organ homogenates on 7H10 agar plates containing 10% OADC, cycloheximide (10 µg/ml), and ampicillin (50 µg/ml). Plates were incubated for 4 weeks at 37°C before CFU were enumerated. CFU counts were log₁₀ transformed before analysis as mean log₁₀ CFU ± s.d., and compared using Student's t-tests in Prism version 7.0 (GraphPad). Animal experiments were approved by the Swiss Cantonal Veterinary Authority (authorization no. 3082).

ACKNOWLEDGMENTS

We would like to thank Janssen Pharmaceutical, Otsuka Novel Products GmbH, and *Sequella*, Inc for kindly providing the BDQ, DMD, and STZ used in this study, respectively.

FUNDING INFORMATION

This work was funded by the European Community's Seventh Framework Programme under grant agreement 260872.

REFERENCES

1. WHO | Global tuberculosis report 2017. WHO.
2. Maitra A, Bates S, Kolvekar T, Devarajan PV, Guzman JD, Bhakta S. 2015. Repurposing—a ray of hope in tackling extensively drug resistance in tuberculosis. *Int J Infect Dis* 32:50–55.
3. Ramón-García S, Río RG del, Villarejo AS, Sweet GD, Cunningham F, Barros D, Ballell L, Mendoza-Losana A, Ferrer-Bazaga S, Thompson CJ. 2016. Repurposing clinically approved cephalosporins for tuberculosis therapy. *Sci Rep* 6:srep34293.
4. Pagliotto ADF, Caleffi-Ferracioli KR, Lopes MA, Baldin VP, Leite CQF, Pavan FR, Scodro RB de L, Siqueira VLD, Cardoso RF. 2016. Anti-*Mycobacterium tuberculosis* activity of antituberculosis drugs and amoxicillin/clavulanate combination. *J Microbiol Immunol Infect* 49:980–983.

5. Ramón-García S, Ng C, Anderson H, Chao JD, Zheng X, Pfeifer T, Av-Gay Y, Roberge M, Thompson CJ. 2011. Synergistic Drug Combinations for Tuberculosis Therapy Identified by a Novel High-Throughput Screen[∇]. *Antimicrob Agents Chemother* 55:3861–3869.
6. Li W, Sanchez-Hidalgo A, Jones V, Moura VCN de, North EJ, Jackson M. 2017. Synergistic Interactions of MmpL3 Inhibitors with Antitubercular Compounds In Vitro. *Antimicrob Agents Chemother* 61:e02399-16.
7. WHO | Target Regimen Profiles for TB Treatment. WHO.
8. Brečik M, Centárová I, Mukherjee R, Kolly GS, Huszár S, Bobovská A, Kilacsková E, Mokošová V, Svetlíková Z, Šarkan M, Neres J, Korduláková J, Cole ST, Mikušová K. 2015. DprE1 Is a Vulnerable Tuberculosis Drug Target Due to Its Cell Wall Localization. *ACS Chem Biol* 10:1631–1636.
9. Zhang M, Sala C, Hartkoorn RC, Dhar N, Mendoza-Losana A, Cole ST. 2012. Streptomycin-Starved Mycobacterium tuberculosis 18b, a Drug Discovery Tool for Latent Tuberculosis. *Antimicrob Agents Chemother* 56:5782–5789.
10. Makarov V, Lechartier B, Zhang M, Neres J, van der Sar AM, Raadsen SA, Hartkoorn RC, Ryabova OB, Vocat A, Decosterd LA, Widmer N, Buclin T, Bitter W, Andries K, Pojer F, Dyson PJ, Cole ST. 2014. Towards a new combination therapy for tuberculosis with next generation benzothiazinones. *EMBO Mol Med* 6:372–383.
11. Lechartier B, Cole ST. 2015. Mode of Action of Clofazimine and Combination Therapy with Benzothiazinones against Mycobacterium tuberculosis. *Antimicrob Agents Chemother* 59:4457–4463.

12. Matteelli A, Carvalho AC, Dooley KE, Kritski A. 2010. TMC207: the first compound of a new class of potent anti-tuberculosis drugs. *Future Microbiol* 5:849–858.
13. Yano T, Kassovska-Bratinova S, Teh JS, Winkler J, Sullivan K, Isaacs A, Schechter NM, Rubin H. 2011. Reduction of clofazimine by mycobacterial type 2 NADH:quinone oxidoreductase: a pathway for the generation of bactericidal levels of reactive oxygen species. *J Biol Chem* 286:10276–10287.
14. Degang Y, Akama T, Hara T, Tanigawa K, Ishido Y, Gidoh M, Makino M, Ishii N, Suzuki K. 2012. Clofazimine modulates the expression of lipid metabolism proteins in *Mycobacterium leprae*-infected macrophages. *PLoS Negl Trop Dis* 6:e1936.
15. Palomino J-C, Martin A, Camacho M, Guerra H, Swings J, Portaels F. 2002. Resazurin Microtiter Assay Plate: Simple and Inexpensive Method for Detection of Drug Resistance in *Mycobacterium tuberculosis*. *Antimicrob Agents Chemother* 46:2720–2722.
16. Zumla A, Nahid P, Cole ST. 2013. Advances in the development of new tuberculosis drugs and treatment regimens. *Nat Rev Drug Discov* 12:388–404.
17. Tiberi S, Payen M-C, Sotgiu G, D'Ambrosio L, Alarcon Guizado V, Alffenaar JW, Abdo Arbex M, Caminero JA, Centis R, De Lorenzo S, Gaga M, Gualano G, Roby Arias AJ, Scardigli A, Skrahina A, Solovic I, Sulis G, Tadolini M, Akkerman OW, Alarcon Arrascue E, Aleska A, Avchinko V, Bonini EH, Chong Marín FA, Collahuazo López L, de Vries G, Dore S, Kunst H, Matteelli A, Moschos C, Palmieri F, Papavasileiou A, Spanevello A, Vargas Vasquez D, Viggiani P, White V, Zumla A, Migliori GB. 2016. Effectiveness and safety of

- meropenem/clavulanate-containing regimens in the treatment of MDR- and XDR-TB. *Eur Respir J* 47:1235–1243.
18. Van der Paardt A-FL, Akkerman OW, Gualano G, Palmieri F, Davies Forsman L, Aleksa A, Tiberi S, de Lange WCM, Bolhuis MS, Skrahina A, van Soolingen D, Kosterink JGW, Migliori GB, van der Werf TS, Alffenaar J-WC. 2017. Safety and tolerability of clarithromycin in the treatment of multidrug-resistant tuberculosis. *Eur Respir J* 49.
 19. Gopal M, Padayatchi N, Metcalfe JZ, O'Donnell MR. 2013. Systematic review of clofazimine for the treatment of drug-resistant tuberculosis. *Int J Tuberc Lung Dis Off J Int Union Tuberc Lung Dis* 17:1001–1007.
 20. Migliori GB, Eker B, Richardson MD, Sotgiu G, Zellweger J-P, Skrahina A, Ortmann J, Girardi E, Hoffmann H, Besozzi G, Bevilacqua N, Kirsten D, Centis R, Lange C, TBNET Study Group. 2009. A retrospective TBNET assessment of linezolid safety, tolerability and efficacy in multidrug-resistant tuberculosis. *Eur Respir J* 34:387–393.
 21. Feng X, Zhu W, Schurig-Briccio LA, Lindert S, Shoen C, Hitchings R, Li J, Wang Y, Baig N, Zhou T, Kim BK, Crick DC, Cynamon M, McCammon JA, Gennis RB, Oldfield E. 2015. Antiinfectives targeting enzymes and the proton motive force. *Proc Natl Acad Sci* 112:E7073–E7082.
 22. Li W, Upadhyay A, Fontes FL, North EJ, Wang Y, Crans DC, Grzegorzewicz AE, Jones V, Franzblau SG, Lee RE, Crick DC, Jackson M. 2014. Novel Insights into the Mechanism of Inhibition of MmpL3, a Target of Multiple Pharmacophores in *Mycobacterium tuberculosis*. *Antimicrob Agents Chemother* 58:6413–6423.

23. Lechartier B, Hartkoorn RC, Cole ST. 2012. In vitro combination studies of benzothiazinone lead compound BTZ043 against *Mycobacterium tuberculosis*. *Antimicrob Agents Chemother* 56:5790–5793.
24. 2006. Use of clomiphene citrate in women. *Fertil Steril* 86:S187–S193.
25. Farha MA, Czarny TL, Myers CL, Worrall LJ, French S, Conrady DG, Wang Y, Oldfield E, Strynadka NCJ, Brown ED. 2015. Antagonism screen for inhibitors of bacterial cell wall biogenesis uncovers an inhibitor of undecaprenyl diphosphate synthase. *Proc Natl Acad Sci* 112:11048–11053.
26. Jang WS, Kim S, Podder B, Jyoti MA, Nam K-W, Lee B-E, Song H-Y. 2015. Anti-*Mycobacterial* Activity of Tamoxifen Against Drug-Resistant and Intra-Macrophage *Mycobacterium tuberculosis*. *J Microbiol Biotechnol* 25:946–950.
27. Kalia NP, Hasenoehrl EJ, Ab Rahman NB, Koh VH, Ang MLT, Sajorda DR, Hards K, Grüber G, Alonso S, Cook GM, Berney M, Pethe K. 2017. Exploiting the synthetic lethality between terminal respiratory oxidases to kill *Mycobacterium tuberculosis* and clear host infection. *Proc Natl Acad Sci U S A* 114:7426–7431.
28. Wallis RS, Dawson R, Friedrich SO, Venter A, Paige D, Zhu T, Silvia A, Gobey J, Ellery C, Zhang Y, Eisenach K, Miller P, Diacon AH. 2014. Mycobactericidal Activity of Sutezolid (PNU-100480) in Sputum (EBA) and Blood (WBA) of Patients with Pulmonary Tuberculosis. *PLoS ONE* 9.

29. Sulochana S, Mitchison DA, Kubendiren G, Venkatesan P, Paramasivan CN. 2009. Bactericidal activity of moxifloxacin on exponential and stationary phase cultures of *Mycobacterium tuberculosis*. *J Chemother Florence Italy* 21:127–134.
30. Riccardi N, Del Puente F, Magnè F, Taramasso L, Di Biagio A. 2017. Bedaquiline: a new hope for shorter and better anti-tuberculosis regimens. *Recent Patents Anti-Infect Drug Disc.*
31. Grosset J, Vernon A. 2015. A reader's guide to the bactericidal activity of pyrazinamide and clofazimine alone and in combinations with pretomanid and bedaquiline. *Am J Respir Crit Care Med* 191:871–873.
32. Saliu OY, Crismale C, Schwander SK, Wallis RS. 2007. Bactericidal activity of OPC-67683 against drug-tolerant *Mycobacterium tuberculosis*. *J Antimicrob Chemother* 60:994–998.
33. Xavier AS, Lakshmanan M. 2014. Delamanid: A new armor in combating drug-resistant tuberculosis. *J Pharmacol Pharmacother* 5:222–224.
34. Sharma S, Gelman E, Narayan C, Bhattacharjee D, Achar V, Humnabadkar V, Balasubramanian V, Ramachandran V, Dhar N, Dinesh N. 2014. Simple and Rapid Method To Determine Antimycobacterial Potency of Compounds by Using Autoluminescent *Mycobacterium tuberculosis*. *Antimicrob Agents Chemother* 58:5801–5808.

Figures and Tables

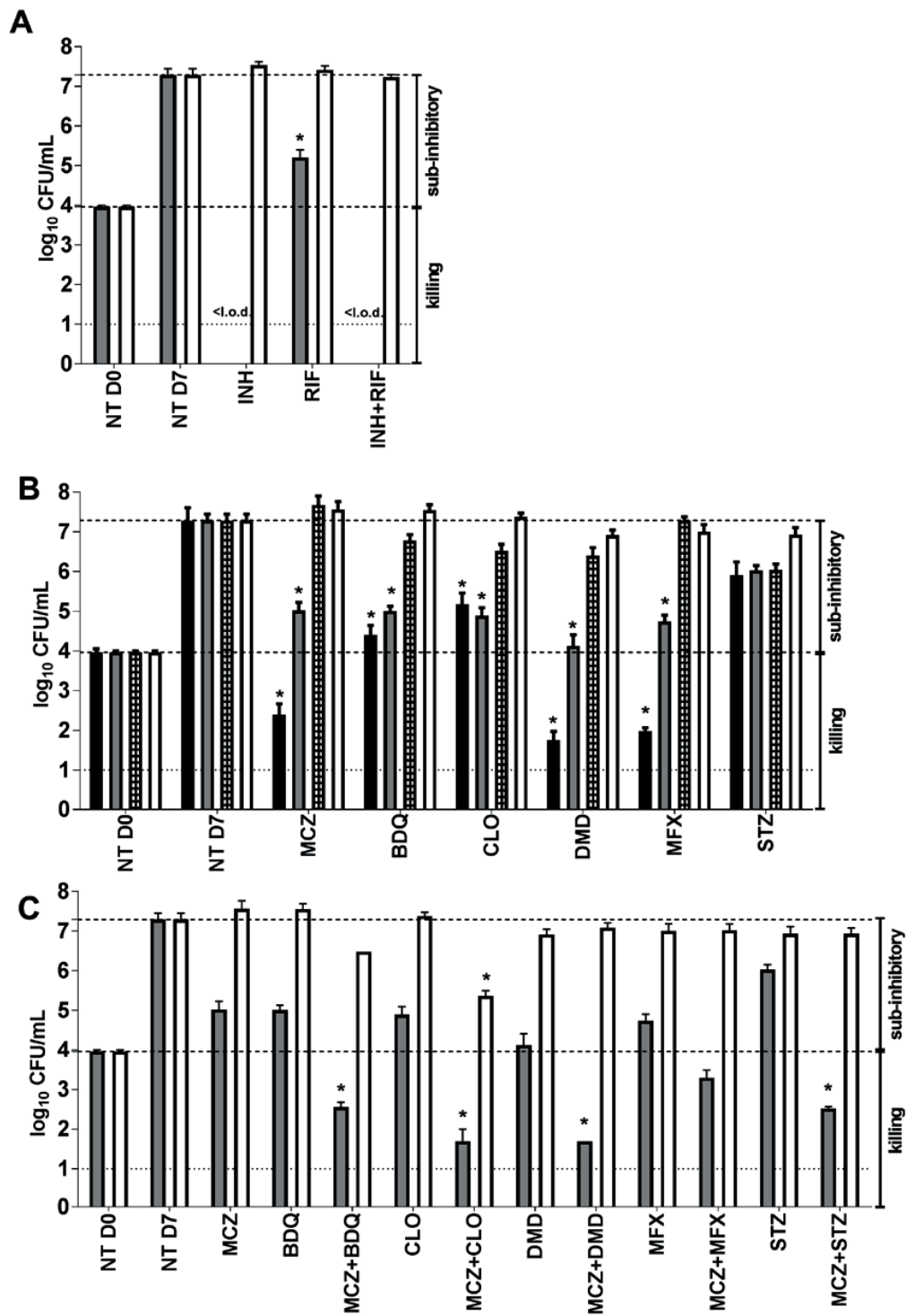


Figure 1: CFU counting after exposure to MCZ in two-drug combinations. (A) NT (non-treated) *M. tuberculosis* H37Rv viability on day 0 and on day 7 was assessed in the presence of INH and RIF, (1X MIC [grey bars] and 0.25X MIC [white bars]) as controls. (B) Activity of drugs tested individually at 2X MIC (black bars), 1X MIC (grey bars), 0.5X MIC (tiled bars) and 0.25X MIC (white bars). (C) The activity of MCZ two-drug combinations at 1X MIC (grey bars) and 0.25X MIC (white bars) of each drug. Faint dashed line represents the limit of detection in the assay. Dark dashed lines represent the number of CFU of the non-treated bacteria at D0 and after 7 days incubation. A decrease of at least 2 log₁₀ in the mean CFU/mL was considered significant (*) compared to the non-treated (NT) control after 7 days incubation (Fig. 1 A and 1B). In combination, a decrease of 2 log₁₀ CFU/mL was considered significant (*) compared to the drugs alone (Fig. 1C); <l.o.d., below the limit of detection.

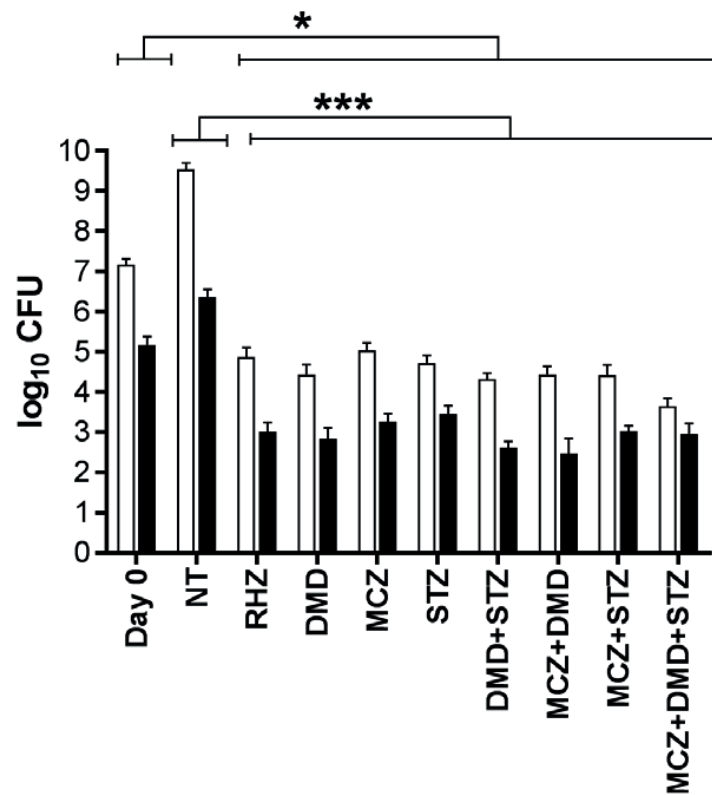


Figure 2: Efficacy of drugs alone or in combination in a mouse model of TB. Drugs were administered by gavage at the following doses: rifampicin (R) = 10mg/kg, isoniazid (H) = 25mg/kg, pyrazinamide (Z) = 150mg/kg, MCZ (MCZ) = 25mg/kg, delamanid (DMD) = 5mg/kg, sutezolid (STZ) = 100mg/kg. White and black columns correspond to the bacterial burden in the lungs and spleens respectively at day 0 (D0) when treatment was initiated, or day 28 (NT, no treatment; regimens as indicated) when treatment ended. Bars represent the mean \pm s.d. of CFUs from five Balb/c mice per group. *, $P \leq 0.03$; ***, $P \leq 0.0002$

Table 1: MIC of the drugs against *M. tuberculosis* H37Rv

Drugs	MIC (µg/mL)
AMK	0.02
BDQ	0.07
CLO	0.20
CLM	24.8
CLR	14.2
DCS	2.80
DMD	0.0017
EMB	0.15
ETO	1.53
INH	0.28
LVX	0.17
LZD	0.34
LZPs	1.4
MEM	1.00
MXF	0.03
MCZ HCl	0.0002
PAS	0.014
PZA	ND ^a
RIF	0.0005
STZ	0.20
TMX	14.22

Abbreviations: AMK, Amikacin; BDQ, Bedaquiline; CLO, clofazimine; CLM, clomiphene; CLR, clarithromycin; DCS, D-cycloserine; DMD, delamanid; EMB, ethambutol; ETO, ethionamide; INH, isoniazid; LVX, levofloxacin; LZD, linezolid; LPZS, lansoprazole sulfide; MEM, meropenem; MXF, moxifloxacin; PAS, para-aminosalicylic acid; PZA, pyrazinamide; RIF, rifampicin; STZ, sutezolid; TMX, tamoxifen.

^aND, not detectable in the conditions tested

Table 2: Combinatory effect of MCZ with first- and second-line drugs against *M. tuberculosis*

H37Rv *in vitro* (checkerboard assay)

Combinations	FICI _m a	FICI _M b	Mean FICI (0.25X MIC) ^c	Mean FICI	Combinatory effect (FICI _m /FICI _M) ^d
MCZ+AMK	1.125	2.000	1.250	1.469	I/I
MCZ+DCS	1.250	3.000	1.125	1.844	I/I
MCZ+EMB	1.125	2.000	1.250	1.844	I/I
MCZ+ETO	1.125	1.500	1.250	1.344	I/I
MCZ+INH	1.063	1.500	1.250	1.236	I/I
MCZ+LVX	1.125	2.000	1.125	1.469	I/I
MCZ+MFX	1.125	2.000	1.250	1.469	I/I
MCZ+PAS	1.125	2.000	1.250	1.469	I/I
MCZ+ RIF	0.750	1.125	1.250	0.922	I/I

^a Represents the lowest FICI observed in this assay

^b Represents the highest FICI observed in this assay

^c Calculated at 0.25X MIC of the first drug indicated in the combination.

^d Combinatory effect: I, indifferent and S, synergism

Table 3: Combinatory effect of MCZ with repurposed or new anti-TB drugs against *M.*

tuberculosis H37Rv *in vitro* (checkerboard assay)

Combinations	FICI _m ^b	FICI _M ^c	Mean FICI (0.25X MIC) ^d	Mean FICI	Combinatory effect (FICI _m /FICI _M) ^e
MCZ+BDQ	0.375	1.250	0.375	0.719	S/I
MCZ+CLM	0.250	1.063	0.250	0.633	S/I
MCZ+CLO	0.375	3.000	0.375	0.719	S/I
MCZ+CLR	1.033	1.250	1.250	1.063	I/I
MCZ+DMD	1.125	2.500	1.125	1.469	I/I
MCZ+LPZs	1.125	2.500	1.250	1.469	I/I
MCZ+LZD	1.125	2.000	1.250	1.328	I/I
MCZ+MEM	1.063	1.500	1.250	1.146	I/I
MCZ+STZ	1.063	2.500	1.250	1.146	I/I
MCZ+TMX ^a	0.625	1.063	0.750	0.935	I/I

^a Combination was assessed using the H37Rv-lux strains as previously reported.

^b Represents the lowest FICI observed in this assay

^c Represents the highest FICI observed in this assay

^d Calculated at 0.25X MIC of the first drug indicated in the combination.

^e Combinatory effect: I, indifferent and S, synergism

Combinations in bold are synergistic

Table 4: Cytotoxicity assay of drug combinations in human HepG2 cells

Drugs/combinations	TD50 ($\mu\text{g/mL}$)^a	TD99 ($\mu\text{g/mL}$)^b
BDQ	9.68	40.47
CLO	0.91	2.82
DMD	52.87	56.81
MCZ	51.16	56.22
STZ	51.32	71.61
BDQ+CLO	0.66	1.99
DMD+BDQ	5.32	14.24
DMD+CLO	0.50	1.07
DMD+STZ	24.85	36.74
MCZ+BDQ	11.19	26.02
MCZ+CLO	1.08	2.61
MCZ+DMD	6.76	21.15
MCZ+STZ	34.50	55.01
MCZ+CLO+BDQ	0.77	2.04
MCZ+DMD+BDQ	3.68	9.01
MCZ+DMD+CLO	0.58	1.77
MCZ+STZ+DMD	5.61	17.23

^a Toxic dose that inhibits 50% of the cell viability

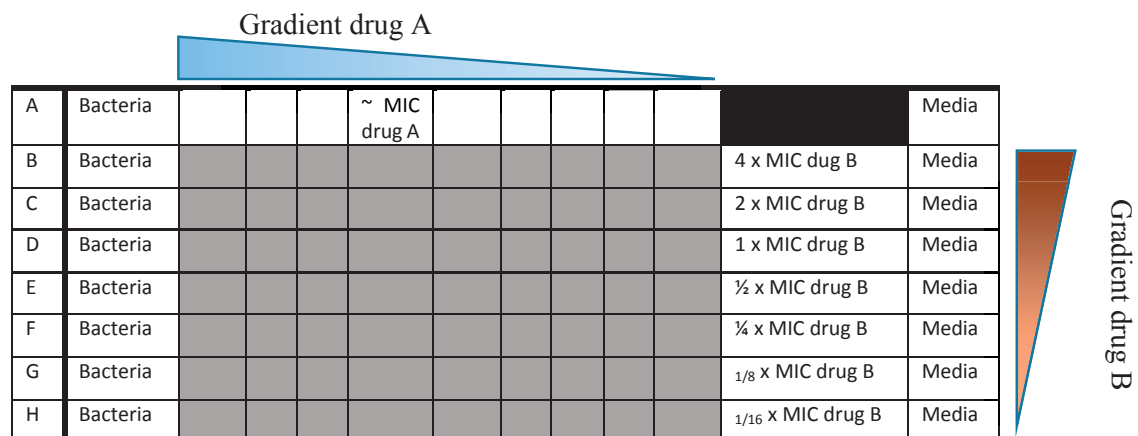
^b Toxic dose that inhibits 99% of the cell viability

Supplemental material

Table S1: *M. tuberculosis* H37Rv viability after treatment with two-drug combinations (Figure 1)

	MIC of each drug		0.25X MIC of each drug	
	log ₁₀ CFU/mL	s.d.	log ₁₀ CFU/mL	s.d.
NT D0	3.950	0.123	3.950	0.123
NT D7	6.996	0.627	6.996	0.627
INH	7.444	0.209	7.496	0.235
RIF	4.543	1.100	7.378	0.214
PZA	7.159	0.064	7.231	0.327
INH+RIF	3.778	0.988	7.224	0.110
INH+RIF+PZA	4.863	1.544	6.628	0.462
MCZ	3.701	1.865	7.235	0.675
BDQ	4.705	0.817	7.289	0.588
MCZ+BDQ	2.531	0.213	6.477	0.000
CLO	3.690	1.748	7.366	0.157
MCZ+CLO	2.000	0.000	5.334	0.223
DMD	3.200	1.137	6.804	0.390
MCZ+DMD	1.699	0.000	7.054	0.213
MFZ	4.690	0.301	6.835	0.503
MCZ+MFZ	3.223	0.380	6.977	0.281
STZ	5.955	0.297	6.780	0.386
MCZ+STZ	2.523	0.064	6.889	0.269
BDQ+DMD	3.914	0.015	7.386	0.257
BDQ+STZ	4.699	0.000	7.521	0.311
CLO+BDQ	1.810	1.404	5.352	1.024
CLO+DMD	3.727	0.225	6.163	0.019
CLO+STZ	4.006	0.211	5.921	0.018
DMD+STZ	4.651	0.069	7.000	0.563
MFZ+BDQ	4.182	0.106	6.393	0.859
MFZ+CLO	5.175	0.041	6.275	0.164

Figure S1: Schematic representation of checkerboard plates as they were prepared for this study.



A

C. glutamicum	1	-----MSEFQVP
M. tuberculosis	1	VARDARKRTSSNFPQLPPAPDDYPTFPDTSTWPVVEPELPAPPYGGPCRPPQHTSKAAAP
S. aureus	1	-----MEKKLINK-----KNTINNYNE
E. coli	1	-----MMISA-----TCPLSE

C. glutamicum	8	EIPAQFLPKHIALVMDGNRWATERGMKRTEGHRGFAVLDDVVDACIELGVPYLSAYAF
M. tuberculosis	61	RIPADRLPNHVAIVMDGNRWATQRLARTEGHRKMGAVVIDIACAIELGKWLSLYAF
S. aureus	18	EIDSSNIPEHIAIIMDGNRWAKKRMPIKGHYEGMOTIKKITRIASDIGVKYLILYAF
E. coli	12	K-LPAHGCRHVAILMDGNRWAKKQCKIRAFGHKAKSVRRRAVSFAANNGTEALTYAF

C. glutamicum	68	STENWRRSTDEVRFMLGFNRDVLRRQRDDLHEKGVVRVWVGRPRPRLWRSVIRELETABEL
M. tuberculosis	121	STENWKRSPDEVRFMLGFNRDVLRRQRDDLKKLGVRIRWVGSRPRLWRSVINELAVAEEM
S. aureus	78	STENWSRPESEVNYIMNLPVNFLKTFELPELEKNVIVETIGFTDKLPKSTIEAINNAKEK
E. coli	71	SSENWNRPAQEVSAIMELFVWALDSEVKSLEHRHNVRIIIGDTSRFNSRLQERIRKSEAL

C. glutamicum	128	TKDNTTMTLAMCVNYGGRAEILDAARDIARLAAEGKLRPEQITEKTFNFLEPDMFDPVD
M. tuberculosis	181	TKSNDVITINVCVNYGGRTTEITEATREIAREVAAGRLNPERITESTIARHLQRPDIPDVD
S. aureus	138	TANNTGLKLIATNYGGRAELVHSLKNNMFDELHQOGLNSDIIDETIYNNHLMTKDYDPDE
E. coli	131	TAGNTGLTLNIAANYGGRWELIVQGVROLAEKVQOQNLQPDQIDEEMLNCHVCMHEAFVD

C. glutamicum	188	LFIRPSGERTSNFLLWQSAYAEVYQDKLPDFTOQDLYDAVLEYAKRRDRFGSA----
M. tuberculosis	241	LFIRTSGEORSSNFWLQAYAYAEYIFQDKLWPDYDRDLWAACEEYASRTRRFGSA----
S. aureus	198	LLIRTSGEORISNFWQSYSEFIFNQKLWPDFDEDELKCKIKIYQSRQRRFGGLSEE-
E. coli	191	LVIRTGGERISNFWQYAYAEYVETDVLWPDFDEQDFEGALNAFANRRERFRFGGTPEGD

C. glutamicum	---	
M. tuberculosis	---	
S. aureus	---	
E. coli	251	ETA

B

	<i>C. glutamicum</i>	<i>M. tuberculosis</i>	<i>S. aureus</i>	<i>E. coli</i>
<i>C. glutamicum</i>	100.00	64.61	37.86	38.17
<i>M. tuberculosis</i>	64.61	100.00	37.94	39.02
<i>S. aureus</i>	37.86	37.94	100.00	39.76
<i>E. coli</i>	38.17	39.02	39.76	100.00

Figure S2: Protein sequence alignments of UppS. Protein sequences from *C. glutamicum* ATCC 13032 (NCgl2203), *M. tuberculosis* H37Rv (Rv2361c), *Staphylococcus aureus* N315 (SA1103) and *Escherichia coli* K12 substr. MG1655 (b0174) were aligned using CLUSTAL Omega (A). Amino acids in red were reported to interact with clomiphene (PDB: 5CQJ). Identities (%) between amino acid sequences (B) were calculated using CLUSTAL 2.1.

Acknowledgements

I would like to express my heartfelt gratitude to the UPCOL members, both past and present, for creating a stimulating, dynamic, and fun environment, for looking out for each other, and for making this experience a truly memorable and meaningful one. I am extremely thankful, first and foremost, to Prof. Stewart Cole, for adopting me when I was lab-less and giving me the opportunity to be part of an incredible team, and for his guidance, supervision, and encouragement throughout these years. Stewart is an inspirational figure and has impressed much on me, including his broad knowledge, sharp observational skills, and humour. I would also like to thank Claudia for her initiation into the P3 lab, for being a great teacher and her patience in teaching, and for always having some time for discussions; Jérémie for his many (wacky) ideas and scientific input on projects, for being always up for scientific and non-scientific discussions, for his motivation and encouragement, for polishing manuscripts and the draft of this thesis; Andréanne for her guidance and collaboration on drug discovery projects, for many fruitful discussions based on her microbiology and drug resistance experience, and for making long P3 times more fun and offering help in hard times (e.g. gavaging mice, 32 REMA plates); Andrej for always having his door open and willing to take time to explain some bioinformatics (and inappropriate jokes); the lab technicians, Anthony, for all the huge initial screens of compounds and help with the mice, Stef, for ensuring the smooth running of the lab, and for always being really kind, Philippe for helping to run the lab and sharing interesting trivia facts; Jan who took time to demonstrate the tricky business of *M. tuberculosis* recombineering; Rita for discussions related to drug discovery and other topics, and for sharing nice moments at MM4TB meetings together with Monica; and to the PhD students, Ye, Nina, Charlotte, Paloma, Raphael, and Sofia, for always being ready to help with experiments, sharing tips and advice, as well as the ups and downs of PhD life. A special mention also to Gaëlle, for her introduction to DprE1 at the beginning; to Benoit, for an engaging project to take over from; to Jean-Yves, for PBTZ interactions and a few fresh air walks; and to Cécile and Suzanne who have enthusiastically and whole-heartedly provided administrative support, and listening ears.

I would also like to thank the chemists, Prof. Karl-Heinz Altmann and his team, Maryline, Tobias, and Patrick, for very fruitful collaborations, for the engaging discussions during our bi-annual meetings, and for generating and synthesising interesting molecules to work with; and to our other collaborators with whom I have had the pleasure of interacting with, Dirk and Prof. Adrie Steyn, Prof. Kevin Pethe, and Prof. Mary Jackson, through email correspondence and/or meetings at conferences, and to Dr. Helena Boshoff for taking time in providing constructive input on the PB project. I am also thankful to members of the labs of the Global Health Institute, particularly the neighbouring Blokesch, McKinney and Lemaitre labs, for the floor interactions in and out of the labs, and for always being willing to lend a helping hand in dire situations, such as when there is a shortage of material; and to my mentor, Prof. Bart Deplancke, for his annual words of encouragement.

I am also very grateful towards members of the now-defunct UPMOORE lab, to Prof. Darren Moore for giving me the opportunity to work in his lab for my Master thesis and for accepting me thereafter as a PhD candidate, for his close guidance and supervision; to Elpida for supervising my Master project and for teaching me many experimental techniques patiently, Guillaume, Roger, Alessandra, Agata, and Liliane, for all the experimental tips and tricks, and scientific advice; and to Duygu, Meghna, and Ece, for sharing the life of Master students.

I also greatly appreciate Prof. Melanie Blokesch, Prof. Karl-Heinz Altmann, Prof. Peter Sander, and Prof. Mary Jackson, for taking time out of their schedules to participate as jury members of the committee.

Last, but certainly not the least, I am extremely thankful for the enriching interactions, inspiration, and support of those whom I have met over the course of my time in Switzerland, for the friendships, for the good times, and for the love and support of those dearest to me.

Caroline Shi-Yan Foo

Chemin du Motte 16b, 1020 Renens, Switzerland

☎ (+41) 78 814 2765 | ✉ caroline.foo@epfl.ch
D.O.B. 31.08.1986 | 🇸🇬 Singaporean

Education

Ph.D candidate, Bioengineering and Biotechnology

Swiss Federal Institute of Technology Lausanne (EPFL)

Aug 2014 - Sep 2018 (expected)

Switzerland

Master of Science, Biomedical Engineering

University of Applied Sciences Aachen

Mar 2010 - Sept 2012

Germany

- Exchange student at EPFL, Switzerland (Nov 2011 - Aug 2012)

Bachelor with Honours, Bioengineering

National University of Singapore

Aug 2005 - May 2009

Singapore

- Exchange student at Technical University of Munich, Germany (Oct 2007 - Aug 2008)

Experience

Ph.D research

Laboratory of Microbial Pathogenesis (UPCOL), Global Health Institute, EPFL

Aug 2014 - present

Switzerland

- Led and managed drug discovery projects for Tuberculosis
- Lead generation and optimisation of 2 new compounds, including target identification and mechanism of action
- Contributed to clinical development support of Tuberculosis drug candidate Macozinone by elucidating mechanisms of resistance, generation of backup series, characterisation of drug interactions

Teaching Assistant

Integrated Laboratory course for Life Sciences, Bachelor course, EPFL

Feb 2014 - Jan 2016

Switzerland

- Supervised groups of students in a laboratory setting
- Demonstration and explanation of biological laboratory techniques, supervision in execution of experiments, discussion and analysis of results
- Grading of lab notebooks and project reports

Research Assistant

Laboratory of Neurodegenerative Research (LMNR), Brain Mind Institute, EPFL

Oct 2012 - Mar 2013

Switzerland

- Investigation of the role of LRRK2 in microRNA regulation by detecting differential expression of microRNAs in Parkinson's disease state
- Elucidation of cellular and molecular mechanisms of LRRK2-linked (Leucine-rich repeat kinase 2) Parkinson's disease using a viral-based gene transfer method in *in vitro* and *in vivo* models

Master thesis research

Laboratory of Neurodegenerative Research (LMNR), Brain Mind Institute, EPFL

Nov 2011 - Aug 2012

Switzerland

- Established neuronal toxicity assays in primary neuronal cultures based on neuronal death, neurite length and branching complexity using Sholl analysis
- Development of primary neuronal culture model of LRRK2-linked Parkinson's disease

Teaching Substitute

Raffles Institution

Jul 2009 - Feb 2010

Singapore

- Conducted lessons in Physics and Biology at the secondary school level
- Prepared students for end-of-year exams, provided extra coaching sessions

Bachelor Project

Nano-Bioanalytics Laboratory, National University of Singapore

Sep 2008 - May 2009

Singapore

- Optimisation of polymer layer production for layer-by-layer encapsulation of pancreatic cells
- Validation of components and presence of polymer layers using UV, IR spectroscopic and biophysical methods

Technical Skills

Laboratory skills

Microbiology, molecular biology, biochemistry, working with cell lines and primary neuronal cultures, recombinant purification and expression of proteins and adenovirus, immunocytochemistry, fluorescent and confocal imaging

Trainings and Certifications

Working in biosafety P1 to P3 laboratory, animal experimentation

Computer skills

Microsoft Office (Word, Excel, Powerpoint), Adobe Photoshop, Illustrator, Latex

Publications

- Tsika E, Kannan M, **Foo CS-Y**, Dikeman D, Glauser L, Gellhaar S, Galter D, Knott GW, Dawson TM, Dawson VL, Moore DJ. 2014. *Conditional expression of Parkinson's disease-related R1441C LRRK2 in midbrain dopaminergic neurons of mice causes nuclear abnormalities without neurodegeneration*. *Neurobiol Dis* 71:345–358.
- **Foo CS-Y**, Lechartier B, Kolly GS, Boy-Röttger S, Neres J, Rybniker J, Lupien A, Sala C, Piton J, Cole ST. 2016. *Characterization of DprE1-Mediated Benzothiazinone Resistance in Mycobacterium tuberculosis*. *Antimicrob Agents Chemother* 60:6451–6459.
- Piton J, **Foo CS-Y**, Cole ST. 2017. *Structural studies of Mycobacterium tuberculosis DprE1 interacting with its inhibitors*. *Drug Discov Today* 22:526–533.
- Piton J, Vocat A, Lupien A, **Foo CS-Y**, Riabova O, Makarov V, Cole ST. 2018. *Structure-based drug design and characterization of sulfonyl-piperazine benzothiazinone inhibitors of DprE1 from Mycobacterium tuberculosis*. *Antimicrob Agents Chemother AAC*.00681-18.
- Lupien A, Vocat A, **Foo CS-Y**, Blattes E, Gillon J-Y, Makarov V, Cole ST. 2018. *An optimized background regimen for treatment of active tuberculosis with the next-generation benzothiazinone Macozinone (PBTZ169)* *Antimicrob Agents Chemother AAC*.
- **Foo CS-Y**, Lupien A, Kienle M, Vocat A, Benjak A, Sommer R, Lamprecht DA, Steyn AJC, Pethe K, Piton J, Altmann K-H, Cole ST. 2018. *Arylvinyllpiperazine amides, a new class of potent inhibitors targeting QcrB of Mycobacterium tuberculosis*. *mBio*.

Conference Proceedings

- More Medicines for Tuberculosis (MM4TB) Consortium Meeting (Paris, France, 29-30th June 2015). "Characterization of DprE1-Mediated Benzothiazinone Resistance in Mycobacterium tuberculosis". *Oral presentation*.
- EMBO Tuberculosis 2016: Interdisciplinary Research on Tuberculosis and Pathogenic Mycobacteria (Paris, France, 19-23th September 2016). Foo CS-Y *et al.*, Characterization of DprE1-Mediated Benzothiazinone Resistance in Mycobacterium tuberculosis. *Poster presentation*.
- Gordon Research Conference: Tuberculosis Drug Discovery and Development (Lucca, Italy, 25-30th June 2017). Foo CS-Y *et al.*, Characterization of DprE1-Mediated Benzothiazinone Resistance in Mycobacterium tuberculosis. *Poster presentation*.

Grants, Achievements & Awards

FEMS Young Scientists Meeting Grant, FEMS Travel Fellowship for EMBO Tuberculosis 2016 conference

June 2016

2nd Best Oral Presentation, MM4TB Consortia Meeting

June 2015

Roche Continents, organised by Roche. 1 out of 100 participants challenging boundaries in science, art & innovation

Aug 2014

Singapore Local Undergraduate Scholarship, OCBC Bank

Aug 2005 - May 2009

Award for Study Abroad, National University of Singapore

Oct 2007 - Aug 2008

Diploma in Piano Performance, Associated Board of Royal School of Music (DipABRSM)

Aug 2000

Languages

English

Native

Mandarin

Fluent

German

B2, Working proficiency

French

B1



Source: Stop TB Partnership